
Synthesis of Amphiphilic Block Copolymers and their Interactions with Model Lipid Membranes

DISSERTATION

zur Erlangung des
Doktorgrades der Naturwissenschaften (Dr. rer. nat.)

der

Naturwissenschaftlichen Fakultät II

der Martin-Luther-Universität
Halle-Wittenberg,

vorgelegt

von Matthias Schulz
geb. am 07. Februar 1984 in Stendal

ausgeführt unter der Leitung von

Prof. Dr. Wolfgang H. Binder
Professor für Makromolekulare Chemie
Martin-Luther-Universität Halle-Wittenberg

Gutachter:

1. Prof. Dr. Wolfgang H. Binder (MLU Halle-Wittenberg)
2. Prof. Dr. André Laschewsky (Universität Potsdam)

„Wer kämpft, kann verlieren.

Wer nicht kämpft, hat schon verloren.“

BERTOLT BRECHT

ACKNOWLEDGEMENTS

Finally, this dissertation is a result of more than three years of work and now it is of great importance for me to thank all those people who in one way or another supported my research and contributed in completion of this work. Without their assistance and the numerous discussions with them this dissertation could never be finished.

I would like to express my special thanks to:

First of all to my supervisor Prof. Dr. Wolfgang H. Binder for giving me the opportunity to perform my PhD on this interesting topic, which has always inspired me and has contributed significantly to broadening my knowledge in this challenging field. Without his guidance, time for scientific discussions, help in writing publications and encouragement during my work, this thesis would not have been possible to finish.

I am really grateful for the support by Jun.-Prof. Dr. Kirsten Bacia (ZIK HALOmem) and her group members (especially Daniela Krüger, Stefan Werner, Dr. Annette Meister, Dr. Sebastian Daum and Claudia Müller) who helped me, made measurements for me and showed me how to deal with confocal Laser Scanning Microscopy (LSM) to perform my own measurements. Thus, successful publications were the result of useful discussions with them, which helped me a lot in understanding and interpreting the data.

I would like to thank also the group of Prof. Dr. Alfred Blume, in particular Peggy Scholtysek Bob-Dan Lechner and Dr. Andreas Kerth, who also helped and made experiments for me such as DSC studies, fluorescence microscopy investigations of monolayers and AFM measurements. Furthermore, I would like to show my appreciation to Prof. Dr. Jörg Kressler and his group for supporting me and allowing me to conduct measurements (Langmuir monolayer studies and confocal LSM investigations of my numerous samples) at their department. I do not want to forget to thank all my colleagues for the friendly and cheerful daily work throughout all the years. It is a great pleasure for me to especially acknowledge Adekunle-Ayodele Olubummo (*alias* Paul) who has worked together with me on this new membrane topic and provided me especially with surface functionalized nanoparticles based on CdSe that have played a crucial role in my studies. The daily work with him, numerous DFG meetings and our mutual support during our dissertations led to many joint publications as well as to a strong friendship.

Special thanks to all my friends (especially the daily *Mensa-team* consisting of Haitham Barqawi, Mark Jbeily, Parvin Zare, Ali Shaygan Nia and my friends from other departments Andreas Hentsch, Eik Koslowski and Daniel Teichmann) who made my time at Martin-Luther-University very special and unforgettable. Furthermore, I am grateful for their support and encouragement during my work as well as in many other situations in my private life.

Finally, I would like to dedicate this thesis to my beloved family with deepest gratitude to all of them. At a time when life seemed to stop, my family always helped me to find a new direction and always stood behind me over all the years – finally helping me to reach this academic degree. My parents deserve the biggest thanks of all offering me an always welcoming home and endless loving support.



Für meine Familie

ABSTRACT

Membranes can be fabricated either from lipid or polymer molecules resulting in the formation of liposomes or polymersomes, respectively. Such self-assembled vesicles are cell-size membrane systems consisting of a microscopic hollow sphere, which exhibits a bilayer of amphiphilic molecules. Many of the polymersomal membrane properties are similar to their lipid analogues, whereby the thermal and mechanical stabilities are often higher. A simple mixing of phospholipids and synthetic block copolymers (BCPs) leads to the formation of hybrid vesicles. The issue of phase separation within these hybrid vesicle membranes plays a central role in creating structural features at the membrane surface, which can selectively interact with natural or synthetic macromolecules (*e.g.* proteins or synthetic nanoparticles).

This thesis investigates the formation of hybrid lipid/polymer vesicles composed of natural lipids (*e.g.* DPPC or DOPC) and synthesized polyisobutylene-*block*-poly(ethylene oxide) (PIB-*b*-PEO) copolymers, and provides details in understanding the effect of membrane incorporated BCPs on the lipid bilayer organization demonstrating *e.g.* the formation of laterally mixed or laterally phase separated vesicle morphologies. The biocompatible di- (PIB_n-*b*-PEO_m) and triblock copolymers (PEO_m-*b*-PIB_n-*b*-PEO_m) were prepared by a combination of living carbocationic polymerization (LCCP) with a Cu(I)-mediated 1,3-dipolar cycloaddition reaction (“click”-reaction) between azide-telechelic PIBs and alkyne-modified PEOs allowing to obtain well-defined BCPs with various block lengths ($n = 35 - 160$; $m = 12 - 48$).

Both types of membranes (liposomes or polymersomes) can undergo lateral phase separation processes, which especially in lipid membranes comply with their biological functions. So-called “lipid rafts” or domains are the consequence of the lateral phase separation within complex lipid mixtures, which can be induced by molecular effects such as length mismatches of the hydrophobic lipid chains and/or by interactions with cholesterol. Herein, it was possible to demonstrate the control of phase separation phenomena in hybrid membranes by simply varying the lipid/polymer composition and temperature. Confocal laser scanning microscopy (LSM) of hybrid vesicles was used to visualize the membrane morphologies either with common membrane dyes, fluorescently labeled BCPs or with a specific antibody, which recognizes the PEO-functionality of the PIB-PEO based BCPs. Control of phase separation in hybrid vesicle membranes further allowed the demonstration of the selective incorporation of hydrophobically modified nanoparticles into the polymer-rich domains. As a result, the formation of biocompatible hybrid vesicles with selectively incorporated nanoparticles can open up new perspectives in controlling physical and mechanical properties of membranes such as nanoporosity, permeability and stiffness to develop effective vesicle carriers.

KURZFASSUNG

Membranen können unter Bildung von Lipo- oder Polymersomen sowohl aus Lipidmolekülen als auch aus synthetischen Polymeren aufgebaut werden. Solche selbstassemblierten, vesikulären Strukturen sind Membransysteme in der Größenordnung von natürlichen Zellen, die, bestehend aus einer Doppelschicht amphiphiler Moleküle eine wässrige Phase einschließen. Die Membraneigenschaften von Polymersomen sind in vielerlei Hinsicht mit denen von Liposomen vergleichbar, jedoch zeichnen sich Polymersome durch deutlich höhere thermische und mechanische Stabilitäten aus. Das Mischen von Phospholipiden und synthetischen Blockcopolymeren führt zur Bildung von Hybridvesikeln, wobei der Aspekt der Phasenseparation eine zentrale Rolle zur gezielten Oberflächenmodellierung dieser Membranen spielt, welche selektive Wechselwirkungen mit natürlichen oder synthetischen Makromolekülen zulassen (z.B. mit Proteinen oder synthetischen Nanopartikeln).

Die vorliegende Arbeit untersucht die Bildung von gemischten Lipid/Polymer-Hybridvesikeln, die aus natürlichen Lipiden (z.B. DPPC oder DOPC) und selbsthergestellten Polyisobutylen-*Block*-Poly(ethylenoxid) (PIB-*b*-PEO) Copolymeren aufgebaut sind, und prüft Effekte der eingelagerten Polymere auf die Organisation der Lipidmembran. Die biokompatiblen Di- (PIB_n-*b*-PEO_m) und Triblockcopolymeren (PEO_m-*b*-PIB_n-*b*-PEO_m) wurden durch eine Kombination der lebenden carbokationischen Polymerisation mit der Cu(I)-vermittelten 1,3-dipolaren Zykoadditionsreaktion („Klick“-Reaktion) zwischen Azid-telechelen PIBs und Alkin-modifizierten PEOs erhalten, die es erlaubt klar definierte Copolymeren mit unterschiedlichen Blocklängen ($n = 35 - 160$; $m = 3 - 48$) herzustellen.

Beide Membransysteme (Lipo- oder Polymersome) können laterale Phasenseparationsprozesse aufzeigen, welche speziell im Fall der Lipidmembranen häufig im Zusammenhang mit ihrer biologischen Funktion stehen. „Lipid-Rafts“ – auch Domänen genannt – sind die Konsequenz lateraler Entmischungphänomene komplexer Lipidmischungen, die durch molekulare Effekte wie unterschiedliche hydrophobe Kettenlängen oder Wechselwirkungen mit Cholesterol hervorgerufen werden können. Hierzu zeigte sich, dass man das Mischungs-/Entmischungsverhalten von Lipid/Polymer-Hybridvesikeln durch das Variieren der Zusammensetzung sowie der Temperatur kontrollieren kann. Konfokale Laser-Scanning-Mikroskopie (LSM) erlaubte Phasenseparationsprozesse mit Hilfe von kommerziellen Membranfarbstoffen, fluoreszenzmarkierten Blockcopolymeren oder spezifischen Antikörpern, welche die PEO-Funktionalität des Blockcopolymeren erkennt und bindet, zu visualisieren. Die Kontrolle der Phasenseparation in den experimentell-erforschten Hybridvesikeln lässt außerdem Untersuchungen zum phasenselektiven Einbau von hydrophoben Nanopartikeln zu. Somit können die untersuchten, biokompatiblen Hybridvesikel mit selektiv eingelagerten Nanopartikeln als Modellsysteme betrachtet werden, die neue Perspektiven hinsichtlich der Kontrolle physikalischer und mechanischer Eigenschaften von Membranen (z.B. Nanoporosität, Permeabilität oder Steifigkeit) eröffnen, um effektive vesikuläre Transportsysteme zu entwickeln.

TABLE OF CONTENTS

ACKNOWLEDGEMENTS	iii
ABSTRACT	v
KURZFASSUNG	vi
I. INTRODUCTION	1
1. Amphiphiles and their self-assembly in aqueous solutions	1
2. Biomembranes and liposomes as model system	5
2.1 Liposome formation methods and properties	6
2.2 Lateral phase separation in liposomal membranes	9
3. Synthetic polymers, vesicle formation and their interaction with lipid bilayers	10
3.1 Polymersomes: membrane properties and preparation methods	12
3.2 Interaction of synthetic polymers with lipid membranes	14
3.3 Pore-formation abilities of synthetic polymers within lipid membranes	18
3.4 Lateral phase separation in polymersomal and hybrid lipid/polymer membranes	19
3.5 Application of lipid/polymer interactions	24
II. SCOPE OF THE THESIS	26
1. Objectives	26
2. Concept	27
III. RESULTS AND DISCUSSION	30
1. Hybrid lipid/polymer giant unilamellar vesicles: effects of incorporated bio-compatible PIB-PEO block copolymers on vesicle properties	31
2. Controlling molecular recognition with lipid/polymer domains in vesicle membranes	45

3. Lateral surface engineering of hybrid lipid/BCP vesicles and selective nano-particle embedding	52
IV. EXPERIMENTAL PART	63
1. Materials	63
2. Methods	63
3. Synthesis	65
3.1 Living carbocationic polymerization of IB and end group modification of telechelic PIBs	65
3.2 End group modification of telechelic PEOs	74
3.3 Azide/alkyne “Click”-reaction to generate PIB-PEO based BCPs	78
3.4 Fluorescent labeling of homo- and block copolymers	83
V. SUMMARY	90
VI. REFERENCES	98
VII. APPENDIX	107
VIII. CURRICULUM VITAE	135

Results of this dissertation have been published:

Parts of the introduction (**chapter I/ 3**) have been published in the review article: **Schulz, M.**; Olubummo, A.; *Binder, W. H., Beyond the lipid-bilayer: interaction of polymers and nanoparticles with membranes. *Soft Matter* **2012**, 8, (18), 4849-4864.

(<http://pubs.rsc.org/en/content/articlelanding/2012/sm/c2sm06999g>)

Text parts of chapter I/ 3.2 to 3.5 and Figures (Figure 8, 9 and 11) were adapted with permission from the Royal Society of Chemistry, copyright 2012.

The results and discussion part (**chapter III**) of this thesis is based on the published articles listed below.

Chapter III/ 1 is based on the published article: **Schulz, M.**; Glatte, D.; Meister, A.; Scholtysek, P.; Kerth, A.; Blume, A.; *Bacia, K.; *Binder, W. H., Hybrid lipid/polymer giant unilamellar vesicles: effects of incorporated biocompatible PIB-PEO block copolymers on vesicle properties. *Soft Matter* **2011**, 7, (18), 8100-8110.

(<http://pubs.rsc.org/en/content/articlelanding/2011/sm/c1sm05725a>)

Text and Figures were adapted with permission from the Royal Society of Chemistry, copyright 2011.

Chapter III/ 2 is based on the published article: **Schulz, M.**; Werner, S.; *Bacia, K.; *Binder, W. H., Controlling Molecular Recognition with Lipid/Polymer Domains in Vesicle Membranes. *Angew. Chem. Int. Ed.* **2013**, 52, (6), 1829-1833.

(<http://onlinelibrary.wiley.com/doi/10.1002/anie.201204959/abstract>)

Text and Figures were adapted with permission from John Wiley and Sons (*License number*: 3231351391335), copyright 2013.

Chapter III/ 3 is based on the accepted article: **Schulz, M.**; Olubummo, A.; Bacia, K.; *Binder, W. H., Lateral Surface Engineering of Hybrid Lipid/BCP Vesicles and Selective Nanoparticle Embedding. *Soft Matter*, **2013**, *Accepted Manuscript*. DOI: 10.1039/C3SM52040D

(<http://pubs.rsc.org/en/content/articlelanding/2013/sm/c3sm52040d>)

Text and Figures were adapted with permission from the Royal Society of Chemistry, copyright 2013.

I. INTRODUCTION

1. Amphiphiles and their self-assembly in aqueous solutions

The term “amphiphile” or “amphiphilic molecule” describes an organic compound that consists of both a hydrophilic head group part (polar) and a hydrophobic chain tail (non-polar), which can associate in aqueous solutions into a variety of supramolecular-ordered structures (*e.g.* micelles, vesicles or planar bilayers). Common amphiphiles are surfactants with one hydrocarbon chain or lipid molecules possessing two hydrocarbon chains. However, the hydrophobic/hydrophilic balance and the molecular geometry of the amphiphile determine which type of supramolecular-ordered structure is formed. In this context, Israelachvili *et al.* proposed a model for understanding the role of these structural aspects in forming different kinds of self-assembled structures.¹

The self-assembly of amphiphilic molecules into well-defined structures is driven primarily by the hydrophobic effect¹ in order to minimize the contact area between water molecules and the hydrophobic chain tails of the amphiphiles, which is extremely unfavorable. The hydrophilic interactions between the neighboring head groups undergo repulsive forces due to ionic and steric reasons. Thus, the formation of micelles or bilayer structures strongly depends on the molecular packing parameter (see **equation 1** and **figure 1A**) considering the geometrical shape of the amphiphile, which takes into account the optimal head group area (a_0), critical hydrophobic chain length (l_c) and the volume of the hydrophobic chain tail (v).¹

$$\text{packing parameter} = \frac{v}{a_0 * l_c} \quad \text{Equation (1)}$$

Consequently, the formation of spherical micelles² with a highly positive curvature was found for amphiphiles with a large ratio of the head group area to the hydrocarbon chain volume (*i.e.* $v/(a_0 * l_c) < 1/3$), as illustrated in **figure 1**. If the packing parameter is in the range of $1/3$ to $1/2$, the amphiphiles self-assemble into cylindrical micelles typical for single-chained lipids with small a_0 values.

The formation of planar bilayer structures requires small values of a_0 and large hydrocarbon chain volumes. This is demonstrated by so-called cylinder-shaped lipids³ exhibiting a characteristic molecule geometry which leads to an equalized ratio of the area occupied by the hydrophilic head group to the hydrophobic volume of the chain tail (*i.e.* $v/(a_0 * l_c) \approx 1$).¹

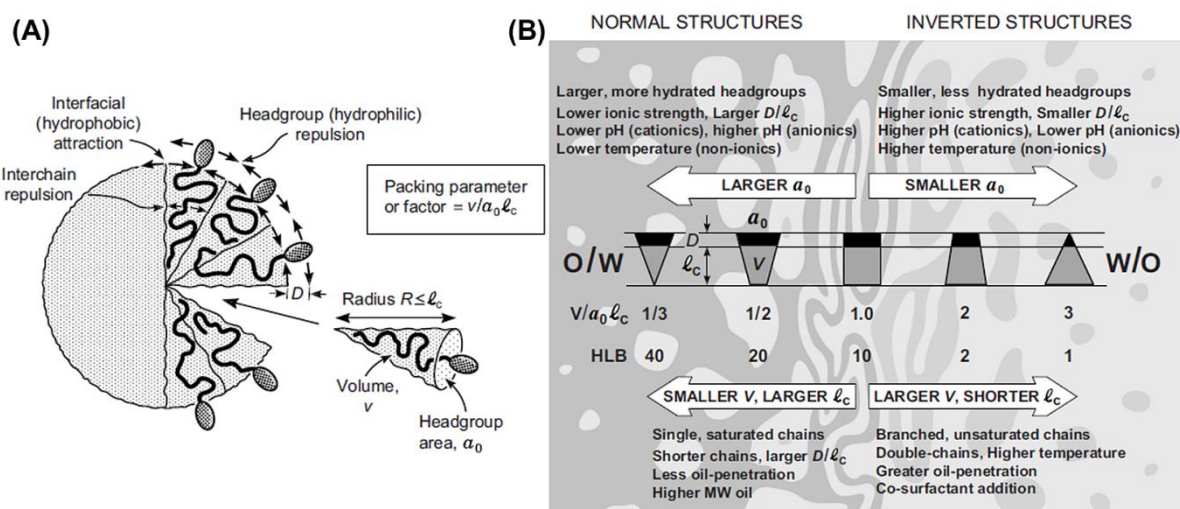
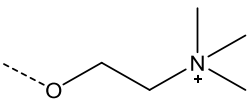
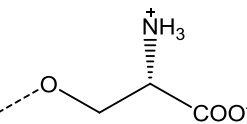
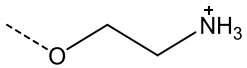


Figure 1. (A) Repulsive head group forces and attractive hydrophobic interfacial forces determine the optimum head group area a_0 . The chain volume v and chain length l_c set limits on how the fluid chains can pack together inside the aggregated structure. (B) The packing parameter $v/(a_0 \cdot l_c)$ and various forces between the head group region (black), hydrocarbon chain region (grey) and at the hydrocarbon-water interface between them together determine the preferred structure of the final aggregate.¹ Figure 1 and figure caption were taken from reference.¹

Flexible bilayers (*i.e.* vesicular structures) require double-chain lipids showing a packing parameter ($v/(a_0 \cdot l_c)$) in the range of 1/2 to 1 (see **figure 2**). As the bilayer edges are exposed to water, the open hydrophobic chain tails were self-closed by forming a curved bilayer structure (increase in lateral pressure) as a consequence of decreasing energetically unfavorable interactions between the lipophilic interior of the open bilayer and excess water.

Most of phospholipids are neutral or charged derivates from glycerol, which differ in their chemical properties and hydrophobic chain lengths of the attached fatty acid chains. Consequently, a variety of bilayer structures with different membrane properties (*e.g.* membrane fluidity, phase behavior or chain melting temperature) are well-known. The hydrophilic head group of phospholipids consists of a phosphate group, which in turn is linked to an amino alcohol compound (*e.g.* choline, ethanolamine or serine) representing the respective phospholipid classes.^{1, 4} The overall properties of self-assembled lipid bilayers (see **table 1**) depend mainly on the chemical structure (saturated or unsaturated hydrocarbon chains) and further on the chain length of the two attached fatty acid chains. Typical chain lengths of phospholipids vary between 14 and 24 carbon atoms.

Table 1. Properties of common phospholipids in modern membrane research (compare also basic chemical structure of the phospholipid in **figure 2B** with the substituent structure (R^1 , R^2 and X) given in **table 1**).

Lipid ^[1]	Degree of saturation	Fatty acid chains (R^1 , R^2)	Head group (X)	Molecular weight [g/mol]	T_m ^[2] [°C]
DLPC		$C_{11}H_{23}$		621.83	-2
DMPC	saturated	$C_{13}H_{27}$		677.93	24
DPPC	($R^1 = R^2$)	$C_{15}H_{31}$		734.04	41
DSPC		$C_{17}H_{35}$		790.15	55
DOPC	unsaturated ($R^1 = R^2$)	$C_{17}H_{33}-\Delta^9$ -cis	choline	786.11	-20
OPPC	unsaturated	$R^1: C_{17}H_{33}-\Delta^9$ -cis $R^2: C_{15}H_{31}$		760.08	-2
DSPS	saturated	$C_{17}H_{35}$		814.06	68
DPPS	($R^1 = R^2$)	$C_{15}H_{31}$		757.95	54
DOPS	unsaturated ($R^1 = R^2$)	$C_{17}H_{33}-\Delta^9$ -cis		810.03	-11
DPPE	saturated ($R^1 = R^2$)	$C_{15}H_{31}$		691.96	63
DOPE	unsaturated ($R^1 = R^2$)	$C_{17}H_{33}-\Delta^9$ -cis		ethanolamine	744.03

^[1] **DL:** 1,2-dilauroyl-; **DM:** 1,2-dimyristoyl-; **DP:** 1,2-dipalmitoyl-; **DS:** 1,2-distearoyl-; **DO:** 1,2-dioleoyl-; **OP:** 1-oleoyl-2-palmitoyl; **PC:** -glycero-3-phosphocholine (zwitterionic lipids); **PS:** -glycero-3-phospho-L-serine (anionic lipids) and **PE:** -glycero-3-phosphoethanolamine (zwitterionic lipids).

^[2] Chain melting temperature of the lipid.

Famous examples of chemical research and membrane studies are the saturated 1,2-dipalmitoyl-*sn*-glycero-3-phosphocholine (DPPC) with 16 carbon atoms and the unsaturated 1,2-dioleoyl-*sn*-glycero-3-phosphocholine (DOPC) with 18 carbon atoms of the hydrophobic acid chains. The self-assembled bilayer morphologies of these two lipid molecules (DPPC or DOPC) showed a completely diverse behavior.⁴ They differ strongly in their chain melting temperature (T_m) and lipid packing parameter forming at room temperature either gel phase (highly rigid) or fluid phase membranes, respectively for DPPC ($T_m = 41.6^\circ\text{C}$) or DOPC ($T_m = -20^\circ\text{C}$). The number of double bonds (*cis*-conformation) located in their hydrophobic chain segments prevent a close packing of the lipid molecules which increases the fluidity of the membrane by decreasing the melting temperature of the respective lipid.⁴ Among the variety of phospholipids, DPPC is one of the major components in biological membranes and showed among others increasing interest in membrane research over the last decades in studying

interaction of lipid bilayers with natural (*e.g.* proteins)⁵ or synthetic nanomaterials (*e.g.* block copolymer or nanoparticles) as reported by several reviews.⁶⁻⁹

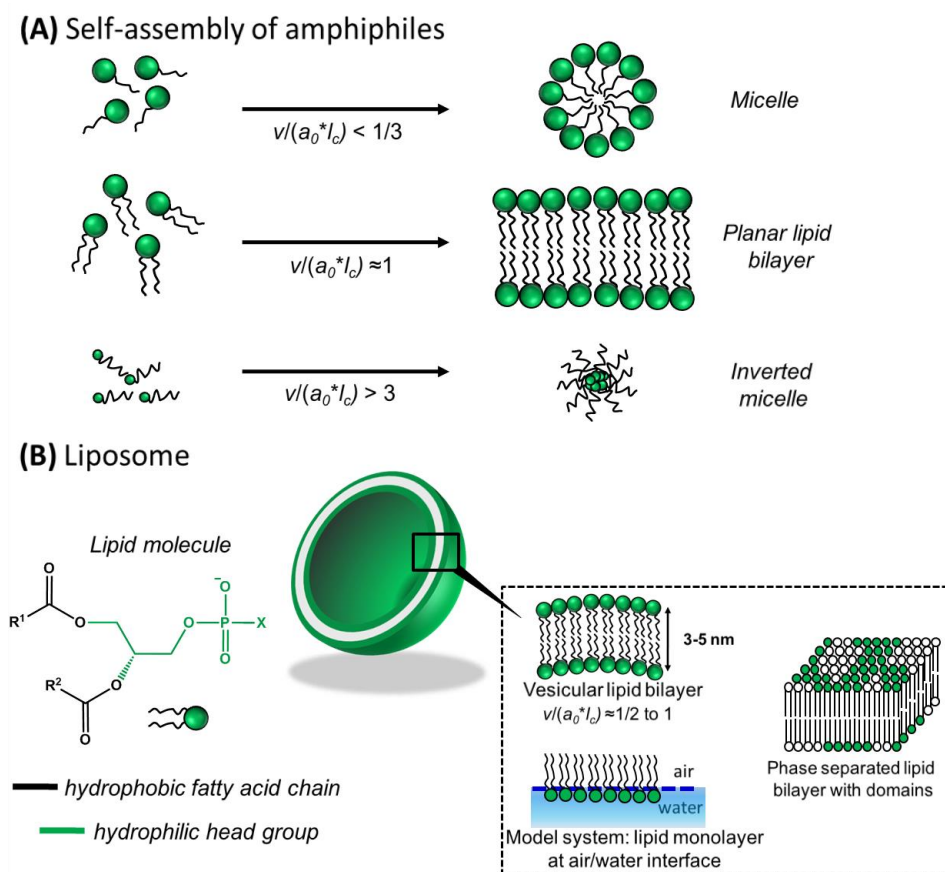


Figure 2. (A) Schematic representation of the amphiphile self assembling in terms of their characteristic packing parameter. (B) Shows the basic chemical structure of lipid molecules (see for R^1 , R^2 and X **table 1**) and their self assembly into vesicular bilayer membranes (*i.a.* the phase separated membrane and the lipid monolayer used as model systems).

Amphiphilic block copolymers (BCPs), the synthetic analogues to lipid molecules, have gained increasing interest in view of their self-assembling behavior in water forming as well supramolecular-ordered structures.¹⁰⁻¹⁴ As demonstrated for lipid and surfactant molecules, the self-assembly of polymer based amphiphiles (*i.e.* block copolymers) depends mainly on the molecular geometry and hydrophobic/hydrophilic balance of the amphiphile resulting in the formation of micellar, tubular or vesicular morphologies.¹² So-called polymersomes are self-assembled vesicles that feature, as same as liposomes, a membrane bilayer, which differentiates the hydrophilic properties inside the aqueous vesicle core from the hydrophobic properties within the bilayer interior.^{5, 11}

Summing up, the self-assembly of amphiphiles like natural lipids or synthetic block copolymer is mainly driven by the hydrophobic effect to prevent energetically unfavorable interactions between the hydrophobic molecule parts and excess water. The resulting (well-defined) supramolecular structure depends strongly on the molecular packing parameter of the amphiphilic compounds.¹⁵

2. Biomembranes and liposomes as model system

Biomembranes are complex assemblies of different type of lipid molecules, proteins and other biological constituents like sterols, glycolipids and enzymes.^{4, 5, 16} Such membranes have many complex functions *in vivo*. Depending on the biological purpose, each cellular membrane has a specific composition, properties and functions to perform. One of the major functions of certain membranes is to act as selective barrier by enabling permeability to ions and small molecules which allows a controlled exchange of the internal with the external cell milieu. In principle a biomembrane is composed of a single phospholipid bilayer in which many guest molecules can be embedded.^{5, 16} These compounds (*e.g.* transmembrane proteins, enzymes or cholesterol) can form channels through the membrane or they have distinct effects on the lipid bilayer organization and the resulting membrane properties. In particular, cholesterol as natural membrane constituent is known to influence the fluidity and permeability of lipid membranes.¹⁷⁻²¹ The specific molecular structure of a series of sterols has shown to promote demixing in lipid vesicles and further an influence on the curvature (positive or negative) of the formed liquid-ordered phases which demonstrates a decisive role in the vesicle budding behavior.^{17, 21}

The phospholipid bilayer²² is a well-defined structure of several thousands of lipid molecules driven by non-covalent lipid-lipid interactions such as *van der Waales*-, hydrophobic-, electrostatic interactions or hydrogen bonding. Singer and Nicolson¹⁶ reported the fluid mosaic model of biological membranes that describes such bilayer assembles as a homogeneous sea of lipids into which guest molecules, in particular proteins, are dispersed with the possibility to move freely around in their fluid lipid matrix. Nowadays, biomembranes are considered to consist of microdomains (so-called lipid rafts^{23, 24}) which differ in their lipid and protein composition from the surrounding membrane areas.³ These domains have further shown to play a fundamental role in cellular processes.^{23, 25-27}

However, the complexity of biological membranes in view of their compositions makes it difficult to study and understand specific effects of single membrane components or

interactions with proteins. Therefore, the membrane research has early focused on model membrane systems,^{4, 28-30} which are composed of few lipid components (binary or ternary lipid mixtures) or at least of one lipid component. So-called liposomes³¹ or lipid vesicles as a dynamic supramolecular structure that encapsulates a small amount of water are well-discussed model membrane systems in literature. These model biomembranes are nowadays used to investigate interaction with natural⁵ or synthetic macromolecules^{6, 7, 9} or in studying the lipid/lipid mixing behavior^{32, 33} and the resulting membrane properties to design effective vesicle carriers for drug-delivery application.

2.1 Liposome formation methods and properties

Liposomes are dynamic supramolecular structures spontaneously formed in aqueous solutions.³⁰ The term “liposome” is in general used for vesicles composed of natural occurring phospholipids with low molecular weights.³⁴ Compared to polymersomes, synthetic vesicles from amphiphilic block copolymers with molecular weights up to 100 kDa leading to dimensions of the molecular bilayer up to 50 nm, the liposomes exhibit a bilayer dimension of 3 to 5 nm.^{13, 35} The resulting membrane properties (*e.g.* the mechanical and thermal stability, bending elasticity or permeability) of vesicles composed of phospholipids are strongly restricted by the bilayer dimension. Whereas polymersomes show much higher mechanical and thermal stabilities^{11, 12} by offering the chance to tune the bilayer dimension by varying the molecular weight of the amphiphilic block copolymers.^{36, 37} Polymersomal membranes showed furthermore a more selective permeability towards polar moieties compared to phospholipid membranes.³⁸

Irrespective of the membrane composition, vesicles can be classified according to their size and lamellarity. Vesicles with diameters smaller than 100 nm are called small unilamellar vesicles (SUVs). The so-called large unilamellar vesicles (LUVs) exhibit a vesicle diameter in the range of about 100 to 1000 nm and the size range of most biological cells (1 to 100 μm) is represented by giant unilamellar vesicles (GUVs). These three different classes of vesicles consist of a single bilayer membrane, whereas multilamellar vesicles (MLVs) are composed of more than one bilayer often as a result of uncontrolled film hydration methods.³⁹

The sizes and lamellarity of vesicles depend mainly on the applied preparation method. Usually the formation of vesicles starts with dissolving the desired amphiphilic compound (*e.g.* lipid or block copolymer) in an appropriate organic solvent and furthermore the solution is used to produce a homogeneously thin film on a substrate (*e.g.* silica or conductive glass

surface).³⁹ Such film can be produced by evaporating the organic solvent with a stream of nitrogen or vacuum. Another possibility to produce a more homogeneously thin film is the spin coating approach. Afterwards, the hydration of the thin dry film (multilayer stacks of bilayers) is performed and the self-assembly of the amphiphiles proceeds. Whereby, the temperature during that hydration step should be above the melting temperature (T_m) of the highest melting component used in the mixture to ensure a successful vesicle formation, which requires curvature fluctuations (see **figure 3**, taken from the reference⁴¹) typical for the liquid-disordered state of the bilayers.^{40, 41}

Simple film hydration results in swelling of the multilayer stacks. Combined with simultaneous shaking or vortexing of the sample, most of the lipids will form MLVs and only few GUVs are obtained.^{29, 39} Once present as MLVs, it is not possible to convert these vesicles into GUVs because a peeling off of the onion-like structure of MLVs is energetically unfavorable.³⁹ Using sonication or freeze-thaw cycles MLVs can be converted into vesicles with diameters smaller than 50 nm (SUVs).²⁹ Furthermore, passing MLV suspensions through polycarbonate membranes with a defined pore size (extrusion) is the most popular method to produce LUVs having diameters of several hundred nanometer.^{29, 39}

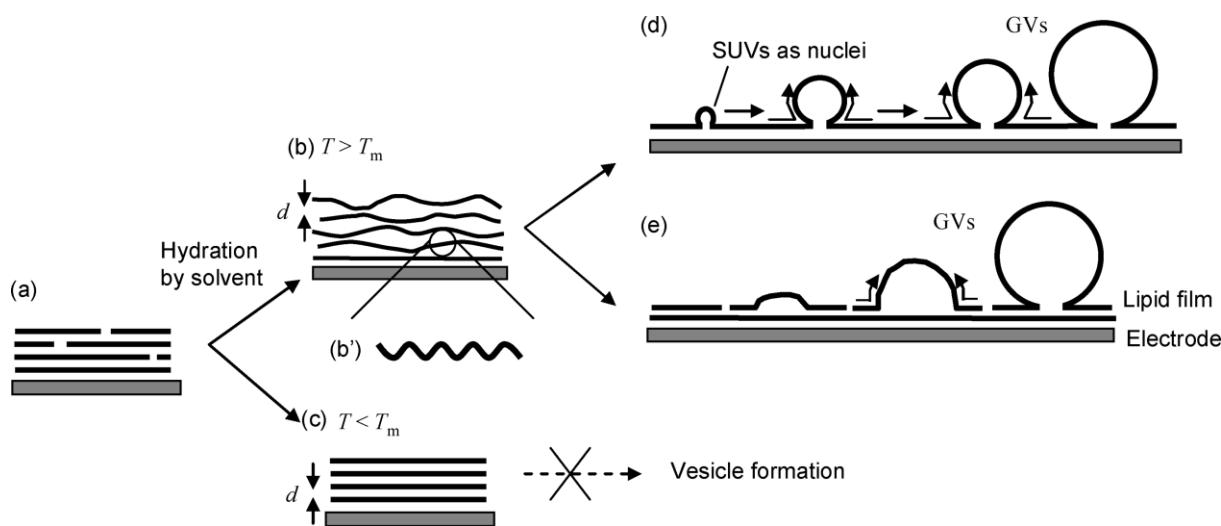


Figure 3. Schematic illustration of the possible mechanism of GUV formation by electroformation method: (a) multilayer stack of membranes before its hydration, (b) membrane multilayer stacks in presence of curvature fluctuations leading to an increase in the bilayer spacing, (b') curvature fluctuations of a free standing bilayer segment, (c) membrane multilayer stack in absence of curvature fluctuations, (d) *expansion model*: SUVs as nuclei resulted from the film hydration growing up to GUVs and (e) *swelling model*: the thin lipid film swelled to increase the curvature of the lipid film.⁴¹

Model (e) refers to the reports of Angelova and her coworkers.^{42, 43} Figure 3 and figure caption were taken from reference.⁴¹

Improvements of the lipid film hydration by applying an externally applied electric field during the swelling process (hydration step) has shown to produce homogenous GUV populations and is currently the most widely used method for preparing giant vesicles. This method is well-known as electroformation method and was originally reported by Angelova and Dimitrov in 1986.^{42, 43} Applying a low-voltage alternating electric field promotes the formation of truly unilamellar vesicles with diameters in the range of about 1 to 100 μm which show high stabilities for days, but the standard electroformation method will not be successful in forming GUVs containing too many charged lipids.³⁹ A further disadvantage of this method is that the electroformed vesicles remain connected to the residual lipid film on the used electrodes.³⁹

Recently, an approach demonstrated some modifications of the electroformation method using a suspension of SUVs and LUVs to deposit the lipids on the electrodes, which ensures a good macroscopic orientation and the control of the aqueous content of the membrane stacks resulting in high GUV formation rates.⁴⁴ Kinetic studies on the giant vesicle formation (*via* electroformation) have shown that the membrane fluidity of vesicles is dominant in the growth behavior of GUVs.⁴¹ Addition of cholesterol in low amounts further demonstrated the formation of small vesicles, whereas at high amounts the GUV formation was drastically inhibited as a consequence of the decrease in membrane permeability that is proportional to the fluidity of the membrane.

Another recently published approach demonstrated an efficient electroformation procedure to prepare supergiant unilamellar vesicles (diameter $> 100 \mu\text{m}$) containing cationic lipids.⁴⁵ Standard electroformation with indium tin oxide (ITO) coated glasses as electrodes showed difficulties in producing cationic GUVs. These difficulties were related to aging of the ITO-glass surfaces during their repeated use. It was demonstrated that mild annealing of the ITO-coated surface in presence of air ensures an efficient reproducible electroformation of supergiant cationic vesicles and prevents the effect of aging.⁴⁵

In addition to the already described preparation methods for liposomes, other methods are known which are not that widely used compared to the electroformation. For example microfluidic techniques allow the formation of defined water/oil (w/o) emulsions or w/o/w double emulsions which can be directly used to prepare giant unilamellar vesicles.³⁹ In this

case the used oil phase is a volatile organic solvent which is not miscible with water (*e.g.* chloroform). The advantage of this technique is that the obtained vesicles exhibit a monodisperse size and uniform shape. Giant vesicles can also be formed from lipids, which are dissolved in a water-miscible solvent. Vesicles were obtained by adding dropwise water to the stirred lipid solution, but this method is not fully explored and yielded only heterogeneous vesicle populations with an average size below 1 μm .³⁹

Due to the large size of giant unilamellar vesicles (1-100 μm), such model membrane systems allow the investigation of real time monitoring of morphological changes (*e.g.* adsorption and binding of proteins or domain formation processes) of individual vesicles by optical and laser scanning microscopy (LSM) techniques or by electron microscopy.⁴⁶⁻⁴⁹ If compared with the size of GUVs used to mimic and study artificial cell processes, the large unilamellar vesicles with a diameter of about 100 nm find applications as drug-delivery systems.³⁹

2.2 Lateral phase separation in liposomal membranes

Phase heterogeneities in the complexity of biomembranes are of functional importance and play a vital role in maintaining cellular functions. So-called “lipid rafts” or domains within lipid membranes are the consequence of lateral phase segregation of complex lipid mixtures (see **figure 4**), which have shown in model membrane studies that such morphological changes can be induced either by temperature,⁵ curvature effects⁵⁰ or by molecular effects such as chain length mismatches of the hydrophobic lipid tails,^{32, 33, 51, 52} by complexation with dications⁵³⁻⁵⁵ and/or by interactions with cholesterol^{21, 56} and sphingophospholipids (*e.g.* ternary mixtures of DOPC, sphingomyelin and cholesterol).⁵⁷

Interaction between proteins and lipid membranes for example the binding of the multivalent protein cholera toxin to receptor (ganglioside GM1) functionalized lipid vesicle membranes showed that crosslinking induced by the protein binding can lead to macroscopic domain formation (see **figure 4B/ III**).⁵⁸

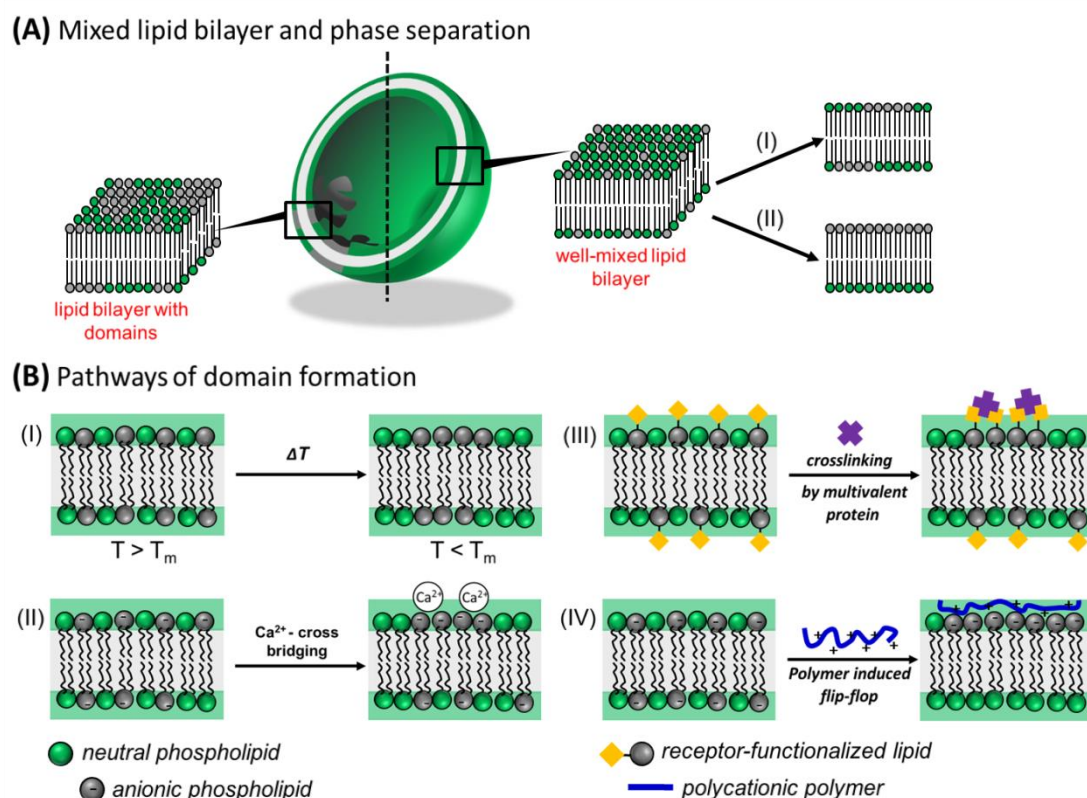


Figure 4. (A) Schematic representation of mixed and phase separated lipid bilayers demonstrating in (A/I) the lateral phase separation of lipid mixtures and in (A/II) the vertical phase separation process. In (B) the different pathways of phase separation (I to IV) in lipid membranes are shown.

Furthermore, interactions between model lipid bilayers and synthetic macromolecules indicated that polymers also promote lateral and/or vertical phase separation phenomena⁵ *e.g.* by flip-flop events between the inner and outer layer of the membrane, as illustrated in **figure 4B/ IV**.^{59, 60}

3. Synthetic polymers, vesicle formation and their interaction with lipid bilayers

Membranes can be fabricated either from lipid or polymer molecules resulting in the formation of lipo- or polymersomes, respectively.^{6, 13} Starting from the initial discovery of Kunitake^{61, 62} and Ringsdorf *et al.*⁶³ liposomes showed a victorious path along the scientific world, using them most widely as delivery systems in medicine for drug formulation or gene transport.

However, the significantly younger polymersomes have gained increasing interest due to significant expansion of their structural variability and chemical properties compared to

liposomes.^{12, 36, 37} In contrast to vesicles composed of lipids, polymersomes show remarkably higher stability and toughness, which offer the usage as robust carriers.^{35, 64}

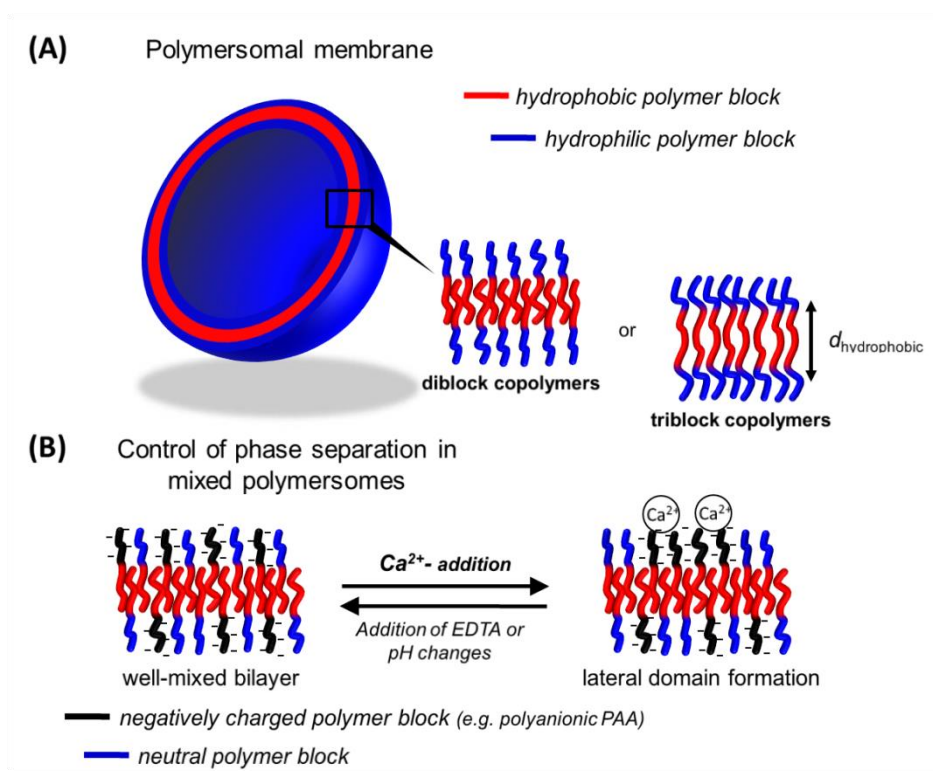


Figure 5. (A) Schematic representation of polymersomal membranes composed of di- or triblock copolymers. (B) Shows the concept of controlling phase separation in mixed polymersomes by addition of Ca^{2+} -ions (crosslinking of anionic BCPs) or removing the cross-linkage by complexation of Ca^{2+} with EDTA (ethylenediaminetetraacetic acid).

Based on the initial work of Discher and Eisenberg¹² a multitude of di- and triblock copolymers has been found up to now to self assemble into polymersomes,^{35, 65-68} opening the possibility to engineer membranes with increased stiffness (bending modulus),⁶⁹ variable thickness ($d_{\text{hydrophobic}}$ in the range of about 8 to 50 nm)⁷⁰ and highly variable chemical composition.^{35, 65} Moreover, in contrast to lipid vesicles, polymersomal membranes can be used to embed significant loads of (hydrophobic) nanoparticles (NPs),^{37, 71-75} even enabling their precise positioning in specific parts of the hydrophobic membrane.⁷⁶ Vesicles containing supramagnetic NPs in the hydrophobic membrane portion^{73, 77, 78} can release their loadings by applying an alternating magnetic field as result of a localized heating of the NPs.⁷⁹⁻⁸²

Nevertheless, many practical applications of polymersomes *e.g.* as delivery system with triggered release of their encapsulants require efficient preparation methods to produce monodisperse vesicles with a controllable size and composition in reproducible high amounts.

3.1 Polymersomes: membrane properties and preparation methods

Preparation techniques known from the formation of liposomes, such as standard film or bulk hydration or electroformation, can also be applied to generate polymersomes.^{13, 35, 39} While such methods provide vesicles which are not uniform in size sonication, freeze-thaw cycles or extrusion methods¹² were used, as same as for liposomes, to produce monodisperse vesicle populations. A disadvantage of such methods is the low encapsulation efficiency, which remains an important challenge to prepare vesicles with high loadings of active materials for delivery applications.

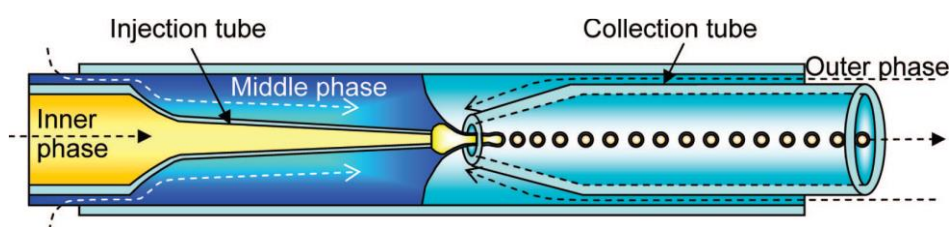


Figure 6. Schematic representation of a microcapillary geometry for generating double emulsion drops as templates for polymersomes. The geometry requires that the outer phase is immiscible with the middle phase, which is in turn immiscible with the inner phase. Both the injection and the collection tube are tapered from glass capillary tube (outer/ inner diameter of 1000/ 580 μm). Typical inner diameters for the injection tube are in the range of 10 to 50 μm .⁸³ Figure 6 and figure caption were taken from reference.⁸³

Herein, microfluidic techniques using capillary microfluidic devices (see **figure 6**),^{84, 85} which prepare w/o/w double emulsion drops as templates^{83, 86} have shown to be very efficient in controlling the size and structure of polymersomes demonstrating further high encapsulation efficiency compared to the commonly used preparation methods.^{78, 87} Weitz *et al.* one of the pioneers in developing such techniques for the formation of well-defined polymersomes, have demonstrated an efficient preparation of photo- and thermoresponsive polymersomes for triggered release by embedding gold NPs into the hydrophobic part of vesicles from a mixture of PEG-*b*-PLA and PNIPAM-*b*-PLGA block copolymers.⁷⁸

Crucial for the wide range of polymersome applications are the properties of the formed membrane. These properties reflect the chemical composition, block length ratio and the molecular weight of the utilized vesicle formers. Depending on the hydrophobic chain length (molecular weight) of the amphiphilic block copolymer, the membrane thickness can be

adjusted “step less” from ~8 to 50 nm with a significant increase in its stability. Critical for this process is the relation between the hydrophobic membrane thickness (d) and the molecular weight (M_w) of the polymer (see **equation 2** and **figure 5**),^{11, 70} whereas the hydrophilic part of the membrane often scales with $d_{hydrophilic} = M_w$.⁸⁸

$$d_{hydrophobic} = M_w^{0.55} \quad \text{Equation (2)}$$

In contrast to lipid membranes, where the overall physicochemistry (*e.g.* permeability, bending moduli or fluidity of components) is determined by the ~5 nm thick lipid bilayer, the membranes of polymersomes offer significantly more variability.

As illustrated in **figure 7**, polymersomes are much more stable and tougher than their lipid analogues and have shown in single-vesicle micromanipulation methods that they are highly deformable (high membrane elasticity) and could be aspirated into micrometer-sized pipettes^{11, 13} appearing comparable in quality to fluid-phase lipid membranes.

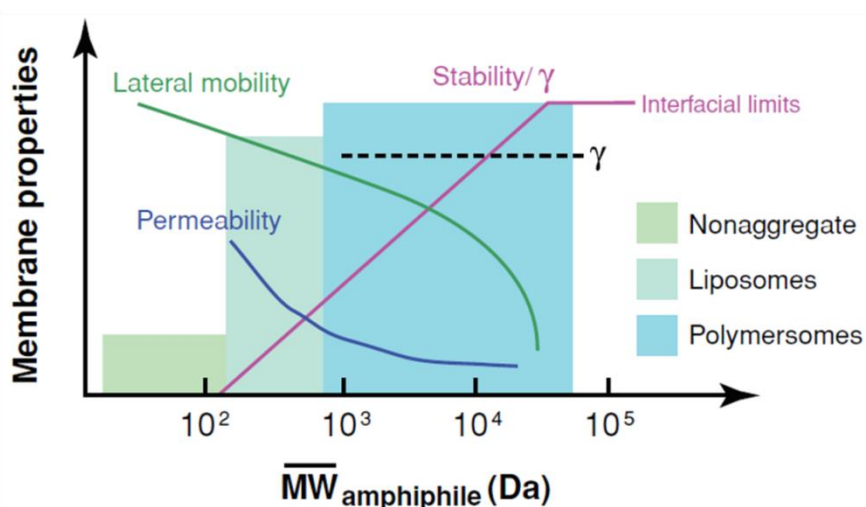


Figure 7. Schematic representation of physical membrane properties versus molecular weight of the corresponding vesicle formers.¹¹ Figure 7 was taken from reference.¹¹

Whereas lipid membranes were optimized by nature rather for fluidity than for stability, the robust polymersomal membranes demonstrate a significantly reduced lateral mobility and permeability with increasing the molecular weight of its polymer building blocks. Measurements of lateral diffusion coefficients and membrane viscosity showed that the fluidity of polymersomal membranes decrease most drastically when the chains are sufficiently long enough to result in chain entanglements.¹¹ Lastly, permeation of water

through membranes composed of synthetic block copolymers has found to be considerably reduced compared to liposomes.¹¹

The high stability and low fluidity of polymersomes combined with efficient preparation methods generating vesicles of controlled size offers applications as transport system, but the development of efficient release mechanism of such systems (target delivery) still remains as a challenge.

3.2 Interaction of synthetic polymers with lipid membranes

Biomembranes mainly act as a selective barrier that regulates the transport between the external and internal environment of the cell protecting against foreign substances.⁵ The incorporation of molecules, in particular synthetic macromolecules (such as polyelectrolytes,^{89, 90} amphiphilic BCPs⁹¹⁻⁹³ or dendrimers^{94, 95}) can drastically change the physiochemical properties of a specific membrane.

The advancing development in designing macromolecules with well-defined architectures and chemical composition, *e.g.* mimicking natural lipid structures, enables the study of selective interactions between synthetic polymers and model membrane systems. Over the years up to 2008 numerous studies reporting on interactions between synthetic polymers and model biomembranes were published.^{7, 9} Control of non-covalent interactions (*e.g.* hydrogen bonding, columbic association or hydrophobic interaction) between macromolecules and lipid membranes is affected primarily by the chemical structure and charge properties of the interaction pairs. When macromolecules interact with lipid membranes a large variety of effects could be observed as illustrated in **figure 8**. As illustrated in **figure 8B**, quite early⁹⁶ an adsorption model of cationic polymers was developed, which describes the ability of a surface bound polymer (polylysine) to induce lateral reorganization and segregation of single membrane components in mixed lipid bilayers (DPPC/DPPA). Recently, detailed studies on this topic have shown that such polycation/liposome complexes can lead to membrane fusion⁹⁷ depending on the conformation of the surface adsorbed polymer chains.

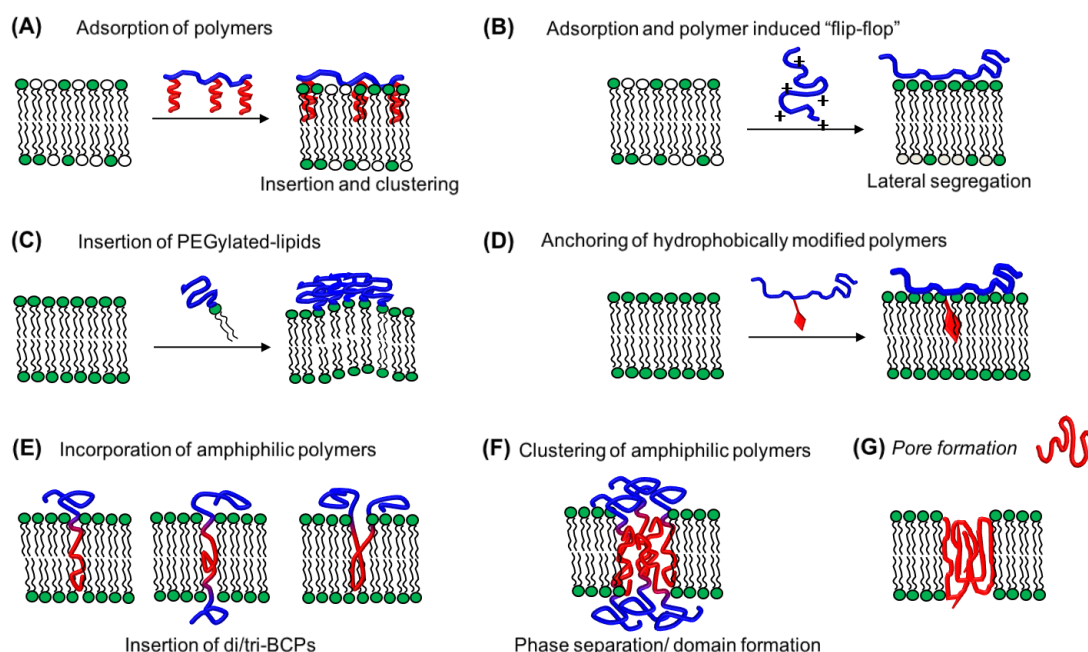


Figure 8. (A-G) Interaction pathways between synthetic polymers and lipid bilayers and their influence on membrane organization showing a large variety of effects dependent on the polymer type. Figure 8 and the corresponding caption were reproduced by permission from the Royal Society of Chemistry (see publication: Schulz *et al.*, *Soft Matter* **2012**, 8, (18), 4849-4864).

Herein, the formed polylysine corona was found to be thin enough to induce membrane fusion by the decrease of electrostatic rejection between similar charged lipid vesicles allowing interliposomal contact and exchange. Polymer anchoring onto lipid bilayers (see **figure 8D**) *via* hydrophobic modifications of their backbone as discussed early⁹⁸ is nowadays an appropriate strategy to reach an effective binding between water-soluble polymers and lipid membranes.⁹⁹ Interestingly, a temperature induced thermo-reversible collapse of liposomal anchored polymer chains (LCST) was found early to induce vesicle budding or transient pore formation suggesting that the hydrophobic side chains of the polymer remains incorporated during the process.¹⁰⁰

A particular area of interest is coulombic association between charged polymers and lipid membranes. In comparison to nonionic polymers, a deep incorporation of charged polymers into the hydrophobic membrane interior is strongly restricted. Instead, the external binding of charged polymers onto liposomal surfaces (**figure 8B**) is driven by electrostatic interactions between the charged polymer units and oppositely charged lipid head groups, forming a polymeric corona on top of the liposome surface.⁶⁰ Most of the recent interaction studies have been performed with positively charged polymers and negatively charged liposomal

surfaces.^{7, 101-103} Few examples describe *pH*-depending interactions between zwitterionic liposome surfaces and positively charged polymers^{90, 104} or anionic polyelectrolytes.^{104, 105} The adsorption of polymeric molecules onto the hydrophilic corona of liposomes can lead to strong effects on the membrane organization.

The binding of cationic polymers to lipid membrane surfaces have shown irreversible rearrangement effects on the lipid bilayer organization leading further to membrane disruption.^{106, 107} Moreover, surface bound cationic polymers are able to promote migration of lipid molecules in one of the liposomal layers (segregation) or between the inner and outer layer (“flip-flop”).^{60, 108} Furthermore, it has been demonstrated that the ability of charged polymers to neutralize the charge state of liposomal surfaces leads to effective polymer/liposome complexation and could end in interliposomal polymer migration⁵⁹ or vesicular membrane fusion by reducing the interliposomal repulsion.⁹⁷ The effect of salt concentration on the adsorption behavior of polyelectrolytes onto lipid membranes was shown by several research groups.^{59, 90, 105} The high sensitivity of formed polymer/liposome complexes against salt addition was demonstrated by interactions between cationic polyethylenimine (PEI) and zwitterionic DMPC vesicles as a function of salt concentration (NaCl).⁹⁰ At low salt concentration aggregation of the polymer/liposome complexes (vesicle aggregation) was observed, whereas at high salt concentrations the aggregation was prevented, concomitant with drastic changes in the DMPC chain melting transition of the hydrocarbon tails, which suggests a strong penetration ability of PEI molecules into the lipid bilayer at high salt concentrations.

Deep penetration of polymers into the hydrophobic membrane interior (see **figure 8E** and **8F**) is primarily driven by hydrophobic interactions typical for neutral polymers. Recently, modern research is concentrated on the penetration ability of amphiphilic block copolymers into lipid mono-¹⁰⁹⁻¹¹² and bilayer systems.^{60, 91, 113, 114} Nonionic block copolymers (BCPs), such as pluronics or poloxamers (PEO-*b*-PPO-*b*-PEO) have been studied extensively, revealing the main parameters governing the interaction between lipid membranes and such amphiphilic polymers.⁹³ Experimental results compared to simulations proved that the hydrophilic/hydrophobic balance and the overall hydrophobicity of the triblock copolymers affect drastically the polymer incorporation into lipid monolayers. Thus, the incorporation activity of poloxamers was found to correlate with its solubility in the subphase (water), as with increasing hydrophobic block lengths the solubility of the BCP decreases and interactions with the lipid alkyl-chains are much stronger resulting in higher squeeze-out

pressures. An early experimental proof showed the temperature dependent association between the poloxamer F-68 (PEO₇₆-PPO₂₉-PEO₇₆) and DPPC monolayer.¹¹¹ An increase in temperature leads to a higher squeeze-out pressures of the triblock copolymer chains from the lipid film as a consequence of the decrease in the closed packing of the lipid molecules at higher temperatures. Herein, it was further demonstrated that the lipid packing density can regulate the poloxamer insertion into lipid monolayers showing distinct effect on the lipid film morphology.¹⁰⁹

Langmuir balance technique coupled with spectroscopic methods such as IRRAS (Infrared Reflection Absorption Spectroscopy) can give a more detailed view on the molecular organization of the interacting components in a mixed monolayer.^{110, 112, 115} IRRAS analysis of mixed monolayers from perdeuterated lipids (DPPC-*d*₆₂) and amphiphilic triblock copolymers (PGMA₁₄-*b*-PPO₃₄-*b*-PGMA₁₄) has shown that the insertion of these amphiphilic polymers into the lipid film leads to mesoscopically to nanoscopically dimensioned lipid cluster surrounded by a polymer network.¹¹⁵

It has been found that the interaction strength between amphiphilic triblock copolymers and lipid membranes strongly depends on the hydrophobicity of the polymer, which can further show membrane solubilization effects.¹¹⁴ Additional experiments proved the effect of temperature on the incorporation ability of poloxamers into lipid bilayers.^{91, 116} Based on isothermal titration calorimetry (ITC) experiments it was shown that pluronic molecules (P388) were incorporated into fluid-phase DMPC liposomes above their main phase transition temperature ($T_m = 24^\circ\text{C}$), whereas gel-phase membranes of DMPC (below T_m) prevent the polymer incorporation.⁹¹

In contrast to amphiphilic polymers, reports on the interaction between dendritic polymers and model biomembranes describing their nature and localization are rather rare.^{94, 117, 118} The importance of such interactions is related to the structure of dendrimers, which exhibit a well-defined highly branched architecture with numerous functional groups on their surface suitable for pharmaceutical applications. Recently, it was reported that the dendrimers strongly interact with the polar head group region of the lipid bilayer, where the polymer incorporation leads to a rearrangement of the lipid hydrogen bonding network.⁹⁴ A deep penetration of the dendritic molecules into the hydrophobic membrane interior is strongly limited due to the polar structure of their hyperbranched polymers.

In comparison to nonionic dendrimers, interaction studies of cationic dendrimers with lipid membranes showed the electrostatic origin of their nature.^{95, 119} Association of cationic

phosphorus dendrimers with negatively charged liposomal surfaces proved strong dendrimer/lipid interactions *via* electrostatic forces which resulted in fluidity changes of the lipid bilayer.⁹⁵

3.3 Pore-formation abilities of synthetic polymers within lipid membranes

An overview of various factors important for the formation of channels and pores in lipid membranes induced by synthetic polymers, including the chemical composition and polymer architecture is given in several reviews.^{7, 9} A relationship between the polymer architecture and the pore formation pathway was extensively described in the literature,⁹ as illustrated in **figure 9A**.

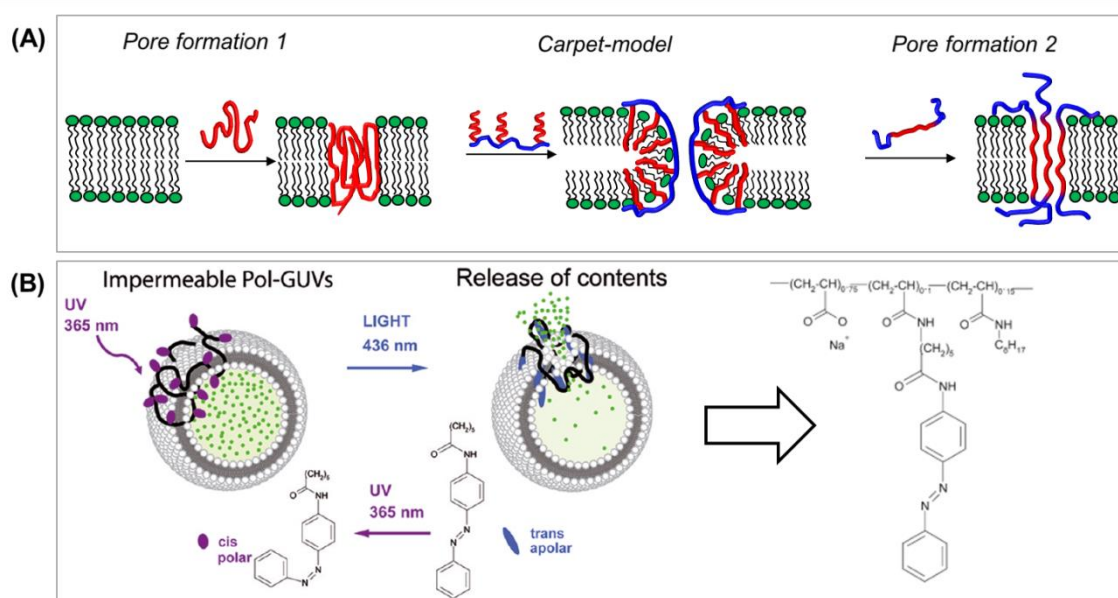


Figure 9. Different pathways of polymer-induced pore-formation into lipid bilayer membranes. Pore formation by full insertion of a polyelectrolyte (pore formation 1), by insertion of an amphiphilic graft copolymer (carpet model) and by incorporation of amphiphilic triblock copolymers (pore formation 2). (B) Illustration of light-induced membrane permeabilization by *cis/trans* photoconversion of modified copolymer chains. The polymer-loaded GUVs maintained impermeable, when irradiated under UV light (436 nm) they become permeable and release their internal content – reprinted with permission from ref.¹²⁰, copy right 2010, American Chemical Society. Figure 9 and the corresponding caption were reproduced by permission from the Royal Society of Chemistry (see publication: Schulz *et al.*, *Soft Matter* **2012**, 8, (18), 4849-4864).

Recently, scientific interest has been concentrated on liposomal release of encapsulated materials from the vesicle interior through the lipid bilayer by controlled breakup mechanisms,

which allows the control of membrane permeability. Accordingly, the group of Tribet¹²⁰ showed for the first time triggered permeabilization of lipid membranes induced by external light irradiation. They found that azobenzene-modified poly(acrylic acid) copolymers embedded into DOPC GUVs can induce membrane perturbation by *cis-trans* photoconversion (see **figure 9B**). The biological relevance of this system was shown in cell culture studies stressing the remarkable influence on the membrane properties under mild conditions. Previous investigations proved nonspecific permeability of lipid bilayers induced by hydrophobically modified poly(acrylic acids).¹²¹ These amphiphilic copolymers can undergo channel-formation in vesicular lipid membranes depending on the polymer concentration. Furthermore, fluorescence microscopy studies of liposomal release confirmed nanometer sized polymer channels (channel radii of 1 to 5 nm) with the ability of transmembrane exchange of small molecules (*e.g.* of albumin and dextran molecules).

3.4 Lateral phase separation in polymersomal and hybrid lipid/polymer membranes

Lateral phase separation phenomena in lipid bilayers with micrometer-sized domains have been extensively studied and reported to be generally induced by a mismatch of the acyl chain length between the lipid components and/or by interactions with cholesterol.

In contrast to this, vesicles composed of block copolymers can display either horizontal or lateral phase separation phenomena caused by the immiscibility of their different polymer building blocks^{122, 123} or by action of cations (*e.g.* Ca^{2+} induced domain formation *via* crosslinking of anionic BCPs in mixture with neutral polymers, see **figure 10** and concept in **figure 5**).^{10, 124}

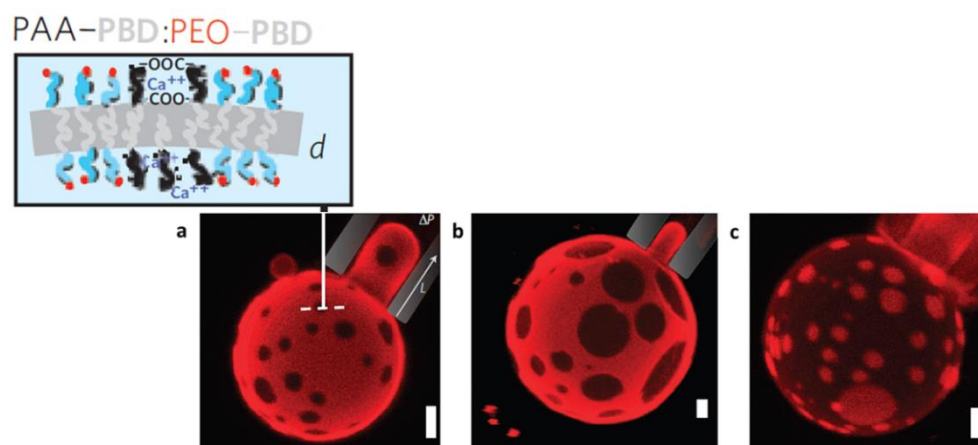


Figure 10. Spotted polymersomes imaged by z-sectioning confocal microscopy during aspiration in micropipettes. (a-c) Cation-induced lateral phase separation of vesicles composed of a charged PAA₇₅-*b*-PBD₁₀₃ BCP and a neutral, fluorescently labeled PEO₈₀-*b*-PBD₁₂₅ BCP, which were formed at *pH* of

4 and 0.1 mM Ca^{2+} -concentration by varying the membrane composition (a) 25 %, (b) 50% and (c) 75% of the charged polymer. The inset in (a) shows a schematic representation of the phase-separated membrane induced by Ca^{2+} -cross-bridging of the anionic polymers. Scale bars: 2 μm . Figure 10 and figure caption were taken from reference.¹⁰

Battaglia and his coworkers¹²² demonstrated that the surface topology of polymersomes at the nanoscale could be controlled by the confined polymer/polymer phase separation as a result of the variation of their membrane compositions. The observed domain shapes (*via* confocal laser scanning and electron microscopy) were reported to appear similar at the micro- and nanolength scales, with dimensions that are linearly proportional to the vesicle diameter. Remarkably, further investigations assessing the rate of polymersome uptake by cells (endocytosis efficiency) as a function of their domain morphology and size have shown that vesicles composed of PEO-*b*-PDPA and PMPC-*b*-PDPA copolymers with small domains (mixtures with molar ratios of 25/75 or 75/25) have considerably higher endocytosis efficiencies as compared to vesicles with large domains (typical for 50/50 mixtures of both BCPs) and to the pure one component polymersomes. Whereas the size of polymersomes seemed to have no effect on how fast such vesicles enter cell populations, but it showed a noteworthy effect on the number of internalized polymersomes per cell.

Another recent study, investigated the dynamics of domain formation and remixing kinetics in spotted polymersomes from mixtures of polyanionic and neutral amphiphiles in the presence of Ca^{2+} -ions (see also **figure 5B** in chapter I/ 3).¹²⁴ It was noted that addition of the calcium chelating agent EDTA (ethylenediaminetetraacetic acid) to phase separated vesicles led to a significant decrease of the domain size within minutes, whereas increasing the *pH* with addition of NaOH showed a viscous fingering of domains and a decrease in domain size within hours (total mixing within days). The large differences in mixing kinetics upon EDTA and NaOH stimuli were proposed to be the result of different disruption mechanisms of the calcium cross-bridging that induces the lateral phase separation within the polymersomal membrane.

Hybrid lipid/polymer membranes are a new class of artificial membranes, which combine the excellent biocompatibility of liposomes with enhanced thermal- and mechanical stabilities of polymersomal membranes.⁶ Such hybrid bilayer types are very young in biochemical/chemical membrane research and have gained enormously increasing interest in the last years. As a result of blending natural occurring phospholipids with synthetic block copolymers,

hybrid lipid/polymer membranes showed also the formation of phase separated membrane morphologies.¹²⁵⁻¹³⁰

In 2005, investigations and considerations concerning the formation of hybrid lipid/polymer vesicles were reported for the first time.¹²⁵ The obtained hybrid vesicles were prepared from mixtures of a synthetic poly(2-methyloxazoline)-*block*-poly(dimethylsiloxane)-*block*-poly(2-methyloxazoline) (PMOXA-*b*-PDMS-*b*-PMOXA) triblock copolymer with egg phosphatidylethanolamine or DPPC. Based on fluorescence quenching experiments a homogeneous lipid distribution (lipid contents smaller than 20 mol%) in the polymer matrix were suggested. No detailed analysis and information of membrane morphologies were performed. Several years later in 2011 two different groups of Vanderlick¹²⁹ and Binder¹²⁸ actually opened this new membrane platform by studying the formation of hybrid lipid/polymer vesicles depending on their compositions. As consequence, they were able to successfully demonstrate membrane heterogeneities either induced by an external stimulus¹²⁹ or by the immiscibility of both membrane components.^{127, 128} Confocal fluorescence microscopy studies proved that it is possible to incorporate high amounts of a non-biocompatible block copolymer (PBd₄₆-*b*-PEO₃₀) into a liposomal membrane (POPC).¹²⁹ The resulting mixed vesicles were prepared by an electroformation method starting from a dry mixed lipid/polymer film. Further investigations concerning the mixing behavior, demonstrated that phase heterogeneities induced by protein binding (Neutravidin) to either biotinylated lipids or block copolymers leads to domain formations. Such strong clustering effects (domain formation) are justified by the fact that one Neutravidin molecule binds to 4 biotin-labeled molecules.

Phase separation phenomena based on the immiscibility of both membrane components, observed by simply varying the lipid/polymer mixing ratio, was demonstrated by our group for the first time.¹²⁸ The incorporation of PIB-PEO based biocompatible polymers into vesicular DPPC membranes varying further their hydrophobicity showed remarkable effects on the lipid bilayer organization (*e.g.* flattening of holes and phase borders or formation of domains).

Similar to bilayer membranes, Langmuir monolayers can serve as a model membrane system to study phase separation phenomena between synthetic polymers and lipids at the air/water interface. Herein, the first report¹³⁰ on mixed lipid/polymer monolayers demonstrated morphological changes in binary mixed monolayers from a lipid (DPPC or

DOPC) and an amphiphilic PMOXA₆₅-*b*-PDMS₁₆₅-*b*-PMOXA₆₅ triblock copolymer *via* a combination of Langmuir film studies and Brewster Angle Microscopy (BAM).

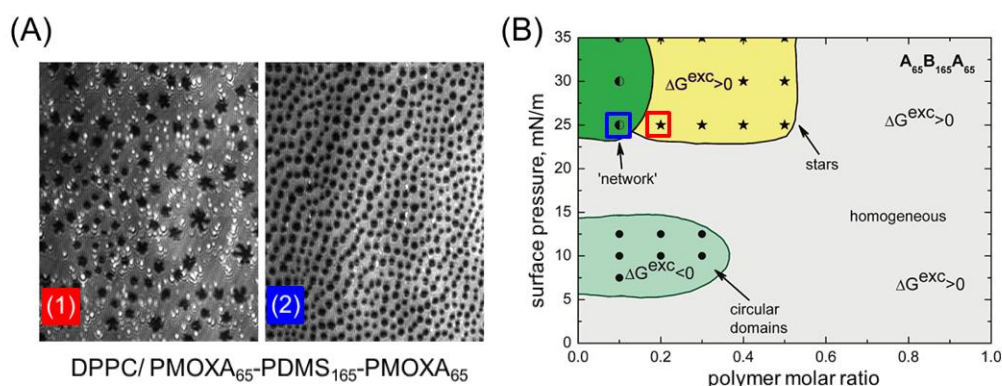


Figure 11. (A) Brewster angle microscopy images of mixed monolayers from A-B-A triblock copolymer and DPPC at 25 mN/m (image width 220 μ m). (1) Mixed film obtained from a polymer to lipid ratio of 0.2 to 0.8 and (2) 0.1 to 0.9. (B) Schematic phase diagram (surface pressure versus mixture composition) obtained for the binary system of PMOXA₆₅-*b*-PDMS₁₆₅-*b*-PMOXA₆₅ and DPPC, illustrating the observations of phase heterogeneities in the mixed monolayers – reprinted with permission from ref.¹³⁰, copyright 2009, American Chemical Society. Figure 11 and the corresponding caption were reproduced by permission from the Royal Society of Chemistry (see publication: Schulz *et al.*, *Soft Matter* **2012**, 8, (18), 4849-4864).

Depending on the lipid/polymer composition it was found that saturated lipid monolayers (DPPC), forming rigid films at room temperature with a high lipid packing density, are much more sensitive to the presence of amphiphilic copolymers showing phase separation phenomena (see **figure 11A**) as compared to mixed monolayers from unsaturated lipid and BCP molecules. In particular the formation of pure lipid domains (DPPC) at high compression states of the mixed film was observed (star-shaped domains at $\pi = 25$ mN/m, compare **figure 11A/ 1** and **11B** red square). In contrast, monolayers composed of DOPC (unsaturated lipid) with specific polymer contents showed only in the low pressure region a tendency to phase separate, whereas at higher surface pressures a homogenous film was observed. Additional visualization techniques monitoring mixed lipid/polymer film morphologies were displayed by studying phase separation phenomena at the air/water interface between fluorescent thermo-responsive block copolymers (RhB-labeled PDMA₂₀₇-*b*-PDEA₁₇₇) and DPPG *via* a laser scanning microscopy technique combined with BAM and AFM (Atomic Force Microscopy).¹³¹ Such combined method allowed a relationship between the observed film morphology and the polymer induced changes by selectively monitoring the

fluorescently labeled polymer molecules. Thus, it has been shown that the BCP molecules (below their LCST) were incorporated into the expanded phase of the lipid film forming mixed domains, whereas an increase in surface pressure (during compression of the mixed film) led to polymer chain expulsion from the lipid monolayer.

Similar to domain-formation in lipid membranes, the structure of the lateral surface of phase separated polymersomes and hybrid lipid/polymer mono- and bilayers is important for future applications, therefore requiring tools to engineer the lateral phase separation process. Such control of demixing of lipid-rich domains from polymer-rich phases in vesicle membranes is provided by thermally driven phase-separation and/or inclusion of cholesterol.¹²⁶ Herein, the control of domain size and shape was achieved by varying the cooling rate (see **figure 12**) and membrane composition, respectively.

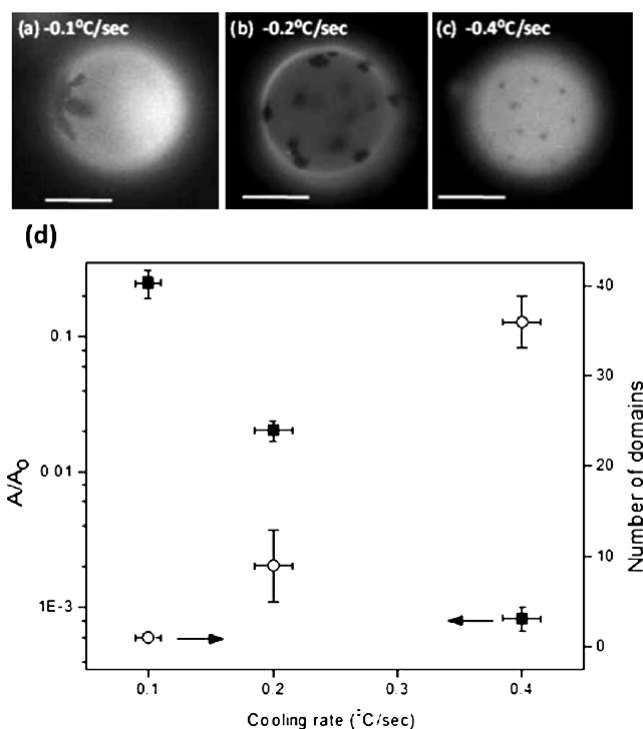


Figure 12. Impact of cooling kinetics. (a-c) Epifluorescence microscopy images of hybrid lipid/polymer vesicles composed of a PBd-*b*-PEO BCP and DPPC (molar ratio of 60/40). Vesicles were prepared at different cooling rates showing an increase in domain size with lowering the cooling rate (a-c). Scale bar represents 10 μm . (d) Number and apparent fraction of individual domains (A/A_0) against cooling rate; A is the apparent area of individual domains and A_0 is the total area of observable membrane.¹²⁶ Figure 12 and figure caption were taken from reference.¹²⁶

The potential fine-tuning of polymersomal and hybrid lipid/BCP membrane morphologies combined with the selective localization of functional nanoparticles^{76, 132} can open up new

perspectives in controlling physical and mechanical properties of the membrane such as nanoporosity, domain structure and stiffness to develop effective vesicle carriers.

3.5 Application of lipid/polymer interactions

Depending on the chemical structure and composition of synthetic polymers, different kinds of interactions and effects on lipid membranes can be expected. For example, polymer adsorption onto cell membranes can be optimized considering surface modifications in cell transplants or life time of polymer/liposome delivery systems. Herein, blood circulation times of liposomal delivery systems *in vivo* are one of the most important points in pharmaceutical and medical applications. The basic concept behind is based on sterical stabilization of the liposome surface by polymers to avoid binding of other molecules. For this purpose synthetically prepared poly(ethylene glycol) (PEG) was shown to be an excellent polymeric shielding device for liposomes, forming a covalently linked hydrophilic corona, which increases blood circulation times¹³³⁻¹³⁵ caused by the fact that PEG-covered liposomes become invisible to macrophages of the blood circulating system. Similar to the efficient PEG long circulation properties *in vivo*, poly(2-oxazoline)-grafted liposomes¹³⁶ have demonstrated comparable results suggesting that this effect is species-independent. In view of cell surface modifications, it was reported that a series of synthetic polymers adsorbed or covalently bound to mammalian cells showed strong differences in the life time of the polymer/cell complex depending on the type of polymer.⁹² Fluorescence microscopy studies with labeled polymers revealed that the investigated polymers were gradually excluded from the cell surface (most of all within 24 hours).

Cationic polymers are currently used as effective antimicrobial agent due to the ability of disrupting cell membranes, otherwise the mechanism of their biocidal activity is poorly understood. In general it has been found that the cationic group structure of polymers is an important factor in the control of membrane activities (*e.g.* binding, destabilization or membrane porosity) promising applications in fields of gene-delivery¹³⁷ or antimicrobial agents.¹³⁸ Thus, the group of Kuroda¹³⁸ has proposed a potential application of poly(methacrylamides) as surface coatings that kill bacteria in case of contact due to the fact that these cationic copolymers selectively disrupt bilayer membranes preventing *e.g.* biofouling processes.

Interaction between polyelectrolytes and model bacteria cell membranes were performed to understand the structural basis of the biocidal activity of these cationic polymers.¹⁰⁶ Herein,

poly(phenylene ethynylene) (PPE)-based polymers with pendant quaternary ammonium groups have shown to be promising candidates for antimicrobial action due to their possibility to disrupt cell membranes. The findings propose that PPE based polyelectrolytes associate with lipid membranes and become incorporated into the hydrophobic membrane interior leading in strong membrane disorganization.

The key element for membrane disrupting by PPE-based polymers was proposed by the chemical structure of the interacting side chain, which was further proved by recent investigations based on a series of cationic phenylene ethynylene oligomers and polymers differing mainly in their chemical side chain structures.¹³⁹ Fluorescence leakage experiments indicated that specific oligomers and polymers showed selective interaction with the high ability to disrupt bacterial cell membrane analogous.

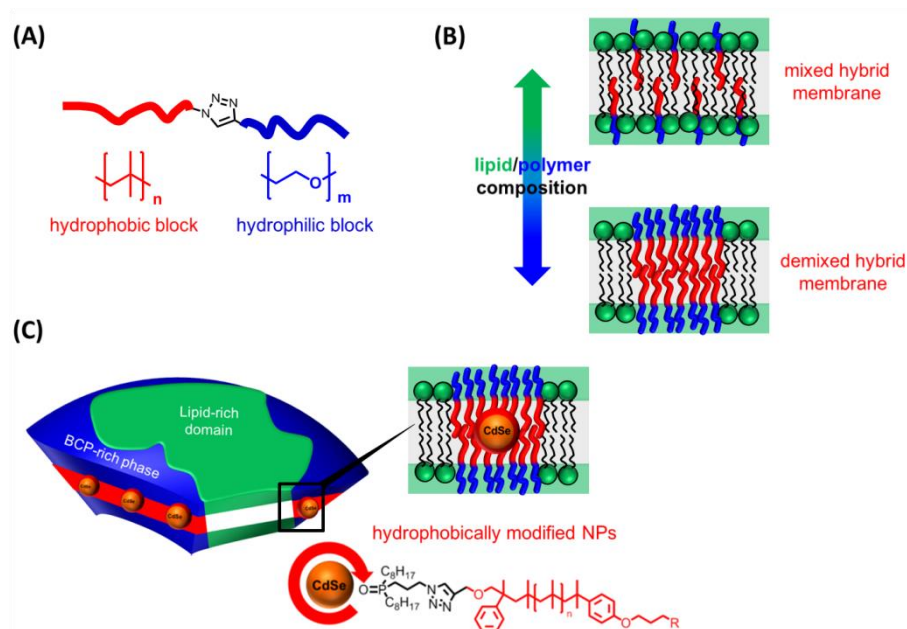
The central point in understanding antimicrobial activity of cationic polymers is the polymer induced membrane disruption. Here, it was found that cationic copolymers with primary amine groups exhibit stronger membrane interactions with higher disrupting abilities than compared to their tertiary or quaternary ammonium counterparts.⁸⁹ The high disrupting activity of primary amine groups against lipid membranes was found to be a result of their enhanced complexation with the phosphate groups of the phospholipids *via* a combination of hydrogen bonds and electrostatic interactions.⁸⁹

II. SCOPE OF THE THESIS

1. Objectives

The main objective of this thesis is to develop a hybrid lipid/polymer membrane system combining the benefits of lipo- and polymersomal membranes.

Therefore, the first objective of this thesis is to prepare amphiphilic di- and triblock copolymers based on polyisobutylene as hydrophobic block and poly(ethylene oxide) as corresponding hydrophilic block segment (see **scheme 1A**). The synthetic pathway will be applied to generate a series of different amphiphilic BCPs varying in their hydrophobic/hydrophilic chain length ratio and furthermore in their BCP architecture.



Scheme 1. Schematic representation of (A) amphiphilic BCP, (B) mixed and demixed hybrid lipid/polymer membrane and (C) phase selective incorporation of hydrophobic nanoparticles into hybrid bilayers.

Subsequently, the formation of hybrid lipid/polymer membranes by blending natural occurring phospholipids with different amphiphilic PIB-PEO based block copolymers in order to understand the effect of such synthetic polymers on lipid membranes is the main objective of this thesis. The self-assembling process of such binary mixtures varying the lipid/polymer composition (**scheme 1B**) should result in the formation of either lateral mixed or demixed bilayer structures. Finally, the concept of phase separated membrane morphologies will be used to demonstrate phase selective interactions of these hybrid membranes with natural (*e.g.* proteins) or synthetic macromolecules (*e.g.* nanoparticles), as illustrated in **scheme 1C**.

2. Concept

The living carbocationic polymerization (LCCP) of isobutylene using two different monovalent initiators (2-chloro-2,4,4-trimethyl-pentane (TMPCl) **2** or α -methylstyrene epoxide (MSE) **4**)¹⁴⁰⁻¹⁴² was applied to generate well-defined chain end functionalized polyisobutylenes, as illustrated in **figure 13**. To realize the covalent connection between the hydrophobic and hydrophilic polymer blocks, chain end modification followed by azide/alkyne “click”-reaction according to literature^{141, 143-145} (see **figure 13A**) were used to prepare different amphiphilic block copolymer structures (compounds **24a-f** or **27a-d**).

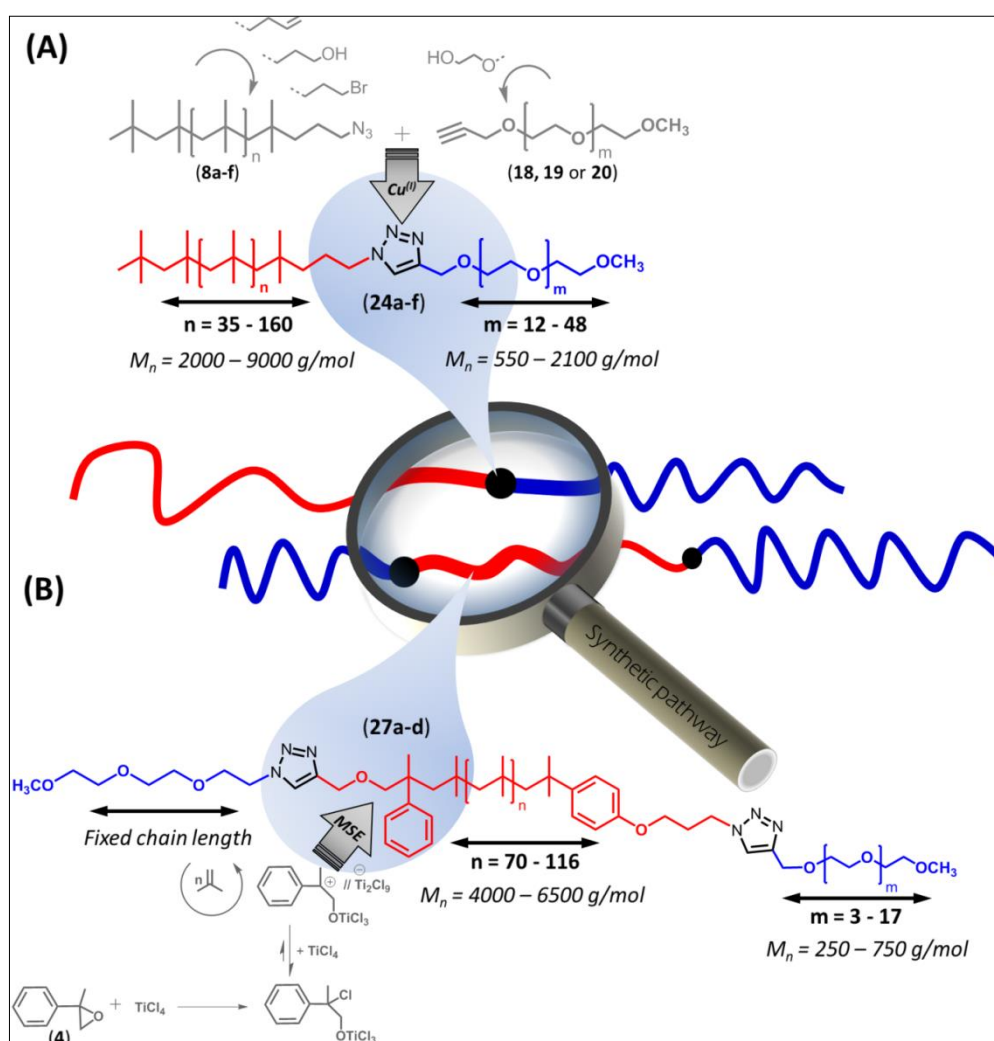


Figure 13. Synthetic concept of the preparation of amphiphilic di- and tri-BCPs varying their chain length ratio and architecture. (A) Shows the azide/alkyne “click”-reaction pathway to covalent connect the hydrophobic (PIB) with the hydrophilic block (PEO) and (B) depicts the structure of nonsymmetric tri-BCPs (**27a-d**) based on PIB and PEO. Using MSE/TiCl₄ as initiator system for the LCCP of isobutylene it is possible to generate an α,ω -telechelic PIB allowing further to attach separately different PEO blocks on each end.

While the electroformation method^{39, 43} has shown to be very efficient in generating vesicles (polymer- and liposomes) with micrometer sizes feasible to study their membrane morphologies by confocal laser scanning microscopy (cLSM), a modified method based on this approach was optimized to study the preparation of electroformed hybrid lipid/polymer vesicles composed of synthesized PIB-PEO based BCPs and phospholipids (see **figure 14**) and to evaluate the influence of the membrane incorporated BCPs on lipid bilayer organization.

In this sense, the *Results and Discussion* part of this thesis is divided into three chapters based on three different publications. The first publication (“*Hybrid lipid/polymer giant unilamellar vesicles: effects of incorporated biocompatible PIB-PEO block copolymers on vesicle properties*” – *Soft Matter* **2011**, 7, 8100-8110; see **1st chapter** of results and discussion), describes the successful formation of hybrid GUVs composed of the natural phospholipid DPPC and two different PIB-PEO based di-BCPs (**24c** and **24e**) showing significant differences in the lipid/polymer mixing behavior and in the formation of completely closed hybrid membrane morphologies.

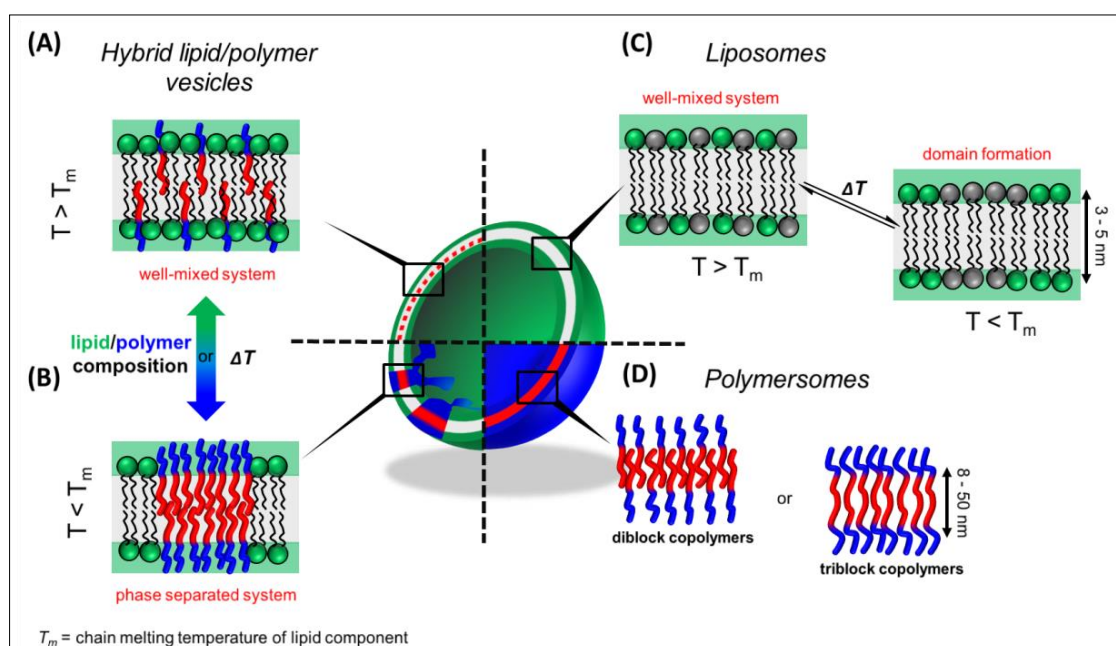


Figure 14. (A and B) Schematic concept of the formation of hybrid vesicles showing different membrane morphologies (well-mixed or phase separated state) as a consequence of varying the temperature and/or the lipid/polymer composition. (C) Concept of liposomal membranes and formation of phase separated morphologies induced by temperature changes. (D) Polymersomes formed by self-assembly of amphiphilic di- and triblock copolymers, which in contrast to liposomes exhibit a significant higher membrane thickness.

To study the biocompatibility of such hybrid membranes and the effect of their membrane composition and morphology (mixed and demixed phase state) in biological recognition processes, the binding of the protein cholera toxin to ganglioside GM1 (glycosphingolipid) functionalized hybrid membranes was another challenge and is described in the second publication (“*Controlling Molecular Recognition with Lipid/Polymer Domains in Vesicle Membranes*” – *Angew. Chem. Int. Ed.* **2013**, 52, 1829-1833; see **2nd chapter** of results and discussion).

According to literature,^{125, 129, 130} membrane heterogeneities can be induced and controlled by variation of the membrane composition and/or temperature. For this purpose, the use of fluorescently labeled BCPs and commonly used membrane dyes (*e.g.* DiDC18^{28, 56} or Rh-DHPE¹⁴⁶) was chosen to selectively prove the presence of either lipid- or polymer-rich domains in phase separated vesicles from DPPC and amphiphilic polymers (**24e**). The initial mixed bilayers (at temperatures above T_m of DPPC) undergo phase separation upon cooling to room temperature¹²⁶ induced by passing the lipid chain melting transition temperature (T_m) (see **figure 14A** and **B**), which results into the formation of polymer-rich phases and rigid DPPC domains (gel-state of the bilayer) – that also constitutes an important aspect of the present work (see also **2nd chapter** of results and discussion). Such control of the membrane phase state by temperature and membrane composition allows further investigation on selective interactions of specific hybrid bilayer parts with functional nanomaterials (*e.g.* synthetic nanomaterials). A defined surface chemistry of nanoparticles has shown to be an efficient strategy to control the localization of particles within the central portion of polymersomal membranes.⁷⁶

The third publication (“*Lateral surface engineering of hybrid lipid/BCP vesicles and selective nanoparticle embedding*” – *Soft Matter* **2013**, *Accepted Manuscript*. DOI: 10.1039/C3SM52040D; see **3rd chapter** of results and discussion), investigates the selective embedding of hydrophobically modified nanoparticles based on CdSe into the polymer-rich phases of demixed hybrid vesicles. For this purpose, a new approach to identify hybrid lipid/polymer membrane heterogeneities was developed. Herein, the BCP molecules were visualized with a specific antibody, which recognizes selectively the PEO functionality of the PIB-PEO BCPs, to clearly identify their position in the lipid bilayer proving further the phase selective incorporation of PIB-modified CdSe NPs into phase separated hybrid membranes.

III. RESULTS AND DISCUSSION

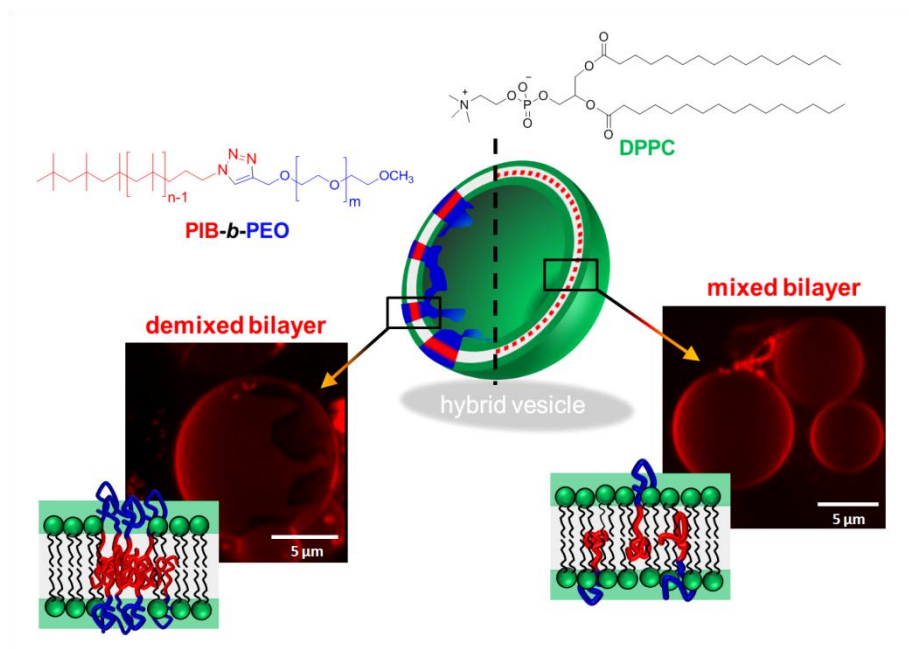
The following chapters of *Results and Discussion* are based on the publications listed below (chapter 1 to 3 based on publication 1 to 3, respectively). The first chapter demonstrates the formation of hybrid lipid/polymer vesicles and examines the mixing/demixing behavior of their membrane constituents. To understand the observed phase separation phenomena in order to address specific receptor/ligand interactions or furthermore the phase selective incorporation of nanoparticles, different methods based on LSM (such as partitioning behavior of common membrane dyes, fluorescent labeling of BCPs or bio-inspired recognition of BCPs by an antibody) were applied to assign the lipid- and polymer-rich domains in phase separated hybrid vesicles, which will be discussed in chapter 2 and 3.

1) Schulz, M.; Glatte, D.; Meister, A.; Scholtysek, P.; Kerth, A.; Blume, A.; *Bacia, K.; *Binder, W. H., Hybrid lipid/polymer giant unilamellar vesicles: effects of incorporated biocompatible PIB-PEO block copolymers on vesicle properties. *Soft Matter* **2011**, 7, (18), 8100-8110.

2) Schulz, M.; Werner, S.; *Bacia, K.; *Binder, W. H., Controlling Molecular Recognition with Lipid/Polymer Domains in Vesicle Membranes. *Angew. Chem. Int. Ed.* **2013**, 52, (6), 1829-1833.

3) Schulz, M.; Olubummo, A.; Bacia, K.; *Binder, W. H., Lateral Surface Engineering of Hybrid Lipid/BCP Vesicles and Selective Nanoparticle Embedding. *Soft Matter*, **2013**, *Accepted Manuscript*. DOI: 10.1039/C3SM52040D.

1. Hybrid lipid/polymer giant unilamellar vesicles: effects of incorporated biocompatible PIB-PEO block copolymers on vesicle properties



ABSTRACT: Self-assembly of lipids and block copolymers into mixed giant unilamellar vesicles (GUVs) and the underlying phase-behavior are reported, based on the well-known assembly of natural lipids and synthetic di- and triblock copolymers in dilute solutions. In this publication the formation of mixed vesicles containing DPPC (1,2-dipalmitoyl-*sn*-glycero-3-phosphocholine) and newly prepared PIB-PEO diblock copolymers (BCP) was investigated via confocal laser scanning microscopy and Langmuir films. Polyisobutylene (PIB) and poly(ethylene oxide) (PEO) are highly biocompatible polymers and their incorporation into DPPC vesicles therefore leads to interesting structural modifications upon the formation of hybrid GUVs. Results of the confocal microscopy studies prove the mixing/demixing behavior of lipid and polymer molecules in the corresponding bilayer membranes. In particular a homogeneously mixed phase below 20 mol% and above 30 mol% of PIB₈₇-*b*-PEO₁₇, but also the formation of demixed phases of DPPC with 20 to 28 mol% of BCP were observed. Lipid/polymer interactions in mixed monolayers were further investigated by Langmuir balance techniques coupled with fluorescence microscopy. It is shown that the typical behavior of DPPC monolayers at the air/water interface is strongly disturbed by the presence of the diblock copolymers, further proving phase separation.

INTRODUCTION

Membranes in living cells require complex mixtures of a multitude of lipids to control essential properties such as fluidity, mechanical stability and the function and spatial organization of membrane proteins.¹ As the physical properties of most lipids are restricted by their chemical structure (in most cases fabricated from glycerol/sphingosine and fatty acids),^{2,3} significant effort has been placed in the generation of artificial cell membranes made from polymers, in particular amphiphilic block copolymers. Based on the initial work of Discher and Eisenberg⁴ a multitude of di- and triblock copolymers has been found to assemble into polymersomes, opening the possibility to engineer membranes with increased stiffness (bending modulus),⁵ variable thickness (ranging from now 10 to 40 nanometres)⁶ and – most importantly –

highly variable chemical composition,⁷ which in turn may show effects of lateral segregation⁸ or induce significant volume changes.⁹ Thus membranes with entirely new properties can be designed, allowing to introduce complex patterns of hydrophilicity,¹⁰ supramolecular entities,^{11, 12} fluorescent moieties¹³ or the incorporation of enzymes.¹⁴ Moreover, in contrast to lipid vesicles, polymersomal membranes can be used to embed significant loads of (hydrophobic) nanoparticles,^{15–19} even enabling their precise positioning in specific parts of the hydrophobic membrane.²⁰ As lipids and polymers differ significantly in their size, interaction energies and also mixing behavior,^{1, 21–23} the composition of membranes built from both of them will reflect the delicate balance already known if only small amounts of an amphiphilic polymer are mixed with an excess of lipid. Thus amphiphilic polymers can incorporate into membranes and strongly influence

transport properties, stability, curvature and they furthermore can induce the formation of channels in the respective lipid membrane.^{24–26} Polyelectrolytes can induce clustering or even flip/flops of lipids in a mixture of charged/neutral lipids, inducing domain-formation.^{27, 28} Up to now only few reports however have been dealing with direct mixtures between amphiphilic (block) copolymers and biological phospholipids within a bilayer membrane. Meier et al.²⁹ have investigated the formation of mixed lipid/polymer-vesicles by studying a triblock copolymer (ABA, poly(oxazoline-polydimethylsiloxane-polyoxazoline)) *via* film-rehydration, ethanol-injection and detergent-removal methods. Based on rhodamine-quenching experiments, a homogeneous distribution of the polymer (~79 mol%) in the giant liposome within a residual sea of lipids was proposed. Matching results were obtained from Langmuir film measurements with the same lipids in mixture, providing first hints that phase separation might occur at specific concentrations of a polymer in the lipid monolayer.^{30, 31} A recent example³² reports a (non-biocompatible) PBD-PEO polymer in mixture with a fluid-phase forming DOPC-lipid demonstrating the phase-homogeneity of the mixture on the surface of the generated giant vesicles in all compositions. Phase separation is only induced when a strong avidin/biotin interaction of biotin-modified polymers caused a clustering of the polymers, subsequently leading to domain formation. In the present work we demonstrate the formation of mixed vesicles (hybrid giant unilamellar vesicles) providing a study of the polymer/lipid mixing/demixing behavior on the vesicle surface *via* confocal laser scanning microscopy. These hybrid giant unilamellar vesicles (GUVs) are composed of a highly biocompatible PIB-PEO diblock copolymer (BCP) and DPPC as a low mobility lipid forming rigid gel-phase membranes. Furthermore, we compare the confocal laser microscopy results with Langmuir film investigations of mixed monolayers of corresponding compositions. Our study relies on synthetically prepared PIB-PEO block copolymers (PIB-PEO BCP) made by a combination of living polymerization and subsequent click-chemistry,³³ enabling us to control the structural influence of diblock copolymers differing in their hydrophobic/hydrophilic balance incorporated into lipid bilayer membranes. In contrast to previous reports,^{32, 34} the synthetic approach allows the fabrication of amphiphilic BCPs with a wide range of structural features, such as chain length variation and changes in the block composition. Based on our investigations, detailed pictures of structural changes in self-assembled DPPC mono- and bilayer architectures induced by incorporated amphiphilic block copolymers could be developed.

RESULTS AND DISCUSSION

1. Preparation of amphiphilic block copolymers

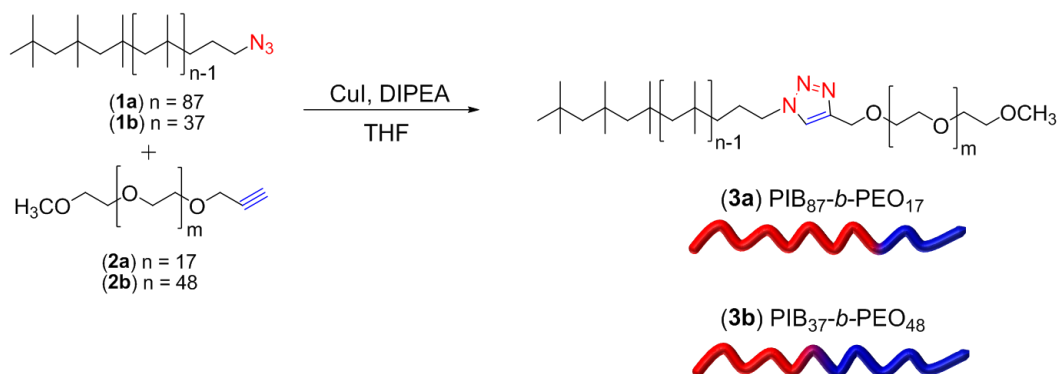
The amphiphilic nature of synthetic PIB-PEO diblock copolymers used in this study enables the preparation of polymersomes *via* a self-assembly process as recently reported¹⁵ by our group. This established behavior of PIB-PEO BCPs forming bilayer membranes with remarkably higher stiffness and stability in contrast to pure liposomes led us to develop a hybrid model system, which allows tuning of the membrane properties. The general approach starts with the synthesis of amphiphilic diblock copolymers varying in their block compositions. Polyisobutylene was chosen as the hydrophobic block, because of its highly flexible chain behavior and excellent biocompatibility, which is in strong contrast to the commonly used PBD-PEO BCPs, where the biocompatibility of the PBD-block is not provided. The preparative strategy relies on the high-yielding azide/alkyne click-reaction to attach covalently hydrophilic PEO chains (**2a**, **2b**) to the hydrophobic PIB (**1a**, **1b**) polymers^{15, 33, 35} (see Scheme 1), resulting in the final polyamphiphilic structure. Telechelic polyisobutylenes bearing azide chain ends (**1a**, **1b**)^{36, 37} and alkyne-telechelic poly(ethylene oxide) (**2a**, **2b**)^{15, 38} had to be prepared referring to well-known literature procedures *via* living polymerization methods, yielding polymers with well-defined molar masses and low polydispersity. The subsequent azide/alkyne click-reaction between azido-telechelic PIB (**1a**, **1b**) and alkyne-telechelic PEO (**2a**, **2b**) was carried out using copper (I) iodide and DIPEA (*N,N*-diisopropylethylamine) as catalyst resulting in quantitative conversions. Results of the final analysis *via* GPC and NMR spectroscopy of the amphiphilic BCPs used in this study are illustrated in Table 1, indicating well-defined structures with respect to molecular weight (M_n) and block composition. Both blocks (PEO and PIB) display glass transition temperatures significantly below room temperature ($T_g(\text{PIB}) = -78^\circ\text{C}$; $T_m(\text{PEO}) = -5^\circ\text{C}$), therefore indicating fully mobile (not glassy) polymer chains.

2. Formation of mixed vesicles (hybrid GUVs)

DPPC-liposomes and hybrid GUVs composed of a binary mixture of DPPC and amphiphilic BCPs were prepared by a modified electroformation method.^{39, 40} The electroformation technique, which uses an alternating low voltage electrical field during the rehydration process of a thin film, was chosen because it promotes the formation of truly unilamellar and particularly large vesicles as illustrated in Fig. 1. DPPC was chosen as the lipid as on one hand stabilities of the resulting GUVs are high, and as on the other hand the difference between the thermal properties, together with the low mobility of the DPPC in comparison with the BCPs nurtured expectations of strong effects within the formed hybrid GUVs. Electroformation of all mixtures was performed at 70°C , *i.e.* above the main transition temperature of DPPC ($T_m = 41.6^\circ\text{C}$) and the T_g/T_m temperatures of PIB and PEO,

which is necessary for the formation of GUVs from pure DPPC and enables lateral mixing of lipid and polymer molecules in hybrid vesicles. All confocal microscopy

images in this study were acquired at room temperature, where liposomes from pure DPPC form a gel phase.



Scheme 1. Synthetic pathway of amphiphilic block copolymers using azide/alkyne-click-chemistry.

To study the mixing/demixing behavior of DPPC and PIB-PEO BCPs in vesicle membranes, different molar mixtures between lipids and the polymers were prepared and subsequently used to form hybrid giant unilamellar vesicles (hybrid GUVs), assuming that the initial mixing ratio of DPPC and polymer in the preparation of the chloroform mixtures represents the GUV composition. However, it cannot be excluded that the observed vesicle populations can differ slightly in their membrane

composition.⁴¹ Structural changes of pure DPPC-liposomes to hybrid GUVs were monitored by confocal laser scanning microscopy (LSM). Here we found that the morphology of the DPPC-liposomes – shape and surface structure – is significantly affected by the incorporation of the amphiphilic polymers, both dependent on the initial mixing ratio and the block composition of the used polyamphiphiles.

Table 1. Experimental data of the prepared diblock copolymers achieved *via* ¹H-NMR and GPC analysis.

polymer	Block composition	$\Phi_{\text{PIB}}^{(c)}$	GPC-results			¹ H-NMR-results
			$M_n^{(a)}$	$M_w^{(b)}$	PDI	$M_n^{(a)}$
3a	PIB ₈₇ -PEO ₁₇	0.84	5350	6580	1.2	5900
3b	PIB ₃₇ -PEO ₄₈	0.44	3970	4930	1.2	4460

^(a) Number average molar mass in g/mol.

^(b) Weight average molar mass in g/mol.

^(c) Volume fraction of PIB-block in the block copolymer.

2.1. Structural modifications at various mixing ratios – confocal microscopy.

First, we optimized the GUV-formation process using pure DPPC and studied the resulting giant liposome characteristics. For visualization of the formed liposomes and further hybrid GUVs, a lipophilic fluorescence dye (DiDC18, see Experimental section) was used. We found that DPPC-GUVs exhibited a deformed morphology with a characteristic hole-defect as shown in Fig. 2. Dark areas were confirmed to be holes by the addition of a water soluble dye, which freely entered these GUVs (data not shown). Upon cooling to room temperature, DPPC bilayers are expected to form a gel phase which is

confirmed by the characteristic multifaceted structure (see Fig. 2B) known for small vesicles.⁴² The size of the observed DPPC-GUVs was in the range of 20 to 50 nm. As described in the literature^{43, 44} the distortion of GUVs made from DPPC under formation of multifaceted structures is observed either under conditions of electroporation or upon addition of low molecular weight alcohols due to a real expansion and thus induction of wrinkles. As neither of our conditions are comparable to electroporation nor added alcohols were used in our GUV-preparations, we clearly assign the observed multifaceted structure to stress induced by the gel phase of the DPPC. In order to exclude the formation of pure polymerosomes, we also tried the preparation of polymer vesicles using the

same conditions as used for all preparations of liposomes and hybrid vesicles (1.3 V/10 Hz and 70°C). However, under these conditions the formation of polymersomes could not be observed, considering the resolution limit of the confocal microscopy. In contrast to pure DPPC-liposomes, GUVs from mixtures of lipids and polymers (30 mol% of **3a**) showed significantly different morphology (see Fig. 2D). The formation and behavior of hybrid GUVs (*i.e.* vesicle size, surface structure and membrane property) depended on the initial mixing ratio. Fig. 3 depicts a systematic overview of the vesicle preparations, indicating significant structural changes with increasing amounts of the polymer component.

GUV preparations using mixtures of DPPC with 0 to 14 mol% of PIB₈₇-*b*-PEO₁₇ (**3a**) show again the formation of vesicles, characterized by the typical DPPC-liposome behavior, *i.e.* displaying a hole-defect and a faceted surface (Fig. 3A and B). Mixtures above 14 mol% of PIB₈₇-*b*-PEO₁₇ yielded GUVs having a completely closed membrane and a uniformly smooth surface. We therefore conclude that the PIB₈₇-PEO₁₇ BCP molecules become incorporated and disturb the close packing of the lipid molecules in the bilayer membrane, leading to smooth and round membranes. The characteristic hole-defect and the multifaceted vesicle surface were absent in all mixtures between 16 and 60 mol% of PIB₈₇-*b*-PEO₁₇ (**3a**).

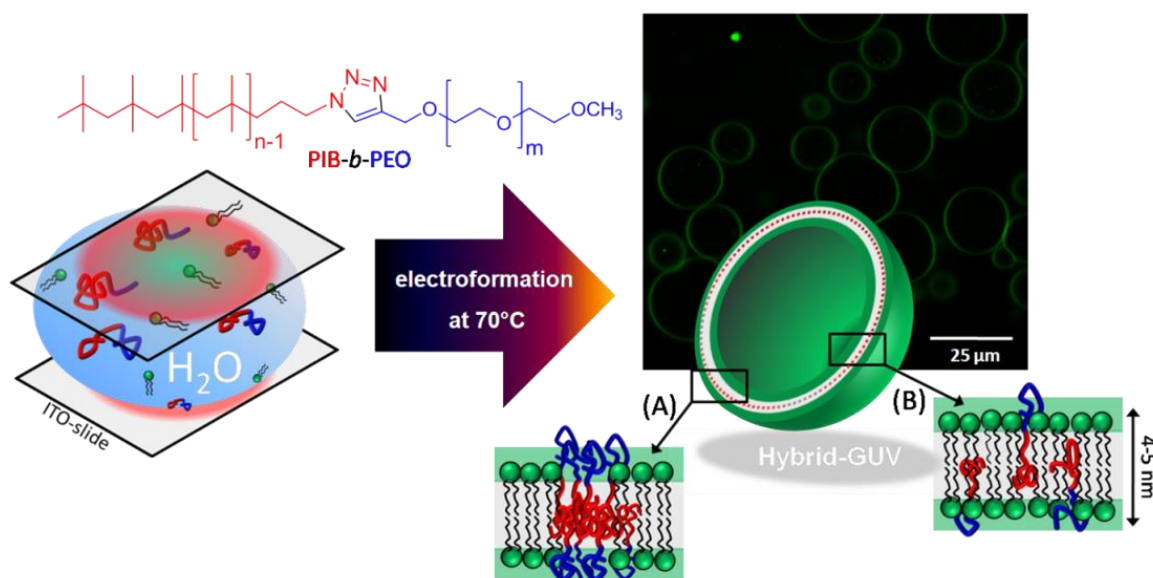


Fig. 1. Schematic view of the preparation of hybrid GUVs composed of a biological phospholipid and a synthetic biocompatible polyamphiphile. The mixed vesicles were prepared by electroformation in water using ITO-coated glasses covered with a thin film of a binary mixed system of lipid/polymer. Vesicle formation was performed at 70°C using an alternating electrical field (1.3 V [650 V*m⁻¹]/10 Hz). (A) and (B) depict a model of possible distributions of both amphiphiles in the hybrid membranes. Polymers may be clustered in the lipid bilayer matrix, *i.e.* they form phases enriched in lipid or polymer (A). Polymers could be homogeneously mixed with the phospholipids (B).

It therefore can be assumed that the block copolymer prevents the formation of extended areas of gel phase. Probably the incorporated BCPs (**3a**) disrupt the gel phase, resulting in smaller islands of gel phase surrounded by BCP molecules. Interestingly differential scanning calorimetry (DSC) of mixtures of DPPC and PIB₈₇-*b*-

PEO₁₇ (**3a**) did not show any change in the DPPC main transition temperature. We suppose that the high curvature of small vesicles, which were prepared by vortexing of the samples at 70°C, precluded the formation of mixed bilayers, despite the BCP incorporation into giant vesicles by electroformation.

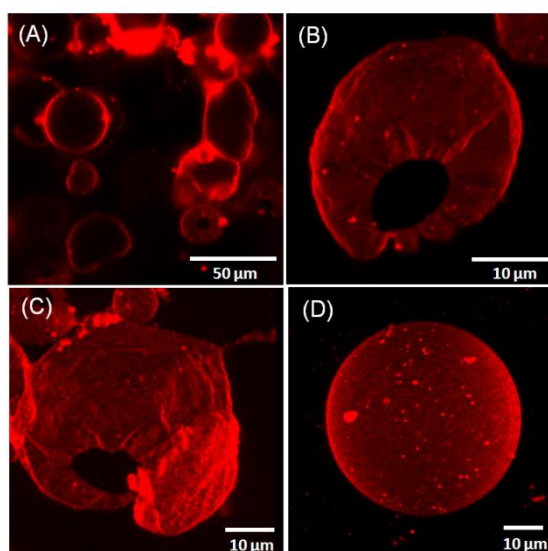


Fig. 2. (A-C) Confocal microscopy images of pure DPPC liposomes recorded at room temperature, *i.e.* below the main transition temperature of DPPC. All formed liposomes show a multifaceted shape of the vesicle membrane as visible in panel (A). The 3D-reconstructions (B and C) demonstrate the hole-defect of the bilayer membrane. Panel (D) depicts a 3D reconstruction of a mixed vesicle loaded with PIB₈₇-*b*-PEO₁₇ (30 mol%), showing a completely closed membrane.

We also examined a second binary mixed system of DPPC with PIB₃₇-*b*-PEO₄₈ (**3b**, Table 1), a BCP with a different hydrophilic/hydrophobic block length ratio compared to compound **3a**. Confocal microscopy investigations showed significant differences in the GUV appearance. As displayed in Fig. 4 and S1 in **appendix A**, hybrid GUVs

from mixtures between 10 and 40 mol% of PIB₃₇-*b*-PEO₄₈ exhibited a morphology that was distinct from pure DPPC GUVs as well as from hybrid vesicles containing the more hydrophobic PIB₈₇-PEO₁₇ BCP. Using the more hydrophilic BCP (**3b**), no smooth and round GUVs were formed.

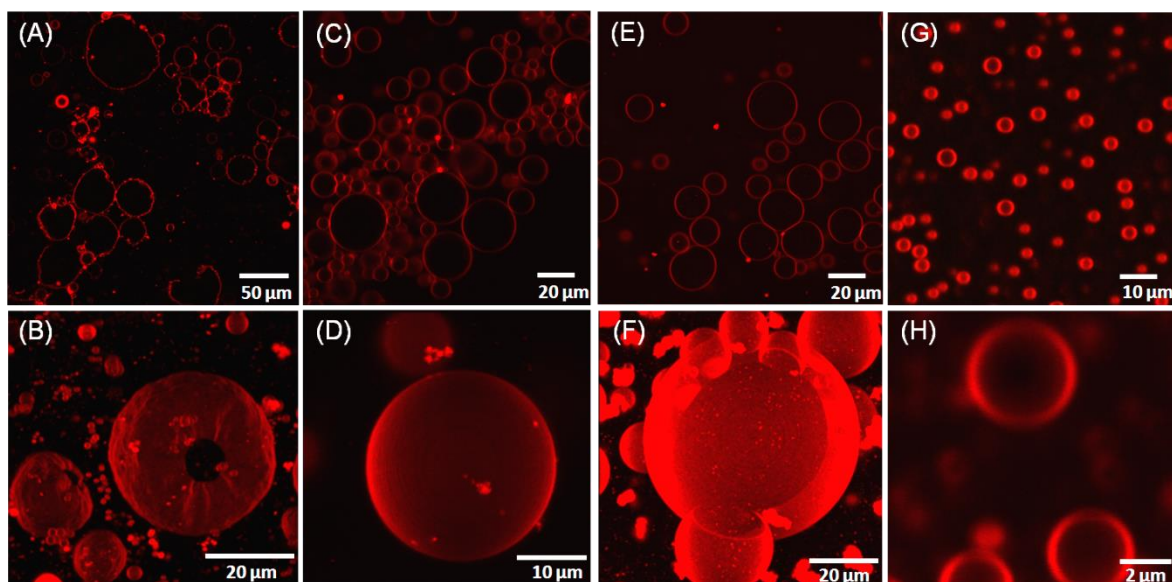


Fig. 3. Confocal microscopy images of different hybrid GUV preparations, prepared with varying ratios of lipid to polymer (PIB₈₇-*b*-PEO₁₇). Panels (A, C, E, G, H) contain single confocal images, panels (B, D, F) represent 3D reconstructions of axial stacks. Panels (A, B) show mixed vesicles obtained from a mixture of 10 mol% of **3a**. The 3D image (B) clearly illustrates the deformations and the characteristic hole-defect of these GUVs. 30 mol% (C, D), 40 mol% (E, F) and 60 mol% (G, H) of BCP was used as the initial mixing ratio. Hybrid vesicle populations loaded with PIB₈₇-*b*-PEO₁₇ have a completely closed bilayer membrane and a smooth surface. The corresponding 3D images in (D) and (F) demonstrate the appearance of a single phase on the scale of visible light microscopy resolution.

Instead, mixed vesicles showed a more ragged surface than those from pure DPPC and exhibited larger holes with more lacerated edges. A further difference to the more hydrophobic polymer was the size of the obtained hybrid GUVs. Whereas vesicle sizes up to ~ 50 nm were obtained from lipid/polymer mixtures using compound **3a**, we observed a wide range of vesicle sizes up to even 200 nm using the PIB₃₇-PEO₄₈ BCP. Obviously, similar to the confocal microscopy studies of DPPC mixtures with **3a**, the incorporated BCP chains (**3b**) affect the packing

behavior of the lipid molecules in the bilayer membrane. The more bulky hydrophilic PEO chains of the PIB₃₇-PEO₄₈ block copolymer may stabilize bilayer edges, resulting in the formation of larger holes (Fig. S1 in **appendix A**). In conclusion both amphiphilic BCPs (**3a** and **3b**) which differ in hydrophobicity show a significant influence on the formation and behavior of hybrid GUVs, in particular on the emergence of phase-borders and the suppression of hole-defects.

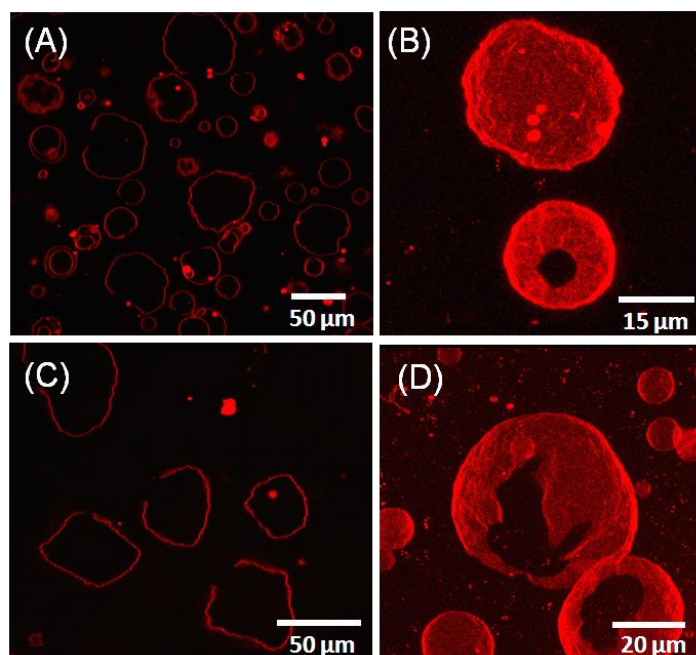


Fig. 4. Confocal microscopy images of hybrid GUVs with incorporated amphiphilic block copolymer chains (PIB₃₇-*b*-PEO₄₈) (**3b**). Panel (A) shows an overview of mixed vesicles at room temperature obtained from a mixture of 10 mol% of **3b** in the preparation. Panel (B) depicts the corresponding 3D-reconstruction of single vesicles, which show a more ragged surface than pure DPPC GUVs. Panels (C) and (D) illustrate hybrid vesicles where 20 mol% of **3b** was used. Membranes contain large holes, which is in strong contrast to the observations using PIB₈₇-*b*-PEO₁₇ (**3a**) as the polymer component, the latter leading to completely closed vesicle membranes.

2.2. Phase separation in hybrid GUVs.

Lateral heterogeneities play important roles in biological membranes⁴⁵ and can be studied in a simplified way in model membranes. The segregation of a specific type of lipid molecules in mixed bilayer membranes can be induced by external stimuli¹ leading to changes in the membrane structures and properties. In the case of lateral phase separation, reorganization of lipids in domains can be induced by a change in temperature, by complexation of charged ions on the outer shell of the membrane^{46, 47} or by the variation of chemical properties of the external milieu (*i.e.* pH-value). As judged by the homogeneous distribution of the fluorescence dye in the vesicle membrane, hybrid GUVs obtained from the initial mixing ratios between 10 and 18 mol% of PIB₈₇-*b*-PEO₁₇ (**3a**) appear to consist of a single phase (compare Fig. 2 and 3), suggesting that the BCP chains are homogeneously

distributed within the lipid bilayer matrix. The same apparent single phase behavior was observed in mixtures above 30 mol% of BCP. Hybrid GUVs forming these mixing ratios did not display any visible demixing phenomena on the spatial scale of light microscopy resolution.

Remarkably, macroscopic domain formation was observed in hybrid GUVs prepared from binary mixtures in the range of 20 to 28 mol% BCP. Confocal microscopy images (Fig. 5) show the formation of extended dark areas in the vesicle membrane, clearly indicating the coexistence of two different phases. This lateral domain formation occurred during the cooling process. Initial monitoring of the same GUVs at temperatures above the main transition temperature of DPPC showed none of the dark domains. The phase separation observed upon cooling indicates a miscibility gap roughly in the range around 20 to 28 mol% of diblock copolymer in mixtures with DPPC. Since the

membrane constitutes a two component system (plus excess water), the two phases must be characterized by different polymer/lipid ratios. Different compositions of the two phases cause differences in amphiphile packing. The lipid analogue DiDC18 used in this study to monitor packing differences enriches in the more ordered gel phase domains of GUVs prepared from phospholipids of different acyl chain lengths (DPPC/DLPC, data not shown),⁴⁸ but segregates from the ordered phase domains in GUVs consisting of two fluid phases (DOPC/sphingomyelin/cholesterol).⁴⁰ We therefore cannot unambiguously assign the brightly labeled areas in Fig. 5 and S2 (**appendix A**) to the lipid-enriched or polymer-

enriched phase. In addition to DiDC18 we examined the partitioning of an alternative membrane dye, namely a rhodamine-labeled phospholipid, within these mixed GUVs and we observed that both DiDC18 and rhodamine-DHPE had the same domain preference (Fig. S3 and S4 in **appendix A**). Based on the visualization of monolayers of the same components (see Section 3.2) it is conceivable that both fluorescent labels were squeezed out of more ordered gel phase domains in hybrid GUVs, in analogy to the dark appearance of the more ordered liquid-condensed domains in mixed BCP/lipid monolayers. Furthermore, time stability of the domains is a further indication of their gel-phase.

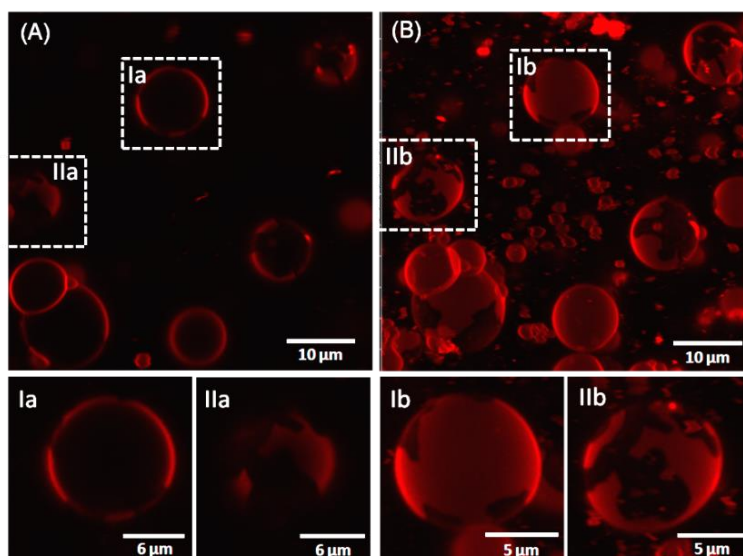


Fig. 5. Confocal microscopy images of hybrid GUVs with incorporated amphiphilic block copolymer chains (**3a**) using DiDC18 for labeling phase heterogeneities. Panel (A) shows an overview of mixed vesicles obtained from a mixture of DPPC and 20 mol% PIB_{87-*b*}-PEO₁₇. Remarkably domains represented by the dark patches in the lipid bilayer membrane are formed. (Ia) and (IIa) show magnified areas of (A). Panel (B) shows the corresponding 3D-reconstruction, indicating the irregular shape of the domain boundaries.

However, it is important to note that mixed monolayers may not be directly comparable to mixed bilayers, because in the latter system the large hydrophobic moieties of the block copolymer need to be accommodated within the hydrophobic core of the bilayer. Fluid phases typically form spherically shaped domains, *i.e.* they assume a geometry that minimizes the length of the domain borders. The irregular borders of the domains observed with the hybrid GUVs (see Fig. 5 and S2 in **appendix A**) suggest that the domains consist of rigid gel domains or gel-type sub-domains, interlaced by polymer. In contrast to the PIB₈₇-PEO₁₇ BCP phase separation was not observed in hybrid GUVs containing the more hydrophilic polymer PIB_{37-*b*}-PEO₄₈ (**3b**). The incorporation of this amphiphile leads to the formation of open membrane fragments without visible domains.

3. Binary mixed monolayers

As one of the goals of our investigations was the understanding of the lipid/polymer interaction in hybrid

vesicles, especially in vesicles achieved from mixtures of DPPC and PIB_{87-*b*}-PEO₁₇ copolymers (**3a**), it was important to study the phase behavior of corresponding mixed monolayers by Langmuir film techniques using identical mixing ratios as used for the GUV formation studies. This method coupled with fluorescence microscopy imaging allows a continuous monitoring of the film morphologies at the air/water interface. Monolayers were labeled with 0.01 mol% rhodamine-DHPE to visualize microstructures (domains). As experimentally shown and in accordance with literature reports,⁴⁹ this fluorescence dye prefers the liquid-expanded (LE) phase of the lipid/polymer film and is largely excluded from ordered phases (*i.e.* liquid-condensed phase, LC). Consequently, phase separation effects can be monitored to estimate the miscibility of lipid/polymer monolayers depending on the prevailing surface pressure. In the first section, we describe the behavior and characteristics of the pure compound isotherms (DPPC and **3a**) to ensure that observed

phenomena in mixed films are results of lipid/polymer interactions.

3.1. Monolayer isotherms of binary mixtures.

The surface pressure-mean molecular area (π -mMA) isotherms of pure DPPC (black curve) and PIB₈₇-PEO₁₇ BCP (**3a**) (olive green) are displayed in Fig. 6. At room temperature (20°C), the DPPC isotherm starts at $\sim 90 \text{ \AA}^2$ per molecule. During further compression a plateau at ~ 7 to $8 \text{ mN}\cdot\text{m}^{-1}$ was observed, which is well-known as the coexisting region of the LE/LC phases.^{50,51} Above the LE/LC plateau, the surface pressure increases sharply (see Fig. 6), indicating a strong condensed behavior of the monolayer. In contrast, the π -mMA isotherm of the diblock copolymer (**3a**) shows a slight increase in the surface pressure over the whole compression range. The lift-off area was found at 380 \AA^2 per molecule, which indicates a well-expanded phase behavior of the monolayer. Film collapse starts at the mMA value of 100 \AA^2 per molecule ($\pi = 41 \text{ mN}\cdot\text{m}^{-1}$), which appears as a plateau. We found that during the collapse formation the surface pressure was completely constant ($\sim 41 \text{ mN}\cdot\text{m}^{-1}$), a typical behavior of PIB-PEO diblock copolymers with comparable hydrophobic block lengths. The observed roll-over collapse agrees well with previous reports comparing the behavior of PIB-PEO copolymer molecules spread on the air/water interface.⁵²

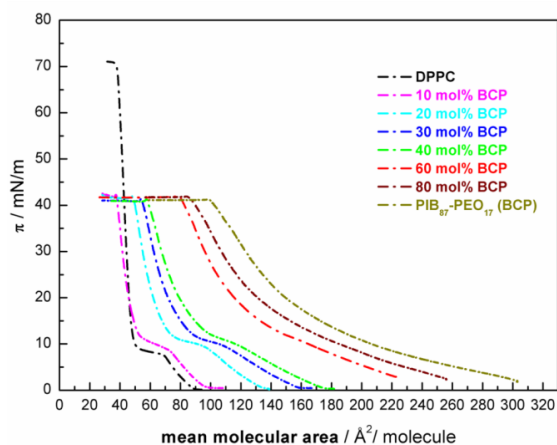


Fig. 6. Langmuir isotherms of the pure compounds (DPPC and **3a**) and the studied lipid/polymer mixtures at 20°C. Black and olive green colored curves represent the isotherms of pure DPPC and PIB₈₇-PEO₁₇ (**3a**), respectively. The π -mMA isotherms of the corresponding mixtures using different lipid/polymer mixing ratios are presented in different colors.

As shown in Fig. 6, the lift-off areas of the π -mMA isotherms from mixtures between 10 and 80 mol% of PIB₈₇-PEO₁₇ (**3a**) increase stepwise with further addition of the polymer component. Thereby the calculated lift-off areas differ from the observed area values. For all mixed isotherms the observed lift-off was smaller than the expected value, based on the mole percent values of the pure compound lift-off areas indicating attractive

lipid/polymer interactions. In the low pressure region between 0 and $8 \text{ mN}\cdot\text{m}^{-1}$ we found a flattening of each isotherm with increasing amounts of **3a** as the BCP chains support the persistence of the expanded phase of the lipid monolayer. This is further proved by monitoring higher surface pressures for the characteristic transition state of the lipid monolayer (LE/LC coexistence region) when increasing the initial mixing ratio of polymer to DPPC.

Compared to the pure DPPC isotherm the formation of the LE/LC plateau in a mixed monolayer from DPPC and 40 mol% of **3a** was observed at $10.1 \text{ mN}\cdot\text{m}^{-1}$ ($\Delta\pi \approx 3 \text{ mN}\cdot\text{m}^{-1}$). Obviously, the amphiphilic polymer molecules affect the rearrangement behavior of the lipid molecules at the air/water interface, resulting in the disturbance of the lipid packing. Furthermore, the LE/LC coexistence region persists up to 60 mol% of PIB₈₇-PEO₁₇, at higher BCP amounts the characteristic plateau of DPPC could not be observed. In contrast, the position of the roll-over plateau of the diblock copolymer (**3a**) was not affected by lipid/polymer interactions and persisted in all mixed monolayers at $\sim 41 \text{ mN}\cdot\text{m}^{-1}$. As mentioned before, the flattening of the mixed isotherms occurs further in the higher surface pressure region from 10 to $40 \text{ mN}\cdot\text{m}^{-1}$, which is attributed to the influence of the polymer component forming a less condensed phase.⁵² As a result the rigid liquid-condensed state of the lipid monolayer is disturbed by the presence of the polymer, which is comparable to the results of the hybrid GUV studies.

3.2. Fluorescence microscopy of binary mixed monolayers.

First, we performed fluorescence microscopy of the pure monolayers (DPPC and PIB₈₇-PEO₁₇). For visualization of the film morphology Rh-DHPE (see Experimental section) was used, which prefers the liquid-expanded phase of the monolayer discussed before. Typically for the DPPC monolayer we observed the LC domain nucleation at the beginning of the plateau at a surface pressure of $7.2 \text{ mN}\cdot\text{m}^{-1}$. Initially, the dark LC domains are bean shaped and with further compression of the film we observed a strong increase in size of these domains, resulting in the formation of chiral domains,^{51, 53} as shown in Fig. S5 (appendix A). Fluorescence microscopy studies of the polymer monolayer showed the formation of a homogeneous film over the whole compression range. Domain formation or further heterogeneities in the film morphology could not be observed. In fluorescence microscopy experiments using mixing ratios from 10 to 40 mol% of PIB₈₇-PEO₁₇ the observed monolayers showed phase separation phenomena over the whole compression range. Fig. 7 presents fluorescence microscopy images of various mixing ratios (between 10 and 40 mol% of **3a**) recorded at different surface pressures, which prove the formation of polymer-rich domains (dark colored) and the nucleation of pure lipid LC domains with fractal shape (black colored). Initially at low surface pressures polymer-

rich domains appeared in the liquid-expanded phase, which are completely circular shaped (at 2 and 3 $\text{mN}\cdot\text{m}^{-1}$). With further compression of the mixed monolayer passing the plateau region, the polymer domains showed an ovate shape, resulting in the formation of mosaic-structures at high surface pressures above 30 $\text{mN}\cdot\text{m}^{-1}$. Typically with increasing polymer content, we found that the separation process leads to an increase in the domain size (see Fig. 7A, E, I and M). Furthermore, the increase in the domain size during the compression of the monolayer was significant. Obviously, some diblock copolymer molecules, which are well-mixed with the expanded lipid film, were squeezed out during the ordering process.

These expelled polymers being merged with the polymer domains result in the observed domain growth. Alternatively, the lipids could also be squeezed into the polymer-rich domains. The different gray scale levels in the fluorescence images indicate that the large polymer-

rich domains (gray colored) contain lipid and labeled lipid molecules (Rh-DHPE). The black regions (no fluorescence intensity) observed between the polymer domains (see Fig. 7C, G, K and O) represent pure lipid domains, which have a high lipid packing density. Further black regions inside the polymer domains at high surface pressure ($\sim 30 \text{ mN}\cdot\text{m}^{-1}$), as clearly visible in Fig. 7H, L and P, support the assumption that the polymer domains contain some liquid-condensed lipid materials.³⁰

The very bright spots (*i.e.* Fig. 7K and O) display areas of the monolayer, where the Rh-DHPE molecules were accumulated after the lipid LE/LC phase transition. At high surface pressures these fluorescently labeled lipids start to diffuse into the polymer-rich domains, forming a bright corona (*i.e.* Fig. 7L and P). Obviously, the polymer domains have a lower packing density compared to the liquid-condensed DPPC phase.

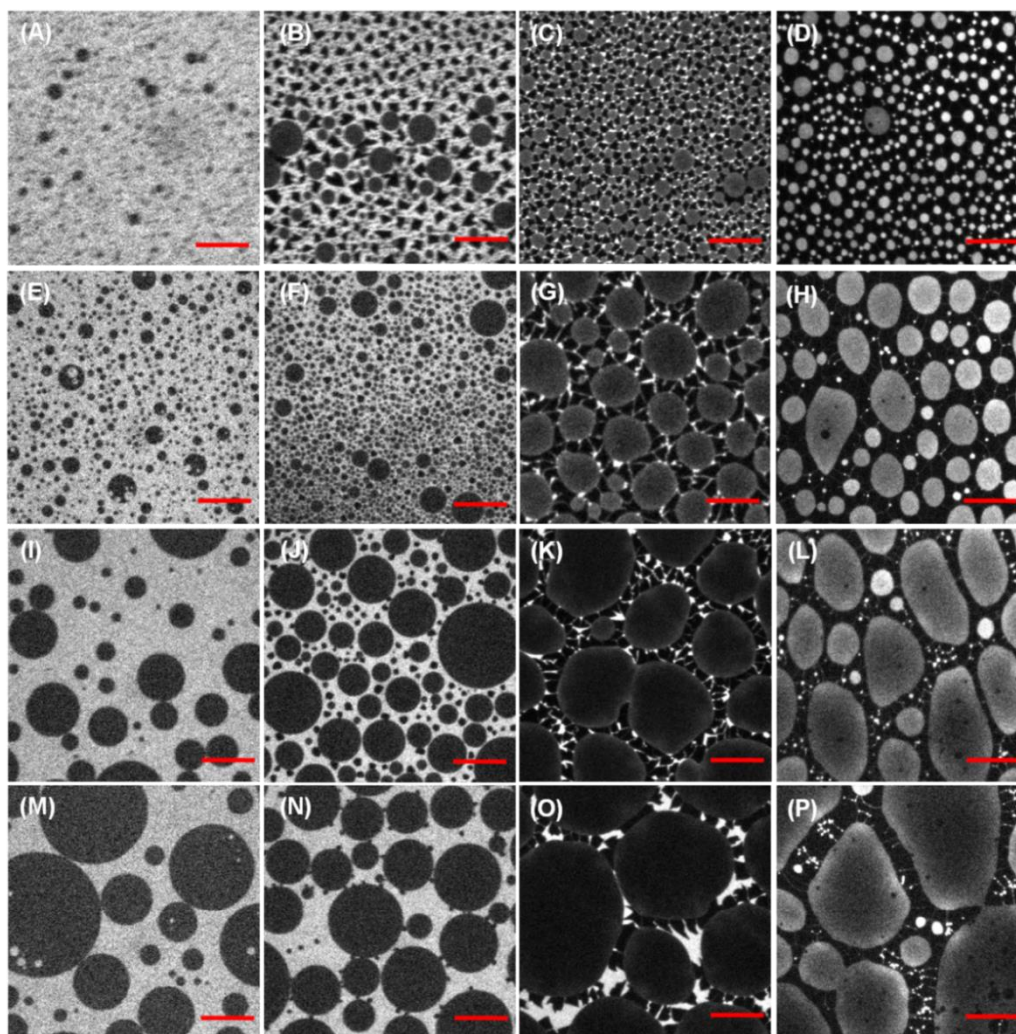


Fig. 7. Fluorescence microscopy images of mixed DPPC/BCP monolayers at the air/water interface at 20°C using different initial mixing ratios: (A-D) 10 mol% of **3a**, (E-H) 20 mol% of **3a**, (I-L) 30 mol% of **3a** and (M-P) 40 mol% of **3a**. The scale bar represents 25 nm. The images of all mixtures were recorded at surface pressures of 3, 10, 12 and 30 $\text{mN}\cdot\text{m}^{-1}$ (from left to right), respectively.

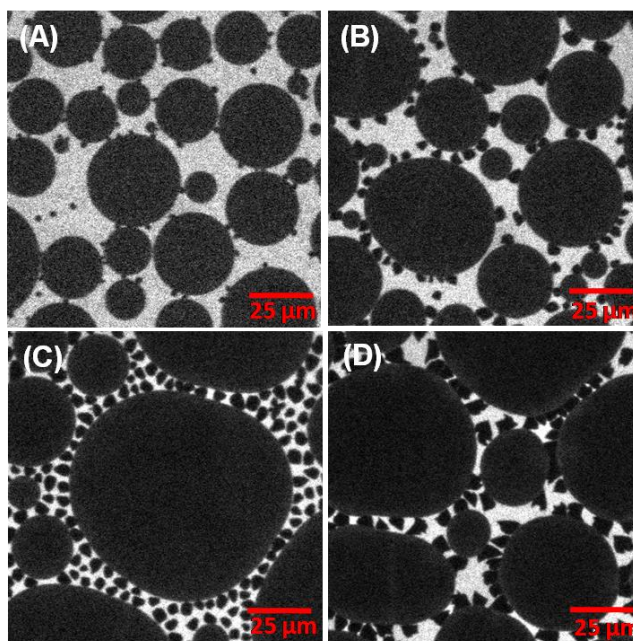


Fig. 8. Fluorescence microscopy images of a mixed DPPC/BCP monolayer (40 mol% of **3a**) at the air/water interface at 20°C, which demonstrates the growth of DPPC domains induced at the polymer boundary surface: (A) 10.0 mN*m⁻¹; (B) 10.9 mN*m⁻¹; (C) 11.7 mN*m⁻¹; (D) 12.2 mN*m⁻¹.

Fluorescence microscopy studies of the mixed monolayer containing 80 mol% of **3a** showed a homogeneous film formation (see ESI, Fig. S6 in **appendix A**) independent of the compression state. The characteristic domain nucleation of DPPC could not be observed, which indicates a homogeneous distribution of the lipid chains in the polymer matrix where lipid/lipid interactions are not feasible.

3.3. Liquid-condensed behavior of DPPC in mixed monolayers.

The behavior of LC domains formed in the LE/LC coexistence region of DPPC is strongly influenced by the presence of diblock copolymer molecules (**3a**). The domain nucleation in the pure DPPC monolayer agrees well with previous reports.^{50, 51} The structural behavior, the growth of the domains and the formed shapes during the compression of the monolayer could be observed as described in the studies of McConlogue and Vanderlick.⁵¹ In binary lipid/polymer mixtures we found significant differences in the isotherm curves and structural changes in the DPPC domains. Depending on the initial mixing ratio, the domain nucleation is shifted to higher surface pressures ($\Delta\pi \approx 4$ to 5 mN*m⁻¹) caused by the increasing influence of the polymer. Furthermore, during the monolayer compression the characteristic DPPC domain transitions, forming bi- and trilobed transition states (Fig. S5 in **appendix A**), were not visible in mixed lipid/polymer monolayers. In all mixtures of DPPC with 10 to 60 mol% of compound **3a** we observed a fractal domain shape of the liquid-condensed phase of DPPC (see Fig. 7 and 8). As a second difference, the size of the LC

domains, which have a high lipid packing density, is strongly decreased in mixed monolayer. On the other hand, the number of DPPC domains increases strongly. Probably, the amphiphilic polymer acts as a dispersant, which prevents the formation of a large LC phase of the lipid. Here we found well-dispersed small liquid-condensed islands of DPPC in mixed monolayers, which is in accordance with the studies of the mixed bilayer membranes. Finally we observed that the domain nucleation in mixtures from 20 to 60 mol% of PIB₈₇-PEO₁₇ BCP occurs on the polymer boundary surface. Fig. 8 shows a more detailed view of the DPPC phase transition in a 40 mol% mixture, where the LC domain nucleation starts at the polymer domain boundaries. The polymer-rich domains, which are well-distributed in the expanded lipid film, serve as nuclei for the formation of small liquid-condensed DPPC islands. As visible in Fig. 8, the domain growth starts in a mixed monolayer using 40 mol% of **3a** at ~10 mN*m⁻¹ and with further compression these domains form a fractal shape as described before.

CONCLUSION AND PERSPECTIVE

The present publication deals with a thorough investigation on mixing lipids (DPPC) and biocompatible block copolymers (PIB-PEO BCP, **3a** and **3b**) in mono- and bilayer structures. A significant effort was directed towards the generation of biocompatible GUVs, where part of the membrane is constituted by the BCP. Electroformation proved to be the method of choice to generate mixed (“hybrid”) GUVs composed of polymers and lipids. At room temperature the mixed vesicles showed a high stability in water suspensions, which makes

our investigated mixed vesicular system attractive for drug delivery applications. Both amphiphilic BCPs (**3a** and **3b**) differing in hydrophobicity show a significant influence on the formation and behavior of hybrid GUVs, in particular the suppression of holes and appearance of phase borders. Mixing/demixing of these lipid and polymeric components proved of high importance, in that

up to 20 mol% and above 30 mol% of the BCP (**3a**), a mixed membrane is observed. However, at mixing ratios from 20 to 28 mol% of the BCP (**3a**) in the membrane, demixing phenomena are clearly observed by confocal laser microscopy of GUVs formed by electroformation (for a schematic drawing see Fig. 9).

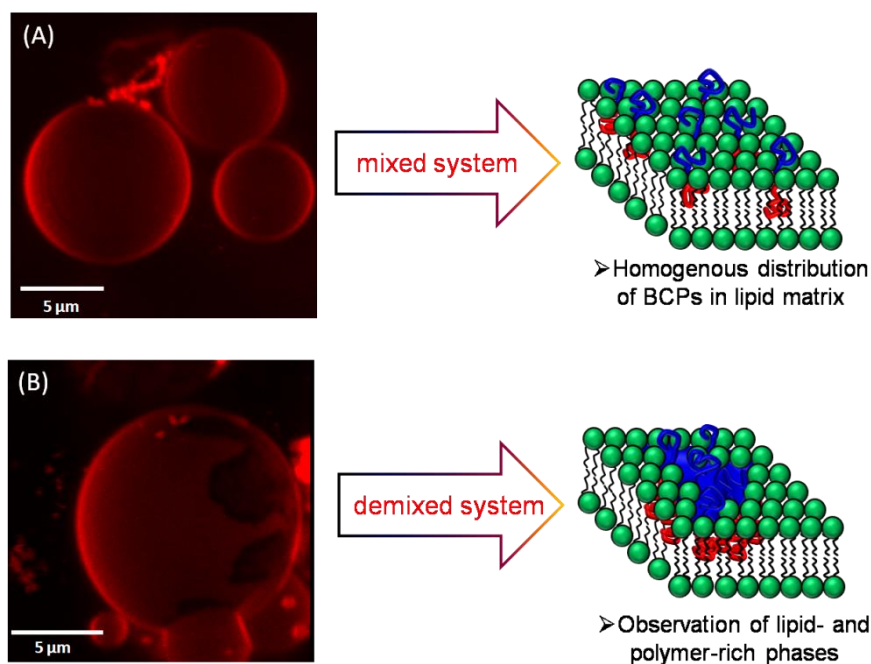


Fig. 9. Confocal microscopy images and the model of distribution of BCP chains in a lipid bilayer matrix for different compositions. (A) Hybrid GUVs from mixtures of 14 to 18 mol% of BCP show a single phase behavior at confocal microscopy resolution, suggesting that polymers may be homogeneously distributed in the lipid matrix. (B) Mixtures containing 20 to 28 mol% of the polymer (**3a**) show a demixed vesicle membrane, indicating a phase separated system.

To understand mixing/demixing phenomena in lipid bilayer membranes loaded with BCP chains in detail, further investigations such as Langmuir-isotherms and morphology studies in mixed monolayers were performed. For all mixed isotherms the observed lift-off was smaller than the expected value, based on the mole percent values of the pure compound lift-off areas indicating attractive lipid/polymer interactions. The rigid liquid-condensed state of the lipid monolayer is disturbed by the presence of the polymer, which is comparable to the results of the hybrid GUV studies. Additionally, in fluorescence microscopy experiments using mixing ratios from 10 to 40 mol% of PIB_{87-b}-PEO₁₇ the observed monolayers showed phase separation phenomena over the whole compression range, which again is indicative of the formation of partially mixed phases, consisting of “seas” of “lipid-rich” and “polymer-rich” domains. Therefore a “sharp” phase boundary containing exclusively segregated pure lipid- and polymer-phases cannot be assumed. The presented hybrid GUVs clearly are the first example of truly biocompatible vesicles where mixtures of a biocompatible BCP and a lipid (DPPC) are fabricated into vesicular membranes by electroformation. We envision a

bright future for such mixed vesicles, located in controllable membrane-moduli, adjustable drug delivery or gas permeability. Further experiments concerning the dynamics (*via* Fluorescence Correlation Spectroscopy) of the individual domains are in progress and will be reported soon.

EXPERIMENTAL SECTION

1. Materials

All chemicals were purchased from *Sigma-Aldrich* (*Schnelldorf*, Germany) and were used as received unless otherwise stated. All solvents, which were used for the workup procedures, were distilled prior to use. Toluene and tetrahydrofuran (THF) were predried over potassium hydroxide for several days, refluxed over sodium/benzophenone and freshly distilled under an argon atmosphere before usage. Azido-functionalized PIB (**1a**, **1b**) as shown in Scheme 1 was synthesized and characterized as reported elsewhere.^{36, 37, 54} The corresponding alkyne-terminated PEO (**2a**, **2b**) was prepared *via* phase transfer catalysis using sodium

hydroxide powder and propargyl bromide as described by Dimonie and Teodorescu³⁸ and according to Binder and Sachsenhofer.¹⁵

1,2-Dipalmitoyl-*sn*-glycero-3-phosphocholine (DPPC, $M = 734.05 \text{ g}\cdot\text{mol}^{-1}$) was purchased from *Avanti Polar Lipids (Alabaster, AL, USA)*, 1,1'-dioctadecyl-3,3',3'-tetramethylindodicarbocyanine perchlorate (DiDC18, $M = 959.92 \text{ g}\cdot\text{mol}^{-1}$) and 1,2-dihexadecanoyl-*sn*-glycero-3-phosphoethanolamine-*N*-(lissamine rhodamine B sulfonyl) (Rh-DHPE, $M = 1267.68 \text{ g}\cdot\text{mol}^{-1}$) were purchased from *Invitrogen (Karlsruhe, Germany)* and used without further purifications.

1.1. Preparation of amphiphilic diblock copolymers (diblock copolymers) (3a, 3b).

As shown in Scheme 1 the preparation of amphiphilic diblock copolymers was performed under Cu(I)-mediated conditions using CuI/*N,N*-diisopropylethylamine (DIPEA) as catalytic system. According to the modified procedure of Binder and Sachsenhofer¹⁵ azido-telechelic PIB (**1a**, **1b**) (1 equiv.), alkyne-terminated PEO (**2a**, **2b**) (1.1 equiv.), DIPEA (40 equiv.) and Cu(I)-iodide (0.1 equiv.) were dissolved in THF and stirred at 50°C. After 48 hours the crude product was purified by a silica-flash column to remove the catalyst residue. The final amphiphilic diblock copolymer (**3a**, **3b**) was achieved in quantitative yields after column chromatography using silica gel and a solvent mixture of chloroform to methanol, 20 to 1. The molecular characteristics of the used PIB-PEO diblock copolymers in this study are illustrated in Table 1.

2. Measurements

2.1. Surface pressure (π) measurements.

Surface pressure (π) measurements of the pure compounds and of different binary mixed systems of PIB-PEO BCP and DPPC at the air/water interface *via* Langmuir film technique were performed using a Langmuir trough system (*KSV, Helsinki, Finland*) with a maximum available surface of 76.800 mm². To minimize dust the trough was kept in a closed box. The used subphase (water) was purified by a Purelab Option system (*ELGA Ltd., Celle, Germany*). Before each measurement was started the trough was purified four times with distilled water and two times with ultrapure water (total organic carbon < 5 ppm; conductivity < 0.055 $\mu\text{S}\cdot\text{cm}^{-1}$). All compression measurements were performed at constant temperature (20°C) realized by a circulating water bath system. The investigated mixture of copolymers and DPPC was dissolved in chloroform (HPLC grade, *Sigma Aldrich*) at a concentration of 1 mM. Defined amounts of the prepared solutions (different molar ratios of DPPC to BCP) were spread on the subphase using a digital microsyringe (*Hamilton*). Each surface pressure measurement using a compression rate of 5 mm²·min⁻¹ was

started 15 minutes after spreading to ensure the full evaporation of the solvent and a uniform monolayer formation.

2.2. Fluorescence monolayer investigation.

Fluorescence microscopy imaging of monolayers at the air/water interface was performed using an "Axio Scope.A1 Vario" epifluorescence microscope (*Carl Zeiss MicroImaging, Jena, Germany*). The microscope was equipped with a Langmuir Teflon trough with a maximum area of 264 cm² and two symmetrically moveable computer-controlled Teflon barriers (*Riegler & Kirstein, Berlin, Germany*). The trough was positioned on an x-y stage (*Märzhäuser, Wetzlar, Germany*) to be able to move the film surface with respect to the objective lens to any desired surface area. The x-y-z motion control was managed by a MAC5000 system (*Ludl Electronic Products, Hawthorne, NY, USA*). The trough was enclosed with a homebuilt Plexiglas hood to ensure a dust-free environment, the temperature of 20 °C was maintained with a circulating water bath and the whole setup was placed on a vibration-damped optical table (*Newport, Darmstadt, Germany*). The air/water surface was illuminated using a 100 W mercury arc lamp, a long-distance objective (LD EC Epiplan-NEOFLUAR 50x) was used and the respective wavelengths were selected with a filter/beam splitter combination, which is appropriate for the excitation and detection of Rh-DHPE (*Zeiss filter set 20: excitation band-pass BP 546/12 nm, beam splitter FT 560 nm, emission band-pass BP 575-640 nm*). Images were recorded using an EMCCD camera (ImageEM C9100-13, *Hamamatsu, Herrsching, Germany*). Image analysis and data acquisition were done using AxioVision software (*Carl Zeiss MicroImaging, Jena, Germany*). All presented images show areas of individually contrast-adjusted raw data.

Monolayer films of DPPC/BCP mixtures and pure compounds were prepared with an entire spreading concentration of 1 mM chloroform (HPLC-grade, *Carl Roth, Karlsruhe, Germany*). The concentration of the fluorescently labeled rhodamine-DHPE in the spreading solution was 0.01 mol% and was used for all measurements. Microscopy images were taken during compression of the monolayer using a compression speed of 4.6 cm²/min.

2.3. Electroformation – preparation of hybrid GUVs.

The giant unilamellar vesicles (GUVs) were prepared by applying an alternating low-voltage electric field during the hydration process of a thin lipid/polymer film. The DPPC/PIB_{87-b}-PEO₁₇ mixtures were prepared in HPLC-grade chloroform, dried under a continuous N₂-stream and dissolved in a defined solvent volume at 10 mg·ml⁻¹. Optically transparent indium-tin-oxide (ITO) coated coverslips (*GeSiM, Großberkmannsdorf, Germany*), which

were used as electrodes, were coated with a thin amphiphile film. Both manual spreading and spin coating of the amphiphile solution were tested, with spin coating yielding a more homogeneous appearance of the film. After the preparation of a thin film on two coverslips, these were placed in a capacitor-type configuration at a distance of 2 mm using a home built flow-chamber. The chamber was filled with deionized water (~300 ml). Finally, the ITO-slips were connected to a pulse generator (Conrad, Germany) and an alternating sinusoidal voltage ($U_{\text{eff}} = 1.3 \text{ V}$, $\nu = 10 \text{ Hz}$) was applied for 4 hours. During the whole electroformation process, the coverslips were heated to 70°C , *i.e.* safely above the main transition temperature of DPPC ($T_m = 41.6^\circ\text{C}$).

2.4. Confocal microscopy.

Confocal microscopy images were obtained on a commercial confocal-laser scanning microscope- LSM 710 (Carl-Zeiss, Germany) using a C-Apochromat 40x/1.2 N.A. water immersion objective. Lipophilic carbocyanine DiDC18 was used as membrane label and was excited with a HeNe laser at 633 nm. Furthermore, Rh-DHPE was also used as fluorescence dye, which was excited with an Argon-Ion-laser at 488 or 514 nm. Imaging of all GUV samples was performed after cooling to room temperature unless otherwise stated.

ACKNOWLEDGEMENTS

We thank the grants DFG BI 1337/6-1 (WHB) and BL 182/23-1 (AB) within the Forschergruppe FOR-1145 (MS), the grants DFG INST 271/249-1; INST 271/247-1; INST 271/248-1, the BMBF ZIK program (FKZ 03Z2HN22 to KB) and ERDF grant 124109001 for financial support.

REFERENCES

- [1] W. H. Binder, V. Barragan and F. M. Menger, *Angew. Chem., Int. Ed.*, **2003**, 42, 5802-5827.
- [2] T. Kunitake, *Physical Chemistry of Biological Interfaces*, ed. A. Baszkin and W. Norde, **2000**, Marcel Dekker, Inc., New York, NY, pp. 283-305.
- [3] H. Ringsdorf, B. Schlarb and J. Venzmer, *Angew. Chem.*, **1988**, 100, 117-162.
- [4] D. E. Discher and A. Eisenberg, *Science*, **2002**, 297, 967-973.
- [5] D. E. Discher, H. Bermudez and D. A. Hammer, *Langmuir*, **2004**, 20, 540-543.
- [6] L. Ma and A. Eisenberg, *Langmuir*, **2009**, 25, 13730-13736.
- [7] A. Mecke, C. Dittrich and W. Meier, *Soft Matter*, **2006**, 2, 751-759.
- [8] D. E. Discher, D. A. Christian, A. Tian, W. G. Ellenbroek, I. Levental, K. Rajagopal, P. A. Janmey, A. J. Liu and T. Baumgart, *Nat. Mater.*, **2009**, 8, 843-849.
- [9] S. Yu, T. Azzam, I. Rouiller and A. Eisenberg, *J. Am. Chem. Soc.*, **2009**, 131, 10557-10566.
- [10] H. Kukula, H. Schlaad, M. Antonietti and S. Forster, *J. Am. Chem. Soc.*, **2002**, 124, 1658-1663.
- [11] R. J. Thibault, O. Uzun, R. Hong and V. M. Rotello, *Adv. Mater.*, **2006**, 18, 2179-2183.
- [12] R. J. Thibault, T. H. Galow, E. J. Turnberg, M. Gray, P. J. Hotchkiss and V. M. Rotello, *J. Am. Chem. Soc.*, **2002**, 124, 15249-15254.
- [13] P. P. Ghoroghchian, P. R. Frail, K. Susumu, D. Blessington, A. K. Brannan, F. S. Bates, B. Chance, D. A. Hammer and M. J. Therien, *Proc. Natl. Acad. Sci. U. S. A.*, **2005**, 102, 2922-2927.
- [14] A. Napoli, M. J. Boerakker, N. Tirelli, R. J. M. Nolte, N. A. J. M. Sommerdijk and J. A. Hubbell, *Langmuir*, **2004**, 20, 3487-3491.
- [15] W. H. Binder and R. Sachsenhofer, *Macromol. Rapid Commun.*, **2008**, 29, 1097-1103.
- [16] W. H. Binder, R. Sachsenhofer, D. Farnik and D. Blaas, *Phys. Chem. Chem. Phys.*, **2007**, 9, 6435-6441.
- [17] S. Lecommandoux, O. Sandre, F. Chécot, J. Rodriguez-Hernandez and R. Perzynski, *Adv. Mater.*, **2005**, 17, 712-718.
- [18] W. Mueller, K. Koynov, K. Fischer, S. Hartmann, S. Pierrat, T. Basche and M. Maskos, *Macromolecules*, **2009**, 42, 357-361.
- [19] G. Gopalakrishnan, C. Danelon, P. Izewska, M. Prummer, P.-Y. Bolinger, I. Geissbühler, D. Demurtas, J. Dubochet and H. Vogel, *Angew. Chem., Int. Ed.*, **2006**, 45, 5478-5483.
- [20] Y. Mai and A. Eisenberg, *J. Am. Chem. Soc.*, **2010**, 132, 10078-10084.
- [21] D. Beyer, G. Elender, W. Knöll, M. Kühner, S. Maus, H. Ringsdorf and E. Sackmann, *Angew. Chem., Int. Ed.*, **1996**, 35, 1682-1685.
- [22] J. Simon, M. Kühner, H. Ringsdorf and E. Sackmann, *Chem. Phys. Lipids*, **1995**, 76, 241-258.
- [23] H. Ringsdorf, E. Sackmann, J. Simon and F. M. Winnik, *Biochim. Biophys. Acta, Biomembr.*, **1993**, 1153, 335-344.
- [24] W. H. Binder, *Angew. Chem., Int. Ed.*, **2008**, 47, 3092-3095.
- [25] C. Tribet and F. Vial, *Soft Matter*, **2008**, 4, 68-81.
- [26] F. Vial, A. G. Oukhaled, L. Auvray and C. Tribet, *Soft Matter*, **2007**, 3, 75-78.
- [27] A. A. Yaroslavov, T. A. Sitnikova, A. A. Rakhnyanskaya, E. G. Yaroslavova, D. A. Davydov, T. V. Burova, V. Y. Grinberg, L. Shi and F. M. Menger, *J. Am. Chem. Soc.*, **2009**, 131, 1666-1667.
- [28] A. A. Yaroslavov, N. S. Melik-Nubarov and F. M. Menger, *Acc. Chem. Res.*, **2006**, 10, 702-710.
- [29] W. Meier, T. Ruysschaert, A. F. P. Sonnen, T. Haefele, M. Winterhalter and D. Fournier, *J. Am. Chem. Soc.*, **2005**, 127, 6242-6247.
- [30] W. Meier, K. Kita-Tokarczyk, F. Ite, M. Grzelakowski, S. Egli and P. Rossbach, *Langmuir*, **2009**, 25, 9847-9856.

- [31] T. Haefele, K. Kita-Tokarczyk and W. Meier, *Langmuir*, **2005**, 22, 1164-1172.
- [32] J. Nam, P. A. Beales and T. K. Vanderlick, *Langmuir*, **2011**, 27, 1-6.
- [33] W. H. Binder and R. Sachsenhofer, *Macromol. Rapid Commun.*, **2007**, 28, 15-54.
- [34] Z. Cheng and A. Tsourkas, *Langmuir*, **2008**, 24, 8169-8173.
- [35] M. Rother, H. Barqawi, D. Pfefferkorn, J. Kressler and W. H. Binder, *Macromol. Chem. Phys.*, **2010**, 211, 204-214.
- [36] W. H. Binder, L. Petraru, T. Roth, P. W. Groh, V. Pálfi, S. Keki and B. Ivan, *Adv. Funct. Mater.*, **2007**, 17, 1317-1326.
- [37] W. H. Binder and D. Machl, *J. Polym. Sci., Part A: Polym. Chem.*, **2005**, 43, 188-202.
- [38] M. Dimonie and M. Teodorescu, *Makromol. Chem. Rapid Commun.*, **1993**, 14, 303-307.
- [39] M. I. Angelova and D. S. Dimitrov, *Faraday Discuss. Chem. Soc.*, **1986**, 81, 303-311.
- [40] K. Bacia, P. Schwille and T. Kurzchalia, *Proc. Natl. Acad. Sci. U. S. A.*, **2005**, 102, 3272-3277.
- [41] S. Veatch and S. Keller, *Biophys. J.*, **2003**, 84, 725-726.
- [42] M. Andersson, L. Hammarstroem and K. Edwards, *J. Phys. Chem.*, **1995**, 99, 14531-14538.
- [43] R. L. Knorr, M. Staykova, R. S. Gracia and R. Dimova, *Soft Matter*, 2010, 6, 1990-1996.
- [44] H. V. Ly and M. L. Longo, *Macromol. Symp.*, **2005**, 219, 97-122.
- [45] K. Simons and E. Ikonen, *Nature*, **1997**, 387, 569-572.
- [46] W. Knoll, G. Schmidt, H. Rötzer, T. Henkel, W. Pfeiffer, E. Sackmann, S. Mittler-Neher and J. Spinke, *Chem. Phys. Lipids*, **1991**, 57, 363-374.
- [47] J. R. Silvius and J. Gagne, *Biochemistry*, **1984**, 23, 3241-3247.
- [48] J. Korlach, P. Schwille, W. W. Webb and G. W. Feigenson, *Proc. Natl. Acad. Sci. U. S. A.*, **1999**, 96, 8461-8466.
- [49] M. Dyck and M. Lösche, *J. Phys. Chem. B*, **2006**, 110, 22143-22151.
- [50] G. Ma and H. C. Allen, *Langmuir*, **2006**, 22, 5341-5349.
- [51] C. W. McConlogue and T. K. Vanderlick, *Langmuir*, **1997**, 13, 7158-7164.
- [52] H. Li, R. Sachsenhofer, W. H. Binder, T. Henze, T. Thurn-Albrecht, K. Busse and J. r. Kressler, *Langmuir*, **2009**, 25, 8320-8329.
- [53] P. Krüger and M. Lösche, *Phys. Rev. E: Stat. Phys., Plasmas, Fluids, Relat. Interdiscip. Top.*, **2000**, 62, 7031.
- [54] W. H. Binder, M. J. Kunz, C. Kluger, G. Hayn and R. Saf, *Macromolecules*, **2004**, 37, 1749-1759.

oxide copolymer (PIB₈₇-*b*-PEO₁₇; BCP **1**) and 1,2-dipalmitoyl-*sn*-glycero-3-phosphatidylcholine (DPPC; **2**) that were functionalized with ganglioside GM1 (**3**); we

then studied the binding of cholera toxin B (CTB) to these hybrid membranes either in the laterally mixed or demixed phase state (Figure 1).

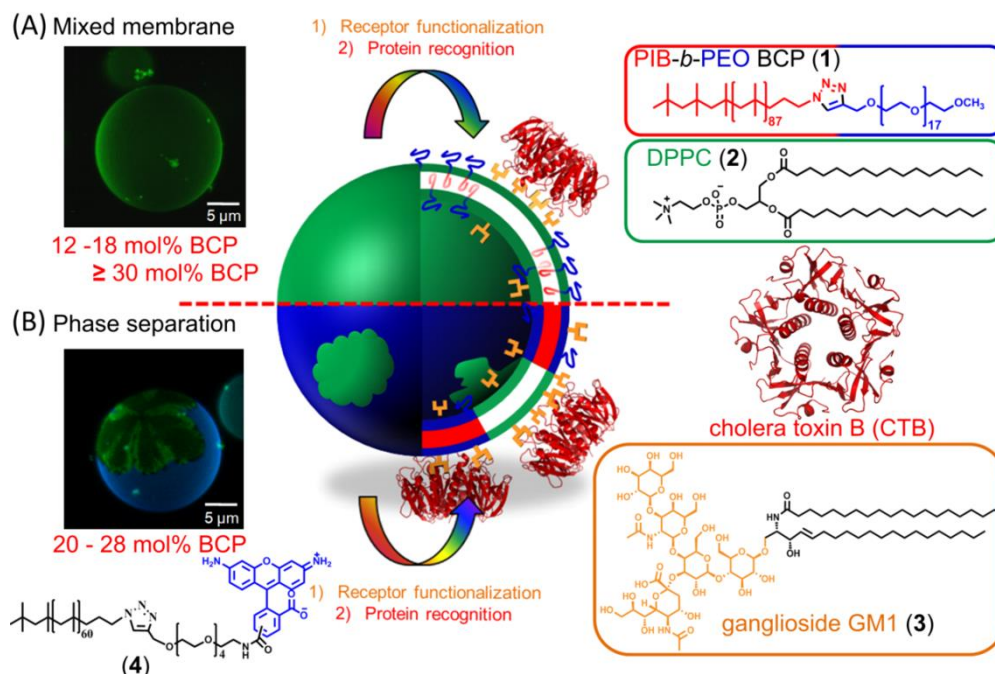


Figure 1. Binding of cholera toxin B to either mixed or phase-separated hybrid vesicles composed of DPPC (**2**) and the biocompatible PIB₈₇-*b*-PEO₁₇ block copolymer (**1**) at various lipid/BCP mixing ratios and containing ganglioside GM1 (**3**). A) Confocal microscopy image of a hybrid vesicle typical for compositions of 12 to 18 mol% and above 30 mol% of BCP **1**; Rh-DHPE as the fluorescent lipidic tracer. B) Image of a phase-separated hybrid vesicle typically obtained for compositions containing 20 to 28 mol% of BCP **1**, fluorescently labeled BCP **4** (blue), and a lipid-enriched domain (DiDC18 (green)).

RESULTS AND DISCUSSION

When the designed amphiphilic block copolymer **1** is incorporated into gel-phase vesicles of DPPC, it induces phase heterogeneities within the “hybrid vesicle membrane”^[15] that can display a two dimensional, lateral domain structure, as illustrated in Figure 1. The membrane morphology of these vesicles appears uniform at the resolution of confocal microscopy (roughly 200-300 nm) when prepared from mixtures containing less than 20 mol% and more than 28 mol% of BCP. In contrast, it is phase-separated into a patched membrane in the narrow compositional range between 20 and 28 mol% of BCP. Figure 1B shows a confocal microscopy image of such a phase-separated GUV (see also Figure 2), prepared from a mixture with 20 mol% of BCP (**1**) and 80 mol% of DPPC (**2**), where individual domains were visualized by the incorporation of the fluorescently labeled BCP **4**, which was selectively excited at $\lambda_{\text{exc}} = 488$ nm (blue region in Figure 1B), and the lipid-analogue membrane dye DiDC18 ($\lambda_{\text{exc}} = 633$ nm; green region in Figure 1B). We found that the phase separation process leads to the formation of a less-ordered polymer-enriched

phase (see Figure 2 and **appendix B**) and a lipid-enriched domain (black patch in Figure 2A, C), the latter being depleted of polymer molecules.

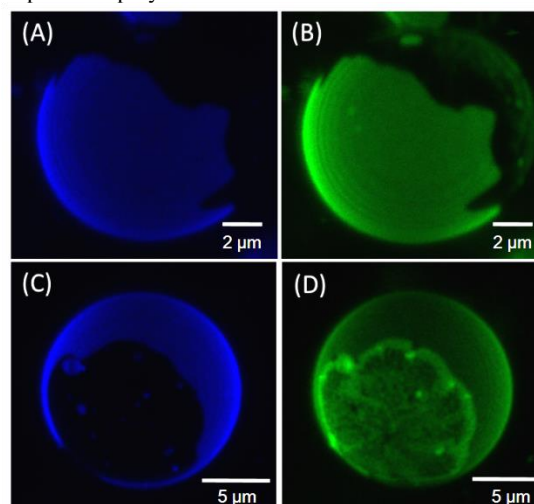


Figure 2. Confocal microscopy images of phase-separated hybrid DPPC/PIB₈₇-*b*-PEO₁₇ vesicles (20 mol% BCP **1**) visualizing phase inhomogeneities by different phase-labeling behavior of a rhodamine-labeled lipid (Rh-DHPE, panel B), the

fluorescently labeled BCP **4** (panels A and C), and DiDC18 (panel D). Panels A and C: three-dimensional reconstruction from axial stacks of a hybrid GUV using compound **4** (excited at 488 nm, in blue). Panel B: same hybrid GUV as in (A) using the Rh-DHPE dye (excited at 561 nm, in green) (preferential incorporation of the dye into the polymer-enriched phase). Panel D: same hybrid GUV as in (C) using DiDC18 as membrane dye (excited at 633 nm, in green). As reported in the literature, the lipid dye Rh-DHPE ($\lambda_{\text{exc}} = 561$ nm) is largely excluded from ordered phases in mono- and bilayer membranes (e.g., liquid condensed phases^[15, 17]).

In Figure 2B, Rh-DHPE is preferentially incorporated into the polymer-enriched phase (compare with Figure 2A) which indicates a less-ordered phase state, whereas the black patches in Figure 2A, B consist of a more-ordered DPPC-enriched phase. Additional experiments using DiDC18 ($\lambda_{\text{exc}} = 633$ nm) to visualize membrane heterogeneities in hybrid GUVs (20 mol% of BCP **1**)

showed a variable degree of enrichment of DiDC18 in the lipid-enriched phase (compare black patch in Figure 2C with 2D) supporting the assumption that this particular phase consists of a gel-like DPPC domain (ordered lipid phase).^[18a, b]

Functionalization of the hybrid vesicles by the addition of ganglioside GM1 (**3**) to the mixtures (e.g. DPPC/BCP/GM1 80:20:0.1) did not lead to changes in the respective phase state, proving that the incorporation of roughly 0.1 mol% of GM1 does not perturb the phases. Continuously varying the lipid/ BCP composition resulted in the formation of different GUV types with stable phase states. At increasing concentrations of compound **1** the lipid/BPC mixtures first formed a mixed state (12-18 mol%), then a phase-separated state (20-28 mol%), and finally another mixed state (≥ 30 mol%). These vesicles were stable over time (monitored over several hours).

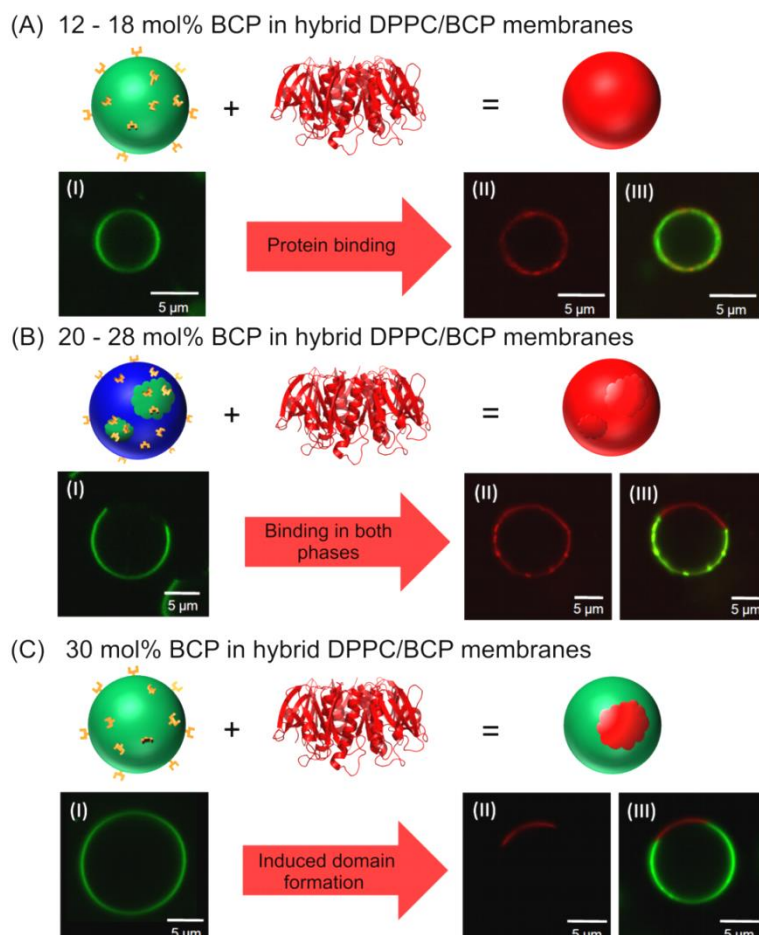


Figure 3. Effect of the hybrid membrane morphology on the protein (CTB) binding behavior; Rh-DHPE (green; excited at 561 nm) Alexa 488-labeled CTB (red; excited at 488 nm). A) Mixed DPPC/BCP membranes (12 to 18 mol% BCP **1**), before (I) and after (II, III) CTB binding. B) Mixed DPPC/BCP (1) membranes (20 mol% BCP **1**) before (compare B/I) and after CTB-binding (see B/II). C) At more than 28 mol% BCP (**1**): mixed membrane morphology (C/I) after CTB binding forms large GM1-containing lipid domains (red; see C/II). Panels A/III, B/III, and C/III are the corresponding overlay images of both dyes.

The thermally driven phase separation leads to macroscopic domain structures, which are stable over time, also suggesting a thermodynamically stable state. Subsequently, the bacterial protein cholera toxin B (CTB) binds specifically to GM1 (**3**) in a highly cooperative process, as the multivalent toxin contains five equal binding sites, each able to interact with one GM1 lipid. The binding affinity of the pentameric toxin has been reported to be about $5 \times 10^9 \text{M}^{-1}$.^[19] Upon addition of CTB (5.3 μM) to the vesicle solution (see the Supporting Information in **appendix B**), selective binding of the fluorescently labeled CTB ($\lambda_{\text{exc}} = 488 \text{ nm}$, colored in red) to the functionalized vesicle membrane occurred rapidly.

As a result, we were able to monitor the lateral distribution of the CTB-bound GM1 within the hybrid vesicle membrane (see Figure 3) depending on the lipid/BCP membrane composition. It should be noted that gel-phase vesicles composed of DPPC with 0.1 mol% of GM1 (**3**) did not exhibit the protein binding (CTB) under our experimental conditions, whereas a fluid membrane system composed of DOPC lipids ($T_m = -20^\circ\text{C}$) containing 0.1 mol% of GM1 showed uniform CTB binding over the entire GUV surface (see **appendix B**). A comparison between the membrane morphology before (visualized with Rh-DHPE; green) and after the CTB binding (Figure 3A) indicated that hybrid GUVs composed of lipid/BCP mixtures containing 12 to 18 mol% BCP display CTB binding over the entire GUV surface. In contrast, with phase-separated GUVs (DPPC/BCP/GM1 = 80:20:0.1) CTB incubation results in the recognition of both domain types by the protein, proving that the GM1 lipids are incorporated into the polymer-enriched phase as well as into the lipid-enriched domains (Figure 3B and the Supporting Information in **appendix B**). When a mixture of DPPC/BCP/GM1 (70:30:0.1) was used, which generated GUVs with a mixed membrane morphology, the morphology changed significantly upon addition of CTB.

Within minutes after protein incubation, protein binding and the formation of large GM1-enriched lipid domains was observed (Figure 3C/I before and 3 C/II after addition of CTB), indicating lateral reorganization during the binding process between CTB and GM1. The kinetics of this phenomenon was fast, taking place within minutes. Thus, we conclude that the highly cooperative binding of the multivalent CTB in the case of hybrid GUVs with 30 mol% BCP leads to the formation of a more ordered GM1-enriched lipid domain, which segregates from the surrounding hybrid bilayer.^[20] The fact that we observed only one or at most a few macroscopic domains per vesicle over several hours

rather than many small domains reflects the thermodynamic stability of the vesicles. At a vesicle composition of around 40 mol% of BCP and above in mixtures with DPPC, the obtained hybrid vesicles containing 0.1 mol% of GM1 (**3**) showed no protein binding to the receptor-functionalized GUV membrane. This is probably due to steric hindrance caused by the long PEO chains of the BCPs (17 ethylene oxide units per BCP). At higher BCP content, the PEO chains appear to form a polymer brush, which blocks the receptor from binding CTB.

At a vesicle composition of around 40 mol% of BCP and above in mixtures with DPPC, the obtained hybrid vesicles containing 0.1 mol% of GM1 (**3**) showed no protein binding to the receptor-functionalized GUV membrane. This is probably due to steric hindrance caused by the long PEO chains of the BCPs (17 ethylene oxide units per BCP). At higher BCP content, the PEO chains appear to form a polymer brush, which blocks the receptor from binding CTB.

Next, we tried to determine the effect of the lipid/BCP composition and the resulting lateral mobility in the membrane on the recognition between CTB and GM1. These vesicles showed different lateral distributions of the membrane-bound CTB when the lipid/BCP composition was varied.

To this end, lateral diffusion processes within unmodified hybrid DPPC/PIB_{87-b}-PEO₁₇ membranes were investigated by FRAP (fluorescence recovery after photobleaching) and FCS (fluorescence correlation spectroscopy) measurements.^[21, 22] Rh-DHPE served as a membrane dye since it should be localized in the more disordered phases in the hybrid membranes.

These techniques (see **appendix B**) provided information about the dynamics in DPPC as well as in hybrid membranes and revealed the effect of incorporated BCP molecules on the organization of the lipid membrane (see Figure 4). For a better understanding of the membrane dynamics in hybrid membranes, we first performed the lateral diffusion analysis of pure DPPC membranes by FRAP (Figure 4A). An irreversible bleaching of the irradiated membrane region was observed, confirming the gel-phase state of the liposomal bilayer at room temperature (which is below the T_m of 41.6°C). In contrast to the high rigidity of pure DPPC bilayers at room temperature, hybrid membranes exhibited a clear increase in the lateral diffusion, which was evident from the faster recovery rates with increasing polymer amounts (see Figure 4A and the Supporting Information in **appendix B**).

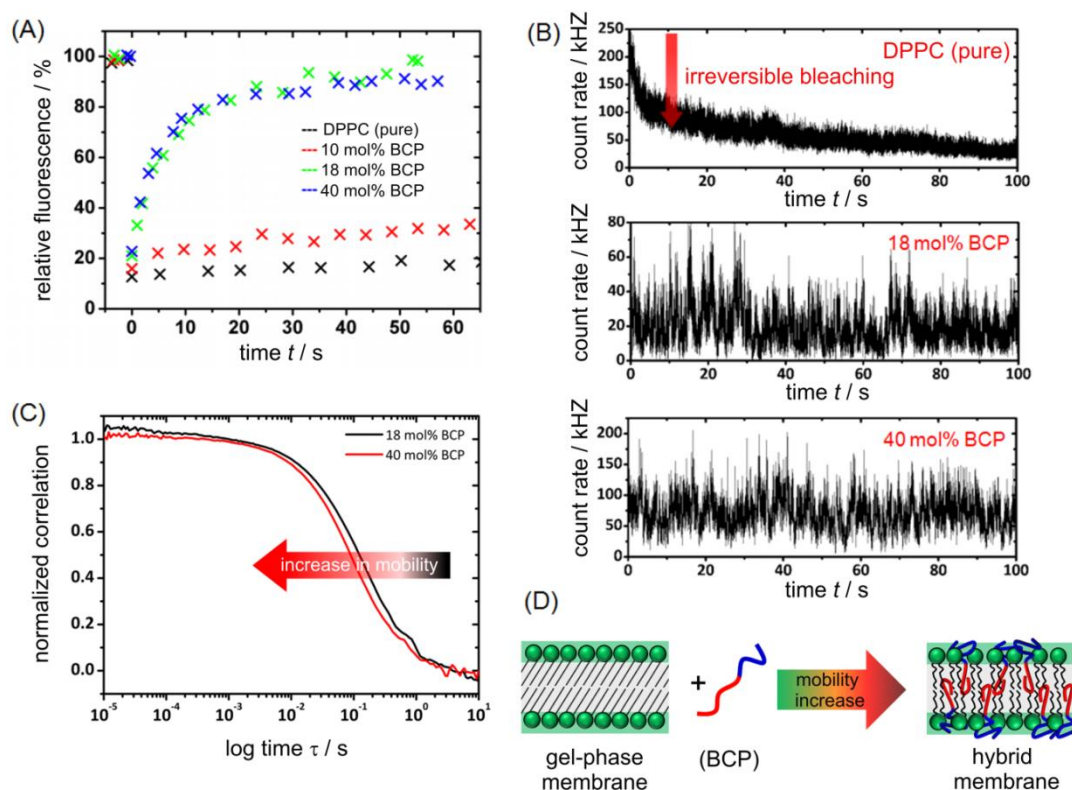


Figure 4. Membrane mobility analysis of Rh-DHPE-labeled DPPC and hybrid membranes by FRAP and FCS measurements for BCP contents ranging from 0 to 40 mol%. A) Normalized fluorescence versus time, recorded during FRAP experiments. At low or zero BCP content (black curve), little fluorescence recovery has occurred in the bleached area after 1 min. At 18 mol% (green curve) and 40 mol% of BCP (blue curve), the recovery has a half-time of roughly 4 s and is almost complete after 1 min. B) Fluorescence intensity traces obtained on pure DPPC and hybrid vesicle membranes with 18 mol% and 40 mol% BCP **1**. C) Fluorescence autocorrelation functions for selected mixtures using 18 mol% (black) and 40 mol% BCP (red). The lateral mobility increases with increasing polymer content because of the incorporated BCP molecules breaking up the rigid lipid packing in the DPPC membranes, as depicted schematically in (D).

Indeed, our experimental FRAP results show that the incorporation of amphiphilic BCPs into gel-phase DPPC membranes strongly affects the lipid organization, shifting it to a more mobile system.

A more detailed picture of membrane dynamics and organization is given by FCS.^[22, 23] In an FCS experiment, fluctuations in fluorescence intensity observed for a defined detection volume report on the diffusion of labeled membrane molecules within the plane of the membrane. Autocorrelation analysis of the monitored fluctuations in the fluorescence time traces (Figure 4B) yields information about the diffusion times (τ_D) and the corresponding diffusion coefficients (D), which are characteristic of each selected membrane composition.

FCS analysis of pure DPPC membranes confirms the results obtained by FRAP. Figure 4B (top) presents a typical fluorescence intensity trace from pure DPPC membranes; a rapid decrease in the fluorescent intensity due to bleaching is observed, indicating a very low lateral mobility of the fluorescent dye which cannot be analyzed by standard FCS models.

Significantly different results were obtained with the hybrid membranes. The fluctuating signal in the

fluorescence traces obtained from samples prepared with 18 mol% and 40 mol% BCP (Figure 4B) indicated that the molecular mobility in the mixed membranes is significantly higher and enabled the analysis of the autocorrelation curves (see Figure 4C). Differences between the correlation curves are significant and prove that the hybrid membrane sample with 40 mol% BCP (red curve) has shorter diffusion times ($\tau_D = (89.5 \pm 2.5)$ ms; $D = 1.6 \times 10^{-13} \text{ m}^2\text{s}^{-1}$), corresponding to a higher lateral mobility of the membrane components. For the sample with 18 mol% BCP, we determined a diffusion time of (120 ± 10) ms ($D = 1.2 \times 10^{-13} \text{ m}^2\text{s}^{-1}$). As depicted schematically in Figure 4D, the incorporation of amphiphilic PIB₈₇-*b*-PEO₁₇ (**1**) into gel-phase membranes of DPPC leads to a disorder of the lipid bilayer caused by the BCP molecules. As a consequence, the lateral mobility is much greater than that in pure DPPC bilayers.

CONCLUSION

In conclusion, the lipid/BCP composition of hybrid GUVs and their resulting morphologies play a significant role in the successful binding of cholera toxin B to the receptor-functionalized vesicle surfaces. The interplay

between CTB binding and reorganization of the hybrid membrane is highlighted by the observation of GM1-enriched lipid domains in hybrid vesicles containing 30 mol% BCP. This lipid/BCP composition is particularly interesting in view of the phase-specific binding of membrane proteins to receptor functionalized hybrid vesicle surfaces, which combine the features of polymer membranes and liposomes. Furthermore, the successful protein recognition on mixed as well as phase-separated membrane morphologies demonstrates the high biofunctionality of our system. Such hybrid membrane systems can serve as biomimetic models to understand biological receptor/ligand recognition on hybrid vesicles, which can be fine-tuned in their lateral organization and mobility by varying the lipid/BCP composition.

EXPERIMENTAL SECTION

Materials and methods used for this study are given in the Supporting Information (**appendix B**). Furthermore, the novel synthesis of the fluorescently labeled PIB-*b*-PEO BCP (**4**) and the procedure of the protein binding studies are given in the Supporting Information.

Hybrid DPPC (**2**)/PIB-PEO BCP (**1**) giant unilamellar vesicles (GUVs) were prepared as described previously^[15] using an electroformation method.^[24] For the visualization of the resulting hybrid GUVs and their membrane heterogeneities, different membrane dyes (DiDC18, Rh-DHPE, fluorescently labeled diblock copolymer **4**) were added to the initial mixture at a total amount of 0.5 mol%. For the surface functionalization of mixed DPPC/PIB-PEO BCP (**1**) membranes with ganglioside GM1 molecules, all lipid/polymer mixtures of various compositions were additionally mixed with 0.1 mol% of GM1. The lipid/polymer mixtures containing 0.1 mol% of GM1 were prepared in chloroform, dried under a continuous N₂ stream, and dissolved in a defined solvent volume to reach a total concentration of 10 mgmL⁻¹. The final mixtures were used to generate a homogenous thin film on optically transparent indium-tin-oxide (ITO)-coated coverslips using a spin-coating method. After the preparation of the thin films on two coverslips (electrodes), the coverslips were placed in a capacitor-type configuration with a separation of 2 mm using a home-built flow-chamber. The flow chamber was filled with a sucrose solution (96 mosmolL⁻¹). The conditions for the electroformation process were applied as reported previously.^[15]

All binding studies between cholera toxin B and GM1-modified liposomal (DPPC or DOPC) or hybrid membranes composed of DPPC and BCP **1** were conducted at room temperature (20°C) using CTB (5 mg) dissolved in a sucrose solution (ca. 100 mL). The dilute solutions of CTB were prepared immediately prior to use. After the electroformation process, the prepared GUVs

with incorporated GM1 receptor molecules were first cooled down to room temperature and then monitored by laser scanning microscopy, which revealed changes in the membrane morphologies. Subsequently, GUVs were treated with the protein solution. The CTB solutions were injected into the flow chamber, which contained the freshly prepared GUVs, using a microsyringe. All experiments were performed with the fluorescently labeled cholera toxin.

ACKNOWLEDGEMENTS

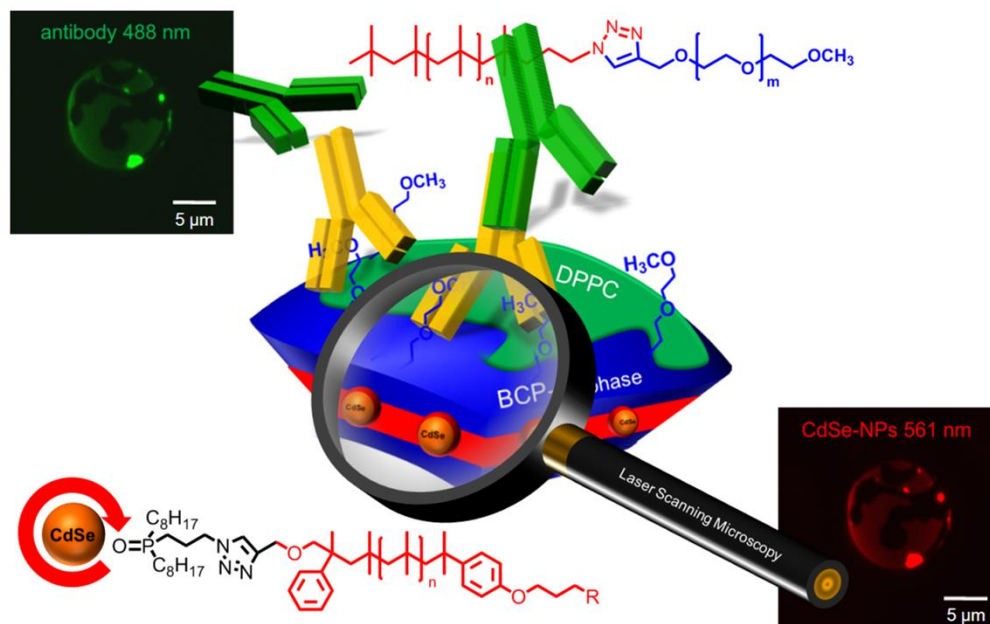
This work was supported financially by the Deutsche Forschungsgemeinschaft (grant BI 1337/6-1 (W.H.B., M.S.) within the Forschergruppe FOR-1145; grants DFG INST 271/249-1, INST 271/ 247-1, INST 271/248-1 (W.H.B.)), the BMBF (ZIK HALOmEm, FKZ 03Z2HN22 (K.B., S.W.)), and ERDF (grant 1241090001).

REFERENCES

- [1] T. Kunitake, *Physical Chemistry of Biological Interfaces* (Eds.: A. Baszkin, W. Norde), Marcel Dekker, New York, **2000**, p. 283.
- [2] W. H. Binder, V. Barragan, F. M. Menger, *Angew. Chem.* **2003**, 115, 5980; *Angew. Chem. Int. Ed.* **2003**, 42, 5802.
- [3] D. E. Discher, A. Eisenberg, *Science* **2002**, 297, 967.
- [4] V. Malinova, S. Belegriou, D. de Bruyn Ouboter, W. Meier, *Adv. Polym. Sci.*, Springer Berlin/ Heidelberg, **2011**.
- [5] M. Schulz, A. Olubummo, W. H. Binder, *Soft Matter* **2012**, 8, 4849.
- [6] W. H. Binder, *Angew. Chem.* 2008, 120, 3136; *Angew. Chem. Int. Ed.* **2008**, 47, 3092.
- [7] K. Simons, E. Ikonen, *Nature* **1997**, 387, 569.
- [8] K. Simons, E. Ikonen, *Science* **2000**, 290, 1721.
- [9] C. LoPresti, M. Massignani, C. Fernyhough, A. Blanazs, A. J. Ryan, J. Madsen, N. J. Warren, S. P. Armes, A. L. Lewis, S. Chirasatitsin, A. J. Engler, G. Battaglia, *ACS Nano* **2011**, 5, 1775.
- [10] L. Luo, A. Eisenberg, *Angew. Chem.* 2002, 114, 1043; *Angew. Chem. Int. Ed.* **2002**, 41, 1001.
- [11] D. E. Discher, D. A. Christian, A. Tian, W. G. Ellenbroek, I. Levental, K. Rajagopal, P. A. Janmey, A. J. Liu, T. Baumgart, *Nat. Mater.* **2009**, 8, 843.
- [12] A. Olubummo, M. Schulz, B.-D. Lechner, P. Scholtyssek, K. Bacia, A. Blume, J. Kressler, W. H. Binder, *ASC Nano* **2012**, 6, 8713.
- [13] W. Meier, T. Ruyschaert, A. F. P. Sonnen, T. Haefele, M. Winterhalter, D. Fournier, *J. Am. Chem. Soc.* **2005**, 127, 6242.
- [14] J. Nam, P. A. Beales, T. K. Vanderlick, *Langmuir* **2011**, 27, 1.

- [15] M. Schulz, D. Glatte, A. Meister, P. Scholtyssek, A. Kerth, A. Blume, K. Bacia, W. H. Binder, *Soft Matter* **2011**, 7, 8100.
- [16] M. Chemin, P.-M. Brun, S. Lecommandoux, O. Sandre, J.-F. Le Meins, *Soft Matter* **2012**, 8, 2867.
- [17] M. Dyck, M. Lęsche, *J. Phys. Chem. B* **2006**, 110, 22143.
- [18] a) J. Korlach, P. Schwille, W. W. Webb, G. W. Feigenson, *Proc. Natl. Acad. Sci. USA* **1999**, 96, 8461; b) C. H. Spink, M. D. Yeager, G.W. Feigenson, *Biochim. Biophys. Acta* **1990**, 1023, 25.
- [19] S. Lauer, B. Goldstein, R. L. Nolan, J. P. Nolan, *Biochemistry* **2002**, 41, 1742.
- [20] A. T. Hammond, F. A. Heberle, T. Baumgart, D. Holowka, B. Baird, G.W. Feigenson, *Proc. Natl. Acad. Sci. USA* **2005**, 102, 6320.
- [21] K. Bacia, D. Scherfeld, N. Kahya, P. Schwille, *Biophys. J.* **2004**, 87, 1034.
- [22] K. Bacia, P. Schwille, *Methods Mol. Biol.* **2007**, 398, 73.
- [23] K. Bacia, P. Schwille, T. Kurzchalia, *Proc. Natl. Acad. Sci. USA* **2005**, 102, 3272.
- [24] The electroformation method was originally reported by Angelova et al.: M. I. Angelova, D. S. Dimitrov, *Faraday Discuss. Chem. Soc.* **1986**, 81, 303.

3. Lateral surface engineering of hybrid lipid/BCP vesicles and selective nanoparticle embedding



ABSTRACT: Bio-inspired recognition between macromolecules and antibodies can be used to reveal the location of amphiphilic block copolymers (BCPs) in model biomembranes and their subsequent scaffolding with nanoparticles (NPs). Potential applications of this novel class of lipid/BCP membranes require an understanding of their compositional heterogeneities with a variety of different molecules including natural proteins or synthetic NPs, whose selective incorporation into a specific part of phase separated membranes serves as a model system for the targeted delivery of therapeutics. We demonstrate the selective incorporation of polymer-functionalized CdSe NPs into the polymer-rich domains in vesicular hybrid membranes using 1,2-dipalmitoyl-*sn*-glycero-3-phosphocholine (DPPC, $T_m = 41^\circ\text{C}$) or 1,2-dioleoyl-*sn*-glycero-3-phosphocholine (DOPC, $T_m = -20^\circ\text{C}$) as the lipid component. Furthermore, we demonstrate a novel method to detect PIB-PEO based amphiphilic BCPs on liposomal surfaces by a PEO binding antibody (anti-PEO). As a result, hybrid membrane morphologies, which depend on the lipid/BCP composition, are selectively monitored and engineered.

INTRODUCTION

When synthetic polymers or nanoparticles interact with lipid membranes, the final morphology is strongly determined by the charge, composition and size of the interacting components,¹⁻³ which in turn can induce phase separation phenomena. Hybrid lipid/polymer membranes, as recently reported,⁴⁻⁶ are of great interest due to their promising applications as drug- and gene-delivery systems. The blending of phospholipids and block copolymers to form hybrid membranes could offer new technical applications in pharmaceutical or biomedical fields, where it is of particular interest to combine the biofunctionality of liposomes with the tremendous mechanical stability and functional variability of polymersomes membranes.^{7, 8} To achieve the application of such hybrid systems utilizing their combined benefits, it is essential to investigate their biocompatibility, their phase behavior and stability as well as the interaction

behavior of these hybrid membranes with biological membrane components (e.g. with proteins and glycolipids)^{9, 10} or biocompatible, surface-modified nanoparticles.^{11, 12} The concept of phase-separated membranes (domains or rafts)^{1, 2, 13, 14} can be used in mimicking biological membrane processes by exploiting interactions of lipid/BCP membrane morphologies with natural or synthetic nanomaterials (e.g. quantum dots), which can selectively interact with specific domains depending on their surface coverage and functionality. Controlling the localization of preformed nanoparticles in amphiphilic block copolymers or lipid composites which are prepared by self-assembly in selected solvents have invoked significant interest of numerous research groups due to the potential application in medicine.¹⁵⁻²³

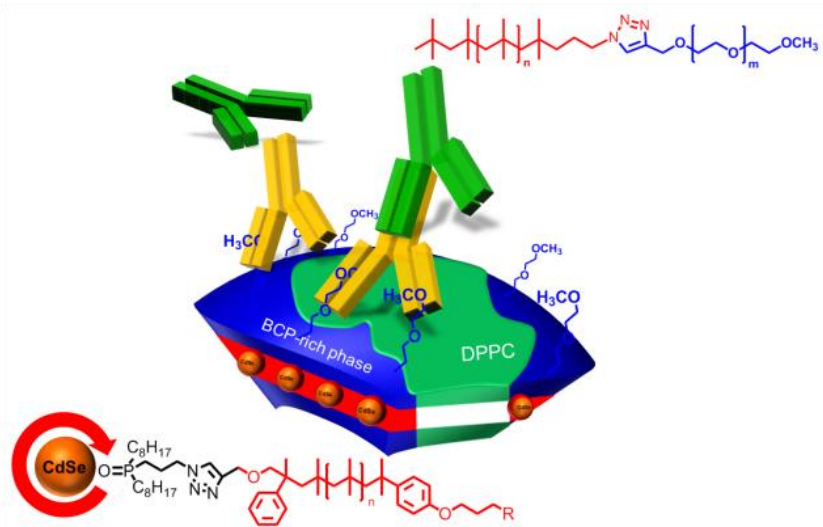
In lipid vesicles, nanoparticles can be selectively located within the aqueous vesicle core^{16, 24} or within the hydrophobic lipid bilayer interior,^{17, 22, 25, 26} by functionalizing the nanoparticles either with hydrophobic

or hydrophilic moieties. In polymersomes, Eisenberg *et al.*²⁰ demonstrated that coating of the nanoparticles with diblock copolymers similar in structure to that of the vesicle membrane-core, allows the particles to be preferentially localized in the central portion of the membrane wall. Another strategy to selectively localize surface-engineered nanoparticles in polymersomes involves the co-assembly of nanoparticles with the block copolymer in solution during the process of polymersome formation, as shown by Binder¹⁶ and Lecommandoux *et al.*,²⁷ who generated a well defined vesicular structure where the hydrophobic or hydrophilic nanoparticles were located in the membrane interior or within the hydrophilic vesicle cavity.

By mixing both lipid and polymer constituents, mixed lipid/polymer vesicles can be generated,^{6, 5} which represent biocompatible hybrid vesicles, *e.g.* composed of DPPC and biocompatible PIB-PEO based block copolymers. Similar to domain-formation^{1, 2, 13, 14} in lipid vesicles the structure of the lateral surface is important for future applications, therefore requiring tools to engineer the lateral phase separation on mixed vesicles. One way to control the lateral phases in *e.g.* DPPC/PIB₈₇-*b*-PEO₁₇ BCP vesicles is achieved by varying the composition of the hybrid membrane. When an amphiphilic block copolymer (PIB-PEO) is incorporated into gel-phase vesicles made from DPPC in amounts ranging from 20 to 28 mol% of the BCP, phase heterogeneities within the hybrid membrane are induced, forming a two-dimensional lateral domain structure. However, the membrane morphologies of hybrid vesicles appear uniform on length scales above the optical resolution of confocal microscopy (roughly 200-300 nm) when prepared with less than 20 mol% or more than 28

mol% of the respective BCP. Similar examples⁴ demonstrating membrane homo- and heterogeneities in hybrid vesicles from a poly(dimethylsiloxane)-*graft*-poly(ethylene oxide) copolymer in mixture with either DPPC or POPC have been reported, where mixtures of 50 mol% of the polymer and POPC formed hybrid vesicles with domains, which separated into pure liposomes and polymersomes with time (vesicle budding and fission). A second approach to control lateral phase segregation is possible by applying an external driving force, where a cross-linking process of membrane constituents on the hybrid vesicle surface leads to the formation of large domains,⁶ *e.g.* by crosslinking with the multivalent protein NeutrAvidin binding to either biotinylated lipid or copolymer molecules. An additional control of demixing of lipid-rich domains from polymer-rich phases in vesicle membranes is provided by thermally driven phase separation and inclusion of cholesterol.²⁸ Herein, the control of domain size and shape was achieved by varying the cooling rate and membrane composition, respectively.

We have recently shown¹¹ that the localization of nanoparticles can be selectively controlled in mixed 1,2-dipalmitoyl-*sn*-glycero-3-phosphocholine and PIB₈₇-*b*-PEO₁₇ monolayers at the air/water interface by specifically engineering the nanoparticle surfaces with polymer ligands. Preferential incorporation of NPs can be the result of forming PIB brushes on the nanoparticle surfaces, which leads to the specific interaction of the PIB-covered particles with the BCPs within the phase-segregated hybrid membrane. A similar approach was reported by Eisenberg *et al.* demonstrating selective particle localization in case of polymersomes with specifically polymer-covered Au-NPs.²⁰



Scheme 1. Schematic representation of the selective incorporation of CdSe NPs into the polymer-rich domains of phase separated hybrid DPPC/BCP vesicles proving membrane heterogeneities by antibody-mediated monitoring of BCP molecules.

In this paper, we demonstrate a method to detect compositional membrane heterogeneities of hybrid lipid/BCP vesicles *via* a bio-inspired recognition between antibodies and membrane incorporated BCPs (see Scheme 1). As a result, we are able to specifically monitor the BCP molecules within the membrane by PEO binding antibodies (anti-PEO) thus detecting the phase state in laterally mixed or laterally demixed membranes. PIB₈₇-*b*-PEO₁₇ BCP, well known to incorporate into DPPC membranes, showed significant effects on the lipid phase behavior and control of receptor/protein recognition processes.^{5, 9} In order to understand the role of the membrane fluidity on the lipid/BCP mixing behavior, we studied mixtures of the BCP with either DPPC ($T_m = 41.6^\circ\text{C}$) or with DOPC ($T_m = -20^\circ\text{C}$), *i.e.* two phospholipids which form membranes in the gel state or fluid state at room temperature, respectively. Control of membrane heterogeneities by the lipid/BCP composition were proved by the PEO-binding antibodies, which showed significant differences in the phase labeling behavior compared to the commonly used Rh-DHPE membrane dye. The selective labeling of BCPs within the hybrid membrane showed the formation of polymer-rich domains and revealed further small heterogeneities in apparently uniform vesicular membranes which were not detected by Rh-DHPE. Furthermore, we were able to demonstrate the selective incorporation of hydrophobic PIB-covered CdSe NPs into either hybrid DPPC/BCP or DOPC/BCP bilayers in the phase separated and non-phase separated case.

EXPERIMENTAL PART

MATERIALS

The diblock copolymer (PIB₈₇-*b*-PEO₁₇) with a polydispersity ($\text{PDI} \leq 1.2$), used in this study, was synthesized in our laboratories *via* a combination of a living carbocationic polymerization method and the approach of the azide/alkyne-“click”-reaction, as reported previously.⁵ The hydrophobic PIB-covered CdSe nanoparticles were synthesized and labeled with rhodamine B according to a previously published procedure.¹¹ 1,2-Dipalmitoyl-*sn*-glycero-3-phosphocholine (DPPC, $M = 734.05 \text{ g/mol}$) and 1,2-dioleoyl-*sn*-glycero-3-phosphocholine (DOPC, $M = 786.11 \text{ g/mol}$) were purchased from *Avanti Polar Lipids* (*Alabaster*; *AL*, USA). The fluorescence dyes used in this study for imaging experiments, 1,1'-dioctadecyl-3,3,3',3'-tetramethylindodicarbocyanine perchlorate (DiDC18; $M = 959.92 \text{ g/mol}$) and 1,2-dihexadecanoyl-*sn*-glycero-3-phosphoethanolamine-N-(lissaminerhodamine B sulfonyl) (Rh-DHPE, $M = 1267.68$) were purchased from *Invitrogen* (*Karlsruhe*, Germany) and used without further purifications. The fluorescently labeled diblock copolymer dye (PIB₆₀-*b*-PEO₄-fluor488) ($\lambda_{\text{max}} = 488\text{nm/excitation}$) was prepared as previously described⁹ and used to label the polymer-rich phase as a comparison to the antibody-mediated monitoring of the BCPs.

Antibodies (anti-PEO and secondary antibody).

Monoclonal rabbit IgG antibody (Ab) against PEO recognizing the methoxy-terminated poly(ethylene oxide) (PEG-RabMAb) was purchased from *EPITOMICS* (*Burlingame*, *CA*, USA) and used for the PEO binding experiments. A polyclonal goat anti-rabbit secondary IgG Ab covalently labeled with Dylight 488 dye ($\lambda_{\text{max}} = 494 \text{ nm/excitation}$) was purchased from *EPITOMICS* (*Burlingame*, *CA*, USA). The secondary Ab specifically recognizes the anti-PEO, which allows the monitoring of the PIB-PEO based BCP molecules within the hybrid membrane by confocal laser scanning microscopy using an excitation wave length of 488 nm.

METHODS

Hybrid lipid/BCP vesicle formation.

The formation of hybrid lipid/BCP giant unilamellar vesicles (GUVs) was obtained as described previously⁵ based on an electroformation method reported by Angelova *et al.*²⁹ Water, which was used for the study, was purified using a *Purelab Option system* (*ELGA Ltd.*, *Celle*, Germany), yielding ultra-pure water. Lipid and polymer were mixed at the indicated mixtures in chloroform (HPLC grade, *Sigma Aldrich* (*Schnelldorf*, Germany)). For the purpose of visualization of the resulting hybrid GUVs and observed membrane heterogeneities (phase separation phenomena), different membrane dyes (DiDC18, Rh-DHPE or labeled di-BCPs) were added to the initial mixture with a total amount of 0.5 mol%. All experiments demonstrating the selective incorporation of hydrophobic CdSe-NPs into phase separated hybrid membranes were performed with a molar nanoparticle to lipid ratio of 1 to 1500 to ensure the stability of the resulting vesicles over time. Higher nanoparticle loadings (NP/lipid of 1/1000 and above) destroyed the hybrid vesicles.

Binding studies (anti-PEO and secondary antibody incubation).

All binding studies between PEO binding Abs and hybrid membranes consisting of either DPPC or DOPC with incorporated PIB-*b*-PEO copolymers were conducted at room temperature (20°C). A dilution of anti-PEO ($5\mu\text{L}$; 1mg/mL in buffer) in $100 \mu\text{L}$ water was prepared freshly before each usage. After the electroformation process, the GUVs with incorporated BCP molecules were first cooled down to room temperature. Changes in their membrane morphology were monitored by confocal laser scanning microscopy. Afterwards, using a microsyringe, $100 \mu\text{L}$ of the anti-PEO solution was injected into the flow chamber, which contained the freshly prepared GUVs. After 1 hour incubation with the primary Ab (anti-PEO), the vesicle solution was carefully washed by rinsing the flow chamber with water to remove excess of free primary Ab. Subsequently, the fluorescently labeled anti-rabbit secondary Ab ($5\mu\text{L}$, 1mg/mL in PBS) was diluted in 100

μL (water) and injected into the flow chamber. The recognition process was followed by laser scanning microscopy.

Vesicle analysis by laser scanning microscopy (LSM).

Confocal microscopy images were obtained on a commercial confocal laser scanning microscope – LSM 710 ConfoCor 3 (Carl-Zeiss, Germany) using a C-Apochromat 40x/1.2 N.A. water immersion objective. Lipophilic carbocyanine DiDC18 was used as a membrane dye and was excited with a HeNe laser at 633 nm. Rh-DHPE, a head group-labeled lipid, was also used to monitor membrane heterogeneities in hybrid vesicles, which was excited with a DPSS-laser at 561 nm. The binding of anti-PEO to the hybrid vesicle surfaces was monitored by the green-labeled secondary antibody, which recognizes the primary Ab, using the 488 nm laser line of an Argon-Ion laser. The fluorescently labeled di-BCP dye (PIB₆₀-*b*-PEO₄-fluor488) was also excited at 488 nm using the Argon-Ion laser. The hydrophobically modified CdSe NPs, which were fluorescently labeled with rhodamine B (see Fig. S1 in **appendix C**), were excited with a DPSS laser at 561 nm. All GUV imaging studies, *i.e.* the monitoring of phase heterogeneities by antibody binding as well as the selective incorporation of NPs into the hybrid lipid/BCP membranes, were performed after cooling to room temperature (20°C) unless otherwise stated.

RESULTS AND DISCUSSION

Identification of phases in hybrid membranes from DPPC/BCP mixtures

As known from previous investigations, the incorporation of the amphiphilic PIB-PEO BCPs into DPPC vesicles^{5,9} results in the formation of hybrid lipid/BCP membranes. Varying the molar composition of such membranes (DPPC/BCP-ratio) a two-dimensional domain morphology showing either uniform membranes or laterally phase segregated structures is observed, however without assignment of the phases to the respective component. As the recognition functionality and specificity of antibodies can be applied towards selective molecule targeting we focused on a novel method to selectively detect the incorporated PIB-PEO based BCPs and the resulting morphologies *via* a PEO-recognizing antibody system. A PEO-binding rabbit IgG monoclonal antibody and a secondary polyclonal goat anti-rabbit IgG antibody were selected, covalently labeled with a green-fluorescent dye (Dylight 488 dye) to enable a detection of compositional membrane heterogeneities in lipid/BCP GUVs directly by confocal microscopy.³⁰ This antibody is highly specific for the PEO-chain of the respective BCP, thus allowing differentiation of the PEO-part within the mixed hybrid lipid/BCP membranes.

Figure 1 shows confocal microscopy images of a phase separated vesicle obtained from mixtures of DPPC with 24 mol% of BCP. As visible by the selective antibody binding, we observed a polymer-rich phase (see Figure 1, green channel) and macroscopic DPPC-rich domains (black patch in Figure 1A).

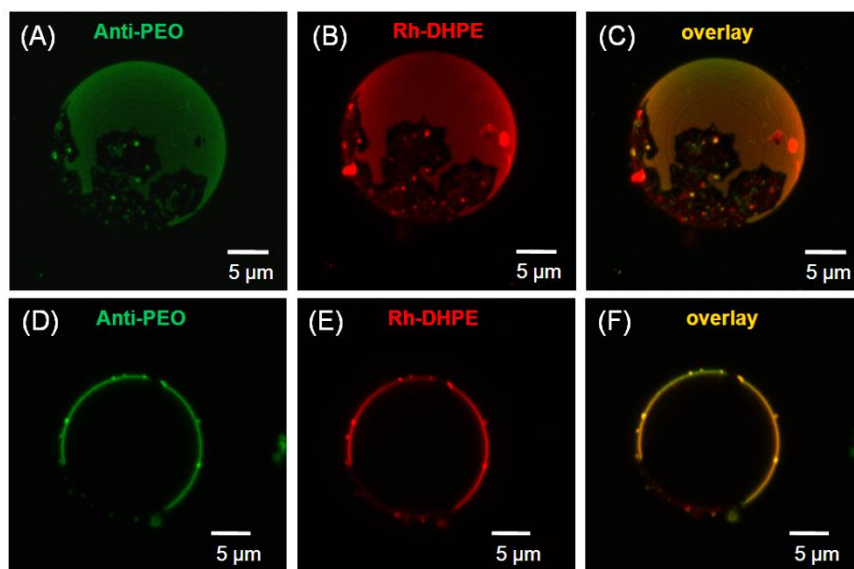


Figure 1. Confocal microscopy images of hybrid GUVs prepared from a mixture of DPPC with 24 mol% of BCP demonstrating the antibody-mediated proof of phase separated membrane morphologies. (A-C) 3D-reconstruction of an axial series of confocal slices from a phase separated vesicle typical for this lipid/BCP composition. Antibody monitoring (green area in panel A and D, excited at 488 nm) indicates the polymer-rich phase. (D-F) Single GUV slice images near the vesicle equator, same vesicle as shown in (A-C), proving the partitioning behavior of the Rh-DHPE dye (red area in panel B and E, excited at 561 nm) compared to the antibody labeled BCP molecules (D). Panel (C) and (D) Overlay images of both dyes.

Recognition of the BCPs chains by the antibody thus proves⁹ that the Rh-DHPE is preferentially incorporated into the polymer-rich phase (compare green with red channel in Figure 1) being largely expelled from the highly ordered DPPC-domains (see also **appendix C** Figure S5). When the DPPC-lipid constituted the major

component in mixture with the BCP in amounts up to 10 mol%, the obtained hybrid vesicles showed a faceted surface with a uniform fluorescence of the Rh-DHPE dye within the membrane (see Figure S3 in **appendix C**, red channel).

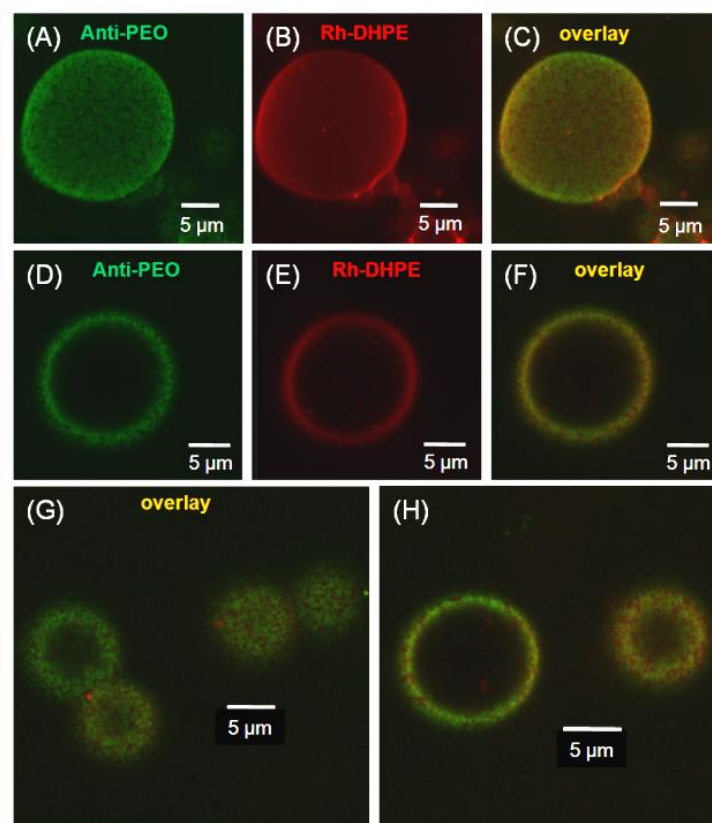
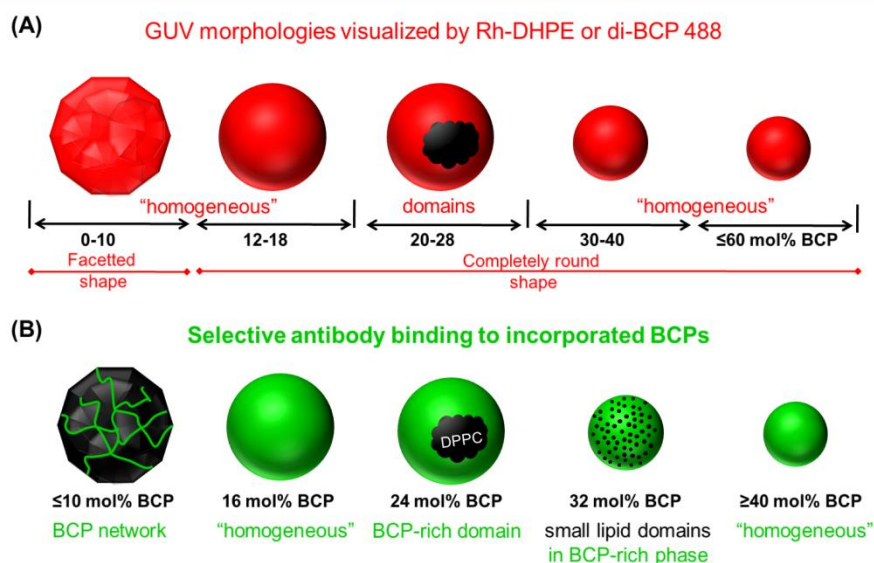


Figure 2. Confocal microscopy images of hybrid GUVs from a mixture of DPPC with 32 mol% of BCP, monitoring membrane heterogeneities *via* antibody-mediated detection of membrane incorporated BCPs (antibody: green areas in panel A and D) in contrast to the uniform fluorescence of Rh-DHPE (visualized in red, see panel B and E). (A-C) 3D-reconstruction of an axial series of confocal slices from a typical vesicle obtained for this lipid/BCP composition. (D-F) Images of a GUV near the vesicle equator (G, H). Overlay images of GUVs, showing the small heterogeneities.

The specific BCP recognition by the antibody revealed a network-like morphology of the incorporated BCP molecules (see green channel in Figure S3, **appendix C**), assuming that the gel-phase state of the DPPC bilayer at room temperature leads to macroscopic lipid-rich islands with a high conformational order, surrounded by squeezed out BCP molecules. Upon cooling, the vesicular hybrid membrane undergoes a phase transition from a fluid (above $T_m = 41.6^\circ\text{C}$ of DPPC) to a highly rigid state. Thus, the low amount of incorporated BCPs (< 10 mol%) is not sufficient to prevent the formation of the gel-phase state (as previously proven by FRAP- and FCS-measurements)⁹ – as a result the BCP chains are expelled from the highly ordered DPPC islands concentrating at the edges of these areas. Higher polymer contents (above 12 mol% BCP) showed completely round and smooth vesicle morphologies, hybrid vesicles from mixtures of DPPC with 16 mol% of BCP demonstrated a uniform

distribution of polymers within the hybrid membrane, as shown by the homogeneous binding of antibodies (Figure S4 in **appendix C**). Both uniform fluorescent signals of the labeled antibody and Rh-DHPE (green and red channel, respectively) prove the mixed state of the DPPC/BCP bilayer.

Monitoring the phase state of hybrid vesicles in mixture with 32 mol% of BCP by antibody-binding, small black domains within the hybrid membrane were observed, demonstrating an inhomogeneous distribution of the lipid and polymer molecules (see Figure 2). By comparing the red channel in Figure 2B (showing the uniform fluorescence signal of the Rh-DHPE dye) with the fluorescence signal from the PEO-binding antibody system (Figure 2A), the small heterogeneities (black spots in Figure 2A) can be assigned to DPPC-enriched domains.



Scheme 2. Schematic overview of the apparent hybrid membrane morphologies visualized by (A) the commonly used membrane dye Rh-DHPE and the labeled di-BCP (PIB₅₇-*b*-PEO₄-fluoro 488) compared to the selective binding of the membrane incorporated BCPs by the PEO-binding antibody system (B).

In contrast to Rh-DHPE, the selective BCP-recognition by antibodies revealed clearly a phase separated membrane morphology, as depicted in the overlay images of Figure 2C, 2G and H. Thus, Rh-DHPE is limited in detecting mixing/demixing phenomena in hybrid lipid/polymer membranes and the potential fine tune of such morphologies is impossible, whereas the antibody-binding allows a significantly finer monitoring of membrane heterogeneities. It can however not be excluded that the antibody is responsible for a local segregation of the BCPs due to the multivalent interactions of the antibody with polymer molecules.

Vesicles containing more than 40 mol% of the BCP again show a uniform morphology. No domains could be observed considering the optical resolution limit of the microscope (see Figure S6 in the **appendix C**). Both the fluorescence of the Rh-DHPE dye and of the fluorescently labeled antibody (binding to incorporated BCPs) indicate a random lateral distribution of the lipid and polymer molecules over the whole GUV surface proving the mixed state of membranes from such compositions. Scheme 2 schematically summarizes the different composition dependent membrane morphologies of DPPC/BCP vesicles as revealed by the selective PEO-binding antibody (see **Scheme 2B**) in comparison to the morphologies visualized by Rh-DHPE or the fluorescently labeled BCP. It proves that bio-inspired recognition *via* antibodies shows a significantly higher potential for specifically visualizing membrane heterogeneities and for understanding hybrid lipid/polymer morphologies than commonly used membrane dyes, because the antibody explicitly marks the distribution of the respective BCP constituents in the corresponding phases.

Assignment of hybrid membrane morphologies from DOPC/BCP mixtures

In comparison to the results from hybrid GUVs of DPPC/BCP, a significantly different lipid/polymer mixing behavior can be expected from the use of hybrid vesicles composed of DOPC as lipid component in mixtures with the PIB₈₇-*b*-PEO₁₇ BCP. Due to the low phase transition temperature of DOPC ($T_m = -20^\circ\text{C}$) in contrast to DPPC, the lipid bilayer is now in the fluid state at room temperature (*RT*).

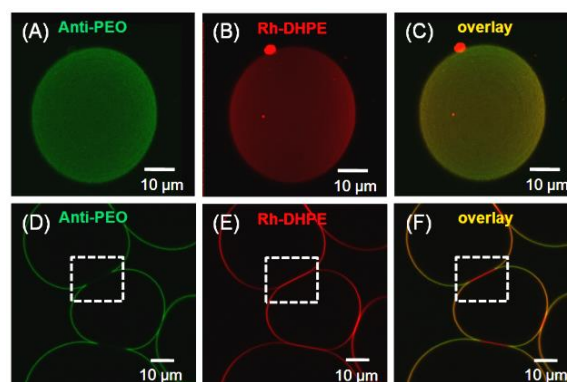


Figure 3. Confocal microscopy images of hybrid GUVs from DOPC mixed with 30 mol% of BCP. Hybrid membrane morphologies are monitored by antibody-binding (panel A and D) and by Rh-DHPE fluorescence (panel B and E). (A-C) 3D-reconstructions of an axial series of confocal slices. (D-F) shows a magnification of hybrid vesicles after addition of antibody. The fluorescent antibody is excluded from membrane areas where two GUVs have hemi-fused (indicated by the white box in D to F). (C and F) Overlay images of the fluorescence from both dyes.

Considering the thermally induced phase separation in DPPC/BCP vesicles (caused by the melting temperature of DPPC), which leads to the formation of highly ordered DPPC-rich domains at RT , we expected that the fluid state of DOPC vesicles at RT results in homogeneous membrane morphologies when mixed with the amphiphilic BCP. Figure 3 presents a typical confocal microscopy image of well-mixed GUVs, prepared from mixtures of DOPC with 30 mol% of BCP, where the vesicle membrane was visualized by Rh-DHPE (see Figure 3B) and by the antibody recognition of the incorporated BCPs.

Uniform fluorescence signals in both channels (green and red channel Figure 3A/B) indicate that the membrane components are randomly distributed within the hybrid bilayer. The indicated areas in Figure 3 D to F demonstrate that binding of the antibodies occurs exclusively to the outer membrane leaflet and confirms that GUVs do not leak (no binding of antibodies: see Figure 3D with 3E). Vesicles prepared from 20 mol% of BCP and 80 mol% DOPC (see Figure S7, **appendix C**) showed a uniform membrane morphology as visualized by the antibody-mediated monitoring of BCPs. Hybrid vesicles from DOPC mixtures with more than 20 mol% BCP also showed uniform binding of the Abs which was stable over time (monitored over several hours), indicating a well-mixed phase state.

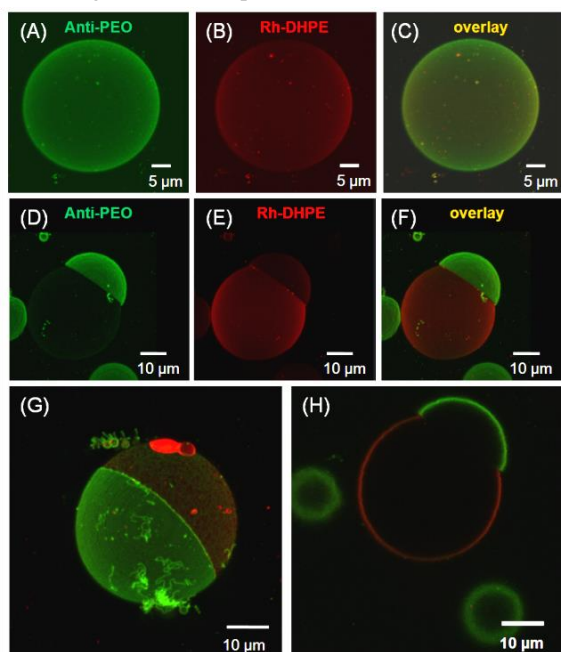


Figure 4. Confocal microscopy images of hybrid DOPC/BCP GUVs prepared from mixtures of DOPC with 10 mol% of BCP illustrating the phase separation and budding processes in hybrid vesicles monitored by the antibody. (A-C) 3D-reconstructions of a series of confocal slices of a hybrid GUV observed within short times (~ 10 min) after incubation of the vesicles with the secondary antibody. (D-F) 3D-reconstructions of a hybrid GUV, shown as equatorial slice in H, obtained 40 minutes after addition of the secondary antibody. Panel (D) shows the

fluorescence signal of the labeled antibody and (E) the fluorescence of the Rh-DHPE indicating a budding process. Panel (G) depicts a 3D-reconstruction of a vesicle (overlay image of Rh-DHPE and antibody) at an early time point during the course of vesicle fission, displaying the large domain boundary line.

Vesicles prepared with ≤ 10 mol% of BCP displayed a different phase behavior and stability. Immediately after electroformation, vesicles appeared well-mixed as depicted in Figure 4A to C, showing a uniform distribution of the Rh-DHPE dye as well as of the surface bound antibodies over the whole GUV surface. Over time, vesicles started to phase separate into large polymer-rich domains as shown in Figure 4G and H (green area) and into DOPC-rich domains (red area in Figure 4H). Moreover, the phase separated GUVs underwent budding.

The 3D-reconstruction of the hybrid vesicle from Figure 4H demonstrated that the phase separation process leads to budding and vesicle fission into polymer-enriched vesicles and polymer-depleted liposomes which are easily identified by the PEO-specific antibody and the Rh-DHPE dye, which label the opposite parts of the membranes (compare Figure 4E and overlay image 4F). The first vesicles undergoing the budding process were observed about 30 to 40 min after the secondary antibody incubation. As a result of the budding and fission process, DOPC-enriched vesicles (labeled in red with Rh-DHPE) which are separated from polymer-enriched vesicles (labeled in green by the antibody) are formed (see overview images of GUVs in Fig. S8 in **appendix C**).

Lipid membranes that exhibit a coexistence of fluid phases are frequently prone to budding processes.^{31, 32, 33} Such event is driven by line tension effects at the domain borders, which are caused by the different compositions of the coexisting domains demonstrating mismatches in membrane thickness³² and/or bending rigidities.⁴ Baumgart *et al.*³² demonstrated for GUVs composed of a ternary mixture of sphingomyelin, DOPC and cholesterol that the line tension drives shape changes to minimize the length of domain boundaries between the coexisting fluid bilayer phases. The shape transformation during the budding process is favored because the energetic cost of the hydrophobic mismatch at the domain boundary is reduced by decreasing its length.³⁴

Consequently, the hydrophobic mismatch between the size of the polymer (PIB_{87-b}-PEO₁₇) and lipid chains plays a role in the formation of well-mixed or phase separated membrane morphologies (≤ 10 mol% of BCP). In the latter case, the significant mismatch between the hydrophobic core thicknesses of the lipid domain with ~ 3 nm³⁵ and the polymer-rich phase with approximately 10 nm, which corresponds to 1-time folded PIB-chain (fully stretched chain ~ 22 nm),³⁶ leads to large energetic costs at the domain boundary causing the vesicle fission event. Considering further the high fluidity of DOPC

membranes and the low amount of incorporated BCPs (10 mol% or less than) we assume that the coexisting phases, the lipid- and the polymer-rich phase, display a fluid character at room temperature as indicated by the formation of circular domains (see Figure 4 and S9). Therefore, we suggest that the hydrophobic mismatch between both phases and the fluid state of the coexisting phases drives the vesicle fission event to completeness, whereas hybrid GUVs from compositions with 20 mol% of BCP and above showed the formation of stable GUVs with a single phase membrane (monitored over hours) displaying neither phase separation nor budding phenomena.

Selective incorporation of PIB-covered NPs into Lipid/BCP membranes

Having identified the different morphological states of the hybrid GUV membranes from lipid/BCP by the antibody-mediated monitoring of BCPs, we proceeded to studying the selective incorporation of polymer-coated CdSe nanoparticles into these hybrid vesicles. Hybrid GUVs with incorporated CdSe NPs were formed by electroformation using the previously reported procedure with a NP to lipid ratio of 1 to 1500.¹¹ Higher nanoparticle loadings (NP/lipid of 1/1000 and above) showed the formation of deformed vesicles leading to the destruction of hybrid membranes within short times after electroformation. Since NPs with diameters smaller than 8 nm are not expected to induce membrane rupture,^{2, 35, 37} we expected that the incorporation of the synthesized PIB-covered CdSe NPs with a diameter of ~ 6 nm results in formation of stable GUVs. To address the specific NP location within a given membrane morphology of hybrid lipid/BCP vesicles, we varied the lipid/polymer composition and the lipid component using either DPPC or DOPC.

NP incorporation into DPPC/BCP membranes

We first investigated the incorporation of hydrophobic CdSe NPs into DPPC/BCP vesicles either in the non-phase separated or phase separated case to enable selective control of NP localization within the polymer-rich domains. Considering the fact that the polymer-functionalized NPs exhibit a brush of polyisobutylene chains on their surface, a selective incorporation of the NPs into the hydrophobic membrane interior of polymer domain could be expected. Based on favored interactions of the NP shell with the PIB chains of the BCP rather than with the hydrophobic lipid tail such selective localization is observed, similar to previous reports for polymersomes controlling NP incorporation by coating the particles with a polymer structure similar to that of the vesicle formers.²⁰

When vesicles were prepared from mixtures with 18 mol% or 40 mol% of the BCP component, the morphology of these hybrid vesicles appear uniform as shown by antibody-mediated monitoring of BCPs and by using the fluorescently labeled di-BCP as membrane dye.

Incorporation of the NPs into these hybrid bilayers showed also a uniform distribution of the particles within the whole membrane (see **appendix C** Figure S11 and S12 A to C). Selective incorporation of PIB-covered NPs into the polymer-rich phase of hybrid GUVs composed of DPPC with a composition between 20 and 28 mol% of the BCP is illustrated in Figure 5.

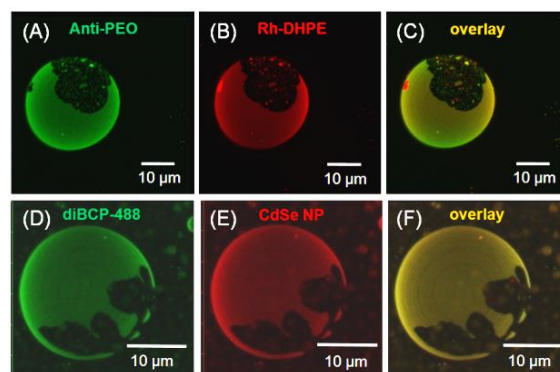


Figure 5. 3D-reconstructions of an axial series of confocal slices of phase separated GUVs composed of DPPC and PIB₈₇-*b*-PEO₁₇ BCP (24 mol% of BCP) without (A-C) and with hydrophobic CdSe NPs (D-F). Fluorescence signal of (A) antibody-mediated monitoring of the BCPs (excited at 488 nm) and (D) the fluorescently labeled diblock copolymer (also excited at 488 nm). Panel (E) shows the fluorescence signal of the modified NPs (excited at 561 nm) demonstrating the selective embedding of the NPs into the polymer-rich phase. (C and F) are the corresponding overlay images of the dyes.

As shown by the partitioning behavior of the di-BCP dye (see Figure 5D) and by the antibody-mediated monitoring of BCPs (Figure 5A), both visualization methods allow the assignment of the polymer-rich phase in heterogeneous vesicles from DPPC and BCP. Rh-DHPE (excited at 561 nm) showed a preferential incorporation into the polymer-rich domains as mentioned before (see section morphologies of DPPC/BCP vesicles). A comparison of the fluorescence intensity signal of the rhodamine-labeled particles with the fluorescence from the di-BCP dye (compare Figure 5E with 5D) proves the preferential incorporation of hydrophobic NPs into the polymer-rich phase (see also **appendix C** Figure S13). Assuming that the favored interactions between the polymer shell of the NPs and the hydrophobic tail of the BCPs causes the selective localization of the particles within the polymer-rich domains, the NP incorporation into the more ordered DPPC-rich domains (black patches in vesicle images in Figure 5) is prevented. Moreover, the difference in the hydrophobic thickness between the lipid- and polymer-rich domains further effects the selective incorporation of the NPs (diameter of ~6 nm) into the thicker polymer-rich phase.

NP incorporation into DOPC/BCP membranes

Finally, we studied the selective incorporation of PIB-covered NPs into phase separated vesicles from DOPC

and the PIB₈₇-*b*-PEO₁₇ BCP at room temperature. The particle incorporation into the polymer-rich phase was proven by applying the antibody-mediated monitoring of the BCPs, as illustrated in Figure 6. For a mixture of DOPC with 10 mol% of BCP, the obtained hybrid GUVs with incorporated CdSe NPs showed the formation of two different phases. Monitoring such vesicles directly *via* the fluorescently labeled NPs (Figure S14 in **appendix C**) after the electroformation process and before incubation of the vesicles with the antibodies confirms that a phase separation process occurs, leading to the formation of a NP-rich phase and a NP-depleted, black phase within the hybrid membrane. Since the black areas do not display a fluorescence signal of the rhodamine-labeled NPs, we assume that this particular phase is the DOPC-rich domain. To prove this assumption, we subsequently incubated the phase separated vesicles with the antibody system (see results in Figure 6).

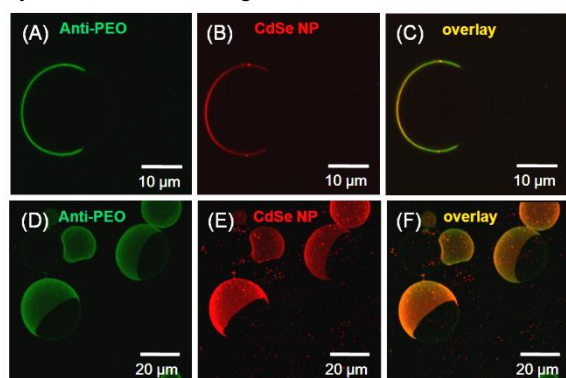


Figure 6. Confocal microscopy images of phase separated GUVs composed of DOPC and PIB₈₇-*b*-PEO₁₇ BCP (10 mol% of BCP) demonstrating the selective incorporation of hydrophobic CdSe NPs into the polymer-rich phase. (A-C) Phase separated hybrid vesicle near the vesicle equator monitoring: (B) the fluorescently-labeled NPs (visualized in red; excited at 561 nm) and (A) the antibodies (visualized in green; excited at 488 nm). Overlay image in panel (C) confirms the selective incorporation of the NPs into the polymer-rich domain. Panels (D to F) 3D-reconstruction of an axial series of confocal slices from an overview of hybrid GUVs.

Antibody-monitoring of the BCPs (Figure 6 A and D) revealed that the particles and BCP molecules are located within the same phase as clearly demonstrated by the overlay images in Figure 6C and 6F. Consequently, the dark domains in the hybrid GUV membranes, as shown in Figure 6, presented the DOPC-rich phases. Thus, we assume that the surface coverage of the CdSe NPs by polymer chains similar to the block copolymer forming the hybrid lipid/BCP membrane plays a significant role in controlling nanoparticle incorporation into specific domains in hybrid vesicles.

CONCLUSION

Investigations of lipid/BCP hybrid membrane morphologies by PEO-recognizing antibodies are

reported as a novel and powerful method for detecting specific compositional membrane heterogeneities within such hybrid systems. Whereas common membrane dyes (*e.g.* Rh-DHPE) are limited in labeling membrane heterogeneities by their phase partitioning behavior, an antibody that selectively recognizes the PEO-functionality of a BCP enables the direct monitoring of the incorporated BCP molecules within the hybrid membrane. Such bio-inspired recognition can reveal specific membrane heterogeneities and furthermore have the potential to fine-tune hybrid lipid/polymer morphologies and the resulting membrane properties by identifying the BCP constituents. In contrast to the binding results of anti-PEO/secondary antibody, the use of membrane dyes (*e.g.* Rh-DHPE) in monitoring phase heterogeneities showed in some cases clear differences in their phase labeling behavior compared to the antibody-mediated BCP monitoring. We observed additional phase heterogeneities in the case of DPPC/BCP vesicles prepared from mixtures of DPPC with 32 mol% of BCP indicating the existence of small lipid-rich domains within the polymer-rich matrix, which were not detected by Rh-DHPE. Furthermore, the significant hydrophobic thickness difference between the lipid and polymer chains have shown to play a major role in forming mixed or demixed membrane morphologies. Thus, in case of DOPC mixtures with low BCP amounts we observed that phase separated vesicles undergo vesicle fission as a consequence of the hydrophobic thickness mismatch between both membrane components which leads to a high line tension at the domain boundaries.

Based on the ability to control the phase separation in hybrid vesicles and the selective targeting of membrane components, we could successfully demonstrate the selective incorporation of hydrophobic PIB covered CdSe nanoparticles into phase separated DPPC/BCP membrane morphologies as well as into fluid DOPC/BCP membranes. The selective localization of the particles within the polymer-rich phases is as a result of the favored interaction between the PIB coatings of the NPs and the hydrophobic membrane interior formed by the PIB-*b*-PEO BCP coupled with the hydrophobic thickness of the polymer-rich phase, which is significantly larger than that of the lipid. The potential fine-tuning of such hybrid lipid/BCP membrane morphologies combined with the selective localization of functional nanoparticles can open up new perspectives in controlling physical and mechanical properties of the membrane such as nanoporosity, domain structure and stiffness to develop effective vesicle carriers.

ACKNOWLEDGEMENTS

We thank Sebastian Daum for advice on antibody experiments and the grants DFG BI 1337/6-1 and DFG BI 1337/7-2 (WHB, MS and AO) within the Forschergruppe FOR-1145, the grants DFG INST

271/249-1; INST 271/247-1; INST 271/248-1 (WHB), the BMBF ZIK program (FKZ 03Z2HN22 to KB) and ERDF (grant 1241090001) for financial support.

REFERENCES

- [1] Binder, W. H.; Barragan, V.; Menger, F. M., Domains and Rafts in Lipid Membranes. *Angew. Chem. Int. Ed.* 2003, **42**, (47), 5802-5827.
- [2] Schulz, M.; Olubummo, A.; Binder, W. H., Beyond the lipid-bilayer: interaction of polymers and nanoparticles with membranes. *Soft Matter* 2012, **8**, (18), 4849-4864.
- [3] Tribet, C.; Vial, F., Flexible macromolecules attached to lipid bilayers: impact on fluidity, curvature, permeability and stability of the membranes. *Soft Matter* 2008, **4**, (1), 68-81.
- [4] Chemin, M.; Brun, P.-M.; Lecommandoux, S.; Sandre, O.; Le Meins, J.-F., Hybrid polymer/lipid vesicles: fine control of the lipid and polymer distribution in the binary membrane. *Soft Matter* 2012, **8**, (10), 2867-2874.
- [5] Schulz, M.; Glatte, D.; Meister, A.; Scholtysek, P.; Kerth, A.; Blume, A.; Bacia, K.; Binder, W. H., Hybrid lipid/polymer giant unilamellar vesicles: effects of incorporated biocompatible PIB-PEO block copolymers on vesicle properties. *Soft Matter* 2011, **7**, (18), 8100-8110.
- [6] Nam, J.; Beales, P. A.; Vanderlick, T. K., Giant Phospholipid/Block Copolymer Hybrid Vesicles: Mixing Behavior and Domain Formation. *Langmuir* 2011, **27**, (1), 1-6.
- [7] Discher, D. E.; Ahmed, F., Polymersomes. *Annu. Rev. Biomed. Eng.* 2006, **8**, 323-341.
- [8] Discher, D. E.; Eisenberg, A., Polymer Vesicles. *Science* 2002, **297**, 967-973.
- [9] Schulz, M.; Werner, S.; Bacia, K.; Binder, W. H., Controlling Molecular Recognition with Lipid/Polymer Domains in Vesicle Membranes. *Angew. Chem. Int. Ed.* 2013, **52**, (6), 1829-1833.
- [10] Thoma, J.; Belegirinou, S.; Rossbach, P.; Grzelakowski, M.; Kita-Tokarczyk, K.; Meier, W., Membrane protein distribution in composite polymer-lipid thin films. *Chem. Commun.* 2012, **48**, (70), 8811-8813.
- [11] Olubummo, A.; Schulz, M.; Lechner, B.-D.; Scholtysek, P.; Bacia, K.; Blume, A.; Kressler, J.; Binder, W. H., Controlling the Localization of Polymer-Functionalized Nanoparticles in Mixed Lipid/Polymer Membranes. *ACS Nano* 2012, **6**, (10), 8713-8727.
- [12] Mai, Y.; Eisenberg, A., Selective Localization of Preformed Nanoparticles in Morphologically Controllable Block Copolymer Aggregates in Solution. *Acc. Chem. Res.* 2012, **45**, (10), 1657-1666.
- [13] Simons, K.; Ikonen, E., Functional rafts in cell membranes. *Nature* 1997, **387**, (6633), 569-572.
- [14] LoPresti, C.; Massignani, M.; Fernyhough, C.; Blanazs, A.; Ryan, A. J.; Madsen, J.; Warren, N. J.; Armes, S. P.; Lewis, A. L.; Chirasatitsin, S.; Engler, A. J.; Battaglia, G., Controlling Polymersome Surface Topology at the Nanoscale by Membrane Confined Polymer/Polymer Phase Separation. *ACS Nano* 2011, **5**, (3), 1775-1784.
- [15] Balazs, A. C.; Emrick, T.; Russell, T. P., Nanoparticle Polymer Composites: Where Two Small Worlds Meet. *Science* 2006, **314**, (5802), 1107-1110.
- [16] Binder, W. H.; Sachsenhofer, R.; Farnik, D.; Blaas, D., Guiding the location of nanoparticles into vesicular structures: a morphological study. *Phys. Chem. Chem. Phys.* 2007, **9**, 6435-6441.
- [17] Bothun, G. D., Hydrophobic silver nanoparticles trapped in lipid bilayers: Size Distribution, bilayer phase behavior, and optical Properties. *J. Nanobiotechnol.* 2008, **6**, 13-23.
- [18] Chen, H. Y.; Abraham, S.; Mendenhall, J.; Delamarre, S. C.; Smith, K.; Kim, I.; Batt, C. A., Encapsulation of Single Small Gold Nanoparticles by Diblock Copolymers. *Chem. Phys. Chem* 2008, **9**, (3), 388-392.
- [19] Glogowski, E.; Tangirala, R.; Russell, T. P.; Emrick, T., Functionalization of nanoparticles for dispersion in polymers and assembly in fluids. *J. Polym. Sci., Part A: Polym. Chem.* 2006, **44**, 5076-5086.
- [20] Mai, Y.; Eisenberg, A., Controlled Incorporation of Particles into the Central Portion of Vesicle Walls. *J. Am. Chem. Soc.* 2010, **132**, (29), 10078-10084.
- [21] Binder, W. H.; Sachsenhofer, R., Polymersome/Silica Capsules by 'Click'-Chemistry. *Macromol. Rapid Commun.* 2008, **29**, (12-13), 1097-1103.
- [22] Gopalakrishnan, G.; Danelon, C.; Izewska, P.; Prummer, M.; Yves Bolinger, P.; Geissbühler, I.; Demurtas, D.; Dubochet, J.; Vogel, H., Multifunctional Lipid/Quantum Dot Hybrid Nanocontainers for Controlled Targeting of Live Cells. *Angew. Chem. Int. Ed.* 2006, **45**, 5478-5483.
- [23] Chen, Y.; Bothun, G. D., Lipid-Assisted Formation and Dispersion of Aqueous and Bilayer-Embedded Nano-C60. *Langmuir* 2009, **25**, (9), 4875-4879.
- [24] Dubavik, A.; Sezgin, E.; Lesnyak, V.; Gaponik, N.; Schwille, P.; Eychmüller, A., Penetration of Amphiphilic Quantum Dots through Model and Cellular Plasma Membranes. *ACS Nano* 2012, **6**, (3), 2150-2156.
- [25] Qiu, D.; An, X.; Chen, Z.; Ma, X., Microstructure study of liposomes decorated by hydrophobic magnetic nanoparticles. *Chem. Phys. Lipids* 2012, **165**, (5), 563-570.
- [26] Chen, Y.; Bose, A.; Bothun, G. D., Controlled Release from Bilayer Decorated Magnetoliposomes via Electromagnetic Heating. *ACS Nano* 2010, **4**, (6), 3215-3221.

- [27] Lecommandoux, S.; Sandre, O.; Chécot, F.; Rodriguez-Hernandez, J.; Perzynski, R., Magnetic Nanocomposite Micelles and Vesicles. *Adv. Mater.* 2005, **17**, (6), 712-718.
- [28] Nam, J.; Vanderlick, T. K.; Beales, P. A., Formation and dissolution of phospholipid domains with varying textures in hybrid lipo-polymersomes. *Soft Matter* 2012, **8**, (30), 7982-7988.
- [29] Angelova, M. I.; Dimitrov, D. S., Liposome electroformation. *Faraday Discuss. Chem. Soc.* 1986, **81**, 303-311.
- [30] *To test the specificity of the antibody (Ab) system against the PEO-functionality of PIB-PEO based BCPs, a dotblot experiment was carried out (see exact procedure **appendix C**). DPPC as lipid component, the polyisobutylene homopolymer and the PIB_{87-b}-PEO₁₇ BCP were plotted at different concentrations on a nitro-cellulose membrane and subsequently stepwise incubated with the Ab-solutions. Afterwards, the binding was proved by fluorescence analysis (see Figure S2, **appendix C**). The Ab-binding was only observed in case of the BCP, whereas DPPC and the PIB-homopolymer showed no recognition by the Ab system. Furthermore, we performed control experiments in the bilayer showing in case of pure DPPC liposomes neither binding nor unspecific adsorption of the antibodies (data not shown). Finally, we examined the effect of the secondary Ab on hybrid vesicles (e.g. 80/20 mixture of DOPC/BCP) without incubating vesicles before with the primary Ab demonstrating that no adsorption or binding of the secondary Ab to hybrid vesicle surfaces (data not shown) was observed. In summary, we found that only the Ab system consisting of the anti-PEO and the secondary Ab showed high specificity against the BCPs, whereas lipid components or the PIB-homopolymer were not recognized.*
- [31] García-Sáez, A. J.; Chiantia, S.; Schwille, P., Effect of Line Tension on the Lateral Organization of Lipid Membranes. *J. Biol. Chem.* 2007, **282**, (46), 33537-33544.
- [32] Baumgart, T.; Hess, S. T.; Webb, W. W., Imaging coexisting fluid domains in biomembrane models coupling curvature and line tension. *Nature* 2003, **425**, (6960), 821-824.
- [33] Bacia, K.; Schwille, P.; Kurzchalia, T., Sterol Structure determines the separation of phases and the curvature of the liquid-ordered phase in model membranes. *PNAS* 2005, **102**, (9), 3272-3277.
- [34] Lipowsky, R., The morphology of lipid membranes. *Curr. Opin. Struct. Biol.* 1995, **5**, (4), 531-540.
- [35] Discher, B. M.; Won, Y.-Y.; Ege, D. S.; Lee, J. C. M.; Bates, F. S.; Discher, D. E.; Hammer, D. A., Polymersomes: Tough Vesicles Made from Diblock Copolymers. *Science* 1999, **284**, (5417), 1143-1146.
- [36] Li, H.; Sachsenhofer, R.; Binder, W. H.; Henze, T.; Thurn-Albrecht, T.; Busse, K.; Kressler, J., Hierarchical Organization of Poly(ethylene oxide)- block -poly(isobutylene) and Hydrophobically Modified Fe₂O₃ Nanoparticles at the Air/Water Interface and on Solid Supports. *Langmuir* 2009, **25**, (14), 8320-8329.
- [37] Ginzburg, V. V.; Balijepalli, S., Modeling the Thermodynamics of the Interaction of Nanoparticles with Cell Membranes. *Nano Lett.* 2007, **7**, (12), 3716-372.

IV. EXPERIMENTAL PART

1. MATERIALS

All chemicals were purchased from Sigma-Aldrich (*Schnelldorf*, Germany). The starting reagent for the synthesis of the bifunctional initiator the 5-*tert*-butyl-isophthalic acid was used without further purification. Isobutylene (Sigma Aldrich, 98.5 %), which was used for the polymerization process, was passed through a gas drying column prior to use and condensed at -80°C under argon. The chemicals, which were employed for the preparation of polyisobutylene and the end group modification: titanium tetrachloride (99.5%), 2,6-di-*tert*butylpyridine (stored at +4°C), allyltrimethylsilane (ATMS) (stored at +4°C), *meta*-chloro-peroxybenzoic acid (72%), 0.5 mol/l THF solution of 9-borabicyclo[3.3.1]nonane (stored at +4°C), 1,3-dicyclohexylcarbodiimide (99%), 4-dimethylaminopyridine (99%), hexynoic acid (99%), α -methylstyrene (99%) and propargyl bromide (99%) were all used without further purifications. All solvents, which were employed for the work up procedures, were first distilled before use. Predried dichloromethane (over CaCl₂) was freshly distilled over CaH₂ and degassed with argon prior to use. Hexane used as polymerization solvent was refluxed over concentrated sulphuric acid for at least 7 days to remove olefin impurities, followed by an extraction procedure with a basic solution and refluxed over calcium hydride before using. THF was predried over potassium hydroxide for several days and freshly distilled over sodium/benzophenone prior to use.

2. METHODS

¹H- and **¹³C-NMR spectra** were performed on a *Varian Gemini 2000* (200 and 400 MHz) FTNMR spectrometer using *MestRec-C* (4.9.9.6) software for data interpretation. The measurements were done in deuterated chloroform (CDCl₃: 7.26 ppm (1H) and 77.0 ppm (¹³C)). All chemical shifts (δ) are reported in parts per million (ppm) relative to tetramethyl silane (TMS); coupling constants (*J*) are given in Hertz (Hz) using standard abbreviations (s = singlet; d = doublet; t = triplet; m = multiplet).

GPC analysis was performed on a *Viscotek GPCmax VE2001* system combined with a *Viscotek TDA30L* (triple detector array). Polyisobutylene standards in the range of 340-87.600 Da purchased from PSS (Polymer standard service) were used for conventional external calibration using a *Viscotek VE3580* refractive index detector. The polystyrene-

divinylbenzene based column set consists of a HHR – HGuard – 17369 pre-column followed by a GMHHR – N – Mixed Bed 18055 (1000 - 4 x 105 Da) and a G2500HHR - 17354 (100 – 2 x 104 Da) column. The detector and the column temperature were held constant at 35°C with flow rates of 1 mL/minute. The investigated samples were dissolved in THF (>99.9%), analyzing the results of the GPC analysis were achieved using *OmniSec* (4.5.6) software.

IR-spectra were recorded on *Bruker Vertex 70* FT-IR spectrometer and evaluated by *OPUS* (6.5) software. Samples were measured with *golden gate unit* combined with a *RT DLa TGS* detector.

TLC (thin layer chromatography) was performed with TLC aluminium sheets silica gel 60 F254 being purchased from *Merck*. As oxidation reagents a cerium molybdate solution –“blue stain” – (1 g $\text{Ce}(\text{SO}_4)_2 \cdot 4\text{H}_2\text{O}$, 2.5 g $(\text{NH}_4)_6\text{Mo}_7\text{O}_{24} \cdot 4\text{H}_2\text{O}$, 6 mL conc. H_2SO_4 and 90 mL H_2O) and a solution of 1 g $\text{Ce}(\text{SO}_4)_2 \cdot 4\text{H}_2\text{O}$, 2.75 mL conc. H_2SO_4 and 47 mL H_2O were used.

MALDI-TOF-MS measurements were performed on a *Bruker Autoflex III* system (*Bruker Daltonics*) operating in reflectron and linear modes. Data evaluation was carried out on *flexAnalysis* software (3.0). Ions were formed by laser desorption (smart beam laser at 355 nm, 532 nm, 808 nm and 1064 nm \pm 5 nm; 3 ns pulse width; up to 2500 Hz repetition rate), accelerated by voltage of 20 kV and detected as positive ions. The matrix solution was prepared by dissolving 1,8,9-anthracenetriol (dithranol) or *trans*-2-[3-(4-*tert*-butylphenyl)-2-methyl-2-propenylidene]malononitrile (DCTB) in THF at a concentration of 20 mg/mL. Polymer samples were dissolved in THF at a concentration of 5 or 10 mg/mL. AgTFA, LiTFA or NaTFA were dissolved at a concentration of 1 mg/mL in THF. Solutions of the matrix, polymer and salt were mixed in defined volume ratio and 1 μL of each mixture was spotted on the MALDI-target. The rhodamine B labeled polyisobutylene (**30**) was dissolved in pure THF (5 mg/mL) without adding any salt to it and spotted on the MALDI-target. The instrument was externally calibrated with a 25 poly(ethylene glycol) (PEG) standard ($M_p = 2000$ g/mol) applying a quadratic calibration method with an error of 1-2 ppm.

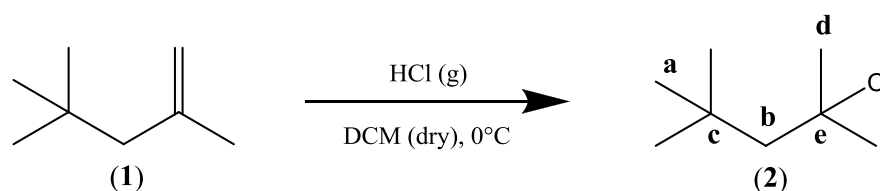
ESI-TOF-MS measurements were performed on a Bruker Daltonics micrOTOF time-of-flight ESI-MS system. Spectra were recorded in the positive mode with an accelerating voltage of 4.5 kV, a transfer line with 180°C and a scan range of 50-15000 m/z . Spectra were processed on a *Bruker Daltonics ESI compass 1.3 for micrOTOF* (Data Analysis® 4.0). Samples were prepared by dissolving 5 mg of the polymer (di- and tri-BCPs) in a mixture of

THF/ACN/methanol of 90/5/5 (v/v/v). Fluorescently labeled BCPs (di- and tri-BCPs labeled with rhodamine or fluor 488 dye) were dissolved in THF/MeOH of 80/20 (v/v) without adding a salt to the solution. Afterwards, 150 μL of these solutions are directly injected into ESI-source using a syringe pump (*KD Scientific Inc., Massachusetts, USA*) with an injection speed of 50 $\mu\text{L}/\text{min}$.

3. SYNTHESIS

3.1 Living carbocationic polymerization of IB and end group modification of telechelic PIBs

3.1.1 Synthesis of monovalent initiator (TMPCl) (2)¹⁴⁷



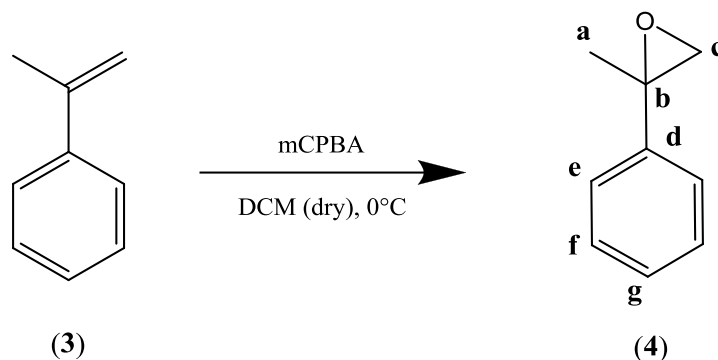
According to a literature procedure of Kennedy *et al.*¹⁴⁷, the monovalent initiator TMPCl (2) was obtained by the addition reaction of HCl to the double bond of 2,4,4-trimethylpent-1-ene resulting in the *Markovnikov* product. In a one-necked round-bottom flask the starting material (1) (2.15 g, 19.1 mmol) dissolved in dry DCM (5 mL) is added. The solution was cooled to 0°C (ice bath) and dry, gaseous hydrochloric acid, prepared by dropping concentrated sulfuric acid over sodium chloride, is added *via* a slow stream over a period of 4 hours. Afterwards, the inert solvent was removed fast under reduced pressure at 0°C, yielding compound 2 as a pale yellow liquid. The monovalent initiator compound 2, which is further used for the LCCP of IB without purification, was stored under an argon atmosphere in a freezer.

Yield: 2.0 g, (70 %).

¹H-NMR (400 MHz, CDCl₃): δ (ppm) 1.87 (s, 2H_b), 1.67 (s, 6H_d), 1.05 (s, 9H_a).

¹³C-NMR (400 MHz, CDCl₃): δ (ppm) 71.7 (C_e), 57.8 (C_b), 34.7 (C_d), 32.3 (C_c), 31.4 (C_a).

3.1.2 Synthesis of the LCCP initiator α -methylstyrene epoxide (MSE) (**4**)^{148, 149}



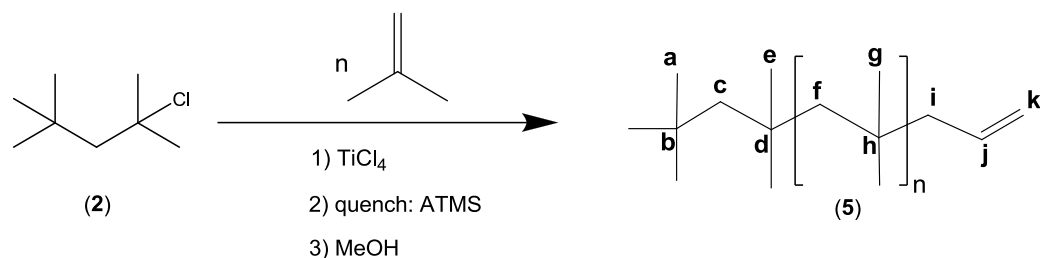
According to the literature procedure of Puskas *et al.*,¹⁴⁸ α -methylstyrene epoxide (**4**) was synthesized by the reaction of the corresponding olefin (**3**) (1 equiv.) with *meta*-chloroperoxybenzoic acid (mCPBA) (10 equiv.) in DCM at room temperature. Methylstyrene (4 g, 3.6 mL, 0.034 mol) was vacuum-distilled prior to use. In a three-necked round bottom flask equipped with a mechanical stirrer and a dropping funnel compound (**3**) was charged dissolved in DCM (80 mL). The mixture solution was cooled to 0°C with an ice bath and stirred while adding drop-wise mCPBA (6 g, 0.037 mol, 1.1 equiv.) dissolved in 70 mL of DCM. After 3 hours at 0°C the reaction mixture was washed 5 times with a 10% Na₂CO₃ solution till all the excess mCPBA is removed. Afterwards the mixture was washed with saturated solution of NaCl. The combined organic layers were dried with Na₂SO₄ and subsequent the solvent was removed by rotary evaporation. The resulting slightly yellow compound **4**, which is further used for the LCCP of IB without purification, was stored under an argon atmosphere in a freezer.

Yield: 2.7 g, (59 %).

¹H-NMR (400 MHz, CDCl₃): δ (ppm) 7.39-7.31 (m, 5H (H_e+H_f+H_g), 2.95 (d, $J = 5.43$ Hz, 1H_c), 2.81 (d, $J = 5.43$ Hz, 1H_{c'}), 1.73 (s, 3H_a).

¹³C-NMR (400 MHz, CDCl₃): δ (ppm) 141.2 (C_d), 128.7 (C_g), 127.5 (C_f), 125.3 (C_e), 57.1 (C_b), 56.9 (C_c), 22.0 (C_a).

3.1.3 Synthesis of monovalent allyl-telechelic polyisobutylene (**5**)^{140, 147, 150}



The synthesis of mono functionalized polyisobutylenes bearing allyl-chain end was accomplished according to literature.^{140, 147, 150} The reaction apparatus was dried and flushed with argon three times. The solvents (DCM and hexane) used for the polymerization process were of absolute dry and all reagents were added *via* syringe into the reaction apparatus. The reaction was carried out under an argon atmosphere at -80°C and the used isobutylene concentration was 1.0 mol/L. The three necked round-bottom flask equipped with a mechanical stirrer, an argon inlet/ outlet and a septum was charged with *n*-hexane (60 ml), dichloromethane (40 ml), DMA (46.3 μL , equiv.) and DtBP (112.5 μL , equiv.). Afterwards, the starting solution was cooled down to -80°C and the initiator TMPCl (**2**) (0.45 g, 3.0 mmol, 0.52 mL) was added *via* a syringe to the reaction flask. At -80°C the stirred solution was treated with the catalyst titanium tetrachloride (0.77 mL, 7.0 mmol) and the colour changed to yellow.

At -40°C condensed isobutylene (8.96 mL, 0.1 mol) was rapidly injected into the reaction flask and the resulting mixture was stirred for 20 minutes. Subsequently, the reaction was quenched with the addition of allyltrimethylsilane (1.4 mL, 9.0 mmol). After another period of 20 minutes under stirring, the solution was treated with MeOH (10 mL) to deactivate titanium tetrachloride and the yellow colour changed back to colourless. The solution was transferred into a one-necked flask and concentrated by evaporating the solvent. The remaining product was precipitated from *n*-hexane into acetone (200 mL). The acetone was decanted and obtained polymer was redissolved in *n*-hexane and precipitated again. Finally, the compound was dried in high vacuum to yield compound **5** as colorless, flexible polymer.

Yield: 5.2 g, (94 %).

^1H -NMR (400 MHz, CDCl_3): δ (ppm) 5.85 (m, 1H_j), 5.01 (m, 2H_k), 2.0 (d, 4H_i), 1.40 (br, 2n H_f), 1.09 (s, 6n H_g), 0.98 (s, 15H (H_a+ H_e)).

^{13}C -NMR (400 MHz, CDCl_3): δ (ppm) 136.1 (C_j), 116.7 (C_k), 59.5 (C_f), 58.9 (C_e), 58.2 (C_g), 50.3 (C_i), 38.2 (C_h), 37.9 (C_d), 32.6 (C_b), 32.4 (C_a), 31.2 (C_g), 31.0 (C_e).

Table 2. Experimental results of isobutylene polymerization using TMPCl/TiCl_4 as initiator system.

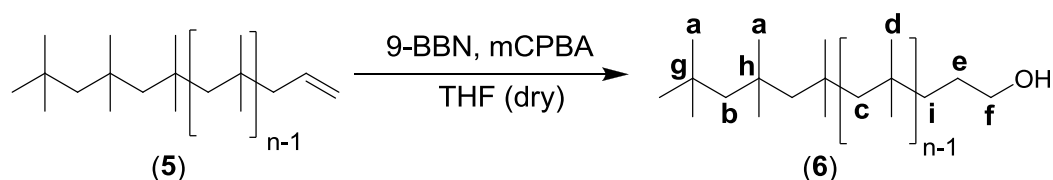
Entry	Sample	$M_n^{1)}$ (theory)	Characterization				Yield ²⁾ [%]
			$M_n^{1)}$ (GPC)	$M_w^{1)}$ (GPC)	PDI	$M_n^{1)}$ (NMR)	
1	PIB ₃₇ -allyl (5a)	2000	2100	2730	1.3	2280	90
2	PIB ₃₅ -allyl (5b)	2000	1900	2360	1.2	2050	92
3	PIB ₆₀ -allyl (5c)	3000	3100	3720	1.2	3450	95
4	PIB ₇₀ -allyl (5d)	4000	3750	4880	1.3	3900	94
5	PIB ₈₇ -allyl (5e)	5000	4900	6070	1.2	4920	92
6	PIB ₁₆₀ -allyl (5f)	9000	9040	11800	1.5	8800	89

¹⁾ Number average molecular weight in [g/mol].

²⁾ Isolated mass of the polymers.

3.1.4 End group modification of monovalent polyisobutylene

3.1.4.1 Synthesis of monovalent hydroxyl-telechelic polyisobutylene (**6**)^{145, 151}



A three-necked, round bottom flask, equipped with a magnetic stirrer, a septum and an argon inlet/outlet was heated and several times flushed with argon. After charging with the allyl-telechelic PIB (**5**) (1.5 g, 0.75 mmol) and freshly distilled THF (120 mL), the solution was bubbled with argon to remove oxygen. Subsequently, a 0.5 M solution of 9-borabicyclo[3.3.1]nonane (9-BBN) in THF (13.5 mL, 6.77 mmol) was added *via* a syringe to the stirred solution. The reaction was accomplished at room temperature for 7 hours and later the mixture was cooled down to 0°C, followed by the addition of MeOH (4 mL) used as a phase transfer agent. Afterwards, the colorless solution was treated with solid *m*CPBA (3.9 g, 22.6 mmol) in several steps and the resulting mixture was stirred over night. Then *n*-hexane (100 mL) was added and the organic phase separated, followed by extraction with distilled water ($pH = 9$) for five times. Thereafter, the organic phase was washed with a mixture of

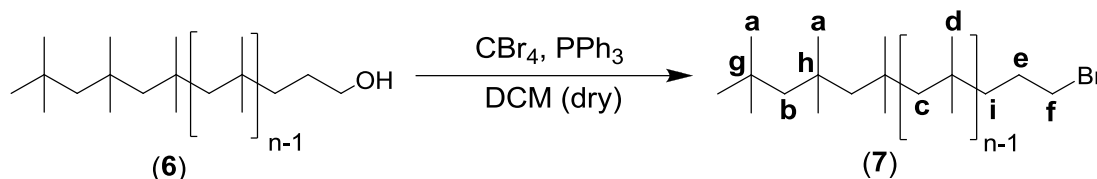
MeOH and water (50:50), with distilled water for five times and finally dried over Na₂SO₄. The filtered solution was placed in a rotary evaporator to remove the solvent. The crude product was dissolved in *n*-hexane and precipitated in MeOH three times. Finally, the colorless polymer was dried under high vacuum to yield compound **6**.

Yield: 1.25 g, (83 %).

¹H-NMR (400 MHz, CDCl₃): δ (ppm) 3.60 (t, *J* = 6.87 Hz, 2H_f), 1.40 (br, 2n H_c), 1.09 (s, 6n H_d), 0.98 (s, 15H_a).

¹³C-NMR (400 MHz, CDCl₃): δ (ppm) 64.0 (C_f), 59.5 (C_c), 58.8 (C_b), 41.4 (C_i), 37.9 (C_h), 32.6 (C_g), 31.2 (C_d), 30.9 (C_a), 27.8 (C_e).

3.1.4.2 Synthesis of monovalent bromo-telechelic polyisobutylene (**7**)^{143, 144}



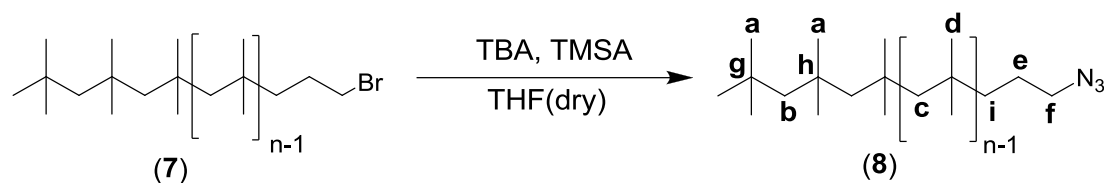
The bromo-telechelic polyisobutylene (**7**) was obtained *via* the well-known Appel-reaction.¹⁵² Thus, a round-bottom three-necked flask was charged with hydroxyl-telechelic PIB (**6**) (0.66 g, 0.34 mmol, 1 equiv.) and 10 equiv. of CBr₄ (0.66 g, 1.98 mmol) were dissolved in DCM (30 mL). Subsequent, the solution was ice-cooled and drop wise a solution of PPh₃ (0.18 g, 1.65 mmol, 10 equiv.) in CH₂Cl₂ (10 mL) was added. The reaction proceeded under stirring over night at room temperature. The solvent was removed and the residue was dissolved in *n*-hexane (two times). After filtration of the combined hexane phases, the product **7** (*R_f* = 0.9) was recovered under evaporation of the solvent and subsequent purified by column chromatography (hexane/ ethyl acetate = 40/1) to remove residual phosphine oxide.

Yield: 0.55 g, (84 %).

¹H-NMR (400 MHz, CDCl₃): δ (ppm) 3.35 (t, *J* = 6.92 Hz, 2H_f), 1.82 (m, 2H_e), 1.40 (br, 2n H_c), 1.09 (s, 6n H_d), 0.99 (s, 15H_a).

¹³C-NMR (400 MHz, CDCl₃): δ (ppm) 59.5 (C_c), 58.8 (C_b), 37.9 (C_h), 44.1 (C_i), 36.3 (C_f), 32.6 (C_g), 31.2 (C_d), 30.9 (C_a), 29.1 (C_e).

3.1.4.3 Synthesis of monovalent azido-telechelic polyisobutylene (**8**)^{143, 144}



The conversion into the corresponding azido-telechelic PIB (**8**) was performed *via* nucleophilic substitution with trimethylsilyl azide (TMSA) and tetrabutylammonium fluoride (TBAF). Thus, a 100 mL round-bottom three-necked flask, which was flame-dried and flushed with argon several times, was filled with compound **7** (0.55 g, 0.27 mmol, 1 equiv.) dissolved in freshly distilled anhydrous THF (50 mL) *via* a syringe. Subsequent, the reaction flask was treated with a solution of TBAF in THF (1.65 mL, 1.65 mmol, 6 equiv.) and trimethylsilyl azide (190 μ L, 1.65 mmol, 6 equiv.). The resulting reaction mixture was heated to 50°C and stirred for 5 h under an argon atmosphere. After removal of the solvent, the crude product was dissolved in *n*-hexane (100 mL) and extracted with distilled water (four times). The organic layer was dried over sodium sulfate, filtered and subsequently the solvent removed under reduced pressure. Thereafter, the achieved product was dried in high vacuum to constant weight yielding the final azido-telechelic PIB (**8**) in quantitative amounts (see results in **table 3**).

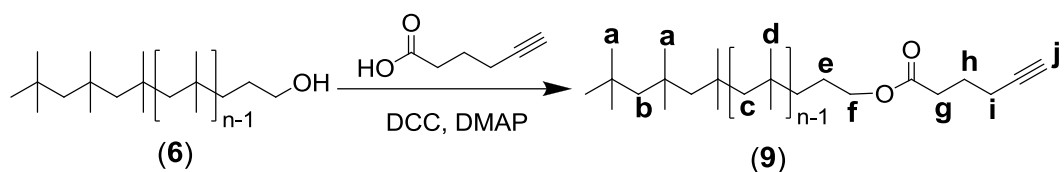
Yield: 0.45 g, (82 %).

¹H-NMR (400 MHz, CDCl₃): δ (ppm) 3.23 (t, $J = 6.98$ Hz, 2H_f), 1.82 (m, 2H_e), 1.40 (br, 2n H_c), 1.09 (s, 6n H_d), 0.99 (s, 15H_a).

¹³C-NMR (400 MHz, CDCl₃): δ (ppm) 59.5 (C_c), 58.8 (C_b), 52.9 (C_f), 42.2 (C_i), 37.9 (C_h), 32.6 (C_g), 31.2 (C_d), 30.9 (C_a), 24.3 (C_e).

FT-IR: ν (cm⁻¹) = 3000-2700 (C-H), 2095 (N₃).

3.1.5 Synthesis of monovalent alkyne-telechelic polyisobutylene (9)¹⁵³



The hydroxy-telechelic polyisobutylene (6) was linked to hex-5-ynoic acid *via* an esterification reaction using *N,N'*-dicyclohexylcarbodiimide (DCC) and a catalytic amount of 4-dimethylaminopyridine (DMAP). A 25-mL one-necked round bottom flask equipped with a magnetic stirrer was charged with DCC (52.0 mg, 0.25 mmol, 1.1 equiv.) and DMAP (2.8 mg, 0.023 mmol, 0.1 equiv.) under dry argon atmosphere. The hydroxy-telechelic PIB (6) (0.5 g, 0.23 mmol) and 1.1 equivalent of hex-5-ynoic acid (28.6 μ L, 0.25 mmol, 1.1 equiv.) were dissolved in dichloromethane (15 mL) and added to the reaction flask. The reaction proceeded for 24 hours, after filtration of the formed *N,N'*-dicyclohexylurea the solvent was removed under reduced pressure. The crude product was redissolved in *n*-hexane and precipitated in methanol. Finally, the alkyne-telechelic PIB (9) was purified by column chromatography using a solvent mixture of *n*-hexane and THF (80:3, $R_f = 0.37$).

Yield: 0.45 g, (90 %).

¹H-NMR (400 MHz, CDCl₃): δ (ppm) 4.05 (t, $J = 6.7$ Hz, 2H_f), 2.44 (t, $J = 7.4$ Hz, 2H_g), 2.25 (m, 2H_h), 1.96 (t, $J = 2.6$ Hz, 1H_j), 1.85 (t, $J = 7.2$ Hz, 2H_i), 1.61 (m, 2H_e), 1.41 (br, 2n H_c), 1.09 (s, 6n H_d), 0.99 (s, 15H_a).

FT-IR: ν (cm⁻¹) = 3316 (-C \equiv C-H), 3000-2700 (C-H), ~2128 (-C \equiv C-H).

Table 3. Characterization and results of end group modification of the allyl-telechelic PIBs (**5**) to the final azido- or alkyne-telechelic PIBs (**8** or **9**).

Entry	Sample	$M_n^{1)}$ (theory)	Characterization				Yield ²⁾ [%]
			$M_n^{1)}$ (GPC)	$M_w^{1)}$ (GPC)	PDI	$M_n^{1)}$ (NMR)	
1	PIB ₃₈ -N ₃ (8a)	2000	2540	3450	1.3	2680	87
2	PIB ₃₅ -N ₃ (8b)	2000	2250	2790	1.2	2320	82
3	PIB ₆₀ -N ₃ (8c)	3000	3380	4100	1.2	3450	85
4	PIB ₇₀ -N ₃ (8d)	4000	4240	5380	1.3	3900	89
5	PIB ₈₇ -N ₃ (8e)	5000	5150	6380	1.2	4920	78
6	PIB ₁₆₀ -N ₃ (8f)	9000	10300	15860	1.5	--- ³⁾	85
7	PIB ₃₅ -alkyne (9)	2000	2740	3670	1.3	2880	90

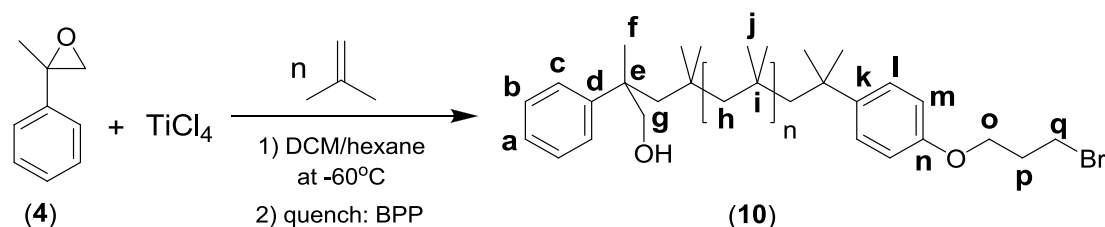
¹⁾ Number average molecular weight in [g/mol].

²⁾ Isolated mass of polymers after conversion to the azide- or alkyne-telechelic PIBs.

³⁾ No NMR analysis performed.

3.1.6 Synthesis of α,ω -telechelic PIBs for nonsymmetric BCPs

3.1.6.1 Synthesis of α -hydroxymethyl- ω -bromo telechelic PIB (**10**)^{148, 154, 155}



The preparation of α -hydroxymethyl- ω -bromo telechelic PIB (**10**) with $M_n = 5000$ g/mol was achieved by a modified procedure of Puskas¹⁴⁹ and Storey et al.¹⁵⁵ as reported elsewhere by Adekunle and coworkers.¹⁵⁴ Under an argon atmosphere, dichloromethane and n-hexane (40/60 mixture), di-*tert*-butylpyridine (*DtBP*) (0.005 mol/L), and initiator (**4**) (0.049 mol/L) were cooled down to -60°C in a three-necked round-bottom flask equipped with a septum and a mechanical stirrer. To the mixture was added a solution of TiCl_4 (0.034 mol/L) and subsequently the polymerization was started by adding condensed isobutylene (1 mol/L) into the reaction mixture *via* syringe. After complete conversion of the monomer (~ 20 minutes), the polymerization mixture was cooled further to -70°C and a quantitative end-capping

reaction was achieved by using an excess of 3-bromopropoxybenzene (BPB) (2.5 equiv per chain end). Finally, after 3 hours, the catalyst was destroyed by addition of methanol (large excess), and the polymer was isolated by repeated precipitation from hexane into methanol. The resulting α -hydroxymethyl- ω -bromo telechelic PIB (**10**) was obtained in a yield of 95%. ($M_{n, GPC} = 4760$ g/mol)

Yield: 2.8 g, (95%).

$^1\text{H-NMR}$ (400 MHz, CDCl_3) δ (ppm): 6.82 (d, $J = 8.79$ Hz, 2H_m), 4.08 (t, $J = 5.78$ Hz, 2H_o), 3.64 (d, $J = 10.77$ Hz, 1H_g), 3.58 (t, $J = 6.53$ Hz, 2H_q), 3.41 (d, $J = 10.78$ Hz, 1H_g), 2.29 (t, $J = 6.23$ Hz, 2H_p).

$^{13}\text{C-NMR}$ (400 MHz, CDCl_3): δ (ppm) 154.1 (C_n), 148.5 (C_d), 141.6 (C_k), 128.4 (C_b), 125.7 (C_i , C_a), 125.1 (C_c), 114 (C_m), 70.1 (C_g), 67.3 (C_p), 53.4 (C_h), 43.8 (C_e), 39.3 (C_j), 30 (C_o), 28 (C_f).

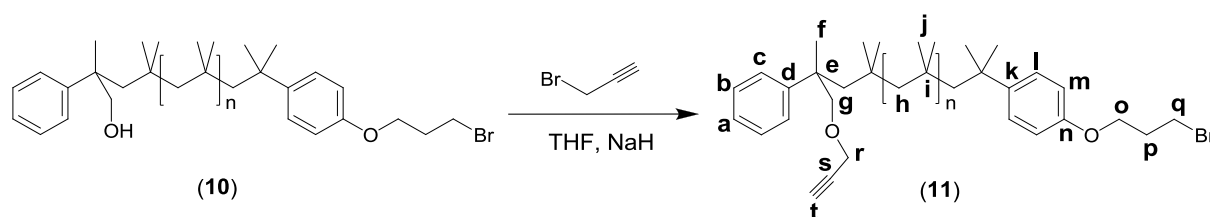
Table 4. Experimental results of isobutylene polymerization using MSE (**4**)/ TiCl_4 as initiator system.

Entry	Sample	$M_n^{1)}$ (theory)	Characterization				Yield ²⁾ [%]
			$M_n^{1)}$ (GPC)	$M_w^{1)}$ (GPC)	PDI	$M_n^{1)}$ (NMR)	
1	HO-PIB ₅₇ -Br (10a)	3000	3190	4950	1.25	3540	92
2	HO-PIB ₇₀ -Br (10b)	4000	3920	5060	1.29	4260	89
3	HO-PIB ₈₅ -Br (10c)	5000	4760	5980	1.25	5080	95
4	HO-PIB ₁₁₆ -Br (10d)	7000	6500	7990	1.23	6130	95

¹⁾ Number average molecular weight in [g/mol].

²⁾ Isolated mass of the polymers.

3.1.6.2 Synthesis of α -alkyne- ω -bromo telechelic PIB (**11**)¹⁵⁴



NaH (1.2 equiv.; 17 mg, 0.714 mmol) was washed three times with dry THF under an argon atmosphere to remove the mineral oil and afterwards cooled to 0°C *via* ice bath. α -

hydroxymethyl- ω -bromo telechelic PIB (**10**) (2.5 g, 0.595 mmol) and 15-crown-5 (1 equiv. 0.131 g, 0.595 mmol) were added drop-wise to the sodium hydride solution. The reaction mixture was allowed to stir for 30 min at 0°C. Subsequently, propargyl bromide (80% in toluene, 2 equiv. 0.141 g, 1.2 mmol) was added slowly to the reaction mixture. The ice bath was removed and the reaction was further stirred at 35°C for 48 hours. Finally, the THF was removed *via* rotary evaporation. The residue was dissolved in hexane, washed three times with water, once with brine and after separation the organic phase was dried over Na₂SO₄. The α -alkyne- ω -bromo telechelic PIB (**11**) was isolated by precipitation from hexane into a mixture of methanol/ acetone (1/1) yielding a slight yellow product.

Yield: 2.4 g, (90%).

¹H NMR (400 MHz, CDCl₃): δ (ppm) 6.81 (d, $J = 8.46$ Hz, 2H_m), 4.08 (m, 4H (H_o+H_r)), 3.64 (d, $J = 10.8$ Hz, 1H_g), 3.58 (t, $J = 6.53$ Hz, 2H_q), 3.41 (d, $J = 10.8$ Hz, 1H_{g'}), 2.35 (m, 1H_t) 2.29 (t, $J = 6.23$ Hz, 2H_p).

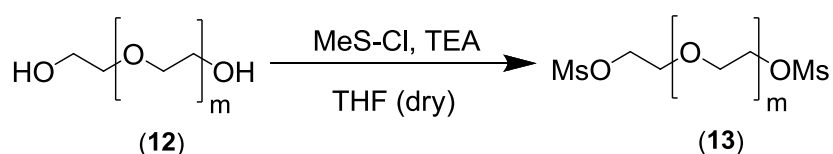
¹³C-NMR (400 MHz, CDCl₃): δ (ppm) 154 (C_n), 148.5 (C_d), 141.6 (C_k), 128.4 (C_b), 125.7 (C_i, C_a), 125.1 (C_c), 114 (C_m), 82.3 (C_g), 75.6 (C_s), 73.4 (C_t), 71.7 (C_r), 67.3 (C_p), 53.4 (C_h), 43.8 (C_e), 32.6 (C_q), 30 (C_o), 28 (C_f).

3.2 End group modification of telechelic PEOs

3.2.1 Synthesis of diazido-telechelic Poly(ethylene oxide) (**14**)^{156, 157}

The azide chain ends were introduced by a two step reaction procedure starting with the mesylation of the hydroxyl-telechelic PEO (**12**) followed by the substitution reaction with sodium azide, according to literature.^{156, 157}

3.2.1.1 Synthesis of mesylated PEO (**13**)^{156, 157}

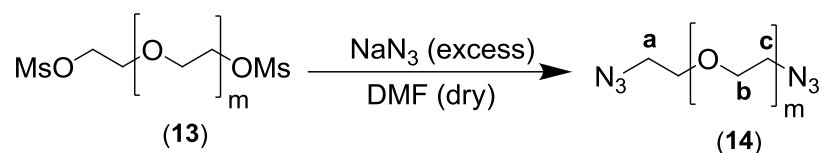


In a two-necked flask, which was flame dried and flushed with argon several times, predried hydroxyl-telechelic PEO (**12**) (M_n = 400 Da, PDI = 1.08) (1 g, 2.4 mmol) dissolved in anhydrous THF (20 mL) was charged and subsequent treated with fresh distilled anhydrous

triethyl amine (TEA) (0.98 g, 9.7 mmol, 4 equiv.). A solution of mesyl chloride (1.1 g, 9.7 mmol, 4 equiv.) in THF (10 mL) was carefully dropped to the reaction mixture and reaction proceeded over night at room temperature. After removal of the solvent, the residue was dissolved in water and five times extracted with dichloromethane. The combined DCM phases were dried over sodium sulfate, filtered and subsequent the solvent removed under reduced pressure. Thereafter, the achieved product (**13**) was short dried in high vacuum yielding a yellow liquid.

Yield: 0.72 g, (52 %).

3.2.1.2 Conversion to the diazido-telechelic PEO (**14**)^{156, 157}



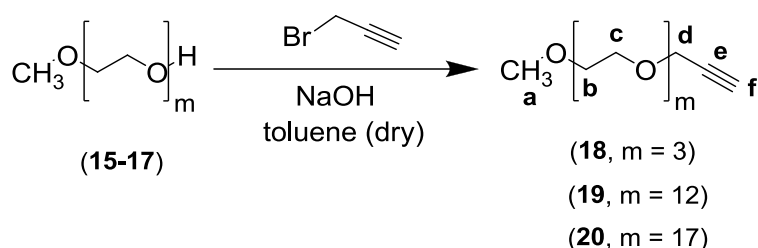
A round bottomed flask was charged with the mesylated PEO (**13**) (0.7 g, 1.2 mmol) and dry DMF (20 mL). The stirred solution was slowly treated with sodium azide (0.4 g, 6.0 mmol, 5 equiv.) and the temperature was raised to 40°C. The reaction mixture was stirred for 48 hours, further the solution was decanted and the solvent removed. The residue was dissolved in water (50 mL), stirred and subsequent three times extracted with DCM (40 mL). Afterwards, the organic phase was dried over Na₂SO₄, filtered and the solvent removed under reduced pressure. Finally, the diazido-telechelic PEO (**14**) was received as orange, viscose liquid.

Yield: 0.49 g, (95 %).

¹H-NMR (400 MHz, CDCl₃): δ (ppm) 3.65-3.60 (m, 38H (H_b+H_c)), 3.35 (t, *J* = 5.3 Hz, 4H_a).

¹³C-NMR (400 MHz, CDCl₃): δ (ppm) 70.7 (C_b), 70.0 (C_c), 50.7 (C_a).

FT-IR: ν (cm⁻¹) = 2102 (N₃).

3.2.2 Synthesis of alkyne-telechelic poly(ethylene oxide) monomethyl ether (18-20)^{144, 158}

Alkyne-telechelic poly(ethylene oxide) monomethyl ethers were prepared according to literature.^{144, 158} A flame dried glass tube was charged with hydroxy-telechelic triethylene oxide (**15**) or poly(ethylene oxide) monomethyl ether (**16** or **17**) ($M_n = 550$ Da or $M_n = 750$ Da, $M_w/M_n = 1.09$) (1.0 g, 1.8 mmol, 1.0 equiv.) and sodium hydroxide (0.7 g, 18.0 mmol, 10.0 equiv.) in toluene (10 mL). A solution of propargyl bromide in toluene (2.0 mL, 18.0 mmol, 10.0 equiv.) was added and the resulting mixture was stirred over night at 50°C. Afterwards, the liquid was decanted and the solvent was removed. The crude product was dissolved in water (10 mL) and extracted three times with DCM (20 mL). Finally, the separated organic phase was dried over sodium sulfate, filtered and the solvent evaporated to achieve (**18-20**) as pale yellow, viscous liquid.

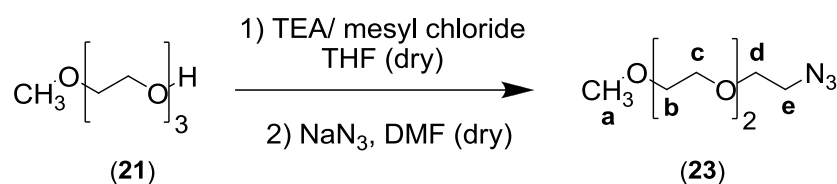
Yield: 0.89 g, (88 %).

¹H-NMR (400 MHz, CDCl₃): δ (ppm) 4.19 (d, $J = 2.35$ Hz, 2 H_d), 3.70-3.51 (m, 4m H (H_b+H_c)), 3.36 (s, 3 H_a), 2.41 (t, $J = 2.34$ Hz, 1 H_f).

¹³C-NMR (400 MHz, CDCl₃): δ (ppm) 79.67 (C_d), 74.4 (C_e), 58.4 (C_f).

FT-IR: ν (cm⁻¹) = 3256 (-C≡C-H), 3000-2700 (C-H), 2117 (-C≡C-H).

3.2.3 Synthesis of α -methoxy- ω -azido telechelic triethylene oxide (TEO) (**23**)¹⁵⁹



Azido-telechelic triethylene oxide (**23**) was prepared in a two step reaction starting with the mesylation of the hydroxyl end group, as reported in the literature.¹⁵⁹ In a two-necked flask, which was flame dried and flushed with argon several times, predried α -methoxy- ω -hydroxy-telechelic TEO (**21**) ($M_n = 164$ Da, $M_w/M_n = 1.08$) (1 g, 6.1 mmol) dissolved in anhydrous THF (20 mL) was charged and subsequent treated with fresh distilled anhydrous triethyl amine (TEA) (1.2 g, 12.2 mmol, 2 equiv.). A solution of mesyl chloride (1.4 g, 12.2 mmol, 2 equiv.) in THF (10 mL) was carefully dropped to the reaction mixture and the reaction proceeded over night at room temperature. After removal of the solvent, the residue was dissolved in water and five times extracted with dichloromethane. The combined DCM phases were dried over sodium sulfate, filtered and subsequent the solvent removed under reduced pressure. Finally, the achieved product (**22**) was short dried in high vacuum yielding a yellow liquid.

The conversion into the α -methoxy- ω -azido-telechelic TEO (**23**) was done as follows: A round bottomed flask was charged with the α -methoxy- ω -mesylated TEO (**22**) and dry DMF (20 mL). The stirred solution was slowly treated with sodium azide (1.2 g, 5 equiv.) and the temperature raised to 40°C. The reaction mixture was stirred for 48 hours, further the solution was decanted and the solvent removed. The residue was dissolved in water (50 mL), stirred and three times extracted with DCM (40 mL). Finally, the organic phase was dried over Na_2SO_4 , filtered and the solvent removed *via* rotary evaporation. The azido-telechelic TEO (**23**) was received as orange, viscose liquid.

Yield: 0.95 g, (90 %).

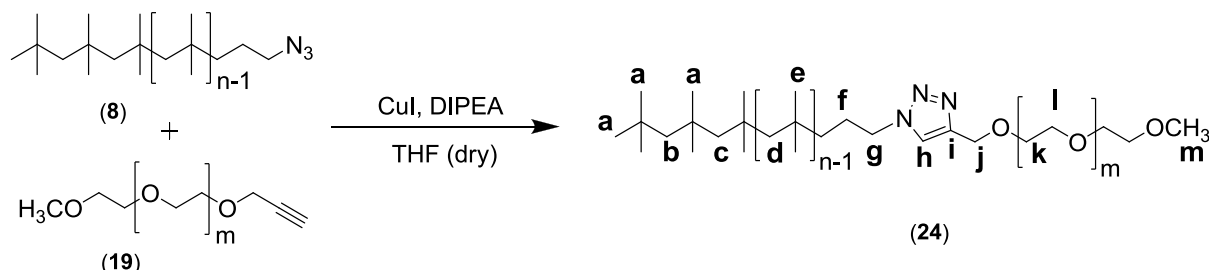
$^1\text{H-NMR}$ (400 MHz, CDCl_3): δ (ppm) 3.65-3.60 (m, 12H ($\text{H}_b + \text{H}_c$)), 3.35 (t, $J = 5.3$ Hz, 2 H_a).

$^{13}\text{C-NMR}$ (400 MHz, CDCl_3): δ (ppm) 70.7 (C_b), 69.9 (C_c), 50.7 (C_e).

FT-IR: ν (cm^{-1}) = 2102 (N_3).

3.3 Azide/alkyne “click”-reaction to generate PIB-PEO based BCPs

3.3.1 Synthesis of amphiphilic PIB-PEO diblock copolymers (24)¹⁴⁴



The azide/alkyne-“click”-reaction was accomplished under an argon atmosphere in a flame dried reaction flask or in a small glass tube. The azide-telechelic PIB (**8**) (50.0 mg, 1.6×10^{-5} mol, 1.1 equiv.) and the alkyne modified PEO (**19**) (8.3 mg, 1.5×10^{-5} mol, 1 equiv.) were charged into the reaction flask. Further the mixture was dissolved in freshly distilled THF (8 mL) and bubbled with a stream of argon over a period of 1 hour to remove the oxygen. The stirred solution was treated with DIPEA (103 μ L, 40 equiv.) and finally with the catalyst copper iodide (0.28 mg, 1.5×10^{-6} mol, 0.1 equiv.). The reaction was accomplished in 2 days at 50°C, followed by filtering the crude product using a flash silica column to separate the catalyst-residues. Subsequent, the solvent was removed under reduced pressure and the product purified by column chromatography on silica gel (CH₃Cl/CH₃OH = 30/1). Finally, the polymer was dried in vacuum to constant weight yielding a pale yellow colored polymer (**24**).

Yield: 37 mg, (68 %).

¹H-NMR (400 MHz, CDCl₃): δ (ppm) 7.54 (s, 1 H_h), 4.67 (s, 2 H_j), 4.26 (t, $J = 7.3$ Hz, 2 H_g), 3.74-3.43 (m, 4m H (H_k+H_l)), 3.36 (s, 3 H_m), 1.98 (m, 4 H (H_b+H_c)), 1.85 (m, 2 H_f), 1.41 (br, 2n H_d), 1.09 (s, 6n H_d), 0.98 (s, 15 H_a).

¹³C-NMR (400 MHz, CDCl₃): δ (ppm) 122.2 (C_h), 109.6 (C_i), 69.7 (C_j), 51.2 (C_g), 25.0 (C_f) (Only resonances for the successful formation of the triazole ring are given).

Table 5. Characterization and experimental results of the synthesized PIB-PEO diblock copolymers *via* azide/alkyne-“click”-reaction using a Cu(I)-iodide as copper(I)-source.

entry	sample	BCP-type	Characterization				Chain length ratio ²⁾	Yield [%]
			M _n ¹⁾ (GPC)	M _w ¹⁾ (GPC)	PDI	M _n ¹⁾ (NMR)		
1	24a	AB	2670	3540	1.3	2250	PIB ₃₇ -PEO ₁₂	30
2	24b	AB	3800	5240	1.2	4790	PIB ₆₇ -PEO ₁₂	78
3	24c	AB	3970	4930	1.2	4460	PIB ₃₇ -PEO ₄₈ ³⁾	82
4	24d	AB	2660	4500	1.6	4320	PIB ₆₀ -PEO ₁₇	67
5	24e	AB	5350	6580	1.2	5900	PIB ₈₇ -PEO ₁₇	80
6	24f	AB	-- ⁴⁾	-- ⁴⁾	-- ⁴⁾	6440	PIB ₈₇ -PEO ₃₇ ³⁾	79

¹⁾ Number or weight average molar mass of the BCPs in g/mol.

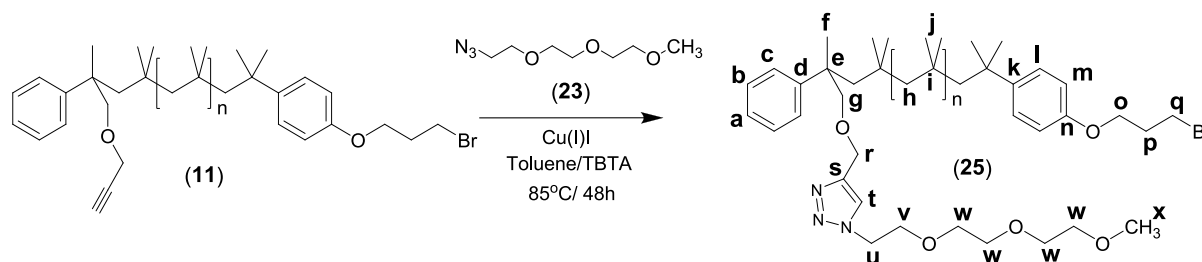
²⁾ Calculated number of the single polymer building blocks by NMR-integration.

³⁾ Alkyne-telechelic PEOs with M_n of 1450 g/mol or 2100 g/mol were used for the azide/alkyne-“click”-reaction (prepared as described in chapter IV/ 3.2.2).

⁴⁾ No GPC analysis performed.

3.3.2 Synthesis of symmetric and nonsymmetric PIB-PEO triblock copolymers

3.3.2.1 Synthesis of α -TEO- ω -bromo telechelic PIB (25)¹⁵⁴



The azide/alkyne-“click”-reaction between α -methoxy- ω -azido telechelic triethylene oxide (TEO) (**23**) and α -alkyne- ω -bromo telechelic PIB (**11**) was conducted under Cu(I)- mediated conditions as follows: Compound (**11**) (1 equiv.), azido-telechelic TEO (**23**) (1 equiv.), tris-(benzyl triazolylmethyl) amine (TBTA) (0.1 equiv.) and Cu(I)-iodide (0.1 equiv.) were dissolved in an argon bubbled toluene (oxygen free) and heated up to 90°C. After 48 hours the solvent was removed *via* rotary evaporation and the crude product was purified by column chromatography on silica gel using a particular procedure (CHCl₃ to remove the unreacted α -

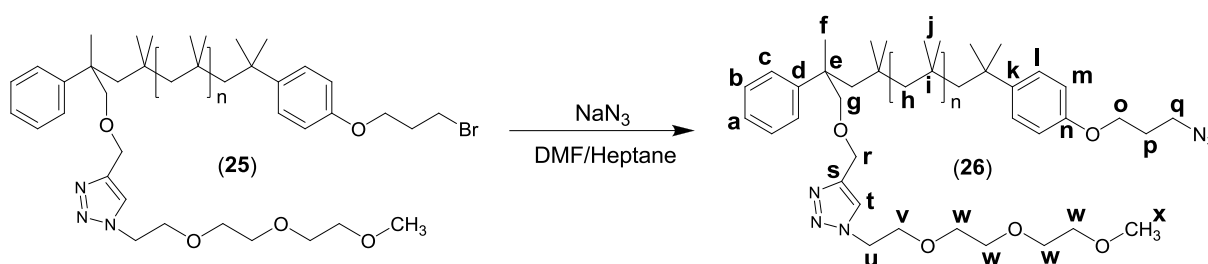
alkyne- ω -bromo telechelic PIB (**11**), $R_f \approx 1$ and followed by $\text{CHCl}_3/\text{CH}_3\text{OH} = 30:1$, $R_f = 0.1$ to remove the unreacted azido-telechelic TEO) yielding the pure α -TEO- ω -bromo telechelic PIB (**25**).

Yield: 1.5 g, (82 %).

$^1\text{H-NMR}$ (400 MHz, CDCl_3): δ (ppm) 7.47 (s, 1H_t), 6.82 (d, $J = 8.41$ Hz, 2H_m), 4.64-4.46 (m, 4H (H_r+H_u)), 4.08 (t, $J = 5.78$ Hz, 2H_o), 3.86 (t, $J = 4.76$ Hz, 2H_v), 3.72-3.47 (m, 12H (H_w+H_q+H_g)), 3.37 (s, 3H_x), 2.29 (t, $J = 6.23$ Hz, 2H_p).

$^{13}\text{C-NMR}$ (400 MHz, CDCl_3): δ (ppm) 154.4 (C_n), 158.8 (C_d), 145.4 (C_r), 142.8 (C_k), 128.8 (C_b), 125.7 (C_l), 125.1 (C_c), 120.9 (C_i), 114.2 (C_m), 81.3 (C_g), 71.8 (C_w), 70.6 (C_w), 69.8 (C_v), 64.8 (C_s), 63.5 (C_p), 59.3 (C_x), 52.9 (C_u), 43.1 (C_e), 32.6 (C_q), 29.3 (C_o), 27.8 (C_f).

3.3.2.2 Synthesis of α -TEO- ω -azido telechelic PIB (**26**)¹⁵⁴



The bromo-telechelic compound (**25**) was converted into the azido-telechelic product as follows: Compound (**25**) (1 g, 0.238 mmol) was dissolved in 100 mL of 50/50 (v/v) mixture of heptane and DMF (two-phase) and treated with sodium azide (14 mg, 2.5 equiv.). The final mixture was heated up to 90°C, upon which it changed to a single phase. The quantitative end group conversion was completed after 5 hours. Afterwards, the reaction mixture was cooled down to room temperature changing back to two phase system. The heptane phase separated and washed three times with deionized water. Finally, the polymer was precipitated into methanol. The obtained product (**26**) was dried under high vacuum.

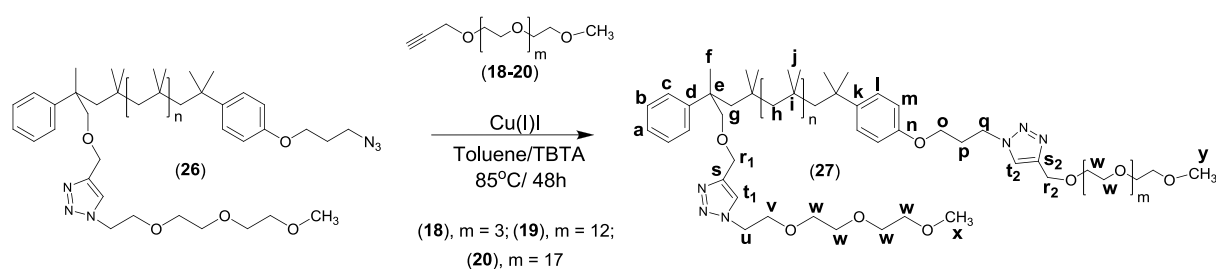
Yield: 0.87 g, (86 %).

$^1\text{H-NMR}$ (400 MHz, CDCl_3): δ (ppm) 7.47 (s, 1H_{t}), 6.82 (d, $J = 8.41$ Hz, 2H_{m}), 4.64-4.46 (m, 4H ($\text{H}_{\text{r}}+\text{H}_{\text{u}}$)), 4.08 (t, $J = 5.78$ Hz, 2H_{o}), 3.86 (t, $J = 4.76$ Hz, 2H_{v}), 3.72-3.47 (m, 12H ($\text{H}_{\text{w}}+\text{H}_{\text{q}}+\text{H}_{\text{g}}$)), 3.37 (s, 3H_{x}).

$^{13}\text{C-NMR}$ (400 MHz, CDCl_3): δ (ppm) 154.4 (C_{n}), 158.8 (C_{d}), 145.4 (C_{r}), 142.8 (C_{k}), 128.8 (C_{b}), 125.7 (C_{l}), 125.1 (C_{c}), 120.9 (C_{i}), 114.2 (C_{m}), 81.3 (C_{g}), 71.8 (C_{w}), 70.6 (C_{w}), 69.8 (C_{v}), 64.8 (C_{s}), 63.5 (C_{p}), 59.3 (C_{x}), 52.9 (C_{u}), 48.3 (C_{q}), 43.1 (C_{e}), 29.3 (C_{o}), 27.8 (C_{f}).

FT-IR: ν (cm^{-1}) = 3000-2700 (C-H), 2095 (N_3).

3.3.2.3 Synthesis of α -TEO- ω -PEO telechelic PIBs (27)



The azide/alkyne-click reaction between α -TEO- ω -azido telechelic PIB (**26**) and α -Methoxy- ω -alkyne-telechelic poly(ethylene oxides) (**18**, **19** or **20**) varying in their repeating unit ($m = 3, 12$ or 17) was conducted under Cu(I)-mediated conditions. Compound (**26**) (1 equiv.), alkyne-telechelic triethylene oxide or poly(ethylene oxide) (**18**, **19** or **20**) (1.1 equiv.), (TBTA) (0.1 equiv.) and Cu(I)-iodide were dissolved in toluene. The reaction mixture was bubbled with argon for 1 h and then heated up to 80°C . After 48 hours, the solvent was removed *via* rotary evaporation and the crude product was purified by column chromatography on silica gel ($\text{CHCl}_3/\text{CH}_3\text{OH} = 30:1$, $R_f = 0.1$ to remove the unreacted alkyne-telechelic PEO) yielding symmetrical or nonsymmetrical α -TEO- ω -PEO telechelic PIB (**27**).

$^1\text{H-NMR}$ (400 MHz, CDCl_3): δ (ppm) 7.59 (s, 1H_{t_2}), 7.47 (s, 1H_{t_1}), 6.82 (d, $J = 8.41$ Hz, 2H_{m}), 4.64-4.45 (m, 8H ($\text{H}_{\text{r}_1}+\text{H}_{\text{u}}+\text{H}_{\text{r}_2}+\text{H}_{\text{q}}$)), 4.01 (t, $J = 5.78$ Hz, 2H_{o}), 3.86 (t, $J = 4.76$ Hz, 2H_{v}), 3.72-3.46 (m, $(4m+8)\text{H}_{\text{w}} + 4\text{H}$ ($\text{H}_{\text{g}}+\text{H}_{\text{q}}$)), 3.37 (s, 6H ($\text{H}_{\text{x}}+\text{H}_{\text{y}}$)), 2.38 (m, 2H_{p}).

$^{13}\text{C-NMR}$ (400 MHz, CDCl_3): δ (ppm) 154.4 (C_n), 158.8 (C_d), 145.4 (C_r), 142.8 (C_k), 128.8 (C_b), 125.7 (C_l), 125.1 (C_c), 121 (C_t), 114.2 (C_m), 81.3 (C_g), 72-70 (C_w), 69.8 (C_v), 64.8 (C_s), 63.5 (C_p), 59-60 (C_x , C_y), 52.9 (C_u), 48.3 (C_q), 43.1 (C_e), 29.3 (C_o), 27.8 (C_f).

Table 6. Characterization and experimental results of end group modification of the α -hydroxymethyl- ω -bromo telechelic PIBs (**10**) and stepwise azide/alkyne-“click”-products to generate symmetric and nonsymmetric triblock copolymers (**27**).

entry	sample	Characterization				Chain length ratio ²⁾	Yield [%]
		M_n ¹⁾ (GPC)	M_w ¹⁾ (GPC)	PDI	M_n ¹⁾ (NMR)		
1	HO-PIB-Br (10c)	4760	5980	1.25	5080	PIB ₈₅	95
2	Alkyne-PIB-Br (11)	4920	6200	1.26	5160	PIB ₈₅	90
3	TEO-PIB-Br (25)	4840	6100	1.26	5360	TEO-PIB ₈₅	82
4	TEO-PIB-N ₃ (26)	4780	5920	1.24	5300	TEO-PIB ₈₅	87
5	TEO-PIB-TEO (27a)	5280	6490	1.23	5500	TEO-PIB ₈₅ -TEO	78
6	TEO-PIB-PEO (27b)	5030	6240	1.24	5930	TEO-PIB ₈₅ -PEO ₁₂	82
7	TEO-PIB-PEO (27c)	4540	5720	1.26	6150	TEO-PIB ₈₅ -PEO ₁₇	67
8	TEO-PIB-TEO (27d)	4220	5270	1.25	5080	TEO-PIB ₇₀ -PEO ₁₂	85

¹⁾ Number or weight average molar mass of the BCPs in g/mol.

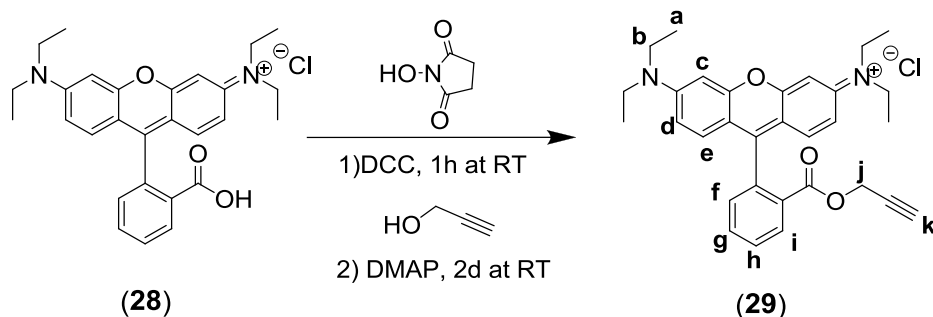
²⁾ Calculated number of the single polymer building blocks by NMR-integration.

Characterization of the tri-BCPs and their pre-steps:

The purity of the final symmetric and nonsymmetric triblock copolymers (**27a-d**) was investigated by HPLC measurements and the desired chemical structure of the tri-BCPs and their pre-steps was proven by NMR spectroscopy and MALDI-TOF MS investigation (see results and methods published recently by our group, “2D-LC/SEC-(MALDI)-MS Characterization of Symmetric and Nonsymmetric Biocompatible PEO_m-PIB-PEO_n Block Copolymers” – *Macromolecules*, **2013**, *46*, 7638-7649.).

3.4 Fluorescent labeling of homo- and block copolymers

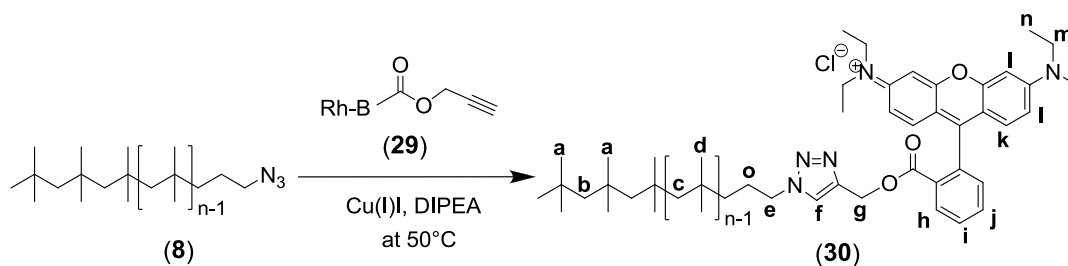
3.4.1 Synthesis of alkyne-modified rhodamine B (Rh B) (**29**)^{160, 161}



The alkyne functionality of rhodamine B was introduced by an esterification reaction according to a modified literature procedure of Wu *et al.*¹⁶¹ using 1,3-dicyclohexylcarbodiimide as esterification agent. Thus, a two-necked-flask, equipped with a septum and N₂ in/outlet, was flame dried and flushed with N₂ two times. A solution of Rh B (**28**) (1.0 g, 2.1 mmol, 1 equiv.) dissolved in fresh distilled anhydrous DCM (30 mL) was filled into the reaction flask *via* a syringe. Subsequent, *N*-hydroxysuccinimide (NHS) (0.27 g, 2.3 mmol, 1.1 equiv.) was added and the reaction proceeded in 1 h at room temperature, followed by the addition of a fourfold excess of propargyl alcohol (0.46 g, 8.3 mmol, 0.45 mL) and a catalytic amount of DMAP (25.3 mg, 0.2 mmol, 0.1 equiv.) dissolved in DCM (2 mL). The resulting mixture was stirred for 2 days at room temperature, followed by precipitation into diethyl ether. The crude product was purified by column chromatography (ethyl acetate/MeOH = 10/2).

Yield: 0.57 g, (53 %).

¹H-NMR (400 MHz, CDCl₃): δ (ppm) 8.36-6.79 (10H, H of benzene ring), 4.64 (s, 2H_j), 3.66 (m, 8H_b), 2.44 (s, 1H_k), 1.22 (q, 12H_a).

3.4.2 Synthesis of rhodamine B labeled polyisobutylene homopolymer (**30**)

The azide/alkyne-“click”-reaction to obtain a fluorescence labeled polyisobutylene homopolymer (**30**) was accomplished under a continuous argon atmosphere in a flame dried reaction flask. The monovalent azido-telechelic PIB (**8**) ($M_n = 1900$ Da, $M_w/M_n = 1.2$) (50.0 mg, 2.6×10^{-5} mol, 1 equiv.) dissolved in THF (5 mL) was charged into the reaction flask. A solution of alkyne-functionalized rhodamin B (**29**) (15.2 mg, 3.2×10^{-5} mol, 1.2 equiv.) dissolved in water (0.75 ml) and DIPEA (240 μ L, 40 equiv.) were added to the stirred solution. Subsequent, the mixture was bubbled with argon to remove the oxygen. Finally, the catalyst Cu(I)-iodide (0.5 mg, 2.6×10^{-6} mol, 0.1 equiv.) and the temperature was raised to 50°C. The above reaction mixture was stirred for 2 days. Furthermore, the mixture was filtered *via* silica flash column and the solvent was evaporated. The crude product was precipitated in acetone and was washed with MeOH three times. Finally, the product was dried to constant weight in high vacuum yielding a violet colored polymer (**30**). The final structure of the fluorescently labeled homopolymer was proved by $^1\text{H-NMR}$ and MALDI-TOF mass spectrometry (see **figure 15**).

Yield: 34 mg (54 %).

$^1\text{H-NMR}$ (400 MHz, CDCl_3): δ (ppm) 8.36-6.79 (10H, H of benzene ring), 7.51 (s, 1H_f), 5.13 (s, 2H_g), 4.26 (t, 2H_e), 3.66 (m, 8H_b), 1.22 (q, 12H_a), 1.55 (m, 14H (H_n+H_o)), 1.40 (br, 2n H_c), 1.09 (s, 6n H_d), 0.98 (s, 15H_a).

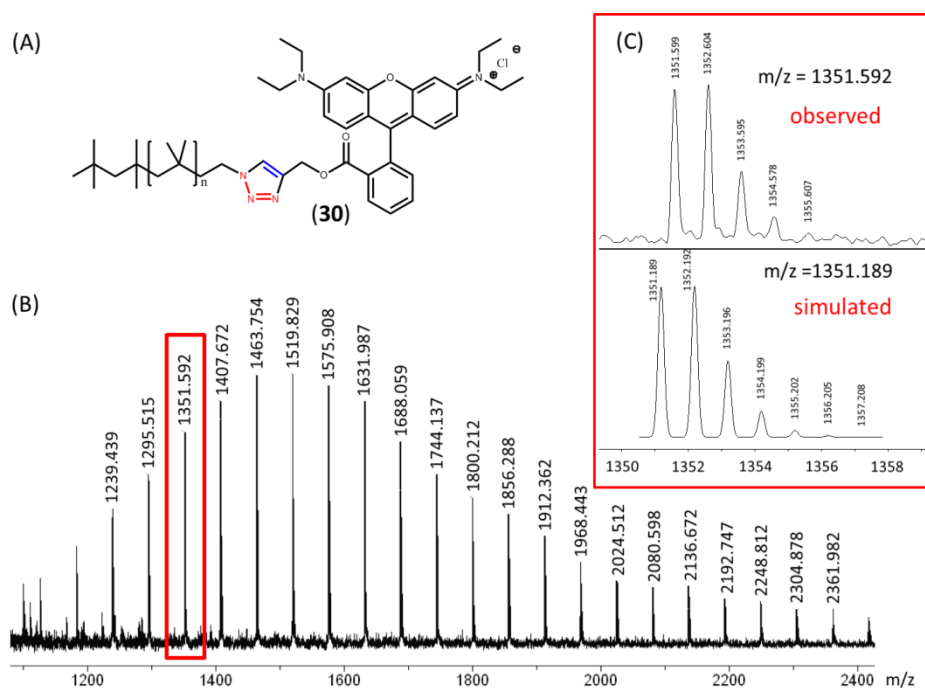
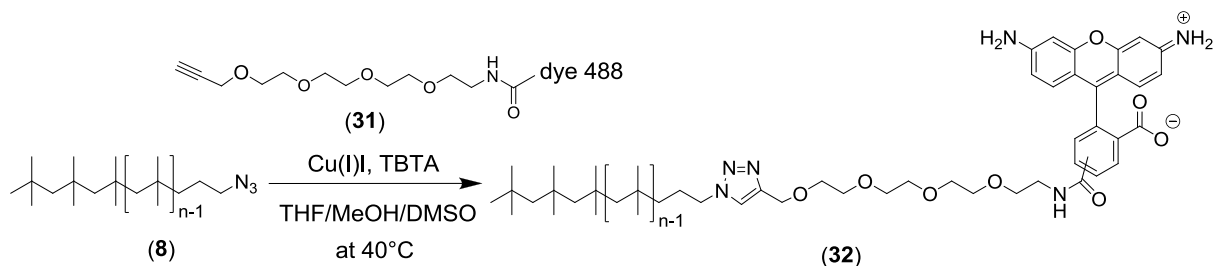
MALDI-TOF MS analysis:

Figure 15. MALDI-TOF mass spectrum of rhodamine B labeled polyisobutylene (**30**). In (A) chemical structure of the desired compound, (B) full view of the recorded mass spectrum and (C) comparison between the observed and simulated isotopic pattern for a singly charged species $[M]^+$ with $M = [C_{41}H_{56}N_5O_3(C_4H_8)_n]$ and $n = 12$.

3.4.3 Synthesis of the fluorescently labeled diblock copolymer (32**)¹⁶²**

For the synthesis of the fluorescently labeled PIB-PEO diblock copolymer (**32**) an azido-telechelic polyisobutylene homopolymer (**8**) (PIB₆₀-N₃, $M_n = 3380$ g/mol with M_w/M_n of 1.2) was prepared and characterized as described in chapter 3.1.4. The corresponding alkyne-functionalized poly(ethylene oxide) block bearing the fluorescent dye (fluor 488 dye, $\lambda_{max} = 494$ nm), which was purchased from *Jena Bioscience GmbH*, was covalently attached to the

polyisobutylene homopolymer *via* Cu(I)-catalyzed azide/alkyne-“click”-reaction. According to the modified procedure of Binder *et al.*,¹⁴⁴ azido-telechelic PIB (**8**) (1 equiv.), acetylene-fluor 488 dye (**31**) (1 equiv.), and tris(1-benzyl-1*H*-1,2,3-triazol-4-yl) methyl]amine (TBTA, 3 equiv.) were dissolved in a solvent mixture of THF, MeOH and DMSO (10/1/0.5), flushed with a stream of argon (~20 min) and subsequently treated with the catalyst Cu(I)-iodide (0.1 equiv.). After 48 hours at 40°C, the crude product was purified by column chromatography to remove the catalyst residues. To remove the contaminating free acetylene-fluor 488 dye (**31**), which was not covalently attached to the PIB block, the final product was precipitated three times using methanol, dissolving undesired compounds. The final structure of the labeled diblock copolymer (**32**) was examined by ESI-TOF MS analysis which confirmed the desired molecular structure of the labeled BCP (see **figure 16**). The absence of free acetylene-fluor 488 in the final product was proven by HPLC.

Yield: 46 mg, (89 %).

ESI-TOF MS analysis:

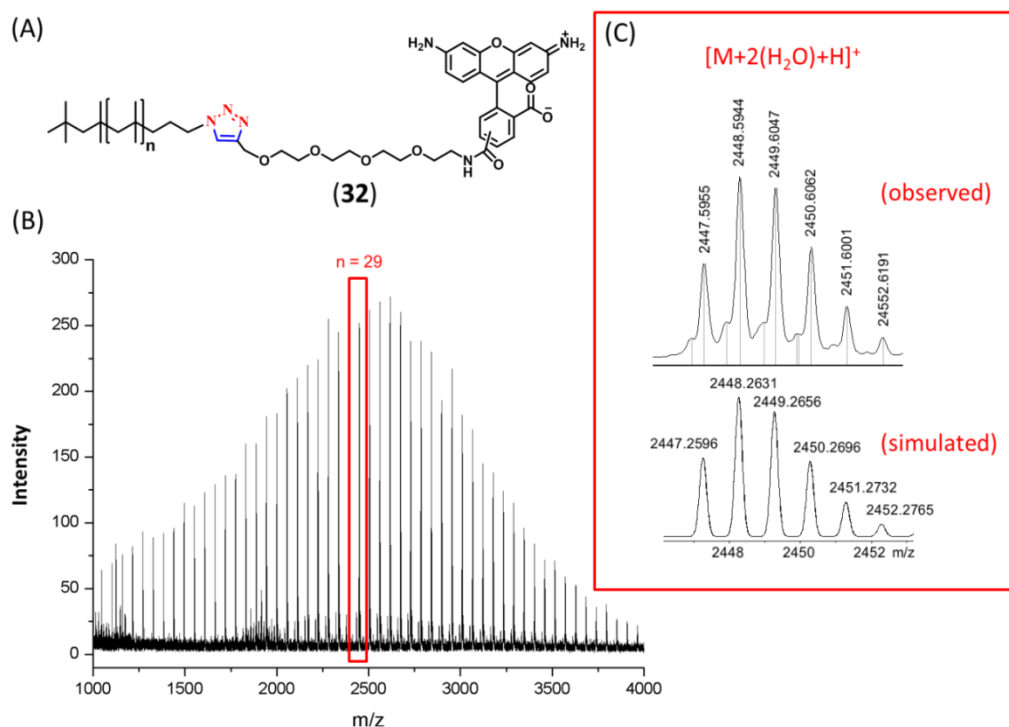
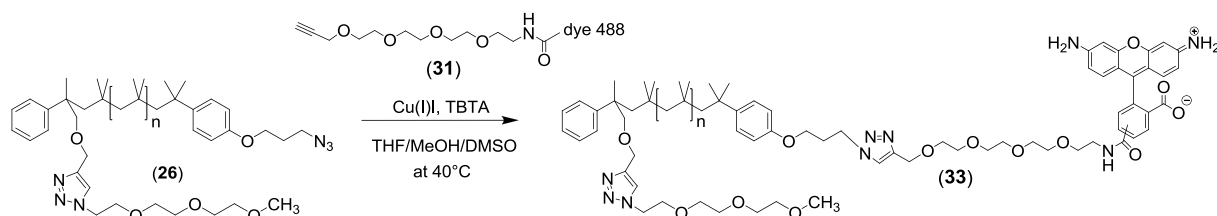


Figure 16. ESI-TOF mass spectrum of the fluorescently labeled di-BCP (**32**). In (A) chemical structure of the desired compound, (B) full view of the recorded mass spectrum and (C) comparison between the observed and simulated isotopic pattern for a singly charged species $[M+2(H_2O)+H]^+$

with $M = [C_{43}H_{56}N_6O_8(C_4H_8)_n]$. The observed side series with significant lower intensities could be assigned to the desired compound **32** (see figure S1 in **appendix B**).

3.4.4 Synthesis of the fluorescently labeled triblock copolymer (**33**)



For the synthesis of the fluorescently labeled triblock copolymer TEO-PIB-PEO₄-dye 488 (**33**), an α -TEO- ω -azido telechelic PIB (**26**) (TEO-PIB₈₅-N₃, $M_n = 4780$ g/mol with M_w/M_n of 1.2) was synthesized and characterized as described in chapter 3.3.2. The corresponding alkyne-functionalized poly(ethylene oxide) block bearing the fluorescence dye (fluor 488), which was purchased from *Jena Bioscience GmbH*, was covalently attached to compound **26** via the Cu(I)-catalyzed azide/alkyne-“click”-reaction. According to the modified procedure of Binder *et al.*,¹⁴⁴ the α -TEO- ω -azido telechelic PIB (1 equiv.), acetylene-fluor 488 dye (**31**) (1 equiv.), and tris(1-benzyl-1*H*-1,2,3-triazol-4-yl) methyl]amine (TBTA, 3 equiv.) were dissolved in a solvent mixture of THF, MeOH and DMSO (10/1/0.5), flushed with a stream of argon (several minutes) and subsequently treated with the catalyst Cu(I)-iodide (0.1 equiv.). After 48 hours at 40°C, the crude product was purified by column chromatography to remove the catalyst residues. To remove free acetylene-fluor 488 dye, the final product was precipitated three times in methanol, dissolving the undesired compounds. The final structure of the labeled triblock copolymer (**33**) was proven by ESI-TOF MS analysis (see **figure 17** and **18**).

Yield: 50 mg, (92 %).

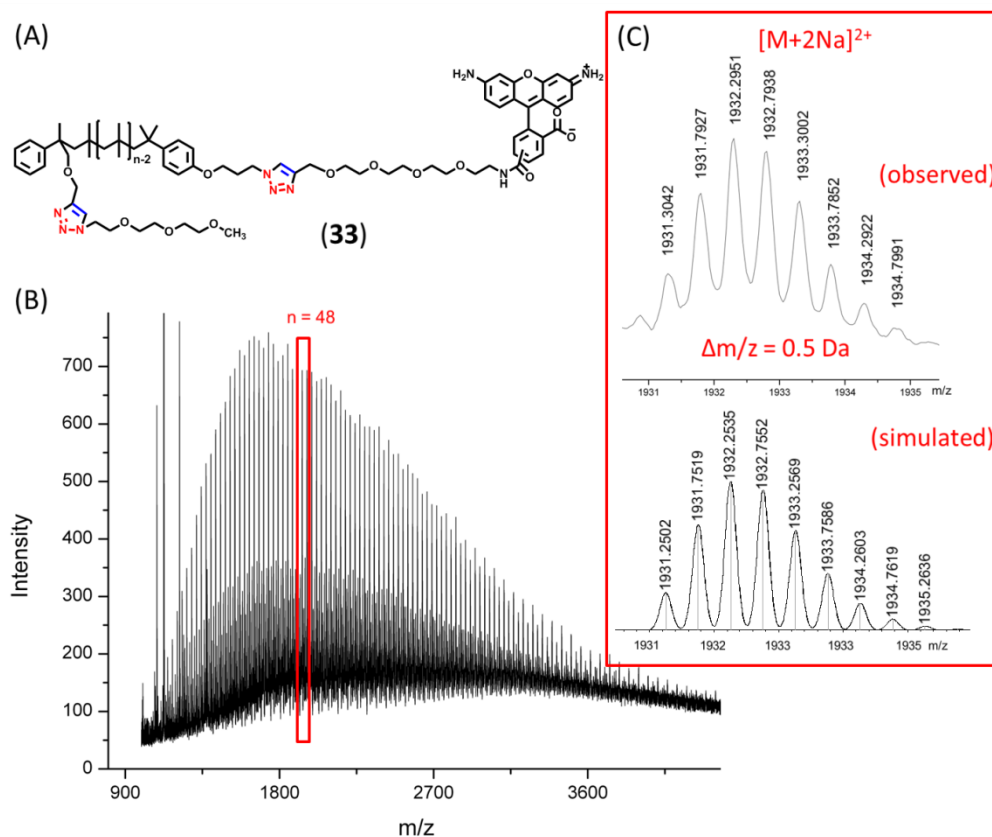
ESI-TOF MS analysis:

Figure 17. ESI-TOF mass spectrum of the fluorescently labeled tri-BCP (**33**). In (A) chemical structure of the desired compound, (B) full view of the recorded mass spectrum and (C) comparison between the observed and simulated isotopic pattern for a doubly charged species $[M+2Na]^{2+}$ with $M = [C_{60}H_{71}N_9O_{13}(C_4H_8)_n]$. The observed side series with lower intensities were further assigned to the desired compound **33** (see **figure 18**).

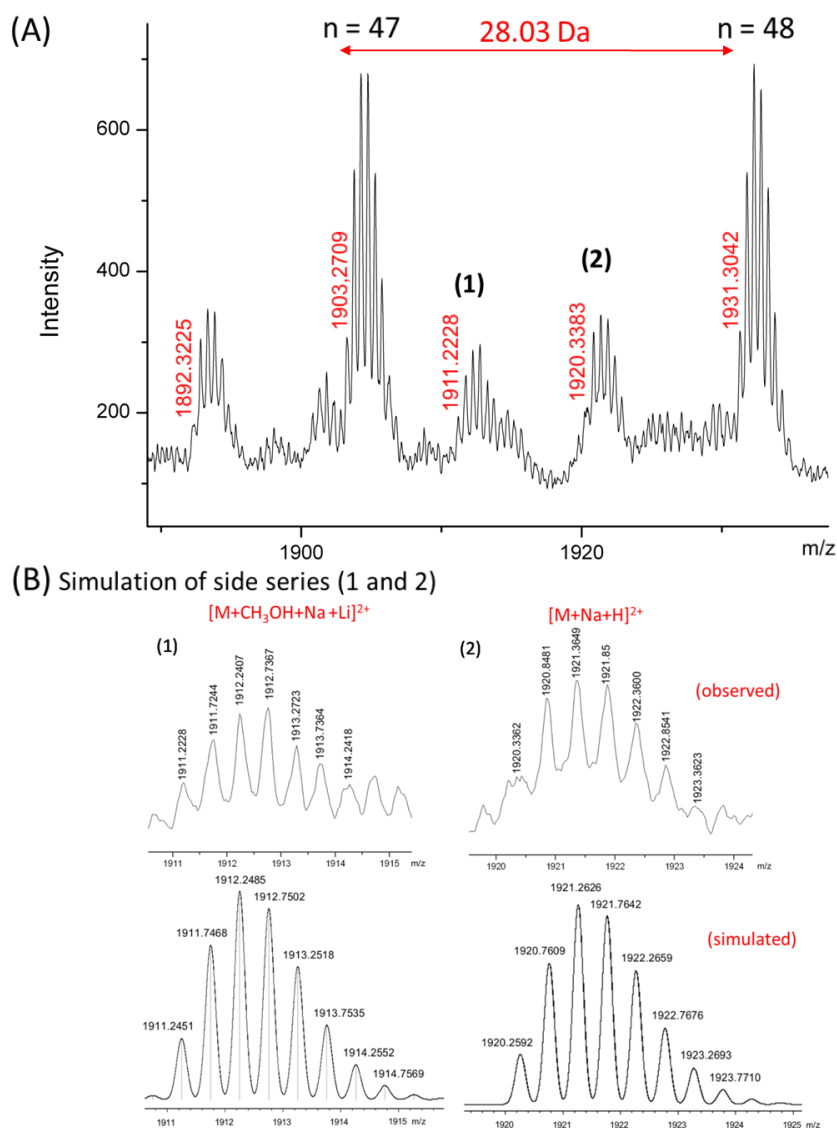
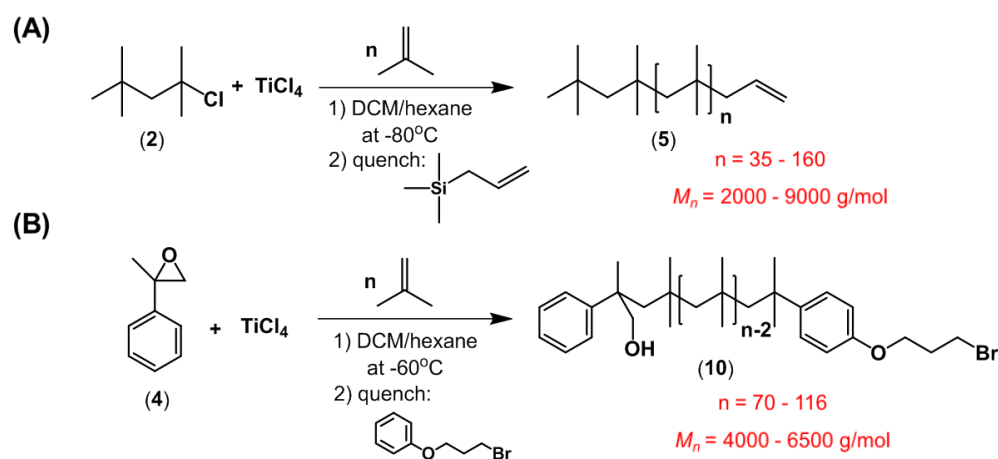


Figure 18. (A) Magnification of the recorded mass spectrum to demonstrate the presence of two side series (1 and 2). (B) Comparison between the observed and simulated isotopic pattern for the different side series, which proved the final structure of the labeled tri-BCP (**33**). Both series (1) $[M+CH_3OH+Na+Li]^{2+}$ and (2) $[M+Na+H]^{2+}$ could be assigned to a doubly charged species of compound **33** with $M = [C_{60}H_{71}N_9O_{13}(C_4H_8)_n]$.

V. Summary

Hybrid lipid/polymer vesicles, mixing/demixing behavior and selective nanoparticle embedding

Summed up, in the present work an efficient method to prepare hybrid lipid/polymer vesicles composed of naturally occurring phospholipids (*e.g.* DPPC or DOPC) and self-prepared amphiphilic polyisobutylene-*block*-poly(ethylene oxide) (PIB-*b*-PEO) copolymers was developed.

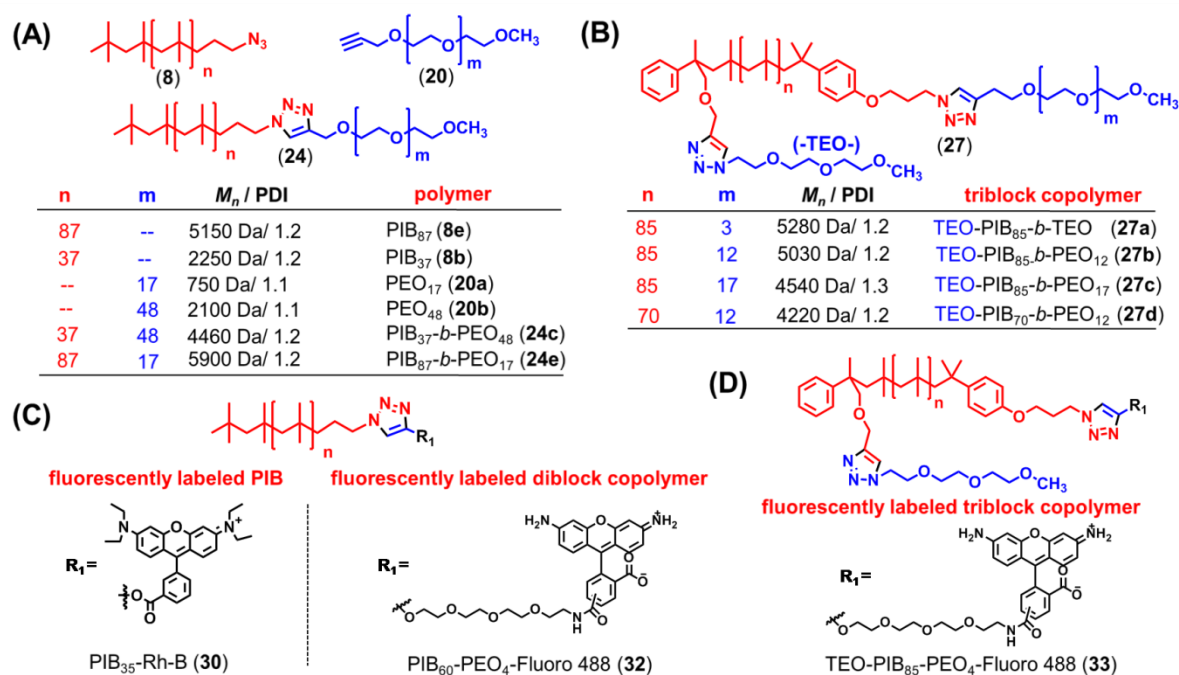


Scheme 2. Synthetic pathway to prepare monovalent allyl-telechelic polyisobutylene (A) and nonsymmetric α,ω -telechelic polyisobutylene polymers (B).

Living carbocationic polymerization (LCCP) of isobutylene (see **scheme 2**) using the monovalent initiator TMPCl (**2**) (2-chloro-2,4,4-trimethyl-pentane) or MSE (**4**) (α -methylstyrene epoxide) with TiCl_4 as coinitiator was successfully applied to generate either monovalent polyisobutylene (**5**) or nonsymmetric α,ω -telechelic polyisobutylene polymers (**10**), respectively. The end group modification of the hydrophobic PIB blocks to the final azide telechelic polymers (**8**) allowed further to covalently connect these molecules with the hydrophilic alkyne-telechelic poly(ethylene oxide) polymers (**20**) *via* the well-known azide/alkyne-“click”-reaction (see polymer structures in **scheme 3**).

In the next step the well-prepared and characterized PIB-PEO based block copolymers (**24a-f** or **27a-d**; compare **scheme 3A** and **3B**), which exhibit similar amphiphilicity as natural lipid molecules, were used to prepare hybrid lipid/polymer vesicles by blending with either DPPC (saturated lipid, T_m of 41.6°C) or DOPC (unsaturated lipid, T_m of -20°C). Herein, the electroformation approach (see conditions in the experimental part of **chapter III/ 1**) was found to be very efficient in generating hybrid vesicles with micrometer sizes feasible to study their membrane morphologies by confocal laser scanning microscopy. Depending on

the molar ratio between the amphiphilic block copolymer and respective lipid, different vesicle morphologies and phase states (mixed or demixed system) were observed (“*Hybrid lipid/polymer giant unilamellar vesicles: effects of incorporated biocompatible PIB-PEO block copolymers on vesicle properties*” – *Soft Matter* **2011**, 7, 8100-8110). It was possible to demonstrate the formation of hybrid GUVs composed of the phospholipid DPPC and two different PIB-PEO based di-BCPs (**24c** and **24e**) which revealed significant differences in the lipid/polymer mixing behavior and particularly in the formation of completely closed membrane morphologies. Both diblock copolymers, the PIB₈₇-*b*-PEO₁₇ (**24e**) and the more hydrophilic PIB₃₇-*b*-PEO₄₈ BCP (**24c**) displaying a longer PEO chain, were successfully embedded into the lipid membrane.



Scheme 3. Schematic representation of the investigated polymer structures. (A) Azide-telechelic polyisobutylene (**8**), alkyne-telechelic poly(ethylene oxide) (**20**) and amphiphilic PIB-PEO based diblock copolymers (**24**) obtained via Cu(I)-mediated azide/alkyne “click”-reaction between compound **8** and **20**. (B) Chemical structures of nonsymmetric triblock copolymers. (C and D) Chemical structures of fluorescently labeled polyisobutylene (**30**) and block copolymers (**32** and **33**).

The incorporation of compound **24c** led to the formation of highly ragged vesicle surfaces over a broad compositional range. Furthermore, the observed hybrid GUVs displayed large open bilayer fragments within the mixed membrane, whereas the PIB₈₇-*b*-PEO₁₇ BCP (**24e**) in mixture with DPPC showed smooth and round vesicle surfaces with a completely closed bilayer membrane. The observed open membrane parts (holes) might be stabilized by the long PEO chains which shield the hydrophobic membrane interior from excess of water.

Interestingly, the interaction of the more hydrophobic BCP (**24e**) and DPPC resulted in the formation of phase separated membrane morphologies in a small compositional range of about 20 to 28 mol% of the BCP.

To study the biocompatibility of such hybrid membranes and the effect of their membrane composition and morphology (mixed or demixed system) in biological recognition processes, the hybrid membranes were functionalized with a natural receptor molecule able to recognize and bind proteins (see publication “*Controlling Molecular Recognition with Lipid/Polymer Domains in Vesicle Membranes*” – *Angew. Chem. Int. Ed.* **2013**, 52, 1829-1833). It was demonstrated that such hybrid lipid/polymer membranes, especially their composition can control the recognition between membrane incorporated receptor molecules and a multivalent protein. The used cholera toxin (protein) binds in a highly cooperative way to ganglioside GM1 receptors (glycosphingolipid), which are known to play a decisive role in cellular recognition processes (cell-to-cell communication in the human nervous system) as surface marker. Confocal microscopy investigations of the protein binding revealed that the GM1 receptor molecules are present in the lipid-rich domains as well as in the polymer-rich phases of demixed GUVs (20 to 28 mol% of compound **24e**). Herein, it was successfully demonstrated that the cholera toxin recognized the GM1-molecules in both phases. At higher polymer amounts (≥ 30 mol% BCP), the initial mixed vesicle morphology changed significantly upon addition of the cholera toxin. Thus, it can be concluded that the increase in membrane fluidity caused by incorporation of polymers (proved by FRAP and FCS studies) and the highly cooperative binding process of the multivalent CTB led in case of hybrid GUVs from DPPC and 30 mol% BCP (**24e**) to the formation of a more ordered GM1-enriched lipid domain. When the polymer was used in amounts of more than 40 mol% in mixtures with DPPC, the obtained hybrid vesicles containing 0.1 mol% of GM1 showed neither recognition nor specific binding of the protein. This is probably due to steric hindrance caused by the PEO chains of the BCPs (17 ethylene oxide units per BCP), whereby at higher BCP contents within the mixed membrane, the PEO chains appear to form a polymer brush, which prevent the receptor/protein recognition.

Fluorescent labeling of di- and triblock copolymers (compound **32** and **33**; see **scheme 3C** and **3D**) was necessary to clearly identify the polymer-rich domains in phase separated lipid/polymer hybrid membranes. The incorporation of amphiphilic PIB-PEO BCPs into model lipid membranes showed over a large compositional range (0 to 60 mol% of BCP) the formation of different membrane morphologies (see **figure 19**). The control over the phase state in hybrid lipid/polymer membranes by simple varying their composition and/or

temperature (above or below the T_m of the lipid) was successfully shown in case of hybrid GUVs obtained from mixtures of DPPC and the PIB₈₇-*b*-PEO₁₇ BCP (**24e**) using 20 to 28 mol% of BCP. Remarkably, above T_m of DPPC the hybrid vesicles depicted a uniform membrane surface (liquid-disordered phase state), whereas upon cooling to RT (below T_m) the hybrid membranes immediately undergo domain formation. The fact that one (see black patch in **figure 19/II**) or mostly few macroscopic domains per vesicle were observed over several hours rather than many small domains reflects the thermodynamic stability of the vesicles.

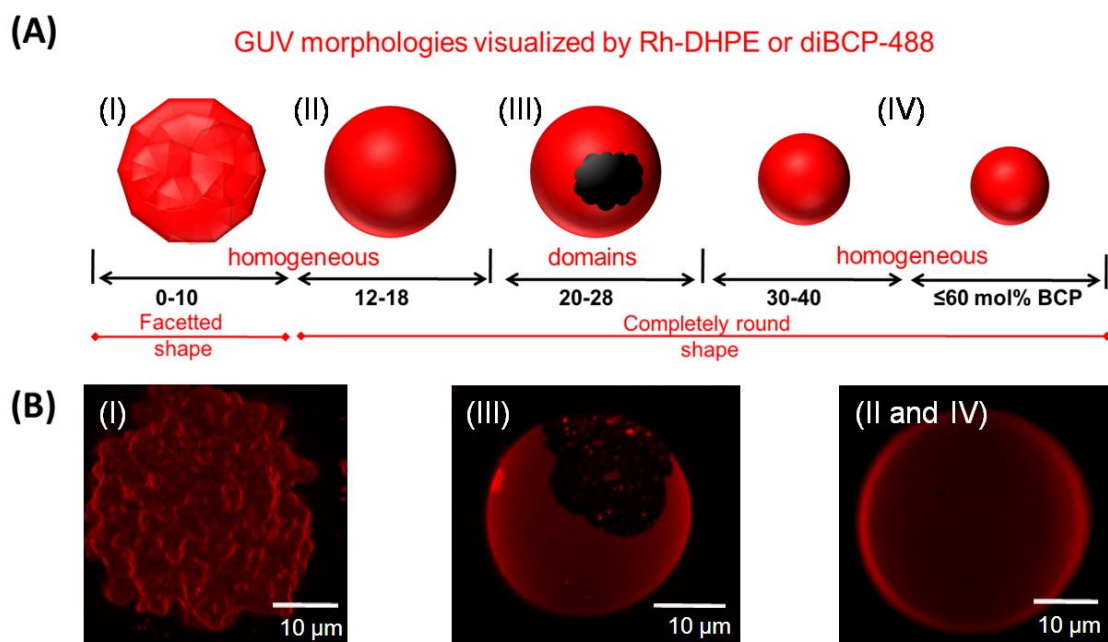


Figure 19. Schematic illustration and results of hybrid GUVs obtained from DPPC and the PIB₈₇-*b*-PEO₁₇ BCP (**24e**) exhibiting different vesicle morphologies (I to IV) and phase states depending on the molar composition between the lipid and polymer component. Compound **32** a fluorescently labeled diblock copolymer (excited at $\lambda_{\max} = 488$ nm) and/or Rh-DHPE (excited at $\lambda_{\max} = 561$ nm) were used to visualize the hybrid membrane morphologies *via* confocal LSM.

The observation of faceted GUVs (0 to 12 mol% BCP) and round GUVs (above 12 mol% BCP, compare **figure 19/I** and **19/II** or **IV**), indicates that a change in the lateral phase state and mobility of membrane components occurred by increasing the amount of BCP within the lipid bilayer. FRAP and FCS measurements (determine the lateral mobility of membrane components) showed clearly that the increase in BCP amount affects the characteristic behavior of rigid DPPC membranes (highly ordered) in such a way that the dense packing of the lipid molecules is drastically changed into a highly mobile membrane system by the polymer incorporation.

Selective proof of specific domains with fluorescently labeled BCPs (compound **32**) (*e.g.* see chemical structure in **figure 20**) and commonly used membrane dyes (*e.g.* DiDC18 or Rh-DHPE) verified that the initial mixed bilayer (at temperatures above T_m of DPPC) undergoes phase separation upon cooling to room temperature forming polymer-rich phases and rigid DPPC-rich domains (gel-state of the bilayer).

Such control of the membrane phase state by temperature and membrane composition allowed further investigations on selective interactions of specific hybrid bilayer parts with functional nanomaterials. A defined surface chemistry of nanoparticles has shown to be an efficient strategy to control the localization of particles within phase separated lipid/polymer membranes.

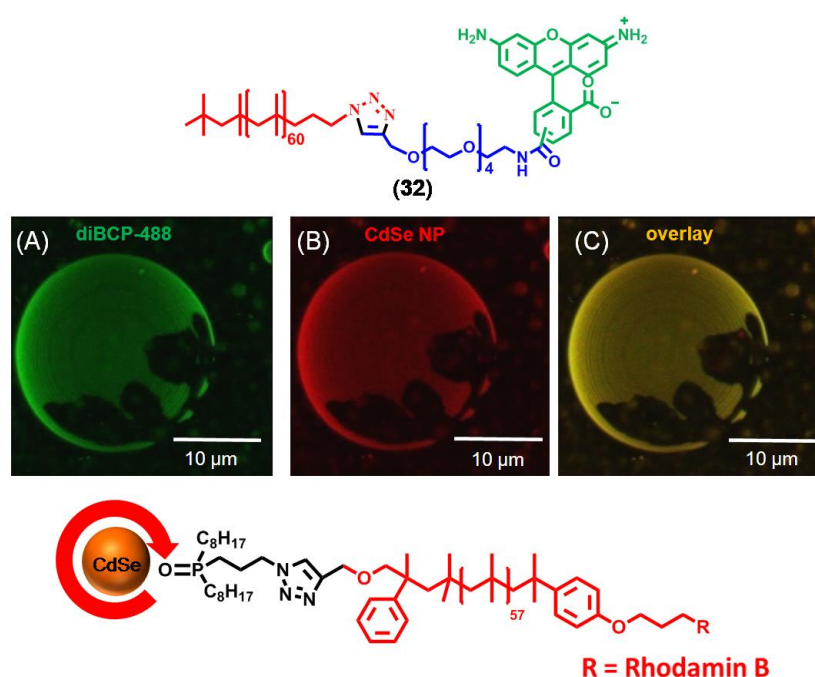


Figure 20. Results of hybrid GUVs and phase selective incorporation of hydrophobically modified nanoparticles. (A) Fluorescently labeled BCP (**32**) (excited at 488 nm, green-colored) within the hybrid membrane (see structure above microscopic vesicle images), (B) fluorescently labeled CdSe-NPs (see structure below microscopic vesicle images), which was excited at 561 nm (red-colored) and (C) overlay image of both excited dyes to clearly demonstrate that NP and BCPs are preferentially partitioned into the same phase preventing their incorporation into the rigid DPPC domains (black patch).

In this context, the third publication (“*Lateral surface engineering of hybrid lipid/BCP vesicles and selective nanoparticle embedding*” – *Soft Matter* **2013**, *Accepted Manuscript*. DOI: 10.1039/C3SM52040D), proved the selective embedding of hydrophobically modified CdSe NPs into the polymer-rich phases of demixed hybrid vesicles. The incorporation of

hydrophobic NPs showed two interesting effects: first, the NPs were distributed within the mixed lipid/polymer membrane depending on the phase state of the hybrid bilayer and second in case of phase separated membrane morphologies it was displayed that the particles and polymers are preferentially incorporated into the same phase, as illustrated in **figure 20**.

In similar experiments with DOPC as fluid membrane component, the NPs were also distributed in accordance to the lipid/polymer mixing state. To conclude, the surface functionalization of the NPs plays a significant role in the phase selective incorporation of the particles into hybrid membranes. Due to preferred interactions between the PIB shell of the CdSe NPs (see chemical structure **figure 20**) and the polyisobutylene chains of the BCPs (**24e**), which form the hydrophobic membrane interior, the particles could be selectively localized within the hydrophobic portion of the polymer-rich phases rather than within the densely packed lipid domains.

To prove our results of the observed phase separation phenomena and the selective NP embedding, a highly selective method to identify membrane heterogeneities without adding a fluorescently labeled molecule to the initial binary lipid/polymer mixtures was developed, considering the fact that such membrane dyes (lipid- or BCP based dyes) can show a different partitioning behavior than the unlabeled ones. Thus, it was possible to develop a specific method to visualize the domain formation process with a specific antibody, which recognizes selectively the PEO functionality of the membrane incorporated BCPs (**24e**). While common membrane dyes such as Rh-DHPE (1,2-dihexadecanoyl-*sn*-glycero-3-phosphoethanolamine-*N*-(lissamine rhodamine B sulfonyl)) or DiDC18 (1,1'-dioctadecyl-3,3,3',3'-tetramethylindodicarbocyanine perchlorate) have shown restrictions in their partitioning behavior visualizing the lipid-rich as well as the polymer-rich phase in hybrid membranes, the identification of specific membrane components by an externally added dye showed advantages. Thus, small membrane heterogeneities within vesicles from mixtures of DPPC and 32 mol% of BCP were monitored, whereas the common membrane dyes displayed a uniform distribution within the hybrid bilayer without observable heterogeneities on the length scales above the optical resolution of the microscope (~200 - 300 nm). When the DPPC-lipid constituted the major component in mixtures with BCP in amounts up to 10 mol%, the obtained hybrid vesicles showed a highly faceted surface (gel state) with a uniform fluorescence of the Rh-DHPE dye within the membrane. The specific antibody-mediated monitoring of BCPs revealed a network-like morphology of the incorporated polymer molecules, assuming that the gel-phase state of the DPPC bilayer at room

temperature leads to macroscopic lipid-rich islands with a high conformational order, surrounded by squeezed out BCP molecules.

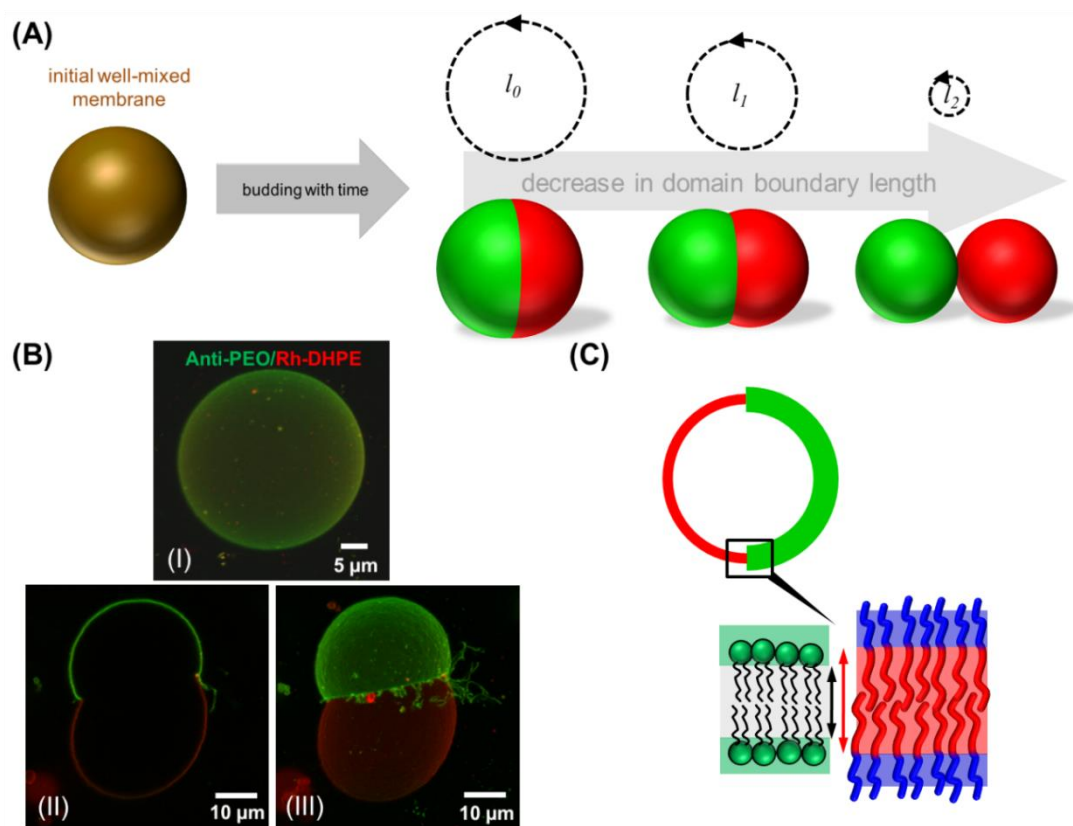


Figure 21. Confocal microscopy results and schematic illustration of the observed vesicle budding process in mixed DOPC/PIB₈₇-*b*-PEO₁₇ BCP GUVs from mixtures with less than 10 mol% of BCP (**24e**). (A) Illustrates the shape transformation during the phase separation and budding of the initial well-mixed vesicles, as shown in (B/I). Such vesicle fission event is favored because the high energetic cost caused by the hydrophobic thickness mismatch between the lipid- and polymer-rich phases (as illustrated in C) at the domain boundary is reduced by decreasing its length (l). (B/II and III) Depict a single confocal slice and a 3D-reconstruction of a series of confocal slices of a hybrid vesicle visualizing the budding process by antibody-mediated monitoring of BCPs (excited at 488 nm, green-colored) and the lipid analogous Rh-DHPE dye (excited at 561 nm, red-colored).

Consequently, the low amount of incorporated BCPs (**24e**) (≤ 10 mol%) was not sufficient to prevent the formation of the gel-phase state (as it was proven by FRAP- and FCS-measurements) – as a result the BCP chains are expelled from the highly ordered DPPC islands concentrating at the edges of these areas.

By varying the lipid component in hybrid GUVs using DOPC (fluid state), which exhibit a totally different phase behavior than the saturated DPPC (gel state) caused by the number of double bonds in their hydrophobic chain tails, it was possible to investigate the effect of fluidity on the stability of lipid/polymer vesicle membranes. As it is shown by recent studies,

the vesicles from BCPs and POPC (fluid phase lipid) undergo phase separation resulting in vesicle budding with time, whereas vesicles from DPPC and BCP did not showed such events (stable over several days).

Therefore, the formation of hybrid vesicles composed of DOPC (fluid component) and PIB₈₇-*b*-PEO₁₇ BCP (**24e**) was investigated. At high amounts of BCP (more than 15 mol%), it was possible to monitor vesicles exhibiting a lateral well-mixed vesicle membrane, which were stable over hours without observable phase heterogeneities on length scales above the optical resolution of the microscope. By monitoring hybrid GUVs obtained from DOPC mixtures with 10 mol% BCP and less (**figure 21**) phase separated membrane morphologies could be clearly identified using the antibody method. These vesicles demonstrated low stabilities resulting in vesicle budding with time that proved the formation of stable DOPC-rich vesicles and polymer-rich vesicles (see **figure 21 B**), which were found to be completely decomposed after hours. The budding process was driven as a result of the line tension at the domain borders caused by the hydrophobic thickness mismatch between the polymer-rich and lipid-rich phases (as illustrated in **figure 21 C**). This mismatch between the size of the polymer (PIB₈₇-*b*-PEO₁₇) and the lipid chains plays a significant role in the formation of either well-mixed or phase separated membrane morphologies (≤ 10 mol% of BCP). In the latter case, the significant mismatch between the hydrophobic core thicknesses of the lipid domain with ~ 3 nm and the polymer-rich phase with approximately 10 nm, which corresponds to one-time folded PIB-chain (fully stretched chain ~ 22 nm), leads to large energetic costs at the domain boundary. Such energetically unfavorable state is minimized by reducing the length of the domain boundary, which drives the vesicle fission to completeness.

VI. REFERENCES

1. Israelachvili, J. N., *Intermolecular and Surface Forces*. 3rd ed.; Elsevier Verlag: 2011 p706.
2. Israelachvili, J., Self-Assembly in Two Dimensions: Surface Micelles and Domain Formation in Monolayers. *Langmuir* **1994**, 10, (10), 3774-3781.
3. Vance, D. E.; Vance, J. E., *Biochemistry of of Lipids, Lipoproteins and Membranes*. 5th ed.; Elsevier Verlag: 2008; p 642.
4. Winter, R., Struktur und Dynamik von Modell-Biomembranen. *Chem. unserer Zeit* **1990**, 24, (2), 71-81.
5. Binder, W. H.; Barragan, V.; Menger, F. M., Domains and Rafts in Lipid Membranes. *Angew. Chem. Int. Ed.* **2003**, 42, (47), 5802-5827.
6. Schulz, M.; Olubummo, A.; Binder, W. H., Beyond the lipid-bilayer: interaction of polymers and nanoparticles with membranes. *Soft Matter* **2012**, 8, (18), 4849-4864.
7. Tribet, C.; Vial, F., Flexible macromolecules attached to lipid bilayers: impact on fluidity, curvature, permeability and stability of the membranes. *Soft Matter* **2008**, 4, (1), 68-81.
8. Amado, E.; Kressler, J., Interactions of amphiphilic block copolymers with lipid model membranes. *Curr. Opin. Colloid Interface Sci.* **2011**, 16, (6), 491-498.
9. Binder, W. H., Polymer-Induced Transient Pores in Lipid Membranes. *Angew. Chem. Int. Ed.* **2008**, 47, 3092-3095.
10. Discher, D. E.; Christian, D. A.; Tian, A.; Ellenbroek, W. G.; Levental, I.; Rajagopal, K.; Janmey, P. A.; Liu, A. J.; Baumgart, T., Spotted vesicles, striped micelles and Janus assemblies induced by ligand binding. *Nat Mater* **2009**, 8, (10), 843-849.
11. Discher, D. E.; Ahmed, F., Polymersomes. *Annu. Rev. Biomed. Eng.* **2006**, 8, 323-341.
12. Discher, D. E.; Eisenberg, A., Polymer Vesicles. *Science* **2002**, 297, 967-973.
13. Discher, B. M.; Won, Y.-Y.; Ege, D. S.; Lee, J. C. M.; Bates, F. S.; Discher, D. E.; Hammer, D. A., Polymersomes: Tough Vesicles Made from Diblock Copolymers. *Science* **1999**, 284, (5417), 1143-1146.
14. Kukula, H.; Schlaad, H.; Antonietti, M.; Förster, S., The Formation of Polymer Vesicles or "Peptosomes" by Polybutadiene-block-poly(L-glutamate)s in Dilute Aqueous Solution. *J. Am. Chem. Soc.* **2002**, 124, (8), 1658-1663.
15. Antonietti, M.; Förster, S., Vesicles and Liposomes: A Self-Assembly Principle Beyond Lipids. *Adv. Mater.* **2003**, 15, (16), 1323-1333.
16. Singer, S. J.; Nicolson, G. L., The Fluid Mosaic Model of the Structure of Cell Membranes. *Science* **1972**, 175, (4023), 720-731.
17. Beattie, M. E.; Veatch, S. L.; Stottrup, B. L.; Keller, S. L., Sterol Structure Determines Miscibility versus Melting Transitions in Lipid Vesicles. *Biophys. J.* **2005**, 89, (3), 1760-1768.
18. Simons, K.; Ikonen, E., How Cells Handle Cholesterol. *Science* **2000**, 290, (5497), 1721-1726.
19. McMullen, T. P. W.; McElhaney, R. N., New aspects of the interaction of cholesterol with dipalmitoylphosphatidylcholine bilayers as revealed by high-sensitivity differential scanning calorimetry. *Biochim. Biophys. Acta* **1995**, 1234, (1), 90-98.
20. Filippov, A.; Orädd, G.; Lindblom, G. r., The Effect of Cholesterol on the Lateral Diffusion of Phospholipids in Oriented Bilayers. *Biophys. J.* **2003**, 84, (5), 3079-3086.
21. Bacia, K.; Schwille, P.; Kurzchalia, T., Sterol structure determines the separation of phases and the curvature of the liquid-ordered phase in model membranes. *PNAS* **2005**, 102, (9), 3272-3277.
22. Sackmann, E., Membrane bending energy concept of vesicle- and cell-shapes and shape-transitions. *FEBS Letters* **1994**, 346, (1), 3-16.

23. Simons, K.; Ikonen, E., Functional rafts in cell membranes. *Nature* **1997**, 387, (6633), 569-572.
24. Semrau, S.; Schmidt, T., Membrane heterogeneity - from lipid domains to curvature effects. *Soft Matter* **2009**, 5, (17), 3174-3186.
25. Simons, K.; Gerl, M. J., Revitalizing membrane rafts: new tools and insights. *Nat. Rev. Mol. Cell. Biol.* **2010**, 11, (10), 688-699.
26. Brown, D. A., Lipid Rafts, Detergent-Resistant Membranes, and Raft Targeting Signals. *Physiology* **2006**, 21, (6), 430-439.
27. Levental, I.; Grzybek, M.; Simons, K., Greasing Their Way: Lipid Modifications Determine Protein Association with Membrane Rafts. *Biochemistry* **2010**, 49, (30), 6305-6316.
28. Spink, C. H.; Yeager, M. D.; Feigenson, G. W., Partitioning behavior of indocarbocyanine probes between coexisting gel and fluid phases in model membranes. *Biochim. Biophys. Acta* **1990**, 1023, (1), 25-33.
29. Weissig, V., *Liposomes: Methods and Protocols, Volume 2: Biological Membrane Models*. Springer New York / Dordrecht / Heidelberg / London: 2010; p 548.
30. Winterhalter, M.; Lasic, D. D., Liposome stability and formation: Experimental parameters and theories on the size distribution. *Chem. Phys. Lipids* **1993**, 64, (1-3), 35-43.
31. Lasic, D. D., *Liposomes: from Physics to Applications*. Elsevier: Amsterdam, 1993.
32. Li; Cheng, J.-X., Coexisting Stripe- and Patch-Shaped Domains in Giant Unilamellar Vesicles. *Biochemistry* **2006**, 45, (39), 11819-11826.
33. Juhasz, J.; Davis, J. H.; Sharom, F. J., Fluorescent probe partitioning in GUVs of binary phospholipid mixtures: Implications for interpreting phase behavior. *Biochim. Biophys. Acta* **2012**, 1818, (1), 19-26.
34. Swiegers, G. F., *Bioinspiration and Biomimicry in Chemistry, Reverse-Engineering Nature*. 1st ed.; John Wiley & Sons, Inc., Hoboken, New Jersey: 2012; p 526.
35. Zhang, X.; Tanner, P.; Graff, A.; Palivan, C. G.; Meier, W., Mimicking the cell membrane with block copolymer membranes. *J. Polym. Sci. Part A: Polym. Chem.* **2012**, 50, (12), 2293-2318.
36. Wang, M.; Zhang, M.; Siegers, C.; Scholes, G. D.; Winnik, M. A., Polymer Vesicles as Robust Scaffolds for the Directed Assembly of Highly Crystalline Nanocrystals. *Langmuir* **2009**, 25(24), 13703-13711.
37. Binder, W. H.; Sachsenhofer, R., Polymersome/Silica Capsules by 'Click'-Chemistry. *Macromol. Rapid Commun.* **2008**, 29, (12-13), 1097-1103.
38. Battaglia, G.; Ryan, A. J.; Tomas, S., Polymeric Vesicle Permeability: A Facile Chemical Assay. *Langmuir* **2006**, 22, (11), 4910-4913.
39. Walde, P.; Cosentino, K.; Engel, H.; Stano, P., Giant Vesicles: Preparations and Applications. *ChemBioChem* **2010**, 11, (7), 848-865.
40. Hishida, M.; Seto, H.; Yamada, N. L.; Yoshikawa, K., Hydration process of multi-stacked phospholipid bilayers to form giant vesicles. *Chem. Phys. Lett.* **2008**, 455, (4-6), 297-302.
41. Shimanouchi, T.; Umakoshi, H.; Kuboi, R., Kinetic Study on Giant Vesicle Formation with Electroformation Method. *Langmuir* **2009**, 25, (9), 4835-4840.
42. Dimitrov, D. S.; Angelova, M. I., Lipid swelling and liposome formation mediated by electric fields. *Bioelectrochem. Bioenerg.* **1988**, 19, (2), 323-336.
43. Angelova, M. I.; Dimitrov, D. S., Liposome electroformation. *Faraday Discuss. Chem. Soc.* **1986**, 81, 303-311.
44. Pott, T.; Bouvrais, H.; Méléard, P., Giant unilamellar vesicle formation under physiologically relevant conditions. *Chem. Phys. Lipids* **2008**, 154, (2), 115-119.

45. Herold, C.; Chwastek, G.; Schwille, P.; Petrov, E. P., Efficient Electroformation of Supergiant Unilamellar Vesicles Containing Cationic Lipids on ITO-Coated Electrodes. *Langmuir* **2012**, 28, (13), 5518-5521.
46. Tanaka-Takiguchi, Y.; Itoh, T.; Tsujita, K.; Yamada, S.; Yanagisawa, M.; Fujiwara, K.; Yamamoto, A.; Ichikawa, M.; Takiguchi, K., Physicochemical Analysis from Real-Time Imaging of Liposome Tubulation Reveals the Characteristics of Individual F-BAR Domain Proteins. *Langmuir* **2013**, 29, (1), 328-336.
47. Heider, E. C.; Barhoum, M.; Edwards, K.; Gericke, K.-H.; Harris, J. M., Structural Characterization of Individual Vesicles using Fluorescence Microscopy. *Ana. Chem.* **2011**, 83, (12), 4909-4915.
48. Fidorra, M.; Heimburg, T.; Bagatolli, L. A., Direct Visualization of the Lateral Structure of Porcine Brain Cerebrosides/POPC Mixtures in Presence and Absence of Cholesterol. *Biophys. J.* **2009**, 97, (1), 142-154.
49. Bacia, K.; Scherfeld, D.; Kahya, N.; Schwille, P., Fluorescence correlation spectroscopy relates rafts in model and native membranes. *Biophys. J.* **2004**, 87, (2), 1034-1043.
50. Parthasarathy, R.; Yu, C.-h.; Groves, J. T., Curvature-Modulated Phase Separation in Lipid Bilayer Membranes. *Langmuir* **2006**, 22, (11), 5095-5099.
51. Wong, B. Y.; Faller, R., Phase behavior and dynamic heterogeneities in lipids: A coarse-grained simulation study of DPPC-DPPE mixtures. *Biochim. Biophys. Acta* **2007**, 1768, (3), 620-627.
52. Shi, Q.; Voth, G. A., Multi-Scale Modeling of Phase Separation in Mixed Lipid Bilayers. *Biophys. J.* **2005**, 89, (4), 2385-2394.
53. Shoemaker, S. D.; Vanderlick, T. K., Calcium modulates the mechanical properties of anionic phospholipid membranes. *J. Colloid Interface Sci.* **2003**, 266, (2), 314-321.
54. Tilcock, C. P. S.; Cullis, P. R.; Gruner, S. M., Calcium-induced phase separation phenomena in multicomponent unsaturated lipid mixtures. *Biochemistry* **1988**, 27, (5), 1415-1420.
55. Haverstick, D. M.; Glaser, M., Visualization of Ca²⁺-induced phospholipid domains. *PNAS* **1987**, 84, (13), 4475-4479.
56. Korlach, J.; Schwille, P.; Webb, W. W.; Feigenson, G. W., Characterization of lipid bilayer phases by confocal microscopy and fluorescence correlation spectroscopy. *PNAS* **1999**, 96, (15), 8461-8466.
57. Baumgart, T.; Hess, S. T.; Webb, W. W., Imaging coexisting fluid domains in biomembrane models coupling curvature and line tension. *Nature* **2003**, 425, (6960), 821-824.
58. Hammond, A. T.; Heberle, F. A.; Baumgart, T.; Holowka, D.; Baird, B.; Feigenson, G. W., Crosslinking a lipid raft component triggers liquid ordered-liquid disordered phase separation in model plasma membranes. *PNAS* **2005**, 102, (18), 6320-6325.
59. Menger, F. M.; Davydov, D. A.; Yaroslavova, E. G.; Rakhnyanskaya, A. A.; Efimova, A. A.; Ermakov, Y. A.; Yaroslavov, A. A., Polymer Migration among Phospholipid Liposomes. *Langmuir* **2009**, 25, (23), 13528-13533.
60. Menger, F. M.; Yaroslavov, A. A.; Melik-Nubarov, N. S., Polymer-Induced Flip-Flop in Biomembranes. *Acc. Chem. Res.* **2006**, 39, (39), 702-710.
61. Kunitake, T., *Physical Chemistry of Biological Interfaces, Editor(s): Baszkin, Adam; Norde, Willem* **2000**, Publisher: Marcel Dekker, Inc., New York, N. Y., 283.
62. Kunitake, T., Synthetic Bilayer Membranes: Molecular Design, Self-Organization, and Application. *Angew. Chem. Int. Ed.* **1992**, 31, (6), 709-726.
63. Ringsdorf, H.; Schlarb, B.; Venzmer, J., Molekulare Architektur und Funktion von polymeren orientierten Systemen Modelle für das Studium von Organisation,

- Oberflächenerkennung und Dynamik bei Biomembranen. *Angew. Chem.* **1988**, 100, 117-162.
64. Malinova, V.; Belegirinou, S.; Bruyn Ouboter, D. d.; Meier, W., Biomimetic Block Copolymer Membranes. In *Adv. Polym. Sci.*, Springer Berlin / Heidelberg: 2011; pp 1-53.
65. Mecke, A.; Dittrich, C.; Meier, W., Biomimetic membranes designed from amphiphilic block copolymers. *Soft Matter* **2006**, 2, (9), 751-759.
66. Kita-Tokarczyk, K.; Grumelard, J.; Haefele, T.; Meier, W., Block copolymer vesicles – using concepts from polymer chemistry to mimic biomembranes. *Polymer* **2005**, 46, 3540-3563.
67. Meier, W., Polymer nanocapsules. *Chem. Soc. Rev.* **2000**, 29, 295-303.
68. Blanazs, A.; Armes, S. P.; Ryan, A. J., Self-Assembled Block Copolymer Aggregates: From Micelles to Vesicles and their Biological Applications. *Macromol. Rapid Commun.* **2009**, 30, 267-277.
69. Bermúdez, H.; Hammer, D. A.; Discher, D. E., Effect of Bilayer Thickness on Membrane Bending Rigidity. *Langmuir* **2004**, 20, (3), 540-543.
70. Ma, L.; Eisenberg, A., Relationship between Wall Thickness and Size in Block Copolymer Vesicles. *Langmuir* **2009**, 25, (24), 13730-13736.
71. Sachsenhofer, R.; Binder, W. H.; Farnik, D.; Zirbs, R., Polymersome-Embedded Nanoparticles. *Macromol. Symp.* **2007**, 254, 375-377.
72. Binder, W. H.; Sachsenhofer, R.; Farnik, D.; Blaas, D., Guiding the location of nanoparticles into vesicular structures: a morphological study. *Phys. Chem. Chem. Phys.* **2007**, 9, 6435-6441.
73. Lecommandoux, S.; Sandre, O.; Chécot, F.; Rodriguez-Hernandez, J.; Perzynski, R., Magnetic Nanocomposite Micelles and Vesicles. *Adv. Mater.* **2005**, 17, (6), 712-718.
74. Mueller, W.; Pierrat, S.; Koynov, K.; Basche, T.; Fischer, K.; Hartmann, S.; Maskos, M., Hydrophobic Shell Loading of PB-b-PEO Vesicles. *Macromolecules* **2009**, 42, 357-361.
75. Gopalakrishnan, G.; Danelon, C.; Izewska, P.; Prummer, M.; Yves Bolinger, P.; Geissbühler, I.; Demurtas, D.; Dubochet, J.; Vogel, H., Multifunctional Lipid/Quantum Dot Hybrid Nanocontainers for Controlled Targeting of Live Cells. *Angew. Chem. Int. Ed.* **2006**, 45, 5478-5483.
76. Mai, Y.; Eisenberg, A., Controlled Incorporation of Particles into the Central Portion of Vesicle Walls. *J. Am. Chem. Soc.* **2010**, 132, (29), 10078-10084.
77. Lecommandoux, S.; Sanson, C.; Diou, O.; Thevènot, J.; Ibarboure, E.; Soum, A.; Brûlet, A.; Miraux, S.; Thiaudière, E.; Tan, S.; Brisson, A.; Dupuis, V.; Sandre, O., Doxorubicin Loaded Magnetic Polymersomes: Theranostic Nanocarriers for MR Imaging and Magneto-Chemotherapy. *ACS Nano* **2011**, 5, (2), 1122-1140.
78. Amstad, E.; Kim, S.-H.; Weitz, D. A., Photo- and Thermoresponsive Polymersomes for Triggered Release. *Angew. Chem. Int. Ed.* **2012**, 51, (50), 12499-12503.
79. Faraudo, J.; Andreu, J. S.; Camacho, J., Understanding diluted dispersions of superparamagnetic particles under strong magnetic fields: a review of concepts, theory and simulations. *Soft Matter* **2013**, 9, (29), 6654-6664.
80. Lee, M. H.; Hribar, K. C.; Brugarolas, T.; Kamat, N. P.; Burdick, J. A.; Lee, D., Harnessing Interfacial Phenomena to Program the Release Properties of Hollow Microcapsules. *Adv. Funct. Mater.* **2012**, 22, (1), 131-138.
81. An, X.; Zhang, F.; Zhu, Y.; Shen, W., Photoinduced drug release from thermosensitive AuNPs-liposome using a AuNPs-switch. *Chem. Commun.* **2010**, 46, (38), 7202-7204.
82. Jain, P. K.; Huang, X.; El-Sayed, I. H.; El-Sayed, M. A., Noble Metals on the Nanoscale: Optical and Photothermal Properties and Some Applications in Imaging, Sensing, Biology, and Medicine. *Acc. Chem. Res.* **2008**, 41, (12), 1578-1586.

83. Shum, H. C.; Kim, J.-W.; Weitz, D. A., Microfluidic Fabrication of Monodisperse Biocompatible and Biodegradable Polymersomes with Controlled Permeability. *J. Am. Chem. Soc.* **2008**, 130, (29), 9543-9549.
84. Kim, S.-H.; Kim, J.; Kim, D.-H.; Han, S.-H.; Weitz, D., *Enhanced-throughput production of polymersomes using a parallelized capillary microfluidic device.* Springer-Verlag: 2013; Vol. 14, p 509-514.
85. Lecommandoux, S.; Perro, A.; Nicolet, C. I.; Angly, J.; Le Meins, J.-F. o.; Colin, A., Mastering a Double Emulsion in a Simple Co-Flow Microfluidic to Generate Complex Polymersomes. *Langmuir* **2011**, 27, (14), 9034-9042.
86. Shum, H. C.; Zhao, Y.; Kim, S.; Weitz, D. A., Multicompartment Polymersomes from Double Emulsions. *Angew. Chem. Int. Ed.* **2011**, 50, 1648-1651.
87. Kim, S.-H.; Shum, H. C.; Kim, J. W.; Cho, J.-C.; Weitz, D. A., Multiple Polymersomes for Programmed Release of Multiple Components. *J. Am. Chem. Soc.* **2011**, 133, (38), 15165-15171.
88. Smart, T. P.; Mykhaylyk, O. O.; Ryan, A. J.; Battaglia, G., Polymersomes hydrophilic brush scaling relations. *Soft Matter* **2009**, 5, 3607-3610.
89. Palermo, E. F.; Lee, D.-K.; Ramamoorthy, A.; Kuroda, K., Role of Cationic Group Structure in Membrane Binding and Disruption by Amphiphilic Copolymers. *J. Phys. Chem. B* **2011**, 115, (2), 366-375.
90. Sikor, M.; Sabin, J.; Keyvanloo, A.; Schneider, M. F.; Thewalt, J. L.; Bailey, A. E.; Frisken, B. J., Interaction of a Charged Polymer with Zwitterionic Lipid Vesicles. *Langmuir* **2010**, 26, (6), 4095-4102.
91. Wu, G.; Khant, H. A.; Chiu, W.; Lee, K. Y. C., Effects of bilayer phases on phospholipid-poloxamer interactions. *Soft Matter* **2009**, 5, (7), 1496-1503.
92. Teramura, Y.; Kaneda, Y.; Totani, T.; Iwata, H., Behavior of synthetic polymers immobilized on a cell membrane. *Biomaterials* **2008**, 29, 1345-1355.
93. Frey, S. L.; Zhang, D.; Carignano, M. A.; Szeleifer, I.; Lee, K. Y. C., Effects of block copolymer's architecture on its association with lipid membranes: Experiments and simulations. *J. Chem. Phys.* **2007**, 127, (11), 114904-12.
94. Mourelatou, E. A.; Libster, D.; Nir, I.; Hatziantoniou, S.; Aserin, A.; Garti, N.; Demetzos, C., Type and Location of Interaction between Hyperbranched Polymers and Liposomes. Relevance to Design of a Potentially Advanced Drug Delivery Nanosystem (aDDnS). *J. Phys. Chem. B* **2011**, 115, 3400-3408.
95. Ionov, M.; Gardikis, K.; Wróbel, D.; Hatziantoniou, S.; Mourelatou, H.; Majoral, J.; Klajnert, B.; Bryszewska, M.; Demetzos, C., Interaction of cationic phosphorus dendrimers (CPD) with charged and neutral lipid membranes. *Colloids Surf., B* **2011**, 82, 8-12.
96. Raudino, A.; Castelli, F.; Gurrieri, S., Polymer-induced lateral phase separation in mixed lipid membranes: a theoretical model and calorimetric investigation. *J. Phys. Chem.* **1990**, 94, (4), 1526-1535.
97. Menger, F. M.; Yaroslavov, A. A.; Sybachin, A. V.; Kesselman, E.; Schmidt, J.; Talmon, Y.; Rizvi, S. A. A., Liposome Fusion Rates Depend upon the Conformation of Polycation Catalysts. *J. Am. Chem. Soc.* **2011**, 133, (9), 2881-2883.
98. Ringsdorf, H.; Sackmann, E.; Simon, J.; Winnik, F. M., Interactions of liposomes and hydrophobically-modified poly-(N-isopropylacrylamides): an attempt to model the cytoskeleton. *Biochim. Biophys. Acta. (BBA) - Biomembranes* **1993**, 1153, (2), 335-344.
99. Zhao, F.; Cheng, X.; Liu, G.; Zhang, G., Interaction of Hydrophobically End-Capped Poly(ethylene glycol) with Phospholipid Vesicles: The Hydrocarbon End-Chain Length Dependence. *J. Phys. Chem. B* **2010**, 114, (3), 1271-1276.

100. Simon, J.; Kühner, M.; Ringsdorf, H.; Sackmanna, E., Polymer-induced shape changes and capping in giant liposomes. *Chem. Phys. Lipids* **1995**, 76, (2), 241-258.
101. Menger, F. M.; Sybachin, A. V.; Ballauff, M.; Kesselman, E.; Schmidt, J.; Talmon, Y.; Tsarkova, L.; Yaroslavov, A. A., Complexation of Anionic Liposomes with Spherical Polycationic Brushes. *Langmuir* **2011**, 27, (9), 5310-5315.
102. Menger, F. M., Remembrances of Self-Assemblies Past. *Langmuir* **2011**, 27, (9), 5176-5183.
103. Menger, F. M.; Yaroslavov, A. A.; Rakhnyanskaya, A. A.; Yaroslavova, E. G.; Efimova, A. A., Polyelectrolyte-coated liposomes: Stabilization of the interfacial complexes. *Adv. Colloid Interface Sci.* **2008**, 142, (1-2), 43-52.
104. Quemeneur, F.; Rinaudo, M.; Maret, G.; Pepin-Donat, B., Decoration of lipid vesicles by polyelectrolytes: mechanism and structure. *Soft Matter* **2010**, 6, (18), 4471-4481.
105. Ngo, A. T.; Cosa, G., Assembly of Zwitterionic Phospholipid/Conjugated Polyelectrolyte Complexes: Structure and Photophysical Properties. *Langmuir* **2010**, 26, (9), 6746-6754.
106. Whitten, D. G.; Ding, L.; Chi, E. Y.; Chemburu, S.; Ji, E.; Lopez, G. P.; Schanze, K. S., Insight into the Mechanism of Antimicrobial Poly(phenylene ethynylene) Polyelectrolytes: Interactions with Phosphatidylglycerol Lipid Membranes. *Langmuir* **2009**, 25(24), 13742-13751.
107. Hong, S.; Leroueil, P. R.; Janus, E. K.; Peters, J. L.; Kober, M.-M.; Islam, M. T.; Orr, B. G.; Baker, J. R.; Banaszak Holl, M. M., Interaction of Polycationic Polymers with Supported Lipid Bilayers and Cells: Nanoscale Hole Formation and Enhanced Membrane Permeability. *Bioconjugate Chem.* **2006**, 17, (3), 728-734.
108. Menger, F. M.; Yaroslavov, A. A.; Sitnikova, T. A.; Rakhnyanskaya, A. A.; Yaroslavova, E. G.; Davydov, D. A.; Burova, T. V.; Grinberg, V. Y.; Shi, L., Biomembrane Sensitivity to Structural Changes in Bound Polymers. *J. Am. Chem. Soc.* **2009**, 131, (5), 1666-1667.
109. Wu, G.; Lee, K. Y. C., Effects of Poloxamer 188 on Phospholipid Monolayer Morphology: An Atomic Force Microscopy Study. *Langmuir* **2009**, 25, (4), 2133-2139.
110. Amado, E.; Kerth, A.; Blume, A.; Kressler, J. r., Infrared Reflection Absorption Spectroscopy Coupled with Brewster Angle Microscopy for Studying Interactions of Amphiphilic Triblock Copolymers with Phospholipid Monolayers. *Langmuir* **2008**, 24, (18), 10041-10053.
111. Frey, S. L.; Lee, K. Y. C., Temperature Dependence of Poloxamer Insertion Into and Squeeze-Out from Lipid Monolayers. *Langmuir* **2007**, 23, (5), 2631-2637.
112. Hussain, H.; Kerth, A.; Blume, A.; Kressler, J., Amphiphilic Block Copolymers of Poly(ethylene oxide) and Poly(perfluorohexylethyl methacrylate) at the Water Surface and Their Penetration into the Lipid Monolayer. *J. Phys. Chem. B* **2004**, 108, (28), 9962-9969.
113. Feitosa, E.; Winnik, F., Interaction between Pluronic F127 and Dioctadecyldimethylammonium Bromide (DODAB) Vesicles Studied by Differential Scanning Calorimetry. *Langmuir* **2010**, 26, (23), 17852-17857.
114. Chieng, Y. Y.; Chen, S. B., Interaction and Complexation of Phospholipid Vesicles and Triblock Copolymers. *J. Phys. Chem. B* **2009**, 113, (45), 14934-14942.
115. Amado, E.; Kerth, A.; Blume, A.; Kressler, J., Phospholipid crystalline clusters induced by adsorption of novel amphiphilic triblock copolymers to monolayers. *Soft Matter* **2009**, 5, 669-675.
116. Wu, G.; Lee, K. Y. C., Interaction of Poloxamers with Liposomes: An Isothermal Titration Calorimetry Study. *J. Phys. Chem. B* **2009**, 113, (47), 15522-15531.

117. Tiriveedhi, V.; Kitchens, K. M.; Nevels, K. J.; Ghandehari, H.; Butko, P., Kinetic analysis of the interaction between poly(amidoamine) dendrimers and model lipid membranes. *Biochim. Biophys. Acta* **2011**, 1808, (1), 209-218.
118. Hong, S.; Bielinska, A. U.; Mecke, A.; Keszler, B.; Beals, J. L.; Shi, X.; Balogh, L.; Orr, B. G.; Baker, J. R.; Banaszak Holl, M. M., Interaction of Poly(amidoamine) Dendrimers with Supported Lipid Bilayers and Cells: Hole Formation and the Relation to Transport. *Bioconjugate Chem.* **2004**, 15, (4), 774-782.
119. Wrobel, D.; Ionov, M.; Gardikis, K.; Demetzos, C.; Majoral, J.-P.; Palecz, B.; Klajnert, B.; Bryszewska, M., Interactions of phosphorus-containing dendrimers with liposomes. *Biochim. Biophys. Acta* **2011**, 1811, (3), 221-226.
120. Tribet, C.; Sebai, S. C.; Cribier, S.; Karimi, A.; Massotte, D., Permeabilization of Lipid Membranes and Cells by a Light-Responsive Copolymer. *Langmuir* **2010**, 26, (17), 14135-14141.
121. Tribet, C.; Vial, F.; Oukhaled, A. G.; Auvray, L., Long-living channels of well defined radius opened in lipid bilayers by polydisperse, hydrophobically-modified polyacrylic acids. *Soft Matter* **2007**, 3, 75-78.
122. LoPresti, C.; Massignani, M.; Fernyhough, C.; Blanz, A.; Ryan, A. J.; Madsen, J.; Warren, N. J.; Armes, S. P.; Lewis, A. L.; Chirasatitsin, S.; Engler, A. J.; Battaglia, G., Controlling Polymersome Surface Topology at the Nanoscale by Membrane Confined Polymer/Polymer Phase Separation. *ACS Nano* **2011**, 5, (3), 1775-1784.
123. Luo, L.; Eisenberg, A., One-Step Preparation of Block Copolymer Vesicles with Preferentially Segregated Acidic and Basic Corona Chains. *Angew. Chem. Int. Ed.* **2002**, 41, (6), 1001-1004.
124. Spinler, K.; Tian, A.; Christian, D. A.; Pantano, D. A.; Baumgart, T.; Discher, D. E., Dynamic Domains in Polymersomes: Mixtures of Polyanionic and Neutral Diblocks Respond More Rapidly to Changes in Calcium than to pH. *Langmuir* **2013**, 29, (24), 7499-7508.
125. Ruyschaert, T.; Sonnen, A. F. P.; Haefele, T.; Meier, W.; Winterhalter, M.; Fournier, D., Hybrid Nanocapsules: Interactions of ABA Block Copolymers with Liposomes. *J. Am. Chem. Soc.* **2005**, 127, (17), 6242-6247.
126. Nam, J.; Vanderlick, T. K.; Beales, P. A., Formation and dissolution of phospholipid domains with varying textures in hybrid lipo-polymersomes. *Soft Matter* **2012**, 8, (30), 7982-7988.
127. Chemin, M.; Brun, P.-M.; Lecommandoux, S.; Sandre, O.; Le Meins, J.-F., Hybrid polymer/lipid vesicles: fine control of the lipid and polymer distribution in the binary membrane. *Soft Matter* **2012**, 8, (10), 2867-2874.
128. Schulz, M.; Glatte, D.; Meister, A.; Scholtysek, P.; Kerth, A.; Blume, A.; Bacia, K.; Binder, W. H., Hybrid lipid/polymer giant unilamellar vesicles: effects of incorporated biocompatible PIB-PEO block copolymers on vesicle properties. *Soft Matter* **2011**, 7, (18), 8100-8110.
129. Nam, J.; Beales, P. A.; Vanderlick, T. K., Giant Phospholipid/Block Copolymer Hybrid Vesicles: Mixing Behavior and Domain Formation. *Langmuir* **2011**, 27, (1), 1-6.
130. Kita-Tokarczyk, K.; Ite, F.; Grzelakowski, M.; Egli, S.; Rossbach, P.; Meier, W., Monolayer Interactions between Lipids and Amphiphilic Block Copolymers. *Langmuir* **2009**, 25, (17), 9847-9856.
131. Romao, R. I. S.; Ferreira, Q.; Morgado, J.; Martinho, J. M. G.; Goncalves da Silva, S.; A. M. P., Microphase Separation in Mixed Monolayers of DPPG with a Double Hydrophilic Block Copolymer at the Air-Water Interface: A BAM, LSCFM, and AFM Study. *Langmuir* **2010**, 26, (22), 17165-17177.

132. Olubummo, A.; Schulz, M.; Lechner, B.-D.; Scholtysek, P.; Bacia, K.; Blume, A.; Kressler, J.; Binder, W. H., Controlling the Localization of Polymer-Functionalized Nanoparticles in Mixed Lipid/Polymer Membranes. *ACS Nano* **2012**, 6, (10), 8713-8727.
133. Immordino, M. L.; Dosio, F.; Cattel, L., Stealth liposomes: review of the basic science, rationale, and clinical applications, existing and potential. *Nanomed.* **2006**, 1, (3), 297-315.
134. Lasic, D. D., Sterically Stabilized Vesicles. *Angew. Chem. Int. Ed.* **1994**, 33, (17), 1685-1698.
135. Needham, D.; Hristova, K.; McIntosh, T. J.; Dewhirst, M.; Wu, N.; Lasic, D. D., Polymer-Grafted Liposomes: Physical Basis for the "Stealth" Property. *J. Liposome Res.* **1992**, 2, (3), 411-430.
136. Zalipsky, S.; Hansen, C. B.; Oaks, J. M.; Allen, T. M., Evaluation of blood clearance rates and biodistribution of poly(2-oxazoline)-grafted liposomes. *J. Pharm. Sci.* **1996**, 85, (2), 133-137.
137. Prevette, L. E.; Mullen, D. G.; Holl, M. M. B., Polycation-Induced Cell Membrane Permeability Does Not Enhance Cellular Uptake or Expression Efficiency of Delivered DNA. *Mol. Pharm.* **2010**, 7, (3), 870-883.
138. Palermo, E. F.; Sovadinova, I.; Kuroda, K., Structural Determinants of Antimicrobial Activity and Biocompatibility in Membrane-Disrupting Methacrylamide Random Copolymers. *Biomacromolecules* **2009**, 10, (11), 3098-3107.
139. Whitten, D. G.; Wang, Y.; Tang, Y.; Zhou, Z.; Ji, E.; Lopez, G. P.; Chi, E. Y.; Schanze, K. S., Membrane Perturbation Activity of Cationic Phenylene Ethynylene Oligomers and Polymers: Selectivity against Model Bacterial and Mammalian Membranes. *Langmuir* **2010**, 26, (15), 12509-12514.
140. Iván, B.; Kennedy, J. P., Living carbocationic polymerization. XXX. One-pot synthesis of allyl-terminated linear and tri-arm star polyisobutylenes, and epoxy- and hydroxy-telechelics therefrom. *J. Polym. Sci., Part A: Polym. Chem.* **1990**, 28, (1), 89-104.
141. Adekunle, O.; Herbst, F.; Hackethal, K.; Binder, W. H., Synthesis of nonsymmetric chain end functionalized polyisobutylenes. *J. Polym. Sci., Part A: Polym. Chem.* **2011**, 49, (13), 2931-2940.
142. Song, J.; Bódis, J.; Puskas, J. E., Direct functionalization of polyisobutylene by living initiation with α -methylstyrene epoxide. *J. Polym. Sci., Part A: Polym. Chem.* **2002**, 40, (8), 1005-1015.
143. Binder, W. H.; Sachsenhofer, R., 'Click' Chemistry in Polymer and Materials Science. *Macromol. Rapid Commun.* **2007**, 28, (1), 15-54.
144. Binder, W. H.; Sachsenhofer, R., Polymersome/Silica Capsules by 'Click'-Chemistry. *Macromol. Rapid Commun.* **2008**, 29, (12-13), 1097-1103.
145. Binder, W. H.; Kunz, M. J.; Kluger, C.; Hayn, G.; Saf, R., Synthesis and Analysis of Telechelic Polyisobutylenes for Hydrogen-Bonded Supramolecular Pseudo-Block Copolymers. *Macromolecules* **2004**, 37, (5), 1749-1759.
146. Dyck, M.; Lösche, M., Interaction of the Neurotransmitter, Neuropeptide Y, with Phospholipid Membranes: Film Balance and Fluorescence Microscopy Studies *J. Phys. Chem. B* **2006**, 110, (44), 22143-22151.
147. Kennedy, J. P., Quasiliving Carbocationic Polymerization. XII. Forced Ideal Copolymerization of Isobutylene with Styrene. *J. Macromol. Sci., Chem.* **1982**, 18, (9), 1367 - 1382.
148. Puskas, J. E.; Brister, L. B.; Michel, A. J.; Lanzendörfer, M. G.; Jamieson, D.; Pattern, W. G., Novel substituted epoxide initiators for the carbocationic polymerization of isobutylene. *J. Polym. Sci., Part A* **2000**, 38, (3), 444-452.

149. Song, J.; Bódis, J.; Puskas, J. E., Direct functionalization of polyisobutylene by living initiation with α -methylstyrene epoxide. *J. Polym. Sci., Part A: Polym. Chem.* **2002**, 40, (8), 1005-1015.
150. Gyor, M.; Wang, H.-C.; Faust, R., Living Carbocationic Polymerization of Isobutylene with Blocked Bifunctional Initiators in the Presence of Di-tert-butylpyridine as a Proton Trap. *J. Macromol. Sci., Pure Appl. Chem.* **1992**, 29, (8), 639 - 653.
151. Iván, B.; Kennedy, J. P.; Chang, V. S. C., New telechelic polymers and sequential copolymers by polyfunctional Initiator-Transfer agents (inifers). VII. Synthesis and characterization α,ω -di(hydroxy)polyisobutylene. *J. Polym. Sci., Part A: Polym. Chem.* **1980**, 18, (11), 3177-3191.
152. Appel, R., Tertiary Phosphane/Tetrachloromethane, a Versatile Reagent for Chlorination, Dehydration, and P&N Linkage. *Angew. Chem., Int. Ed. Engl.* **1975**, 14, (12), 801-811.
153. Schulz, M.; Tanner, S.; Barqawi, H.; Binder, W., H., Macrocyclization of polymers via ring-closing metathesis and azide/alkyne-"click"-reactions: An approach to cyclic polyisobutylenes. *J. Polym. Sci., Part A: Polym. Chem.* **2010**, 48, (3), 671-680.
154. Adekunle, O.; Herbst, F.; Hackethal, K.; Binder, W. H., Synthesis of nonsymmetric chain end functionalized polyisobutylenes. *J. Polym. Sci., Part A: Polym. Chem.* **2011**, 49, (13), 2931-2940.
155. Morgan, D. L.; Storey, R. F., End-Quenching of Quasi-Living Isobutylene Polymerizations with Alkoxybenzene Compounds. *Macromolecules* **2009**, 42, (18), 6844-6847.
156. Hiki, S.; Kataoka, K., A Facile Synthesis of Azido-Terminated Heterobifunctional Poly(ethylene glycol)s for "Click" Conjugation. *Bioconjugate Chem.* **2007**, 18, (6), 2191-2196.
157. Hiki, S.; Kataoka, K., Versatile and Selective Synthesis of "Click Chemistry" Compatible Heterobifunctional Poly(ethylene glycol)s Possessing Azide and Alkyne Functionalities. *Bioconjugate Chem.* **2010**, 21, (2), 248-254.
158. Dimonie, M.; Teodorescu, M., Phase transfer catalysis synthesis of α,ω -diallylpoly(ethylene oxide). *Macromol. Rapid Commun.* **1993**, 14, (5), 303-307.
159. Gruškienė, R.; Čiuta, G.; Makuška, R., Grafting of poly(ethylene glycol) to chitosan at c(6) position of glucosamine units via "click chemistry" reactions. *chemija.* **2009**, 20, (4), 241-249.
160. Wang, D.; Liu, X.-M.; Thakur, A., Efficient Synthesis of Linear Multifunctional Poly(ethylene glycol) by Copper(I)-Catalyzed Huisgen 1,3-Dipolar Cycloaddition. *Biomacromolecules* **2007**, 8, (9), 2653-2658.
161. Wu, J.; Gao, C., Click Chemistry Approach to Rhodamine B-Capped Polyrotaxanes and their Unique Fluorescence Properties. *Macromol. Chem. Phys.* **2009**, 210, (20), 1697-1708.
162. Schulz, M.; Werner, S.; Bacia, K.; Binder, W. H., Controlling Molecular Recognition with Lipid/Polymer Domains in Vesicle Membranes. *Angew. Chem. Int. Ed.* **2013**, 52, (6), 1829-1833.

VII. APPENDIX

Appendix A – *Soft Matter* **2011**, 7, (18), 8100-8110.

Hybrid lipid/polymer giant unilamellar vesicles: Effects of incorporated biocompatible PIB-PEO block copolymers on vesicle properties

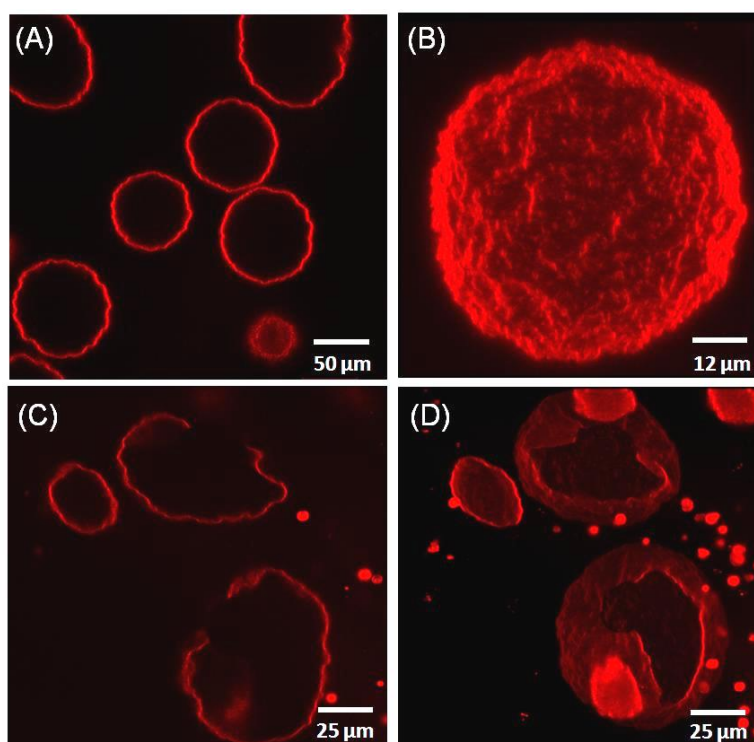


Figure S1. Confocal microscopy images of hybrid GUVs with incorporated amphiphilic block copolymer chains (PIB₃₇-PEO₄₈) (**3b**). (A) Overview of mixed vesicles at room temperature obtained from a mixture of 30 mol% of **3b**. Panel (B) depicts the corresponding 3D-reconstruction of a single vesicle, which shows a vesicle with a highly ragged surface. Panel (C) and (D) illustrate hybrid vesicles prepared from an initial mixing ratio of 40 mol% of PIB₃₇-PEO₄₈. The 3Dreconstruction (D) clearly shows large open fragments of the hybrid membrane.

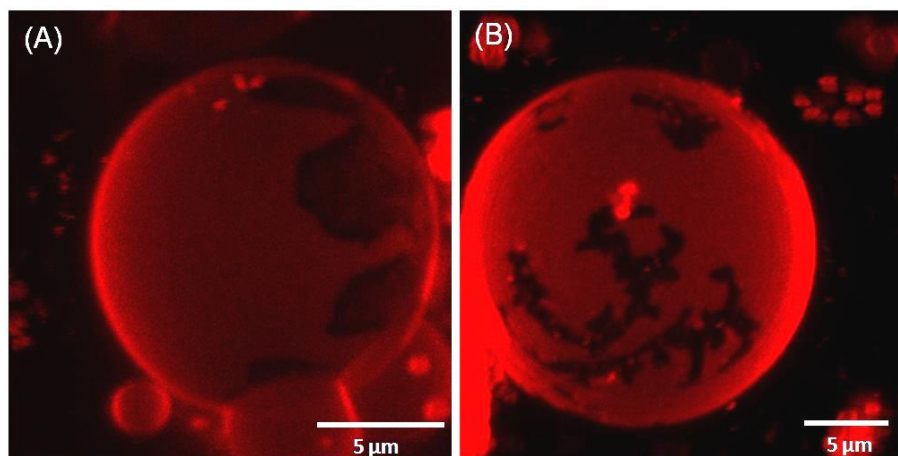


Figure S2. Confocal microscopy images of hybrid GUVs with incorporated amphiphilic block copolymer chains obtained from a mixture of 20 mol% of PIB₈₇-PEO₁₇ BCP using DiDC18 for labeling phase heterogeneities. (A) and (B) depict the 3D-reconstructions of hybrid giant unilamellar vesicles, which exhibit irregularly shaped domains (black patches), indicating a phase separated state of the binary mixed system.

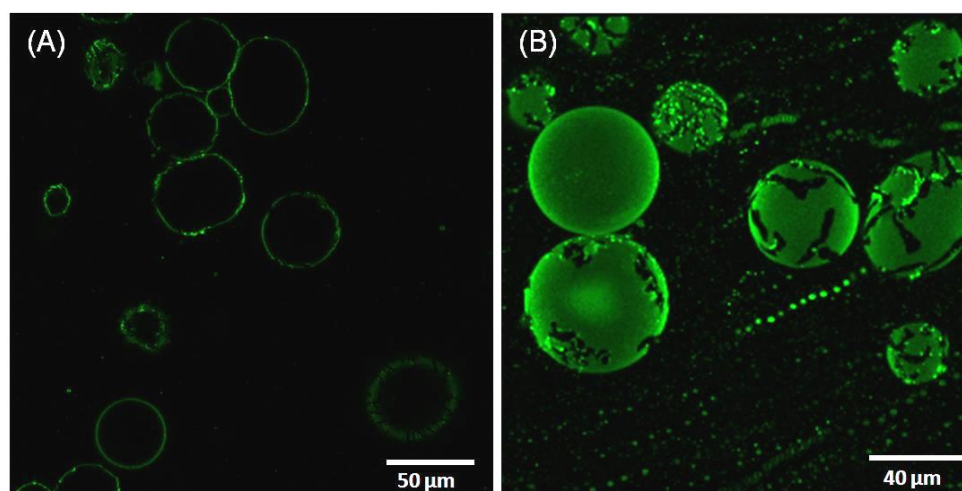


Figure S3. Confocal microscopy images of hybrid GUVs with incorporated amphiphilic block copolymer chains obtained from a mixture of 20 mol% of PIB₈₇-PEO₁₇ using Rh DHPE for labeling phase heterogeneities. Panel (A) shows an overview and panel (B) depicts a 3D-reconstruction of hybrid giant unilamellar vesicles. The same type of irregularly shaped, dark domains, are observed as with DiDC18 as the fluorescent label in Fig.S2.

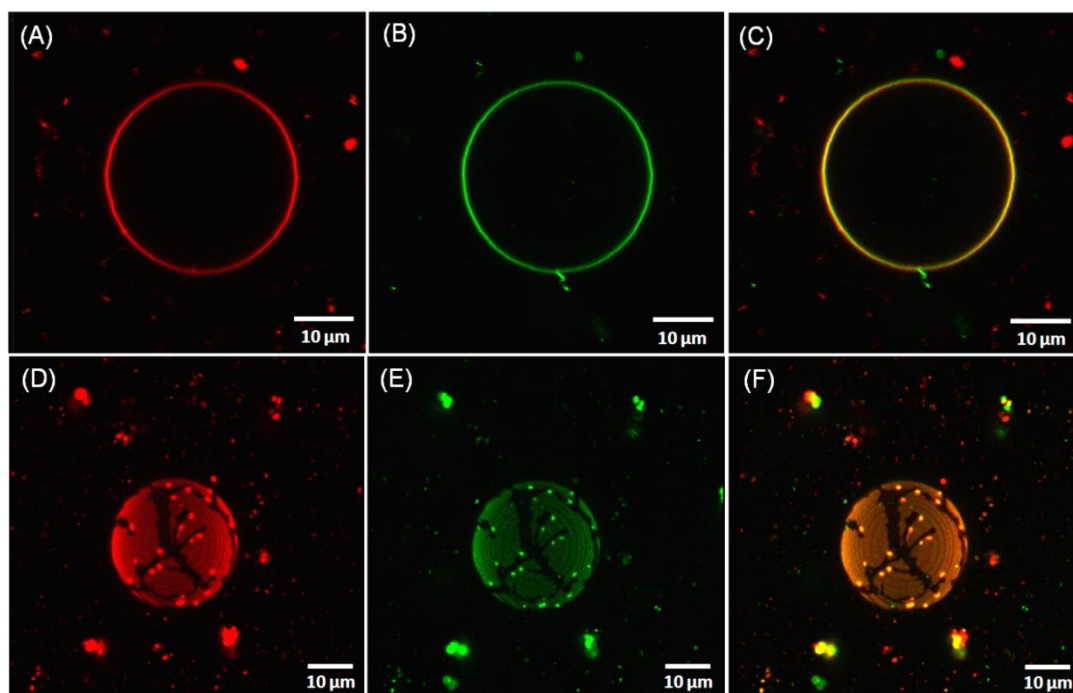


Figure S4. Confocal microscopy images of hybrid GUVs with incorporated amphiphilic block copolymer chains using **30 mol%** (A-C) and **20 mol%** of BCP (**3a**) (D-F). Hybrid GUVs were visualized with two different membrane labels (Rh-DHPE and DiDC18 (0.5 mol%)) to show differences in the phase labeling. Panel (A) and (D) depict a single GUV image where the DiDC18 dye was exclusively excited; Panel (B) and (E) were the Rh-DHPE dye was exclusively excited. Panel (C) and (F) show an overlay of both images, indicating no differences in the phase labeling behavior of both membrane dyes. Panel (D), (E) and (F) are presented as 3D-reconstruction to show the different phases.

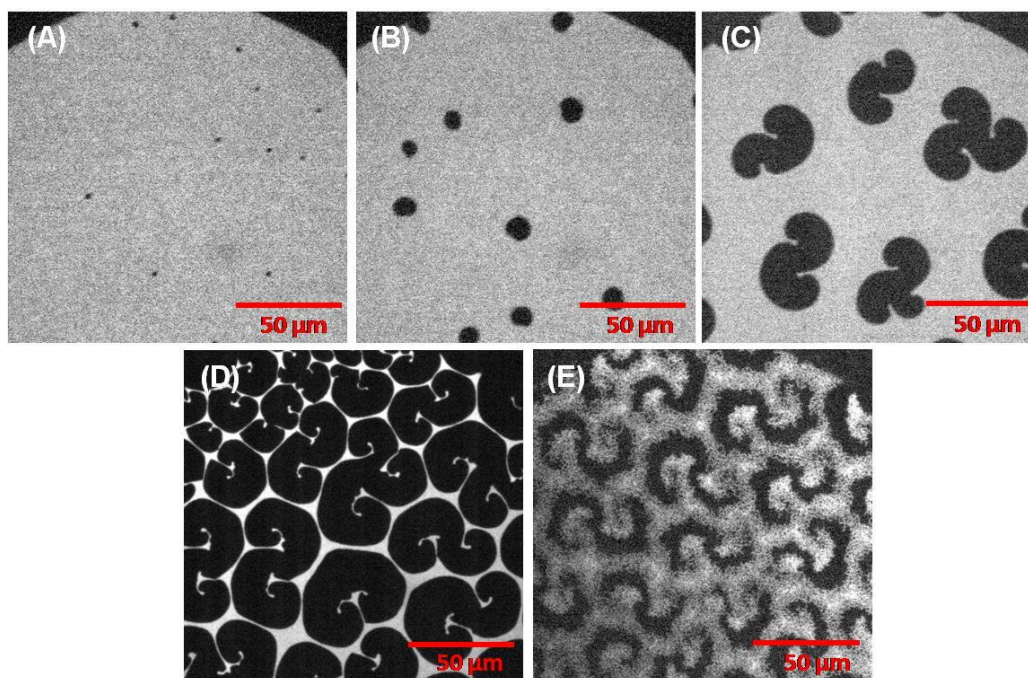


Figure S5. Fluorescence microscopy images of a pure DPPC monolayer at the air/water interface at 20°C recorded at different surface pressures: (A) 7.3 mN/m; (B) 8.0 mN/m; (C) 8.4 mN/m; (D) 12.2 mN/m and (E) 33.8 mN/m.

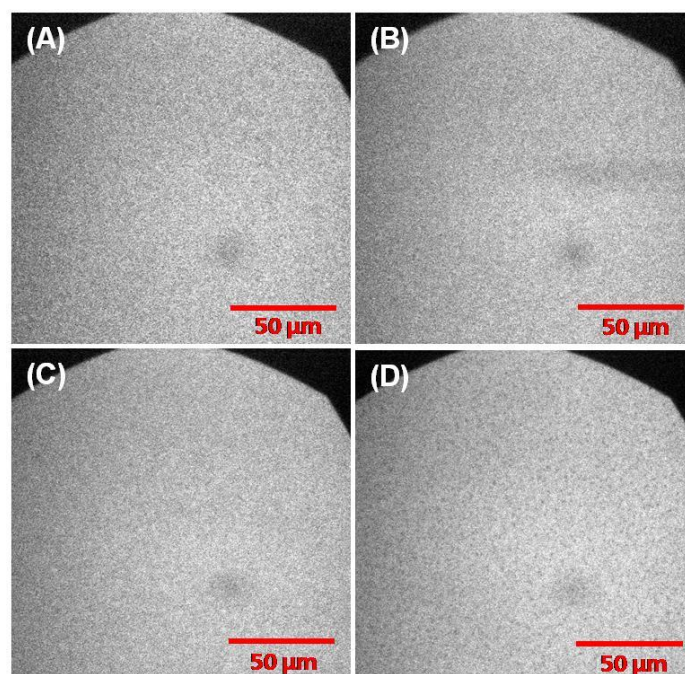


Figure S6. Fluorescence microscopy images of a mixed monolayer of DPPC/ PIB₈₇-PEO₁₇ (80 mol%) at the air/water interface at 20°C recorded at different surface pressures: (A) 3.0 mN/m; (B) 8.0 mN/m; (C) 12.2 mN/m; (D) 30.1 mN/m.

Appendix B – *Angew. Chem. Int. Ed.* **2013**, 52, (6), 1829-1833.

Controlling molecular recognition via lipid/polymer-domains in vesicle membranes

Index:

1. Materials

2. Synthesis of the fluorescently labeled PIB-*b*-PEO BCP (4)

3. Methods

3.1 Vesicle formation

3.2 Modification and formation of hybrid membranes with incorporated GM1 lipids

3.3 Protein binding studies (cholera toxin B)

3.4 Giant vesicle analysis by confocal laser scanning microscopy (CLSM)

3.5 Membrane analysis by FRAP-measurements

3.6 Membrane analysis by FCS-measurements

4. Figures and Schemes

4.1 ESI-TOF analysis of compound **4** (Figure S1).

4.2 Vesicle analysis of phase separated GUVs using compound **4** and a second membrane dye to visualize lateral membrane heterogeneities within the bilayer (Figures S2-S3).

4.3 Incorporation of ganglioside GM1 into hybrid membranes from a mixture of 80 mol% DPPC and 20 mol% BCP (**1**), proving that the incorporation of 0.1 mol% of GM1 does not perturb the phases (Figure S4).

4.4 Schematic illustration of the multivalent cholera toxin B binding five GM1 molecules (Scheme S1).

4.5 Binding studies of cholera toxin B to GM1-functionalized DOPC membranes (fluid system) and hybrid DPPC/BCP (**1**) membranes varying the lipid/BCP composition (Figures S5-S8).

4.6 FRAP analysis for hybrid GUVs using lipid/BCP mixtures with 18 mol% and 40 mol% BCP (**1**) (Figures S9-S10).

1. Materials

All chemicals and solvents, which were used for the synthesis of polymer samples, were purchased from *Sigma-Aldrich (Schnelldorf, Germany)* and used as received unless otherwise stated. Tetrahydrofuran (THF) was predried over potassium hydroxide for several days, refluxed over sodium/benzophenone and freshly distilled under an argon atmosphere before use. PIB-PEO diblock copolymers (PIB₈₇-*b*-PEO₁₇; $M_n = 5900$ g/mol) with a minimal polydispersity ($PDI \leq 1.2$), used in this study, were synthesized in our laboratories *via* a combination of a living carbocationic polymerization method and the approach of the azide/alkyne-“click”-reaction, as reported previously.^[1, 2] 1,2-Dipalmitoyl-*sn*-glycero-3-phosphocholine (DPPC, $M = 734.05$ g/mol), 1,2-dioleoyl-*sn*-glycero-3-phosphocholine (DOPC, $M = 786.11$ g/mol) and ganglioside GM1 were purchased from *Avanti Polar Lipids (Alabaster; AL, USA)* and used without further purifications. The fluorescence dyes used in this study for imaging experiments and membrane dynamic measurements, 1,1'-dioctadecyl-3,3,3',3'-tetramethylindodicarbocyanine perchlorate (DiDC18; $M = 959.92$ g/mol), 1,2-dihexadecanoyl-*sn*-glycero-3-phosphothanolamine-*N*-(lissamine rhodamine B sulfonyl) (Rh-DHPE, $M = 1267.68$) as well as the Alexa 488-labeled cholera toxin subunit B (CTB, $\lambda_{max} = 493$ nm/excitation) were purchased from *Invitrogen (Karlsruhe, Germany)*. For the preparation of the fluorescently labeled diblock copolymer dye (**4**), an acetylene-fluor 488 dye (C₃₂H₃₃N₃O₈, $M = 587.62$ g/mol) was purchased from *Jena Bioscience GmbH (Jena, Germany)*.

2. Synthesis of the fluorescently labeled diblock copolymer (**4**)

For the synthesis of fluorescently labeled PIB-PEO diblock copolymer compound, which is used to monitor the polymer-enriched domains in phase-separated giant unilamellar vesicles (GUVs), an azido-functionalized polyisobutylene homopolymer (PIB₆₀-N₃, $M_n = 3380$ g/mol with PDI of 1.2) was synthesized and characterized as reported elsewhere.^[1] The corresponding alkyne-functionalized poly(ethylene oxide) block bearing the fluorescence dye (fluor 488), which was purchased from *Jena Bioscience GmbH*, was covalently attached to the polyisobutylene homopolymer *via* copper-catalyzed azide/alkyne “click”-reaction. According to the modified procedure of Binder *et al.*,^[1, 2] azido-functionalized PIB (1 equiv.), acetylene-fluor 488 dye (1 equiv.), and Tris(1-benzyl-1*H*-1,2,3-triazol-4-yl)methylamine (TBTA, 3 equiv.) were dissolved in a solvent mixture of THF, MeOH and DMSO (10/1/0.5), flushed with a stream of argon for some time and subsequently treated with the catalyst Cu(I)-iodide (0.1 equiv.). After 48 hours at 40°C, the crude product was purified by a silica-flash column to

remove the catalyst residues. To remove the contaminating free acetylene-fluor 488 dye, which was not covalently attached to the PIB block, the final product was precipitated three times using methanol, dissolving undesired compounds. The final structure of the labeled diblock copolymer was examined by ESI-TOF MS analysis (compare Figure S1). The absence of free acetylene-fluor 488 in the final product was proven by HPLC.

3. Methods

3.1 Vesicle formation

The formation of DPPC/PIB-PEO BCP (**1**) hybrid giant unilamellar vesicles was achieved as described previously^[1] using an electroformation method originally reported by Angelova *et al.*^[3] Water, which was used for the study, was purified *via* passage through a filtering system by *Purelab Option system (ELGA Ltd., Celle, Germany)*, yielding ultra-pure water. Lipid and polymer were mixed at the indicated mixtures in chloroform (HPLC grade, *Sigma Aldrich (Schnelldorf, Germany)*). For the visualization of the resulting hybrid GUVs and their membrane heterogeneities, different membrane dyes (DiDC18, Rh-DHPE or the fluorescently labeled diblock copolymer **4**) were added to the initial mixture at a total amount of 0.5 mol%.

3.2 Modification and formation of hybrid membranes with incorporated GM1 lipids

For the surface functionalization of mixed DPPC/PIB-PEO BCP (**1**) membranes with ganglioside GM1 molecules, all lipid/polymer mixtures varying in their compositions were additionally mixed with 0.1 mol% of GM1. The lipid/polymer mixture containing 0.1 mol% of GM1 was again prepared in chloroform, dried under a continuous N₂-stream and dissolved in a defined solvent volume reaching a total concentration of 10 mg/ml. The final mixtures were used to generate a homogenous thin film on optically transparent indium-tin-oxide (ITO) coated coverslips using a spin coating method. After the preparation of the thin films on two coverslips (electrodes), the coverslips were placed in a capacitor-type configuration at a distance of 2 mm using a home built flow-chamber. The flow-chamber was filled with a sucrose solution (96 mosmol/l). The conditions for the electroformation process were applied as reported previously.^[1]

3.3 Binding studies (cholera toxin B)

All binding studies between cholera toxin B and GM1-modified liposomal (DPPC or DOPC) or hybrid membranes composed of DPPC and BCP (**1**) were conducted at room temperature (20 °C) using CTB (5 µg) dissolved in a sucrose solution (~100 µl). The dilute solutions of

CTB were prepared fresh before use. After the electroformation process, the prepared GUVs with incorporated GM1 receptor molecules were first cooled down to room temperature and after that monitored by laser scanning microscopy, which revealed changes in the membrane morphologies. Subsequently, GUVs were treated with the protein solution. The CTB solutions were injected into the flow chamber, which contained the freshly prepared GUVs, using a microsyringe. All experiments were performed with the fluorescently labeled cholera toxin.

3.4 Giant vesicle analysis by confocal laser scanning microscopy (CLSM)

Confocal microscopy images were obtained on a commercially available confocal-laser scanning microscope (LSM 710/ ConfoCor 3; Carl-Zeiss, Germany) using a C-Apochromat 40x/1.2 N.A. water immersion objective. The lipophilic membrane label DiDC18 was excited with a HeNe laser at 633 nm. The head group labeled Rh-DHPE lipid, which was also used to monitor membrane heterogeneities, was excited with a DPSS-laser at 561 nm. For the monitoring of the cholera toxin B attached to liposomes or hybrid vesicles by binding to their GM1 functionalized vesicular surfaces, an Argon-Ion laser with an excitation wavelength of 488 nm was used. Monitoring of the fluorescently labeled diblock copolymer **4** (PIB₆₀-b-PEO₄-fluor488) was also conducted at 488 nm. All GUV imaging studies, both the monitoring of phase heterogeneities and the interaction studies with cholera toxin B were performed after cooling to room temperature (20 °C).

3.5 Membrane analysis by FRAP-measurements

Fluorescence recovery after photobleaching (FRAP) experiments to determine the mobility of lipid molecules within a prepared hybrid vesicle membrane, were performed with the head group labeled lipid (Rh-DHPE) at 0.5 mol% to ensure the localization of the lipid dye into the more disordered phases. The FRAP measurements were performed on the *LSM 710* confocal laser scanning microscope. Photobleaching in the desired region of the GUV surface was performed using a 561 nm-DPSS-laser at maximal power (5.7 mW before objective). Before and after successful bleaching, a time series of images was acquired. The mean fluorescence intensity in the bleached region, I_{sample} , and the mean fluorescence intensity in an unbleached region of the same size, I_{ref} , were determined. Both intensities were background (B) corrected

and their ratios $I_{rel} = \frac{I_{sample} - B}{I_{ref} - B}$ plotted as a function of time.

3.6 Membrane analysis by FCS- measurements

Fluorescence correlation spectroscopy (FCS) measurements were performed on an *LSM 710/ConfoCor 3* combination setup (*Carl- Zeiss, Germany*) using a C-Apochromat 40x/1.2 N.A. water immersion objective. For FCS experiments, hybrid GUV membranes were labeled with 0.005 mol% of the lipid dye (Rh-DHPE), which was excited at 561 nm using a DPSS-laser. The recorded autocorrelation functions were analyzed using the *ZEN 2009*-software (*Carl-Zeiss, Germany*) and the following model equation^[4]

$$G(\tau) = \frac{1}{N} \cdot \left(1 + \frac{F_{Triplet} \cdot e^{-\frac{\tau}{\tau_{Triplet}}}}{1 - F_{Triplet}} \right) \cdot \frac{1}{1 + \frac{\tau}{\tau_{Diff}}},$$

where N is the mean number of fluorescent particles within the confocal volume during the measurement, $F_{Triplet}$ the average fraction of particles in the triplet state, $\tau_{Triplet}$ the triplet relaxation time and τ_{Diff} the lateral diffusion time of the lipid dye in the membrane. The lateral diffusion time is related to the diffusion coefficient D by

$$\tau_{Diff} = \frac{\omega_0^2}{4 \cdot D},$$

where ω_0 is the radius of the confocal volume in the xy-plane. To determine ω_0 , a calibration measurement on a dye with a known diffusion coefficient is required. Since no reliable diffusion coefficient is available for the 561 nm excitation configuration, which was used in our experiments, the radius of the confocal volume was obtained by interpolation from calibration measurements at excitation wavelengths of 488 nm and at 633 nm, using the known diffusion coefficients of Alexa Fluor 488^[5] and Cy5^[6] and assuming, that the radius of the confocal volume scales with the excitation wavelength.

4. Figures and Schemes

4.1 ESI-TOF MS analysis of the fluorescently labeled PIB-*b*-PEO BCP (4).

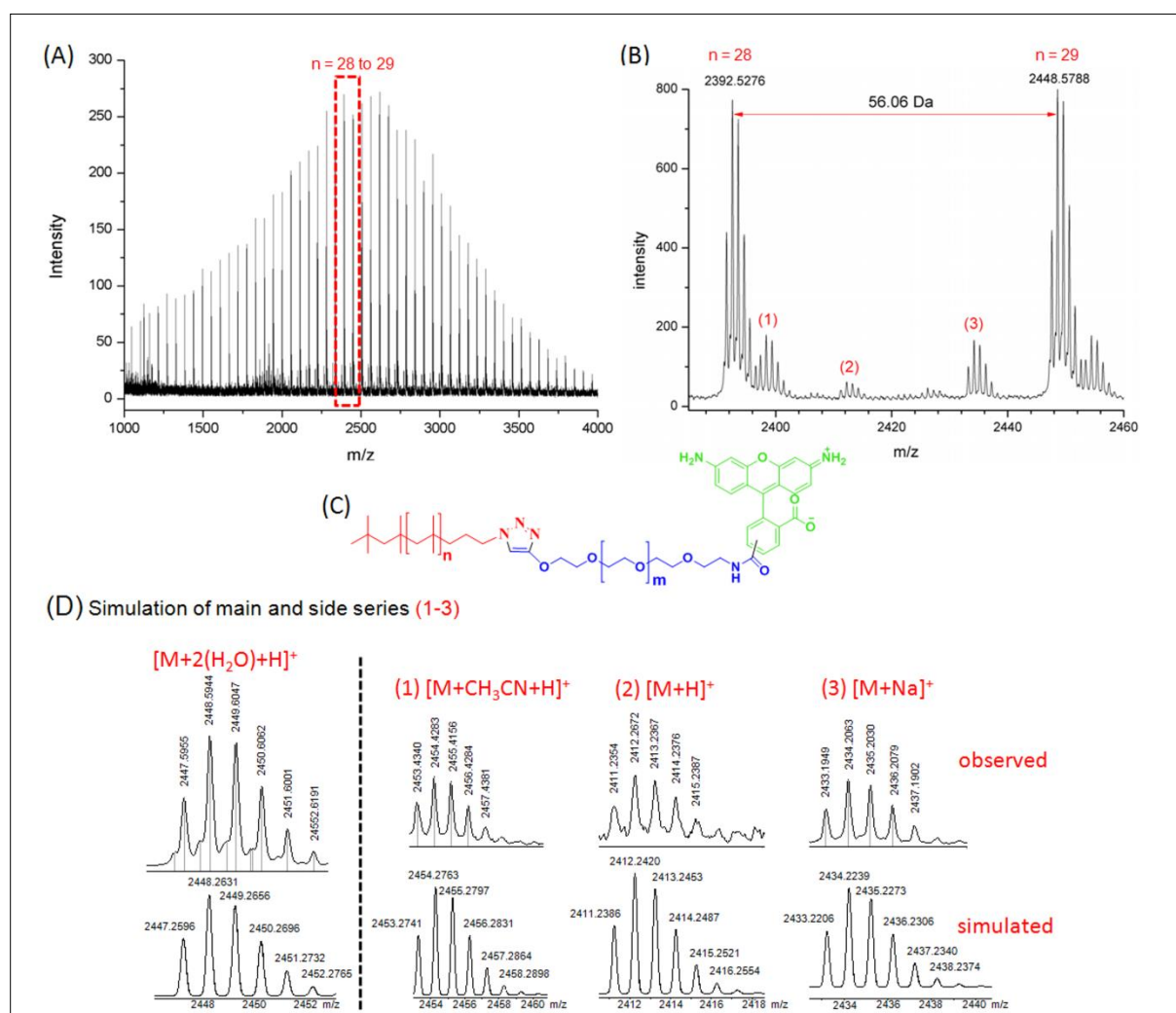


Figure S1. (A) Full view of the ESI-TOF-mass spectrum of the fluorescently labeled diblock copolymer (4) (PIB₆₀-*b*-PEO₄-fluoro-488), (B) magnification showing the $\Delta m/z$ value of 56.06 corresponding to the polymer repeating unit (isobutylene) and (D) comparison between the observed and simulated isotopic patterns of the main and side series proving the final structure of the fluoro 488 labeled diblock copolymer (4), as illustrated in (C) $[M = C_{11}H_{23}N_3(C_4H_8)_n C_{32}H_{33}N_3O_8]^+$.

4.2 Vesicle analysis of phase separated GUVs using compound **4** and a second membrane dye to visualize lateral membrane heterogeneities within the bilayer (Figures S2-S3).

4.3

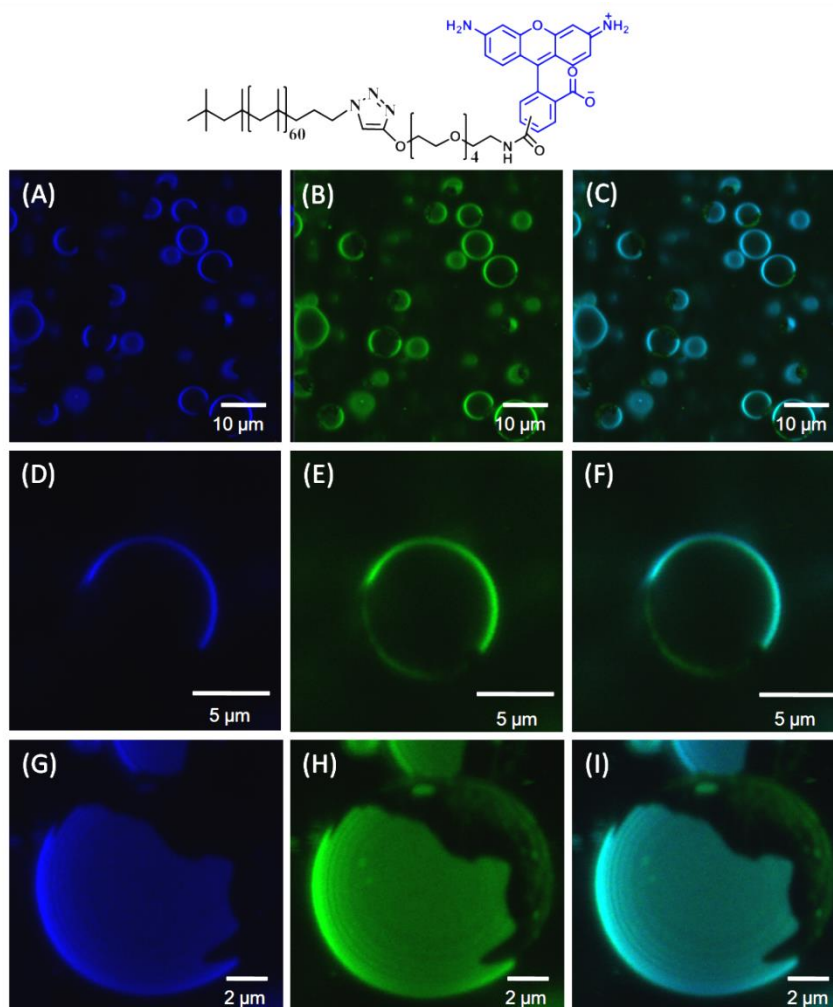


Figure S2. Confocal microscopy images of phase-separated hybrid DPPC/PIB₈₇-*b*-PEO₁₇ GUVs obtained with 80 mol% DPPC and 20 mol% BCP (**1**) at room temperature, demonstrating membrane heterogeneities by the phase labeling behavior of a rhodamine-labeled lipid (Rh-DHPE) and a fluorescently labeled PIB-PEO diblock copolymer **4**. The first row (panels (A), (B) and (C)) shows confocal overview images, the second row shows an equatorial confocal slice of a single GUV and the third row depicts a 3-dimensional reconstruction from an axial series of confocal slices. Panels (A), (D) and (G) depict GUV images where the labeled diblock copolymer dye (blue) was excited at 488nm. Panels (B), (E) and (H) show the Rh-DHPE dye (green), which was excited at 561 nm. Corresponding overlays are shown in panels (C), (F) and (I). Both membrane dyes show preferential partitioning into the same phase. The fact that the diblock copolymer dye (**4**) strongly segregates to this particular phase indicates that this is the polymer-enriched phase (blue-colored domains, panels D and G) and that the other phase is the lipid-enriched phase. Close inspection reveals that, the Rh-DHPE dye is present in both phases, *i.e.*, also in the lipid-enriched phase (compare the single GUV in panel D with E and the 3D-reconstructions of a single GUV in panel G with H). The fact that only a minor quantity of the fluorescently labeled lipid (Rh-DHPE) is observed in the lipid-enriched domain

(slightly green patches in panels F and I) indicates a more ordered, gel-like character of the phase. It is known from literature that Rh-DHPE is largely excluded from ordered phases (*e.g.*, liquid condensed phases),^[1, 7] which accounts for the higher intensity seen from the Rh-DHPE dye in the less ordered, polymer-enriched phases.

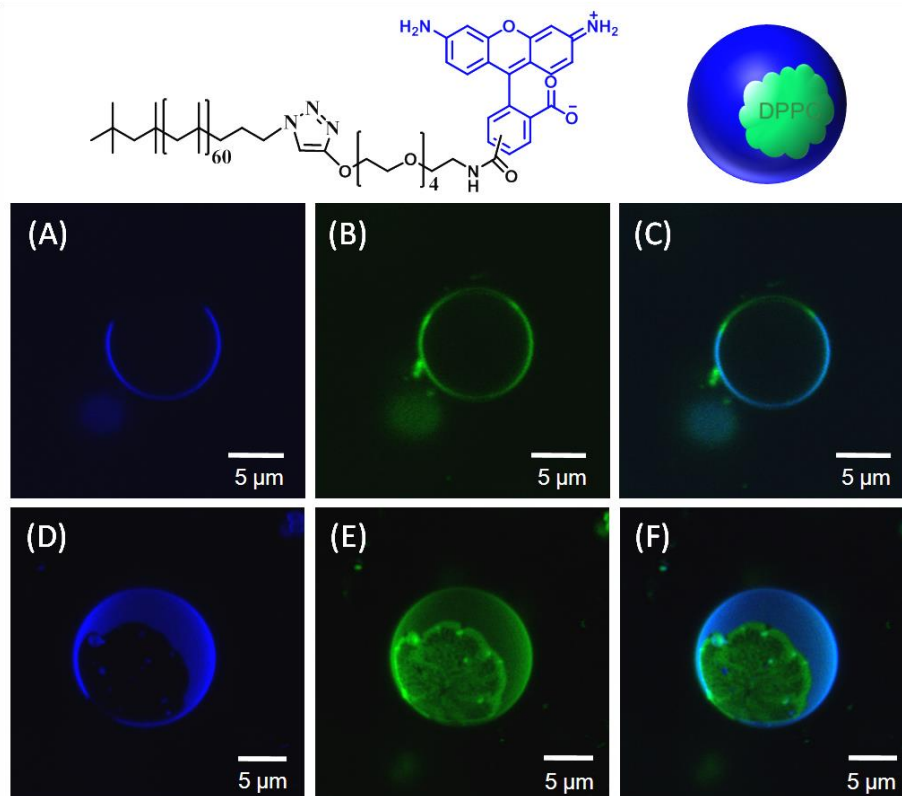


Figure S3. Confocal microscopy images of phase-separated hybrid DPPC/PIB₈₇-*b*-PEO₁₇ GUVs obtained with 80 mol% DPPC and 20 mol% BCP (**1**) at room temperature, demonstrating membrane heterogeneities by the different phase labeling behavior of the DiDC18 dye and the fluorescently labeled diblock copolymer dye (**4**). Panels (A), (B) and (C) show a single, equatorial slice of a GUV; panels (D), (E) and (F) represent 3-dimensional reconstruction from axial stacks. Panels (A) and (D) depict a GUV where the diblock copolymer dye (blue) was excited and imaged; in panels (B) and (E) the fluorescent lipid analog DiDC18 (green) was excited and imaged. Overlays are shown in panels (C) and (F). Same as in Figure S2, the polymer dye (blue) shows a strong preferential partitioning into one domain, marking the polymer-enriched phase. The observed enrichment of the DiDC18 in the other, lipid-enriched domain confirms that the lipid-enriched domain consists of a gel-like phase of DPPC, which is largely depleted of polymer molecules. It is known from literature, that (in contrast to Rh-DHPE) long chain DiD molecules become enriched in the more ordered gel-phase domains of GUVs prepared from phospholipids differing in their acyl-chain length.^[8]

- 4.3 Incorporation of ganglioside GM1 into hybrid membranes from a mixture of 80 mol% DPPC and 20 mol% BCP (**1**), proving that the incorporation of 0.1 mol% of GM1 does not perturb the phases.

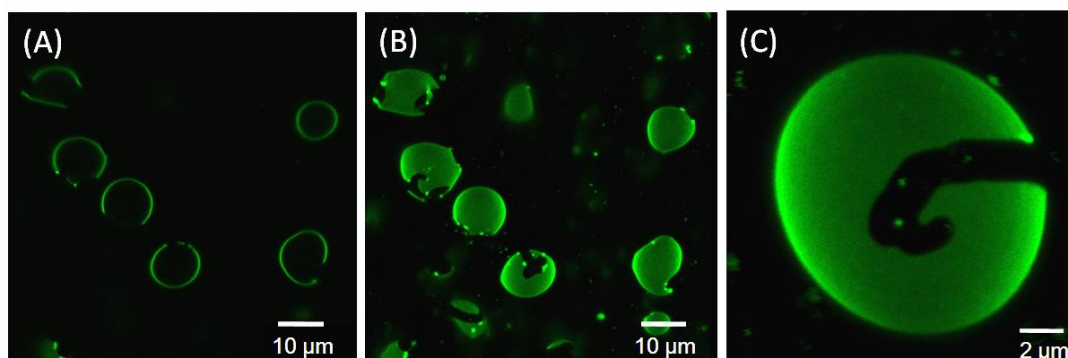


Figure S4. Confocal microscopy images of hybrid DPPC/PIB₈₇-b-PEO₁₇ GUVs composed of DPPC and 20 mol% of PIB₈₇-b-PEO₁₇ BCP (**1**) functionalized with 0.1 mol% of GM1 using Rh-DHPE (green) for labeling phase heterogeneities. Panel (A) depicts an overview of phase-separated vesicles, which show the formation of dark domains typical for hybrid GUVs obtained from mixtures with 20 mol% BCP (**1**). This observation confirms that the incorporated GM1 molecules do not affect the lipid/polymer mixing behavior. Panel (B) shows a 3D-reconstruction of the hybrid GUVs from (A), displaying an irregular shape of the domain boundaries (see also the enlarged view of a single hybrid GUV in panel C).

- 4.4 Schematic illustration of the multivalent cholera toxin B binding five GM1 molecules (orange).



Scheme 1S. Structural illustration of the cholera toxin B pentamer complexed with GM1-type pentasaccharides, demonstrating the binding between one cholera toxin molecule and five GM1 molecules, which is necessary for an effective binding on the vesicular membrane. Crystal structure of the CTB/pentasaccharide complex was taken from the protein data base (PDB-code: 2CHB).

4.5 Binding studies of cholera toxin to GM1-functionalized DOPC membranes (fluid system) and hybrid DPPC/BCP (1) membranes varying the lipid/BCP composition (Figures S5-S8).

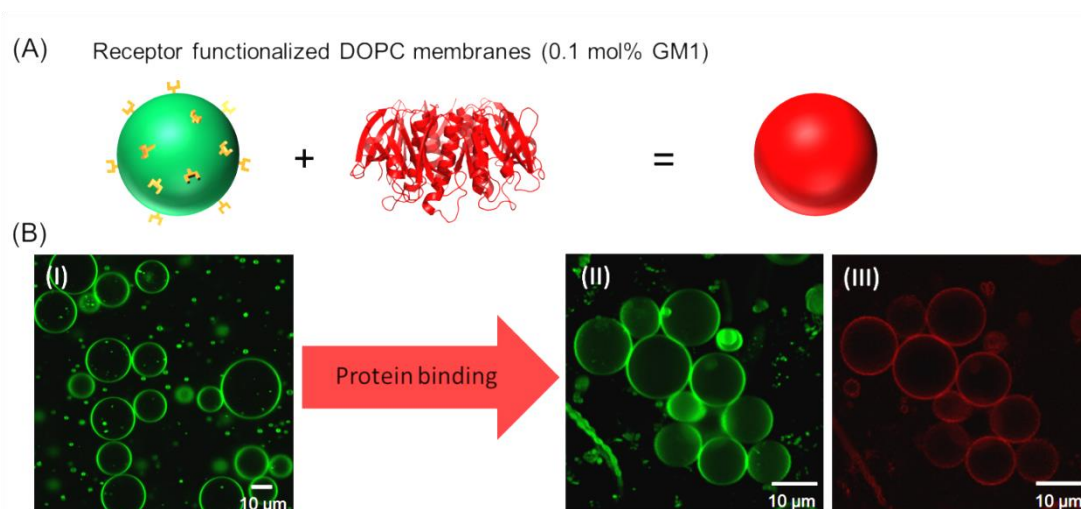


Figure S5. (A) Schematic illustration of the process of CTB binding to liposomes prepared from DOPC with 0.1mol% of GM1. (B/I) Confocal microscopy image of DOPC liposomes before the protein incubation, visualized by the lipid dye Rh-DHPE, which show a uniform appearance in the vesicle membrane. Panel (B/II) depicts liposomes after protein incubation, where the Rh-DHPE was excited at 561 nm (green) and panel (B/III) shows the fluorescence signal from the Alexa 488-labeled CTB protein (red), which also appears uniformly bound over the whole liposomal surface.

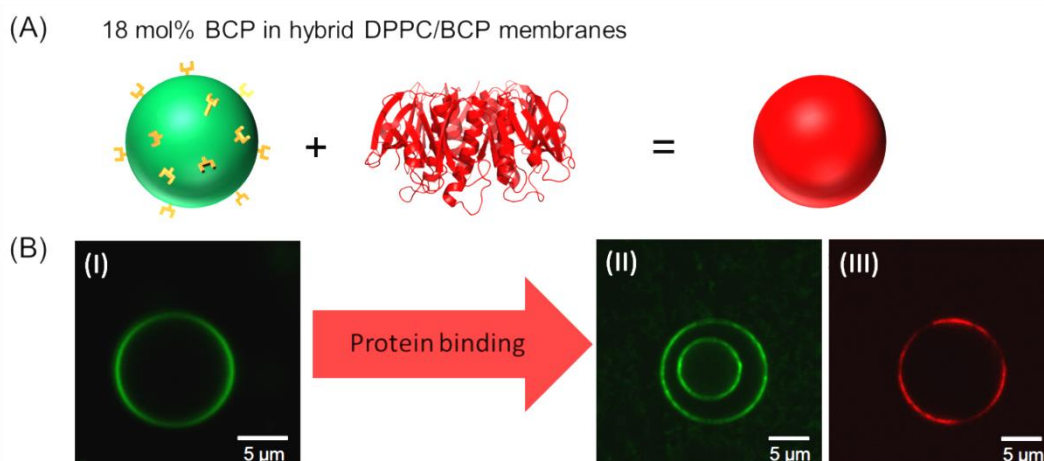


Figure S6. (A) Schematic illustration of the process of CTB binding to GM1-functionalized hybrid GUVs. (B) Confocal microscopy images of hybrid GUVs from mixtures of 82 mol% DPPC and 18 mol% PIB_{87-b}-PEO₁₇ BCP (1), which were functionalized with 0.1 mol% of GM1. Panel (B/I) depicts a hybrid GUV before the CTB incubation, showing a uniform appearance of the Rh-DHPE signal in the vesicle membrane. Panel (B/II) shows a hybrid GUV after the protein incubation, which contains a smaller vesicle, using the lipid dye Rh-DHPE to visualize the membrane. (B/III) shows the same vesicles, monitoring the Alexa 488-labeled CTB protein. The protein, has attached to the outer leaflet of the outer hybrid vesicle by binding to the hydrophilic portion of the incorporated GM1 molecules.

The inner hybrid vesicle displays no CTB binding, because the protein cannot cross the membrane of the outer vesicle.

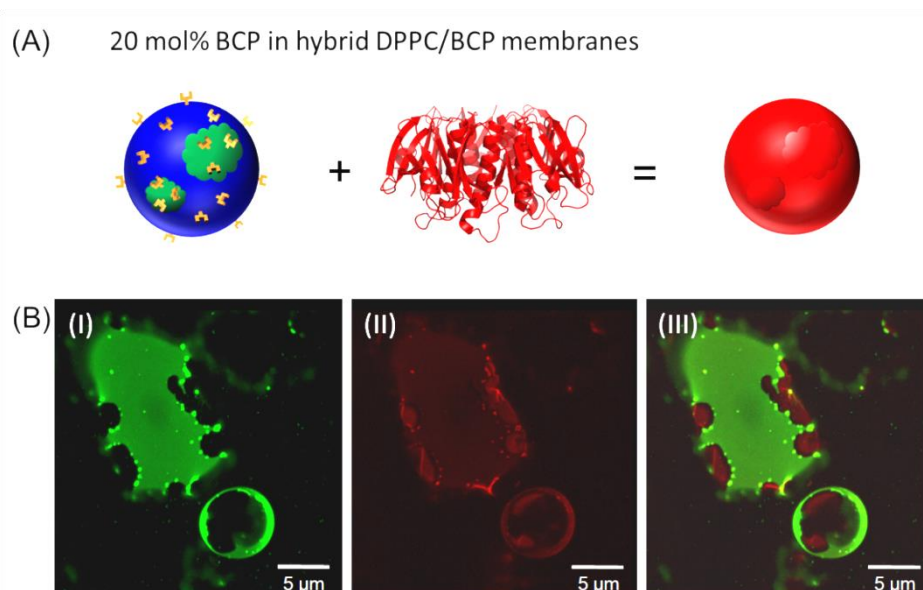


Figure S7. (A) Schematic illustration of the process of CTB binding to GM1-functionalized hybrid GUVs. (B) Confocal microscopy images of GUVs from mixtures of 80 mol% DPPC and 20 mol% PIB₈₇-*b*-PEO₁₇ BCP (**1**), which were functionalized with 0.1 mol% of GM1. Panel (B/I) depicts a 3D-reconstruction of phase separated hybrid GUVs visualizing the membrane heterogeneities with the Rh-DHPE dye (excited at 561 nm, green); Panel (B/II) shows the corresponding image, of the membrane bound Alexa 488-labeled cholera toxin B (red). Panel (B/III) contains the overlay of both images, which demonstrates differences in the phase labeling behavior of Rh-DHPE and CTB. By comparing the signal from the Rh-DHPE (green) to that of the GM1-bound CTB (red), it becomes clear that the protein binds to both phase types (see Panel B/II).

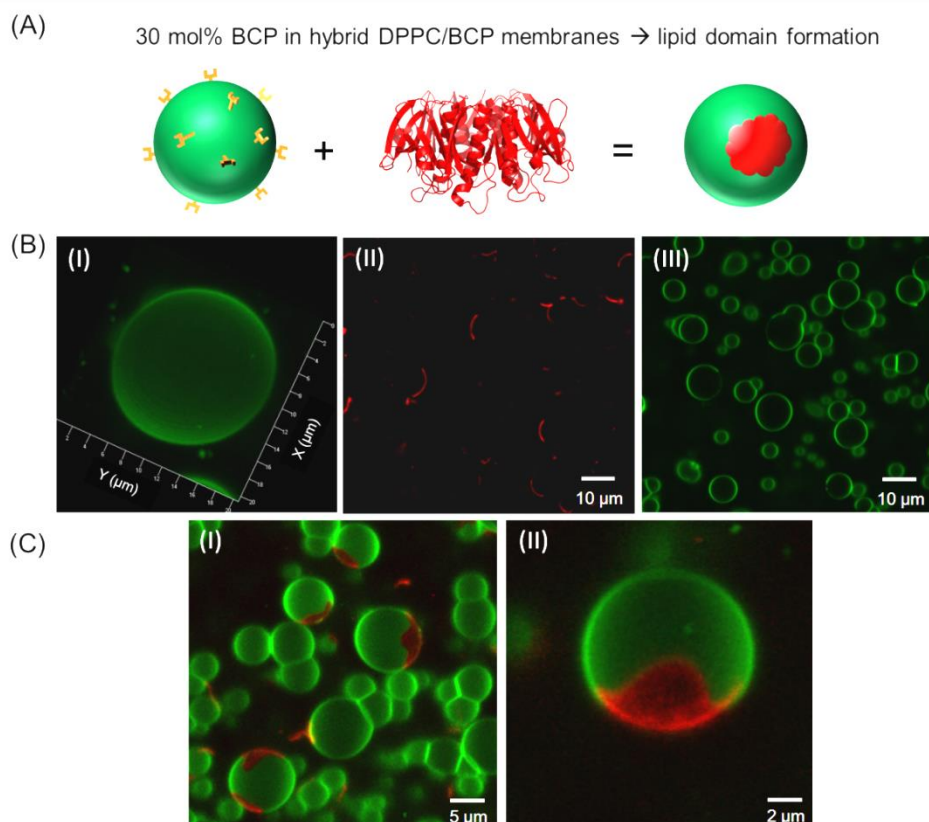


Figure S8. (A) Schematic illustration of the process of CTB binding to GM1-functionalized hybrid GUVs. (B and C) Confocal microscopy images of hybrid GUVs composed of DPPC and 30 mol% of PIB₈₇-*b*-PEO₁₇ BCP (1) functionalized with 0.1 mol% of GM1. Panel (B/I) depicts a 3D-reconstruction of a hybrid GUV before the protein incubation, showing a uniform appearance of the Rh-DHPE signal in the vesicle membrane. Panel (B/II) shows a confocal overview image after the incubation with CTB, monitoring the Alexa 488-labeled CTB bound to GM1, which induced the formation of GM1-enriched domains in the vesicle membranes (red patches) by a crosslinking process. The corresponding overview image (panel B/III), where the Rh-DHPE dye was excited, exhibits that the Rh-DHPE dye is excluded from the GM1-enriched domains, indicating the formation of a more ordered phase. Panels (C/I) and (C/II) depict a 3D-reconstruction of hybrid GUVs after CTB incubation, where both dyes the Rh-DHPE (green) and the Alexa 488-labeled cholera toxin B (red) were excited, demonstrating the CTB-labeled domains formed after protein incubation. Analysis by FRAP and FCS (see Figure 3) revealed that with increasing polymer content the lateral mobility in the membrane is strongly increased, suggesting that the formation of lipid domains after GM1-crosslinking with CTB is due to the higher mobility of GM1 in these membranes (prepared from mixture using 30 mol% BCP 1), compared to gel-phase membranes from DPPC or hybrid membranes obtained from mixtures using 12 to 18 mol% of BCP.

4.6 FRAP analysis for hybrid GUVs using lipid/BCP mixtures with 18 mol% and 40 mol% BCP (1) (Figures S9-S10).

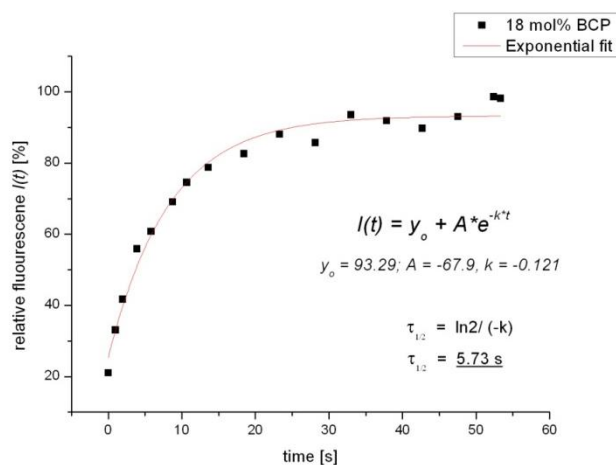


Figure S9. Typical FRAP curve for hybrid GUVs obtained from a 18 mol% BCP mixture using a single exponential fit.

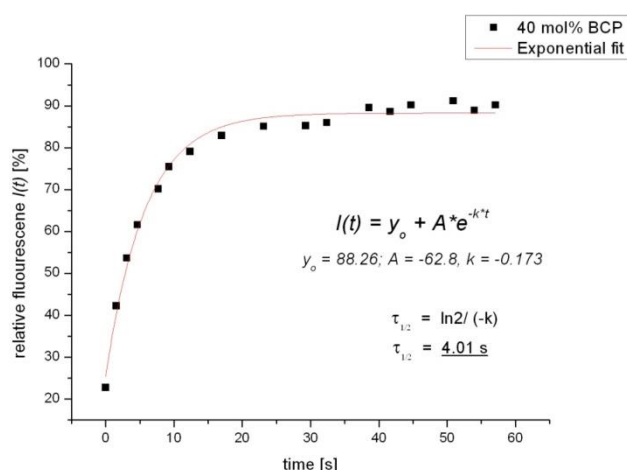


Figure S10. Typical FRAP curve for hybrid GUVs obtained from a 40 mol% BCP mixture using a single exponential fit.

References

- [1] M. Schulz, D. Glatte, A. Meister, P. Scholtyssek, A. Kerth, A. Blume, K. Bacia and W. H. Binder, *Soft Matter*, **2011**, 7, 8100.
- [2] W. H. Binder and R. Sachsenhofer, *Macromol. Rapid Commun.*, **2008**, 29, 1097.
- [3] M. I. Angelova and D. S. Dimitrov, *Faraday Discuss. Chem. Soc.*, **1986**, 81, 303.
- [4] A. M. Melo, M. Prieto, A. Coutinho, *Biochimica et Biophysica Acta* **2011**, 1808, 2559.
- [5] Z. Petrášek, P. Schwille, *Biophys. J.* **2008**, 94, 1437.
- [6] A. Loman, T. Dertinger, F. Koberling, J. Enderlein, *Chem. Phys. Lett.* **2008**, 459, 18.
- [7] M. Dyck and M. Lösche, *J. Phys. Chem. B*, **2006**, 110, 22143.
- [8] J. Korlach, P. Schwille, W. W. Webb and G. W. Feigenson, *PNAS*, **1999**, 96, 8461.

Appendix C – *Soft Matter* 2013, Accepted Manuscript. DOI: 10.1039/C3SM52040D.

Lateral surface engineering of hybrid lipid/BCP vesicles and selective nanoparticle embedding

Figures

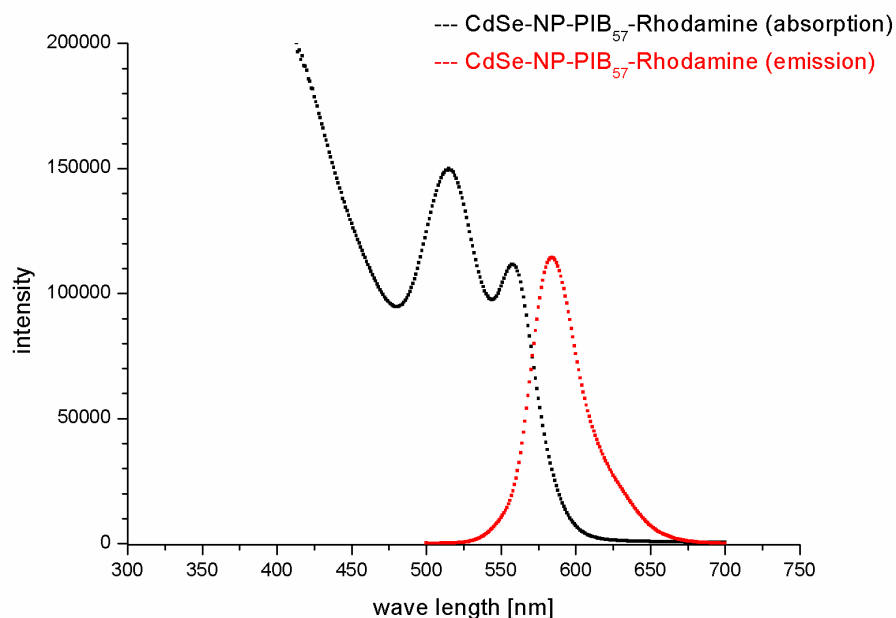


Figure S1. Absorption and emission spectra of hydrophobically modified CdSe nanoparticles, which are covalently labeled with rhodamine-B (excitation, $\lambda_{\text{max}} = 561$ nm).

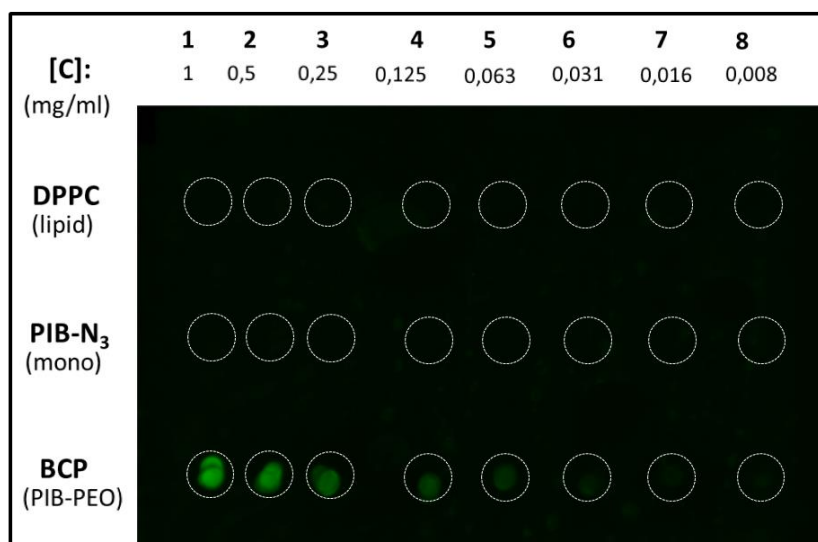


Figure S2. To examine the specificity of the antibody system against the PEO-functionality of PIB-PEO based block copolymers, we performed a dotblot experiment. Therefore, DPPC as lipid component, the PIB-homopolymer and the PIB₈₇-*b*-PEO₁₇ BCP were blotted on a nitro-cellulose membrane varying their concentrations and subsequently the membrane was treated with a solution of dry milk to block unspecific interactions of antibodies with membrane. After 1 hour, the membrane

was washed with buffer solution (three times) and then incubated with the primary antibody (anti-PEO). Afterwards (again 1 hour), the membrane was washed three times with buffer solution (a 20 min) and subsequently the membrane was incubated with the secondary antibody (anti-rabbit, fluorescently labeled with dylight 488 dye). Before the detection of the antibody by fluorescence analysis was carried out, the membrane was washed again three times with buffer solution and slightly dried. The fluorescence analysis (see green areas) is shown in Figure S2 demonstrating that the binding of the antibody system was only observed in case of the blotted BCP sample. DPPC or PIB-homopolymers were not detected by the antibodies confirming the high specificity of antibody system.

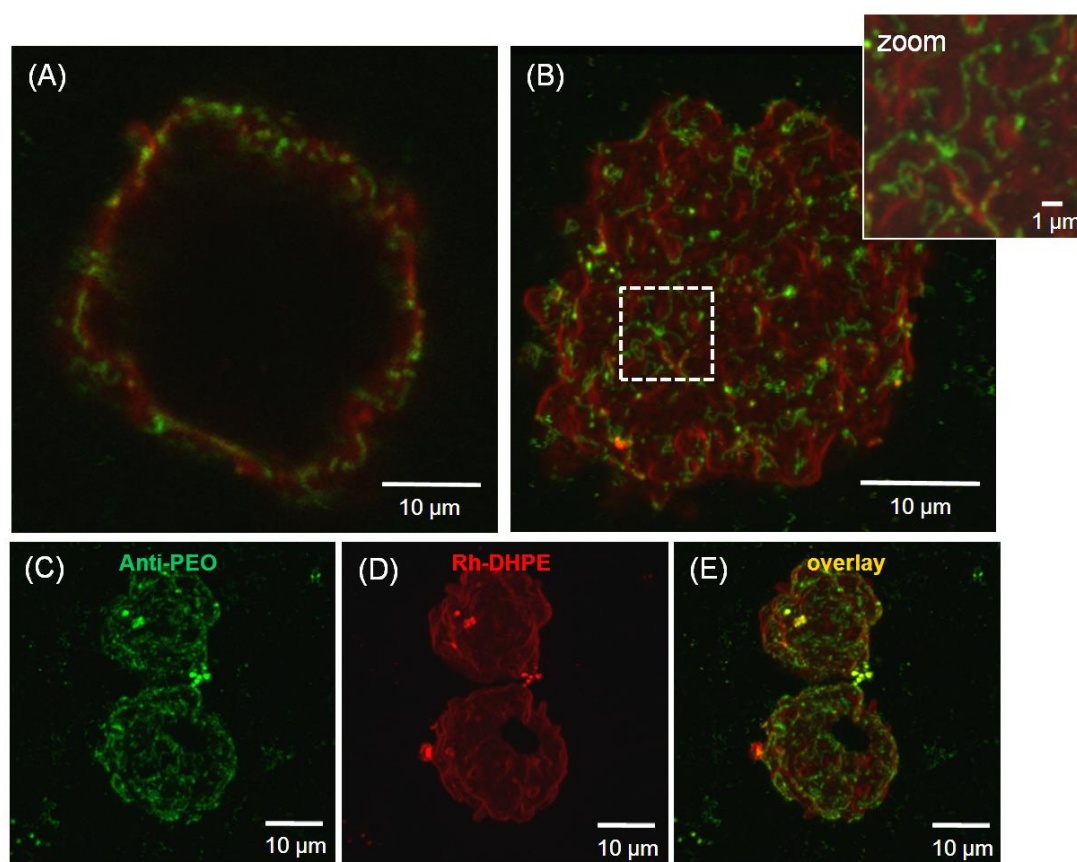


Figure S3. Confocal microscopy images of hybrid GUVs prepared from a mixture of DPPC with 10 mol% of BCP demonstrating that the binding of the antibodies to the incorporated BCPs revealed a network-like morphology of the BCPs within the faceted vesicle surface. Panel (A) depicts an image of a faceted hybrid vesicle, which is typical for such lipid/BCP composition, near the vesicle equator showing the binding of the antibodies to BCPs (green patches in A). (B) 3D-reconstruction of an axial series of confocal slices from the vesicle shown in (A), which proves the network-like morphology of the incorporated BCPs (see green areas in the zoom). Panel (C-E) displays a 3D-reconstruction of single GUVs indicating the uniform distribution of the Rh-DHPE dye over the whole GUV surface (D) and the binding of the antibodies to BCP molecules proving finally heterogeneous distribution of the BCPs in the faceted vesicle surface.

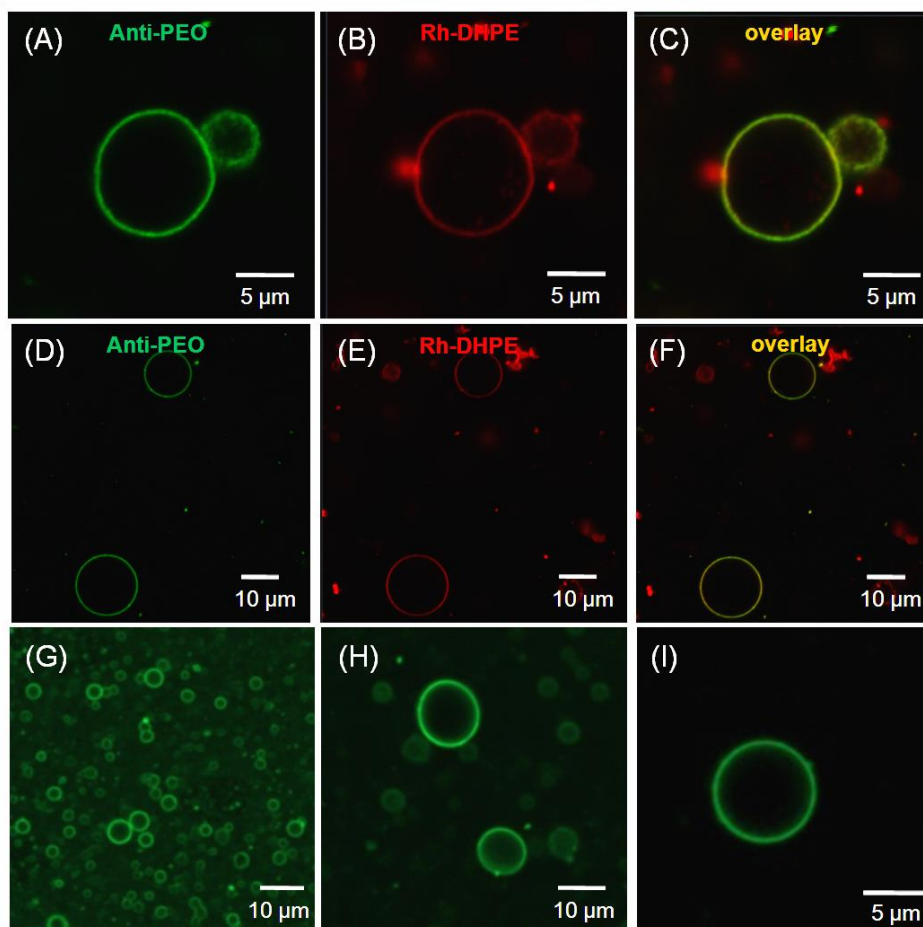


Figure S4. Confocal microscopy images of hybrid GUVs from DPPC mixed with 16 mol% of BCP showing in (A to C) a single vesicle typically obtained for such composition, which demonstrate a random distribution of the membrane components within the mixed bilayer by comparing the fluorescence signal of the antibody with fluorescence of Rh-DHPE dye. (D-F) illustrates an overview of single GUVs proving the mixed membrane morphology by the uniform fluorescence of both dyes. Panel (G to F) shows vesicles from another experiment visualizing the vesicles only by recognition of the membrane incorporated BCPs by antibodies (no additional membrane dye was used). The antibodies bind over the whole hybrid vesicle surface, which indicates that the polymers are randomly distributed in the membrane.

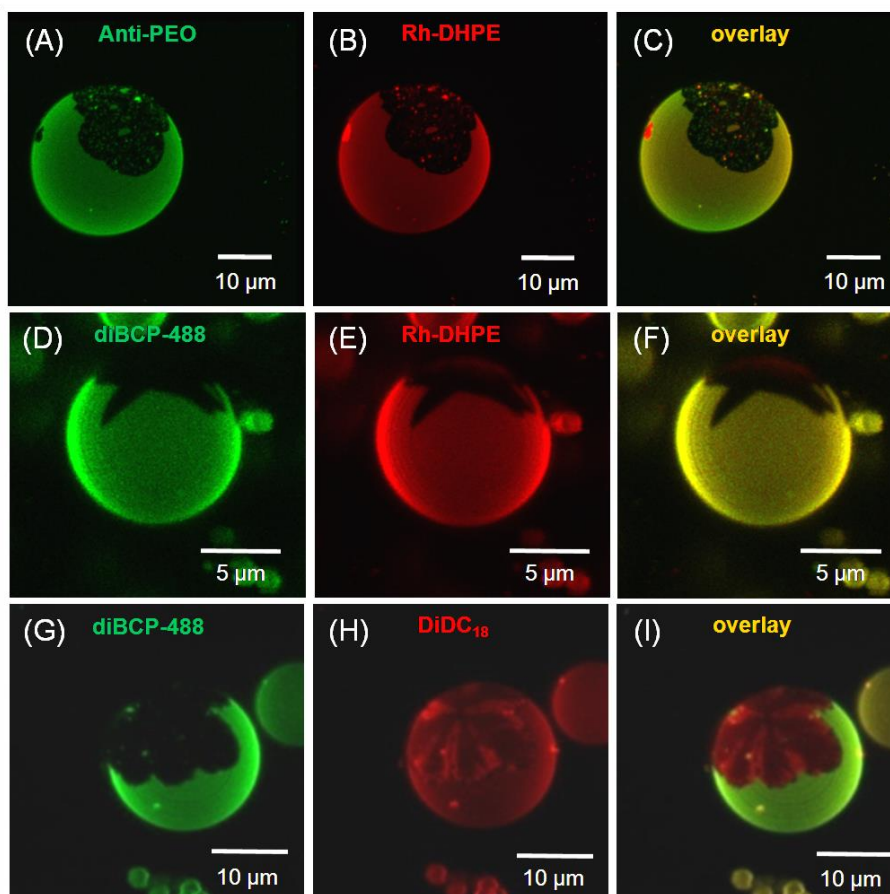


Figure S5. Confocal microscopy images of phase-separated hybrid DPPC/PIB₈₇-*b*-PEO₁₇ GUVs obtained with 76 mol% DPPC and 24 mol% BCP, demonstrating membrane heterogeneities by the phase partitioning behavior of the lipid analogous DiDC18 dye, rhodamine-labeled lipid (Rh-DHPE) and the fluorescently labeled PIB-PEO diblock copolymer (diBCP-488) in comparison to the results of the antibody-mediated monitoring of BCPs (A-C). The first row (panel A to C) shows a 3D-reconstruction of an axial series of confocal slices of a phase separated vesicle where the polymer-rich phase was successfully assigned by the antibody binding (compare panel A, green phase). Panel (D-F) depicts also a 3D-reconstruction of a phase separated GUV, where the polymer-rich phase was successfully assigned by using the fluorescently labeled diblock copolymer (excited at 488 nm, green phase in panel D). The use of Rh-DHPE proves that the membrane dye is preferential incorporated into the polymer-rich phase, as illustrated in panel B and E. Whereas, visualization of phase heterogeneities in hybrid GUVs (Panel G-F, 3D-reconstruction) by the lipid analogous dye DiDC18 showed an enrichment of the dye in the black domain, as proved by the fluorescently labeled block copolymer or antibody binding to be the DPPC-rich phase (compare panel G with H), that this particular phase is formed by highly ordered DPPC molecules. In contrast to the reported phase partitioning behavior of Rh-DHPE,^{1, 2} DiDC18 has shown to become enriched into more ordered gel-phase domains in GUVs prepared from phospholipids, which differ in their acyl-chain lengths.³

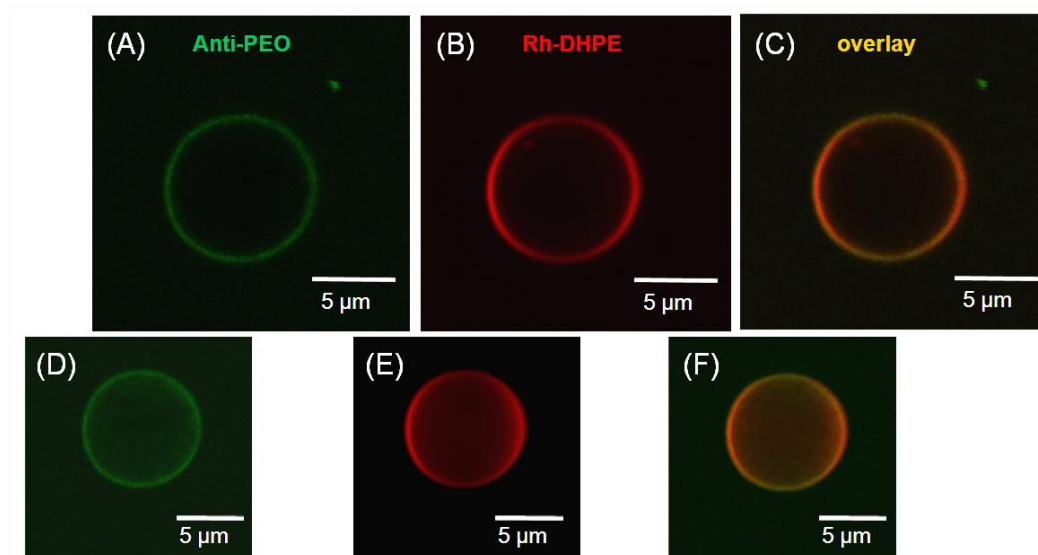


Figure S6. Confocal microscopy images of mixed hybrid DPPC/PIB₈₇-*b*-PEO₁₇ GUVs obtained with 60 mol% DPPC and 40 mol% BCP proving the formation of the mixed phase by antibody-mediated monitoring of membrane incorporated BCP molecules (panel A and D). Panel (A to C) shows a single equatorial slice of a hybrid GUV and panel (D to F) depicts a 3D-reconstruction of an axial series of confocal slice from a vesicle, which is typically obtained for 60/40 mixtures of DPPC and BCP demonstrating a uniform distribution of the antibodies and the Rh-DHPE dye over the whole GUV membrane.

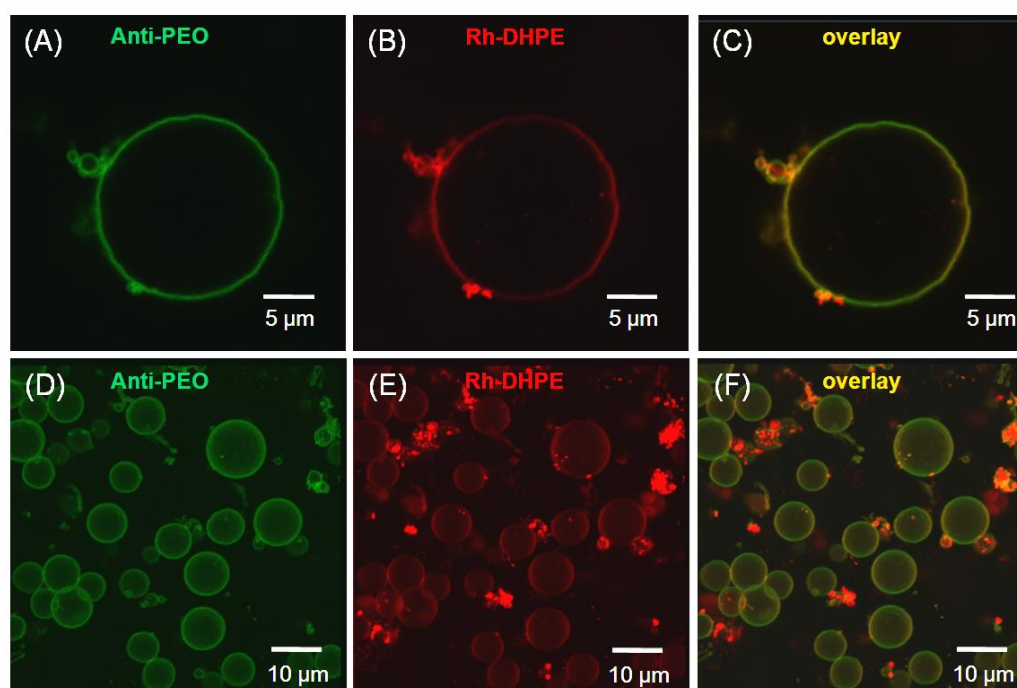


Figure S7. Confocal microscopy images of hybrid GUVs from a DOPC mixture with 20 mol% of BCP showing in (A to C) a single GUV image near the vesicle equator which display that the binding of the antibodies (excited at 488 nm, green) is uniformly observed over whole GUV surface. Panel (B) depicts the same vesicle using Rh-HPE (excited at 561 nm, red) to visualize the membrane

morphology, which showed also a uniform distribution in the membrane. Panel (D-F) shows 3D-reconstruction of an axial series of confocal slices from an overview of hybrid GUVs, which displays the uniform fluorescence signal of the surface bound antibodies and Rh-DHPE for all vesicles proving the mixed state of the hybrid membrane. The obtained GUVs were stable over time (monitored over several hours) demonstrating no phase separation phenomena.

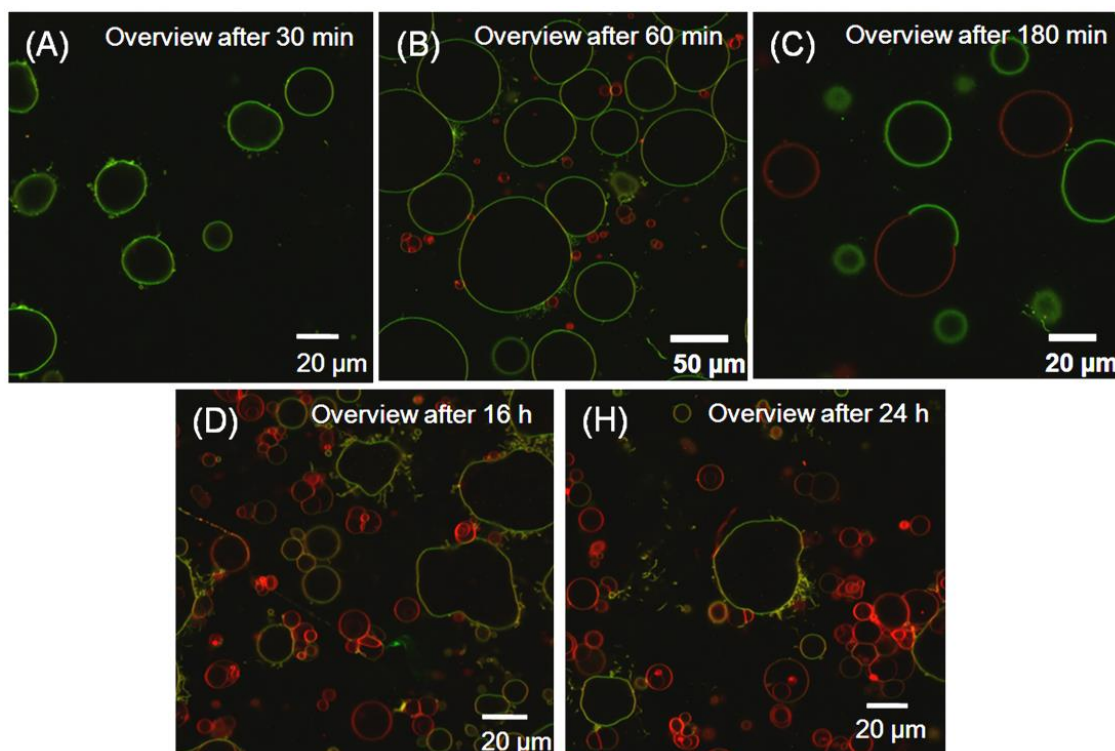


Figure S8. Selective antibody binding revealed that the hybrid vesicles prepared from mixtures of DOPC with 10 mol% of BCP and less polymer content undergo phase separation and a budding process with time. Panel (A to H) depicts confocal microscopy images (overlay image of antibody and Rh-HPE excitation) of hybrid GUVs, which were prepared from DOPC mixture with 10 mol% BCP, near their vesicle equator taken from different vesicles over time. Initially stable GUVs (no red-colored GUVs) were monitored over 24 hours demonstrating the formation of pure DOPC liposomes with time (compare amount of red colored vesicles in overlay images, visualized by Rh-DHPE dye). The analysis of the hybrid vesicles at different times allowed the observation of the budding process proving that the amount of red-colored vesicles is significant increased with time proving that no antibody binds to these vesicles (compare green and red areas in overlay images).

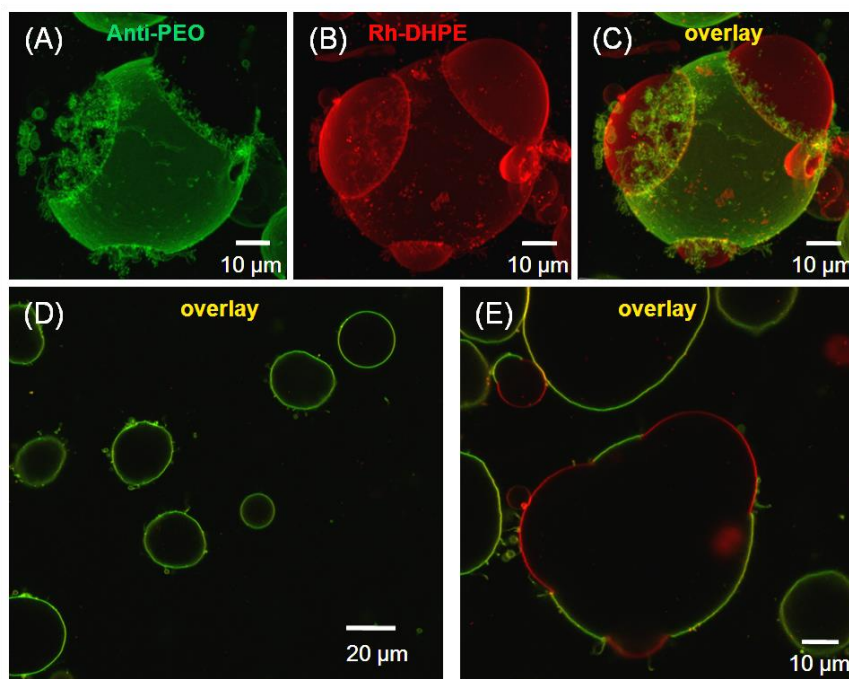


Figure S9. Selective antibody binding revealed that the hybrid vesicles obtained from 10 mol% BCP and less polymer content in mixtures with DOPC undergo phase separation and budding process with time. Panel (A-C) depicts a 3D-reconstruction of an axial series of confocal slices from a hybrid vesicle, which is shown in panel (E) as single slice near the vesicle equator, demonstrating the advanced state of the vesicle budding process (recorded at 85 minutes after secondary antibody incubation). Panel (A) displays the fluorescence signal of the surface bond antibodies (excited at 488 nm, green), panel (B) the fluorescence of the Rh-DHPE dye (excited at 561 nm, red) and panel (C) the overlay image indicating clearly that the vesicle undergoes budding, which results in the formation of polymer-depleted liposomes and polymer-rich vesicles. Panel (D) shows an overview image of hybrid GUVs after a short time after the electroformation process and antibody incubation, where no budding phenomena were observed expecting first stable GUVs.

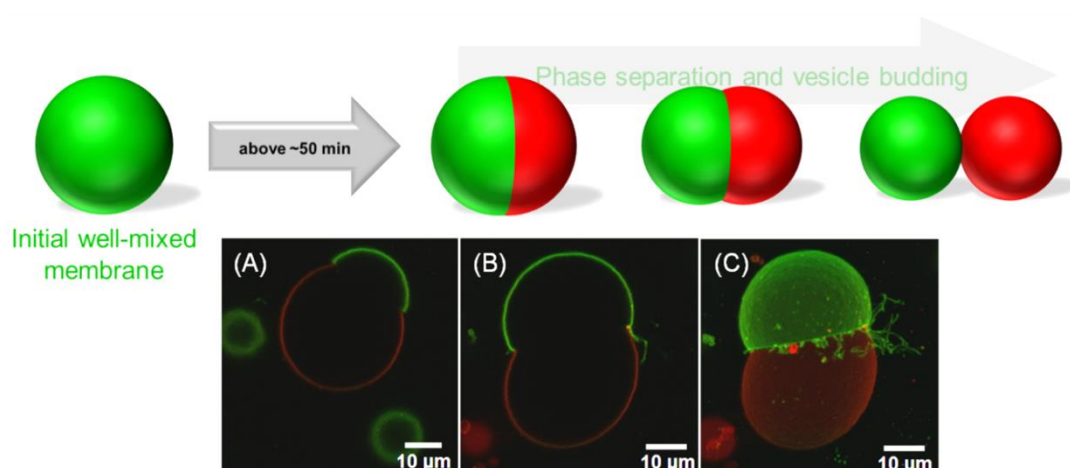


Figure S10. Schematic representation of the vesicle budding process compared to different states of the process obtained by fluorescence monitoring of different vesicles by LSM (panel A to C). During the budding the length of the domain boundary is strongly reduced which drives the vesicle fission process to completeness. Panel (A) shows a vesicle obtained from a mixture of DOPC with 10 mol% of BCP at an early state of the budding process, panel (B) at advanced state of the process and panel (C) depicts the 3D-reconstruction of the vesicle from (B) demonstrating clearly the coexistence of two different phases, the lipid-rich phase (visualized by Rh-DHPE, red area) and the polymer-rich phase (visualized by the fluorescently labeled antibodies, green area).

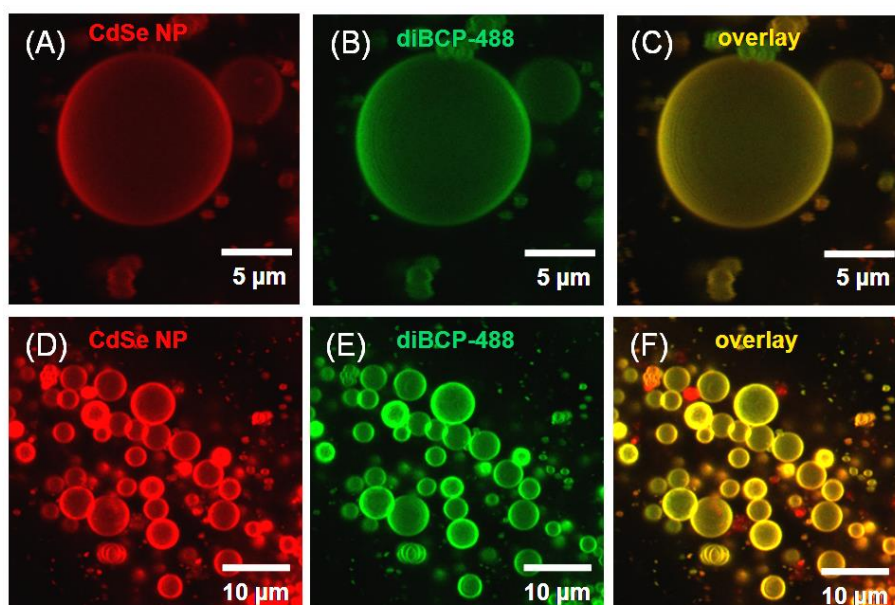
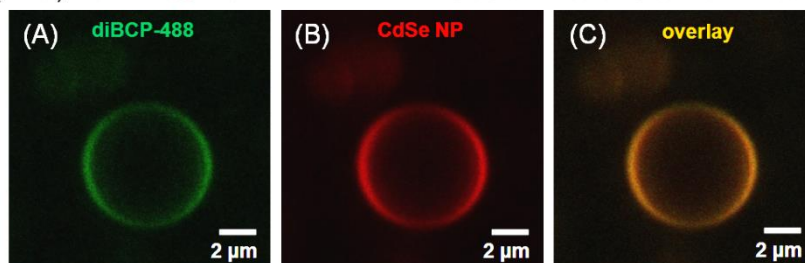


Figure S11. Incorporation of hydrophobically modified CdSe-NPs into DPPC/BCP hybrid membranes at room temperature is presented. (A to C) Confocal microscopy images of hybrid GUVs from a DPPC mixture with 18 mol% of BCP showing a single equatorial slice of a hybrid GUV which demonstrates that the CdSe-NPs (fluorescently labeled with rhodamine B; excited at 561 nm panel A) and the fluorescently labeled diBCP (excited at 488 nm, panel B) are randomly distributed within the

hybrid bilayer proving the mixed membrane state. Panel (D-F) shows 3D-reconstruction of an axial series of confocal slices from an overview of hybrid GUVs, which displays the uniform fluorescence signal of the nanoparticles and labeled BCPs within the mixed bilayer in case of all vesicles proving further the mixed state of the hybrid membrane.

(A-C) 40 mol% BCP with Rh-PIB-CdSe NPs and diBCP 488



(D-F) 20 mol% BCP with Rh-PIB-CdSe NPs and DiDC₁₈

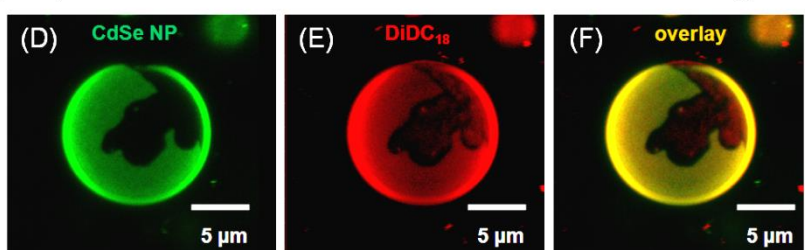


Figure S12. Incorporation of hydrophobically modified CdSe-NPs into DPPC/BCP hybrid membranes is demonstrated in the non-phase separated and phase separated case. The incorporation into mixed vesicles prepared from 60 mol% of DPPC and 40 mol% of BCP is shown in panel (A to C) and the selective localization of the particles in the polymer-rich phase of heterogeneous vesicle morphologies (obtained from mixtures of DPPC with 20 mol% BCP) is depicted in panel (D-F), which shows that the CdSe-NPs (excited at 561 nm) are preferential incorporated into one specific phase (green area in panel D). The enrichment of DiDC₁₈ used as additional membrane dye (panel E) indicates that the black patch in panel (D) consists of an ordered phase of DPPC molecules. The NP monitoring showed clearly that the particles prevent the incorporation into this ordered phase (see black patch in panel D and overlay image panel F).

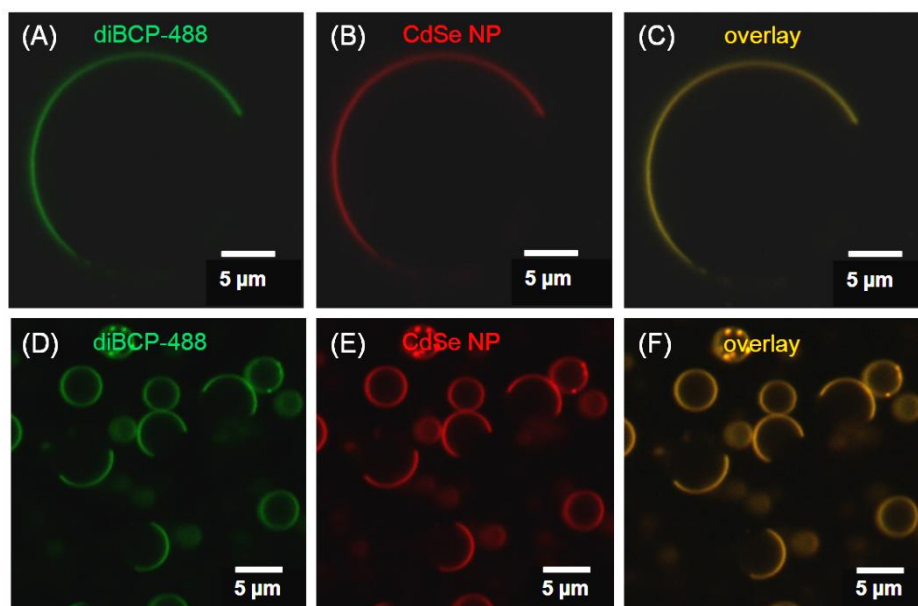


Figure S13. Selective incorporation of hydrophobically modified CdSe-NPs into DPPC/BCP hybrid membranes demonstrating the incorporation into the polymer-rich phase of heterogeneous vesicle morphologies (24 mol% BCP), which is confirmed by co-localization of the CdSe-NPs (fluorescently labeled with rhodamine B; excited at 561 nm panel B) and the fluorescently labeled diBCP (excited at 488 nm, panel A). (D to F) Confocal microscopy images of hybrid GUVs showing a single equatorial slice of the hybrid GUVs, prepared from mixtures of DPPC with 24 mol% of BCP, which demonstrates the formation of different phases and that the fluorescently labeled particles and block copolymers are partitioned into the same phase, preventing the incorporation into the observed black domains (ordered DPPC-rich phases).

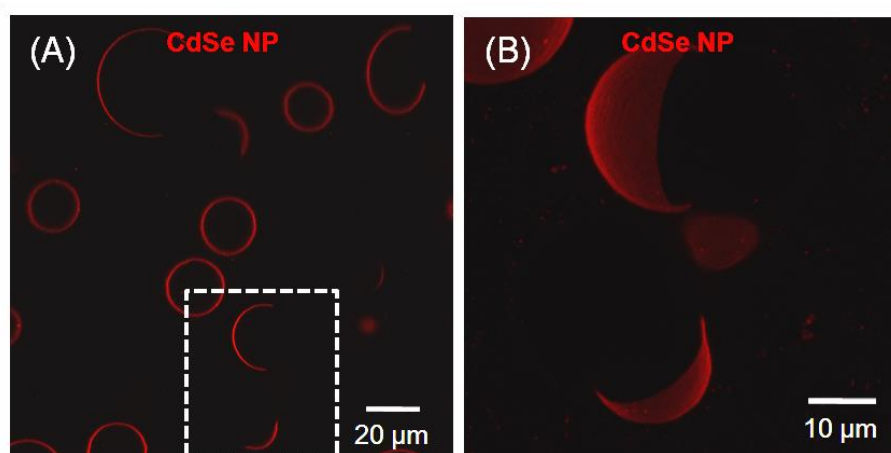


Figure S14. Confocal microscopy images of hybrid GUVs presenting the selective incorporation of hydrophobically modified CdSe-NPs into phase separated DOPC/BCP hybrid membranes (from mixtures of DOPC with 10 mol% BCP). The coexistence of two different phases is displayed by monitoring the fluorescently labeled nanoparticles (excited at 561 nm), which shows the preferential

incorporation of the particles into one of the coexisting phases. Panel (A) depicts a single equatorial slice of hybrid GUVs and panel (B) illustrates a 3D-reconstruction of an axial series of confocal slices of hybrid GUVs (see indicated area in panel A) proving phase heterogeneities already obtained after electroformation process and before the GUVs were incubated with the antibody system.

References

- [1] Dyck, M.; Lösche, M., Interaction of the Neurotransmitter, Neuropeptide Y, with Phospholipid Membranes: Film Balance and Fluorescence Microscopy Studies *J. Phys. Chem. B* 2006, **110**, (44), 22143-22151.
- [2] Schulz, M.; Werner, S.; Bacia, K.; Binder, W. H., Controlling Molecular Recognition with Lipid/Polymer Domains in Vesicle Membranes. *Angew. Chem. Int. Ed.* 2013, **52**, (6), 1829-1833.
- [3] Korlach, J.; Schwille, P.; Webb, W. W.; Feigenson, G. W., Characterization of lipid bilayer phases by confocal microscopy and fluorescence correlation spectroscopy. *PNAS* 1999, **96**, (15), 8461-8466.

Dipl.-Chem. Matthias Schulz

Tel.: 0178/6867745

E-Mail: matthias.schulz@chemie.uni-halle.de

Persönliche Daten

Geburtsdatum: 07.02.1984
Geburtsort: Stendal
Nationalität: deutsch

Familienstand: ledig

Anschrift: Geiststraße 2
 06108 Halle, Sachsen-Anhalt



Beruflicher Werdegang/ Ausbildung

- seit 02/2010** Mitglied in der Forschungsgruppe FOR 1145
Thema: „Strukturbildung von synthetischen polyphilen Molekülen mit Lipidmembranen“
Deutsche Forschungsgemeinschaft (DFG)
- seit 02/2010** Wissenschaftlicher Mitarbeiter an der Martin-Luther-Universität,
 Arbeitsgruppe von Prof. Dr. Wolfgang H. Binder
Dissertation im Fachbereich Makromolekulare Chemie
Thema: „Synthesis of amphiphilic block copolymers and their interactions with model lipid membranes“
Institut für Chemie, Makromolekulare Chemie
- 10/2004 – 11/2009 Hochschulstudium der Chemie/ Abschluss: Diplom (Note 1,0)
Martin-Luther-Universität Halle-Wittenberg
Diplomarbeit: „Macrocyclization of telechelic Polyisobutylenes“
Institut für Chemie, Makromolekulare Chemie

08/1994 – 06/2003 Oberstufenausbildung/ Abschluss: Abitur (Note 1,7)

Diesterweg Gymnasium Tangermünde

08/1990 – 06/1994 Unterstufenausbildung

Comenius Grundschule Tangermünde

Besondere Kenntnisse

- **Fremdsprachen:** Englisch (sehr gut), Russisch (Grundlagen)
- **EDV:** Microsoft Office Paket, Corel Draw, Corel Photo-Paint, Windows Betriebssysteme
- **wissenschaftliche Software:** EndNote, Chem-Sketch, ChemDraw, MestRe-C, Origin Professional, SciFinder, Mikroskopie (Image Analysis): ZEN-2009, ZEN-2011/2012, Leica
- Umfangreiche Kenntnisse im Umgang mit konfokaler **Laser Scanning Microscopy (LSM)** basierend auf Zeiss- oder Leica-Systemen
- **Analytische Methoden:** ^1H -/ ^{13}C -NMR, GPC, IR, UV-VIS, DLS, DSC, HPLC, ESI-TOF MS, MALDI-TOF MS, TGA, HPLC/ESI-TOF MS, Filmwaage/ Langmuir-Blodgett Techn.
- **Sachkunde-Nachweis** gemäß § 5 Abs. 2 der Chemikalien-Verbotsverordnung

Publikationen

- 1) **Schulz, M.**; Tanner, S.; Barqawi, H.; Binder, W., H., Macrocyclization of polymers via ring-closing metathesis and azide/alkyne-“click”-reactions: An approach to cyclic polyisobutylenes. *J. Polym. Sci., Part A: Polym. Chem.* **2010**, 48, (3), 671-680.
- 2) Herbst, F.; **Schulz, M.**; Binder, W. H., Ordentlich dynamisch: Supramolekulare Polymere. *Nachrichten aus der Chemie (NAC)* **2010**, 58, 734-739.
- 3) **Schulz, M.**; Glatte, D.; Meister, A.; Scholtysek, P.; Kerth, A.; Blume, A.; Bacia, K.; Binder, W. H., Hybrid lipid/polymer giant unilamellar vesicles: effects of incorporated biocompatible PIB-PEO block copolymers on vesicle properties. *Soft Matter* **2011**, 7, (18), 8100-8110.
Cover: Soft Matter/ Volume 7/ Number 18/ 21 September 2011/ Pages 7877-8664.
- 4) **Schulz, M.**; Olubummo, A.; Binder, W. H., Beyond the lipid-bilayer: interaction of polymers and nanoparticles with membranes. *Soft Matter* **2012**, 8, (18), 4849-4864.
- 5) Olubummo, A.; **Schulz, M.**; Lechner, B.-D.; Scholtysek, P.; Bacia, K.; Blume, A.; Kressler, J.; Binder, W. H., Controlling the Localization of Polymer-Functionalized Nanoparticles in Mixed Lipid/Polymer Membranes. *ACS Nano* **2012**, 6, (10), 8713-8727.
- 6) **Schulz, M.**; Werner, S.; Bacia, K.; Binder, W. H., Controlling Molecular Recognition with Lipid/Polymer Domains in Vesicle Membranes. *Angew. Chem. Int. Ed.* **2013**, 52, (6), 1829-1833.

- 7) **Schulz, M.**; Olubummo, A.; Bacia, K.; Binder, W. H., Lateral Surface Engineering of Hybrid Lipid/BCP Vesicles and Selective Nanoparticle Embedding. *Soft Matter* **2013**, *Accepted Manuscript*. DOI: 10.1039/C3SM52040D.

Cover: Soft Matter/ Volume X/ 2014/ in press.

- 8) Barqawi, H.; **Schulz, M.**; Olubummo, A.; Binder, W. H., 2D-LC/SEC-(MALDI)-MS Characterization of Symmetric and Nonsymmetric Biocompatible PEO_m-PIB-PEO_n Block Copolymers. *Macromolecules* **2013**, *46*, 7638-7649.
- 9) Olubummo, A.; **Schulz, M.**; Schöps, R.; Kressler, J.; Binder, W. H., Phase Changes in Mixed Lipid/Polymer Membranes by Multivalent Nanoparticle Recognition. *Langmuir* **2013**, *Manuscript submitted*.

Konferenzen und Poster

- 1) 02/2010 in Freiburg (Breisgau)/ *Makromolekulares Kolloquium*: „Blockcopolymer und Nanopartikel an der Luft/Wasser-Grenzfläche“
- 2) 09/2010 in Halle (Saale)/ *Polymertagung P2010*: „Macrocyclization of telechelic polyisobutylenes“
- 3) 09/2012 in Halle (Saale)/ *Polymertagung P2012*: „Hybrid Lipid/Polymer giant unilamellar vesicles (GUVs)“

Konferenzen und Vorträge

- 1) 02/2010 Freiburg (Breisgau)/ *Makromolekulares Kolloquium*: „Blockcopolymer und Nanopartikel an der Luft/Wasser-Grenzfläche“
- 2) 05/2011 Freyburg (Unstrut)/ *Forschergruppe FOR 1145*: „Effect of incorporated amphiphilic BCPs in DPPC mono- and bilayer membranes“
- 3) 11/ 2011 Alterode/ *Forschergruppe FOR 1145*: „Interaction of di- and triblock copolymers with lipid membrane models – Phase separation phenomena in mixed lipid/polymer membranes“
- 4) 06/2012 Oppurg (Thüringen)/ *Forschergruppe FOR 1145*: „Interaction of di- and triblock copolymers with lipid membrane models – Controlling receptor/ligand recognition processes on hybrid vesicle surfaces“
- 5) 09/2012 Halle (Saale)/ *P2012*: „Preparation of amphiphilic BCPs and their incorporation into model bilayer membranes“
- 6) 06/2013 Halle (Saale)/ *Forschergruppe FOR 1145*: „Antibody-mediated proof of hybrid lipid/polymer membrane morphologies“

.....
Matthias Schulz

Eigenständigkeitserklärung

Hiermit erkläre ich an Eides statt, dass ich die vorliegende Dissertation („Synthesis of Amphiphilic Block Copolymers and their Interactions with Model Lipid Membranes“) selbständig und ohne fremde Hilfe verfasst, andere als die von mir angegebenen Quellen und Hilfsmittel nicht benutzt und die den zitierten Werken wörtlich oder inhaltlich entnommenen Stellen als solche gekennzeichnet habe. Weiterhin versichere ich, dass die vorliegende Arbeit noch an keiner anderen Einrichtung zur Begutachtung vorgelegt wurde.

Halle (Saale), den 02.12.2013

.....
Matthias Schulz